U-Pb geochronology of detrital and igneous zircon grains from the Águilas Arc in the Internal Betics (SE Spain): Implications for Carboniferous-Permian paleogeography of Pangea

Citation for published version:
Jabaloy-sánchez, A, Talavera, C, Rodríguez-peces, MJ, Vázquez-vílchez, M & Evans, NJ 2020, 'U-Pb geochronology of detrital and igneous zircon grains from the Águilas Arc in the Internal Betics (SE Spain): Implications for Carboniferous-Permian paleogeography of Pangea', *Gondwana Research*. https://doi.org/10.1016/j.gr.2020.10.013

Digital Object Identifier (DOI):
10.1016/j.gr.2020.10.013

Link:
Link to publication record in Edinburgh Research Explorer

Document Version:
Peer reviewed version

Published In:
Gondwana Research

Gondwana Research

U-Pb geochronology of detrital and igneous zircon grains from the Águilas Arc in the Internal Betics (SE Spain): implications for Carboniferous-Permian paleogeography of Pangea

--Manuscript Draft--

Manuscript Number:	GR-D-20-00209R1
Article Type:	Research Paper
Keywords:	Detrital zircon ages Maximum depositional ages Betic Chain Carboniferous foreland basins
Corresponding Author:	ANTONIO JABALOY, Ph. D. Universidad de Granada Granada, Granada SPAIN
First Author:	ANTONIO JABALOY, Ph. D.
Order of Authors:	ANTONIO JABALOY, Ph. D.
	Cristina Talavera, Ph. D.
	Martín J Rodríguez-Peces, Ph. D.
	Mercedes Vázquez-Vílchez, Ph. D.
	Noreen J Evans, Ph. D.
Abstract:	New U-Pb detrital zircon and U-Pb zircon ages of metaigneous rocks in the Águilas Arc (Betic Chain, SE Spain) allow us to determine the maximum depositional ages of the rocks. Within the Nevado-Filábride Complex, a Late Carboniferous depositional age for the Lomo de Bas schists and quartzites, and a Permian-Triassic maximum depositional age for the Tahal Fm are determined. Within the Alpujárride Complex, the maximum depositional age of the Micaschists and Quartzite Fm is Late Carboniferous and the Meta-detrital Fm was deposited in the Early Permian. Furthermore, the maximum depositional age of the Saladilla Fm in the Maláguide Complex is also Early Permian. The age distribution patterns for the Carboniferous rocks of the Nevado-Filábride and Alpujárride complexes are similar to those from the Cantabrian Zone of the Iberian Massif, suggesting deposition in Carboniferous foreland basins located eastwards of the Iberian Massif. However, age patterns in Maláguide and samples from the North-eastern Iberian Peninsula and South France show strong similarities suggesting that it can be located near those areas in the Late Carboniferous times. The samples with Early Permian maximum depositional ages from the three complexes contain more Paleozoic zircon grains relative to the older Carboniferous samples, but have similar age distribution patterns, suggesting that they were deposited in the same basin. Samples from unconformable Middle Miocene sediments have Early Permian youngest zircon populations and age distribution patterns corresponding to a mixing of detrital zircon grains from the Alpujárride and Maláguide complexes. Furthermore, there is no record of any major felsic rocks formation and/or exhumation event after the Early Permian in those two complexes.
Response to Reviewers:	We have aswered to all the comments and annotations of the reviewers in the "Detailed response to reviewers". The response for the specific comments for Reviewer2 are: We have corrected the inaccuracies found in the Geological setting, shortened it and added a new Table 1 with the lihostratigraphic units of the three tectonic complexes. We have added references to the age of the different units when they are known. We have rewritten the presentation of the results, adding age ranges and /or percentages of the main age groups. We have rewritten the Discussion and Conclusions, deleted four figures, and revised the statements referred to works from other authors. Antonio Jabaloy Sánchez

Cover Letter

UNIVERSIDAD DE GRANADA

To: Joseph G Meert, Ph.D
Associate Editor
Gondwana Research

From: Professor Antonio Jabaloy Sánchez
Departamento de Geodinámica
Facultad de Ciencias
Universidad de Granada
Campus Fuentenueva s/n
18071 Granada (Granada)

Subject: Revised manuscript GR-D-20-00209

Granada, September 2nd, 2020

Dear Associated Editor,

With this letter we are submitting a revised version of the manuscript GR-D-20-00209, entitled "U-Pb geochronology of detrital and igneous zircon grains from the Águilas Arc in the Internal Betics (SE Spain): implications for Carboniferous-Permian paleogeography of Pangea" by Antonio Jabaloy-Sánchez, Cristina Talavera, Martín Jesús Rodríguez-Peces, Mercedes Vázquez-Vílchez, Noreen Joyce Evans.

As requested, we have revised the manuscript, taking into account all comments from the Reviewers. We provide a more detailed explanation in the accompanying Response to Reviewers and greatly appreciate the time invested by each in improving our work. As most of the suggestions from both reviewers were in the annotated PDFs, we quote the location of our revision using the line numbering in the submitted manuscript. However, in our detailed response to the reviewers in red below, we refer to line numbers in the revised manuscript "changes not marked".

All authors have seen and approved the present version of the manuscript and consent to the submission. Thank you very much for your attention to this matter.

Yours sincerely,

Antonio Jabaloy Sánchez
Corresponding Author

UNIVERSIDAD DE GRANADA

Response to Reviewers:

Reviewer #1 comments: Manuscript Number: GR-D-20-00209

“The paper "U-Pb geochronology of detrital and igneous zircons from the Águilas Arc in the Internal Betics (SE Spain): implications for Carboniferous-Permian paleogeography of Pangea" present a large, solid dataset of detrital zircon ages that improves greately the understanding of the controversial paleogeography of the Betic chain in southern Iberia. According to the data presented, the interpretations are solid and properly constructed and discussed (some minor comments in the annotated PDF). The conclusions are innovative and to some extent provoking. The correlation, aided with paleontological criteria, with the Cantabrian zone in northern Iberia sets new constraints not only to the understanding of the Variscan evolution of Western Europe, but also to the complex Mesozoic tertiary evolution of the western Thethyan-Mediterranean realms.

In my opinion, this paper is highly recommended for publication in GR as minor aspects (i.e. duplication of information in the text and figures) are taken into account. All my suggestions can be found in the attached annotated PDF.”

Gabriel Gutiérrez-Alonso

General questions:

First page, no numbering: “This link does not work....”

The Reviewer G. Gutiérrez Alonso refers to the link to the Mendeley datasets. We have improved the link, and also uploaded all Supplementary Material in the submitted revision, using the item category 'e-component'.

Line 1- “Although we all have sometime used the word "zircons" in English it is not correct. Zircon has no plural, it is like bread, you do not buy two "breads", but to bread loafs for example. Use either zircon grains or zircon crystals throughout the whole text.”

Reviewer #1 is correct, and we have revised the ms so that “zircons” are now referred to as “zircon grains”. Thus the title of the manuscript now is: “U-Pb geochronology of detrital and igneous zircon grains from the Águilas Arc in the Internal Betics (SE Spain): implications for Carboniferous-Permian paleogeography of Pangea”.

Line 27- There are not rocks of similar age in the WALZ and the CIZ, so it might not be appropriate to compare those zones with the Betics.

We have deleted the parts of the text that compare our samples with the WALZ and CIZ. The text now reads: “The age distribution patterns for the Carboniferous rocks of the Nevado-Filábride and Alpujárride complexes are similar to those from the Cantabrian Zone of the Iberian Massif” (lines 25 to 27 in the revised manuscript changes not marked).

Line 86- “overriden? subducted implies the existence of oceanic tracts...”

We have changed the text to read:” which was overridden below the Alborán Domain at 18 to 15 Ma…” (lines 90 to 91 in the revised manuscript changes not marked).

Line 107- “sequence? member implies it is part of a formation, if it is describe it beforehand.”

Dr. G. Gutiérrez Alonso is correct and we have deleted the reference to “members” in the description of the lithologies of these rocks. The text now reads:” ....and its succession begins with 600 to 800 m thick graphite-bearing micaschists, quartz schists, and phyllites, which are intercalated with ferruginous quartzite beds (Laborda-López et al., 2015a, b)…” (lines 114 to 116 in the revised manuscript changes not marked).

Line 180- “All this Section could be summarized in Table 1 as it is purely descriptive. See comments in the figure. And provide samples coordinates somewhere!!!”

We have summarized this Section in new Tables 1 and 2, and provided the coordinates of the samples in the new Table 2. As the text in this Section 3 is now reduced to only one sentence, we have combined it with text in the old Section 4.

Line 226- “Supplementary material is not accessible”

We have uploaded all the Supplementary Material in the submitted revision, using the item category 'e-component'.

Lines 243 to 246- “This can be said in the methods”

We have changed this sentence accordingly, and it is now in Section **3. Sampling localities and analytical methods**: in lines 231 to 2346 in the revised manuscript changes not marked.

Lines 263 and 264- “If samples are collected in the Upper Carboniferous (Fig. 4) they should not have Permian zircon grains....

As you have said before the errors are 1sigma. It is quite standard to use 2sigma, which would bring the 284 age error to 10% (28 My) which could fit into the Carboniferous. That makes the data quite difficult to use in order to make any interpretation.”

Dr. G. Gutiérrez-Alonso makes a good point, and the problem originates in the analytical methods section where we stated at lines 235 and 236 that: “Errors used in the calculation are at the 1σ level.” This sentence is confusing as the reader can suppose that the errors within the entire manuscript and in the figures are at the 1σ level. In fact, all data and figure errors are given at the 2σ level, and we have only used 1σ errors during the calculations for the KDE graphics. We have changed the writing in this paragraph, and now it reads (lines 219 to 226 in the revised manuscript changes not marked):

“Ages in the text and figures are quoted as $^{206}Pb/^{238}U$ dates for zircon analysis younger than 1500 Ma and as $^{207}Pb/^{206}Pb$ dates for zircon analysis older than 1500 Ma, while errors are at the 2σ level. Distribution of detrital zircon ages were calculated using DensityPlotter 8.5 (Vermeesch, 2012), with a bin of 40 Ma. An adaptive bandwidth of 40 Ma was applied for the Kernel Density Estimators (KDE); except in the zoom windows from the group of ages younger than c. 541 Ma Ma, where a bin of 10 Ma and an adaptive bandwidth of 10 Ma were applied. Errors used in these KDE calculations are at the 1σ level. (Figs. 5, 6, 9, 10, 13 and 14).”

Dr. G. Gutiérrez-Alonso indicates that the younger zircon age of 284 ± 14 Ma (line 263) is Permian, but as we explain in the next response, we have tried to minimize the risk of using dates from grains with Pb loss using a very conservative calculation for youngest population (see next answer).

Line 264- “is correct here to use mean ages? It is highly dependant on an arbitrary choice of what is the "youngest population"

We have added a paragraph within the new Section 3**. Sampling localities and analytical methods**: lines 235 to 247 in the revised manuscript changes not marked. This new paragraph defines the youngest population in the sense of Dickinson and Gehrels (2009), and justifies our choice of this method to determine the Maximum Depositional Age (MDA) of a sample:

“Among the different strategies to estimate the Maximum Depositional Age (MDA) of a sample, we have chosen a more conservative approach where the youngest population is defined as the weighted mean of the youngest cluster of grains with overlapping 2σ uncertainty (see Dickinson and Gehrels, 2009, for the method, and Sharman and Malkowski; 2020, for a discussion). The original method contemplates the use of three or more grains, however, we have worked with four or more grains in the calculation. Our samples are metadetrital with grains mostly < 400 Ma. The limited curvature of concordia at these young ages combined with the imprecision of the $^{207}Pb/^{235}U$ age, limits the identification of discordance, and, in fact, any level of Pb loss is masked by the uncertainty of the analysis (Bowring and Schmitz, 2003; Ireland and Williams, 2003; Spencer et al., 2016). Therefore, we have tried to minimize the risk of including dates from grains with Pb loss by applying a very conservative youngest population calculation, calculated using Isoplot software (Ludwig, 2003, 2009).”

Line 271- “Statistically, AG-17 is quite different”

Dr. G. Gutiérrez-Alonso is correct and we have changed the text accordingly. The new text reads (lines 281 to 290 in the revised manuscript changes not marked):

“Samples AG-12, AG-14, and AG-18 also have similar age distribution patterns showing a very noticeable Ediacaran component with peak ages between ca. 557 and ca. 618 Ma (between 17.3% and 24.3%, Fig. 5). There are also significant Mesoproterozoic (between 7% and 12%) and Paleoproterozoic (between 17% and 26%) contributions. The Mesoproterozoic population clearly stands out in samples AG-12 and AG-18 with ages clustering at ca. 1001 (7.2%) and 1025 Ma (6.3%), respectively, and the Paleoproterozoic population is clearly identified in sample AG-14 with ages grouping at ca. 1893 and 2032 Ma (13.2%) (Fig. 5). There is a noteworthy difference in sample AG-17; the percentage of Paleozoic ages (36%) in this sample is twice as high as that in the other three samples (15% to 19%) (Fig. 5)."

Line 276- "In order to combine samples, it would be necessary to check their statistical similarity first... (not only by visual inspection of the PDPs or KDEs.

So K-S statistics and/or MDS plots would be very useful to check if the combination of them is significant or not."

Following the suggestion of Dr. G. Gutiérrez-Alonso, we have used the Kolmogorov-Smirnov test (K-S test) and the Multi-Dimensional Scaling methods (MDS) to check the statistical similarity between samples. In order to avoid over-lengthening the revised manuscript, we have added the methodology and results of the K-S test to the Supplementary material, and left only the MDS method in the main manuscript.

When observing the results of both tests, we found that Reviewer#1 is correct and we now only combine samples AG-12, AG-14 and AG-18 from the Lomo de Bas quartzites, and we have changed the text and figures to specify use of that sample combination.

Line 276- "What means nearly? state the concordance percentage used to filter the data."

We have stated the concordance percentage used to filter the data: in the lines 291 and 292 in the revised manuscript changes not marked: "(Concordia ranging between 90% and 110%, Table S1 in Supplementary material)".

Lines 278 to 280- "This is repeated in the pie charts in Figure 9, so it is not necessary to include here (tedious to read)"

We have deleted this sentence, and other similar sentences within **Section 4. Results**.

Line 281- "this means 2 grains... and if the errors are as large as the permian zircon described before.... they are of no use at all."

We agree with Dr. G. Gutiérrez-Alonso, but we have to include them in the description of the results, if not in the interpretation.

UNIVERSIDAD DE GRANADA

Lines 291 to 292- “You say before the youngest is Jurassic”

We have slightly changed these sentences in order to make clear the differences between the age of the youngest zircon grain, and the age of the youngest zircon population. They read now in lines 305 to 309 in the revised manuscript changes not marked: “Individually, samples AG-1 and AG-2 contain Jurassic zircon grains with the youngest zircon grains yielding $^{206}Pb/^{238}U$ dates of 195 ± 8 Ma, and 179 ± 5 Ma, respectively. Both samples also have youngest zircon populations with Permian ages at 275 ± 8 Ma (MSWD = 1.4 and probability = 0.25) and 277 ± 4 Ma (MSWD = 1.12 and probability = 0.35), respectively.”

Line 301- PDD or KDE?

We have stated now that it is a KDE age distribution at line 317 in the revised manuscript changes not marked.

Line 302- Already included in the figure

This is similar to comment on Lines 278 to 280, and we have deleted this sentence.

Line 318- Do they provide a concordia age? If so... that age might be significant

As we have stated previously in the answer to the annotation at Line 264, a problem within the younger-than-400-Ma zircon grains is that the limited curvature of concordia, combined with the imprecision of the $^{207}Pb/^{235}U$ age, limits the identification of discordance, and, in fact, any level of Pb loss is masked by the uncertainty of the analysis (Bowring and Schmitz, 2003; Ireland and Williams, 2003; Spencer et al., 2016). Therefore, we can have perfectly concordant ages with any level of Pb loss in those young zircon grains. A method to determine if Pb loss that is undetectable with a discordance filter is occurring is to note the presence of a tail negatively skewed towards younger ages (see Spencer et al., 2016).

To clarify this problem, we have changed this sentence, and now it reads (lines 335 to 337 in the revised manuscript changes not marked): “There are also 7 slightly younger dates between 264 and 286 Ma defining a tail negatively skewed towards younger ages (Fig. 7), which may relate to Pb loss undetectable with a discordance filter (see Spencer et al., 2016).”

Line 326- which one?

The only known event at this age is the intrusion of Early Jurassic mafic rocks (Puga et al., 2011). Therefore, we have changed the sentence and now it reads (line 346 in the revised manuscript changes not marked): "…linked to the intrusion of Early Jurassic mafic rocks (Puga et al., 2011)."

Line 340- Why not a concordia age?

The Concordia age is within uncertainty of the mean age (287.3 ± 3.4 Ma). The MSWD of the Concordia age is around 13 while the 207 corrected mean age is down to 1.4 and that is why we used the weighted mean.

Line 367- Same as above

Reviewer#1 refers to the comment at Line 276- "In order to combine samples, it would be necessary to check their statistical similarity first... (not only by visual inspection of the PDPs or KDEs. So K-S statistics and/or MDS plots would be very useful to check if the combination of them is significant or not."

We have performed the Kolmogorov-Smirnov test (K-S test) and added its methodology and results in the Supplementary material (Texts S1 and S2, Tables S2 and S3). We have added a last sentence in the Section 3. **Sampling localities and analytical methods**: "Methodology and results of the Kolmogorov-Smirnov test are given in the Supplementary material (Texts S1 and S2, Tables S2 and S3)."

Furthermore, we have added a reference to the K-S test in Table S2 in the Supplementary material, where the values of the similarity are recorded (lines 373 and 375 in the revised manuscript changes not marked): "The age distribution patterns of these 4 aforementioned samples show some similarities (Fig. 9, and see Kolmogorov-Smirnov test-S in table S2 in the Supplementary material).

Line 434-Mean age or concordia age?

As for sample AG-13, we have choosen the mean age and not the Concordia age because of the lower MSWD (0.76 versus 1.9). Both ages are within uncertainty. The Concordia age is 282.3 ± 1.9 Ma.

Line 493- In general the discussion is quite tedious and difficult to follow. The comparisons made based in estimated relative abundances, number of grains and percentages is too complicated to really appreciate the differences. New statistical tools to make this comparisons based in K-S statistics are nowadays available and provide efficient quantitative comparison tools. The use of this tools (MDS) would be of great benefit and help in understanding and following this discussion. (e.g. Vermeesch, P. (2018). Dissimilarity measures in detrital geochronology. Earth-Science Reviews, 178, 310-321.

We thank Dr. G. Gutiérrez-Alonso for this suggestion, which have improved the discussion. We have reduced the comparison between estimated relative abundances and used the Multi-Dimensional Scaling method (MDS) to make a comparison between samples. We have also added the similarity values of the comparison obtained using the K-S test in the Supplementary material.

Dr. G. Gutiérrez-Alonso makes a good point…the old comparisons were too complicated to really appreciate the differences. When we have applied the K-S and MDS methods, the similarity between the Maláguide Complex and Ossa-Morena Zone is no longer supported. The values of the tests indicate that the MC samples are more similar to the samples of NE Iberia and South France. We have changed accordingly the paleogeographic location of the Maláguide realm during the Late Carboniferous in new Figure 16 and in the graphical abstract.

Line 500- Check criteria according to: https://doi.org/10.1016/j.earscirev.2020.103109

In the methodology and discussion, we have added a definition of youngest population and a justification for why we have used it (see answer to comment in Line 264). Specifically, in the beginning of the discussion, we have added in lines 535 to 537 in the revised manuscript changes not marked: “As previously stated, we also provide the youngest populations (see Dickinson and Gehrels, 2009 for the method, and Sharman and Malkowski; 2020 for a discussion).”

Line 521- What criteria is used to discern populations vs. single zircon grains usage. Please explain

Please see our response to the comment at lines 264 and 500.

Line 531- including the variscan remnants in the Betics (Reference to the paper with granite ages)

We have included a reference to the works on the Variscan remnants in the Betics in lines 580 to 582 in the revised manuscript changes not marked: “Furthermore, they could have been sourced from the oldest granitoids within the Variscan remnants in the Betic Chain, essentially the older orthogneisses in the NFC with U-Pb ages of ca. 301 Ma (Gómez-Pugnaire et al., 2004, 2012).”

Line 536-They are also found in Carboniferous rocks from the Cantabrian Zone, see Pastor-Galán et al. 2013 (Gond Res) where the sources are explored. Ordovician zircons may come from the Ollo de Sapo magmatic event, and devonian from the volcanic event that is now starting to be recognized in the Central Iberian Zone (Gutiérrez-Alonso, G., Murphy, J. B., Fernández-Suárez, J., & Hamilton, M. A. (2008). Rifting along the northern Gondwana margin and the evolution of the Rheic Ocean: A Devonian age for the El Castillo volcanic rocks (Salamanca, Central Iberian Zone) . Tectonophysics, 461(1-4), 157-165.) (or in Almadén, sorry, no ref) or from the allochthonous complexes where rocks with silurian and devonian zircons are relatively abundant.

Dr. G. Gutiérrez-Alonso is correct and we have changed the text of the first paragraph in **subSection 5.2. Provenance of zircon in Late Carboniferous samples**, to include those sources.

Line 550- See above

We have deleted this paragraph.

Line 588- It would be necessary also to compare with the data from the Pyrenees (Martínez et al., 2015, GSA Bull, doi: 10.1130/B31316.1)

The reference for this work is Martínez et al. (2016). We have processed their data and compared it to the other Late Carboniferous samples from the Betic Cordillera and the Iberian Massif in a new paragraph in **subSection 5.2. Provenance of zircon in Late Carboniferous samples** (lines 573 to 703 in the revised manuscript changes not marked).

UNIVERSIDAD DE GRANADA

Line 595- Reference

We have added a reference to this statement at line 620 in the revised manuscript changes not marked: "(Jabaloy-Sánchez et al., 2018)"

Line 635- See above

This is similar to the comments at line 536 and line 550, and we have deleted this statement.

Line 805- I would add another line of correlation using the ages of the intrusive rocks reported here and in other previous work. The Permian ages of the intrusives (which are volumetrically minor) are similar to those granites in the CZ, while the WALZ and the CIZ the granite ages are, in general older and the granites significantly more abundant)

Thanks for this suggestion. We have added several sentences at the end of the discussion (lines 864 to 870) in the revised manuscript changes not marked: "Another line of correlation is the age of the felsic intrusive rocks reported here and in previous works (Gómez-Pugnaire et al., 2014; 2012). The Permian age of the volumetrically minor intrusive bodies (301 to 282 Ma, Gómez-Pugnaire et al., 2004, 2012; this work) is similar to granites in the CZ (286 to 297 Ma; Gutiérrez-Alonso et al., 2011), while the significantly more abundant granites in the WALZ and the CIZ are, in general, older (321 to 290 Ma, Martins et al., 2019, and references therein)."

Figure 2- Location (white dot) of Granada is missing

We have added the location of Granada and deleted the two red rectangles in old Figs. 6 and 7.

Figure 3-Make the dots and sample numbers more prominent and provide coordinates of the collected samples in Table 1.

We have made the dots and sample numbers bigger, and also added the coordinates in Table 2.

Figs. 4, 5 and 8- Provide a legend with the lithological symbols, there is plenty of space and the chosen patterns are quite confusing. Same for Fig. 5 and Fig. 8

Figures 4, 5 and 8 could be combined into a single figure (landscape) where it is easier to see the similarities and differences in the different domains

We have provided a legend with the lithological symbols and combined the old Figs. 4, 5 and 8 into a new Figure 4.

Figs 6 and 7 -Is this figure necessary? Same for Fig. 7. Local maps do not provide information regarding detrital zircon ages. They are useful for structural or tectonic purposes, but this paper does not deal with any local geology.

We have deleted the old Figs. 6 and 7.

Table 1- Include number of zircon grains used.

Include in the table the age of the sample (or at least, its putative age)

We have included the putative age of the samples and the Total number of analyses/Conc. Analyses in the new Table 2.

We have also followed the minor suggestions marked in the PDF file by Reviewer #1 including the comments on Figures 1, 2 and 4 that we have changed accordingly.

UNIVERSIDAD DE GRANADA

Reviewer #2 comments: Manuscript Number: GR-D-20-00209

Reviewer #2: This study by Jabaloy-Sánchez and co-authors on U-Pb geochronology in metamorphosed siliciclastic and igneous rocks from the Betic Chains is of relevant scientific interest.

The objective of this study and the volume of U-Pb zircon data and its quality is a very strong point of this contribution.

However, I noticed several weak points that deserve to be corrected and improved. The first concerns some inaccuracies found in the Geological setting (see attached pdf with my annotations). This Section is very long and confusing and it is advisable to present a table with the lithostratigraphy of the three metamorphic complexes. Many references are missing on the ages of the different units.

We have corrected the inaccuracies found in the Geological setting, shortened it and added a new Table 1 with the lihostratigraphic units of the three tectonic complexes. We have added references to the age of the different units when they are known.

The second weak point concerns the presentation of results. This presentation is confusing, lacking age ranges and/or percentages of the main age groups for each sample. The model of presentation of the results that is used for one sample must be kept for the others to facilitate the understanding by the reader.

We have rewritten the presentation of the results, adding age ranges and /or percentages of the main age groups.

Finally, the Discussion and the Conclusions can be improved (see attached pdf with my annotations). Some statements regarding works by other authors are incorrect. The figures are too many and some of them can be merged.

We have rewritten the Discussion and Conclusions, deleted four figures, and revised the statements referred to works from other authors.

I believe that the authors are able to improve this version to make it more interesting for the readers.

Annotations in the pdf:

Line 40- detrital zircon grains

We have added the correction to lines 40 and 41 in the revised manuscript changes not marked: "...corresponding to a mixing of detrital zircon grains".

Lines 68, 69, 72, 74, 75, 77, 86, 89- time-constraints are necessary...

We have added the known constraint ages to the text at lines 70 to 96 in the revised manuscript changes not marked: "The Alpine Betic-Rif orogen is an arcuate Alpine mountain belt outcropping in both South Spain and North Morocco and formed essentially during Late Paleogene-Neogene times (e.g. Platt et al., 2003; Chaluan et al., 2008) (Fig. 1). According to Balanyá and García-Dueñas (1987), this belt comprises: i) a central allochthonous terrain, the so-called Alborán Domain, ii) the South Iberian Domain, which includes the Triassic to Neogene rocks deposited at the southern paleomargin of the Iberian Peninsula, iii) the North African Domain, comprising Triassic to Neogene rocks deposited at the north-western paleomargin of Africa, and iv) the Flysch Trough units with Cretaceous to Neogene slope/rise and abyssal plain deposits (e.g. Chalouan et al., 2008, and references therein). Furthermore, the Alborán Domain, as originally defined by Balanyá and García-Dueñas (1987), included three metamorphic complexes, namely (from bottom to top): the Paleozoic to Mesozoic Nevado-Filábride Complex (NFC), the Paleozoic to Mesozoic Alpujárride Complex (AC) and the Paleozoic to Paleogene Maláguide Complex (MC) (Fig. 1).

Recently this subdivision has been redefined and a new tectonic framework with only three major domains is emerging. Pratt et al. (2015) and Azdimousa et al. (2019) have indicated that the whole Maghrebian Flysch Domain was part of the North African Domain. Moreover, the Alborán Domain has been redefined and now only comprises two tectonic complexes: the lower AC and the upper MC (see Gómez-Pugnaire et al., 2012, and references therein). Accordingly, the NFC is now considered part of the southern paleomargin of the Iberian Peninsula, which was overridden below the Alborán Domain at 18 to 15 Ma (see López-Sánchez Vizcaino et al., 2001; Gómez-Pugnaire et al., 2004; 2012; Platt et al., 2006; Kirchner et al., 2016).

In the Central part of the Betic-Chain, the previously mentioned metamorphic complexes were deformed by three major E-W trending Tortonian antiforms, but eastwards, left-lateral, roughly N-S trending strike-slip faults rotated and translated the folds towards the North to form the Águilas tectonic Arc (Figs. 1, 2)."

Line 93- Will be useful to present a table with the different units from each complex and available ages...

Figs 4, 5 and 8 can be merged

We have made a new Table 1 with the different units from each complex, and also merged the old Figs. 4, 5 and 8 into a new Fig. 4

Line 105- age?

The age of these rocks was unknown before we did the first datation of them, although other orthogneisses in the CNF have yielded Late Carboniferous-Early Permian ages. We have accordingly changed the sentence to read (lines 109 to 113 in the revised manuscript changes not marked): "…rocks include orthogneiss bodies derived from metamorphosed, felsic rocks of unknown age (Álvarez and Aldaya, 1985; Álvarez, 1987), although other orthogneiss bodies within the CNF have yielded Late Carboniferous to Early Permian U-Pb ages (Gómez-Pugnaire et al., 2004, 2012, and references therein)."

Line 118- age?

This comment refers to the age of the Metaevaporite Fm, for which different authors have proposed ages ranging from Permian to Paleogene. We have changed the sentence and now it reads (lines 124 and 125 in the revised manuscript changes not marked): "Moving up section is the Metaevaporite Fm, attributed Permian-Triassic (Leine, 1968; Vissers, 1981) to Paleogene ages (Puga et al., 1996),…"

Line 119- ages?

As outlined above, this comment refers to the age of the Marbles and Calc-Schists Fms, for which different authors have proposed ages varying from Paleozoic to Cretaceous. We have changed the sentence and now it reads (lines 127 and 129 in the revised manuscript changes not marked): "for which pre-Permian to Cretaceous ages have been proposed (Tendero et al., 1993; Gómez-Pugnaire et al., 2012) (Fig. 4, Table 1)."

UNIVERSIDAD DE GRANADA

Lines 181 to 183- or 21??? 8+9+2+2

Thank you for catching this error. The correct total is 21. We have corrected this error at the beginning of **Section 3. Sampling localities and analytical methods**, in line 197 in the revised manuscript changes not marked.

Lines 185 to 211- this information (lines 185-211) could be included in table 1

This comment agrees with Reviewer#1, we have deleted these three paragraphs and included this information in the new Table2 and new Figure 4

Line 234- he group of ages younger than c. 541 Ma

We have changed the sentence and now it reads (lines 223 and 224 in the revised manuscript changes not marked): "…except in the zoom windows of the group of ages younger than c. 541 Ma,"

Line 240- zircon grains

Changed.

Lines 268, 269, 272, 386 to 388, and also lines 479 to 480- %?

We have added the percentages of the components in the description.

Line 277- ???, and Lines 278 to 283- age range for all age groups?

After the suggestion of Reviewer#1, we have changed this paragraph. We have also added the range of ages for all groups. The paragraph now reads (lines 291 to 299 in the revised manuscript changes not marked): "Combining a total of 406 dates (Concordia ranging between 90% and 110%, Table S1 in Supplementary material) obtained from the most similar samples (AG12, AG14 and AG18 of Lomo de Bas quartzites; see Kolmogorov-Smirnov test-S in table S2 in the Supplementary material), the age distribution pattern is characterised by dates ranging from 283 to 3195 Ma (Fig. 5). Within the 67 Paleozoic zircon grains, there are Early Permian (one grain, 283 ± 14, 1.5% with respect to the total amount of Paleozoic grains), Carboniferous (306 ± 4 to 359 ± 8 Ma, 40%), Devonian (368 ± 6 to 405 ± 6 Ma, 9%), Silurian (442 ± 10 Ma, 1.5%), Ordovician (460 ± 12 to 484 ± 8 Ma, 9%) and Cambrian dates (486 ± 7 to 540 ± 7 Ma, 39%) (Fig. 5)."

Lines 302 to 307, 367 to 374, 391 to 393, 396 to 401, 408 to 413, 449 to 451, and also lines 456 to 459- age range for all age groups?

We have added the range of ages from all groups.

Lines 481 to 491-This is not the best way to present the results ... there are no age ranges or percentages ...

Reviewer#2 is correct, and we have added the age ranges and percentages in this paragraph.

Line 497- zircon grains

We have changed the word zircons to zircon grains

Line 497- How many?.

We have rewritten the sentence and now it reads (line 536 in the revised manuscript changes not marked): "…with 4 dates between 284 ± 14 and 323 ± 5 Ma"

Lines 497 and 498, and also lines 499 to 505, 519 to 521- what is the difference between youngest grains and youngest population??? do you mean youngest individual grains?

Lines 499 to 505- you must explain this better...

Reviewer G. Gutiérrez-Alonso also had the same query. We have added a paragraph to explain the difference between the youngest grains and youngest population, and why we have used the latter method. In addition, we have added a sentence in the first paragraph in subsection 5.1. (lines 536 to 538 in the revised manuscript changes not marked): "As previously stated, we also provide the youngest populations (see Dickinson and Gehrels, 2009, for the method, and Sharman and Malkowski; 2020, for a discussion).

Line 506- ????

We have deleted the beginning of this sentence.

UNIVERSIDAD DE GRANADA

Line 5010- Are you considering these orthogneisses as volcanic or plutonic protoliths??? they represent volcanism coeval with deposition or they are intrusive plutons post-deposition?

We have rewritten this second paragraph in subsection 5.1. (lines 548 to 556 in the revised manuscript changes not marked). In this paragraph we discuss how, regardless of whether the orthogneisses is of volcanic or plutonic origin, it is located in the uppermost part of the succession and can help to constrain the depositional age of the rocks: "…are strongly deformed and metamorphosed, making it difficult to determine whether they represent volcanic rocks or intrusive plutons. However, in either case, these units can help define the minimum depositional age of the Lomo de Bas rocks, as they are located in the uppermost part of the succession (see Fig. 4). If they are volcanic rocks coeval with deposition, they indicate the age of the uppermost layers, and if they are plutons which were intruded post-deposition, they constrain the minimum depositional age of the Lomo de Bas rocks."

Lines 524 and 525- in this case you are not preferring a more conservative approach, why?

We do not understand this question, as in this sentence we are using the youngest population of sample AG-5 with a Late Carboniferous age (308 Ma) to determine the Maximum Depositional Age (MDA) as we did with the rest of the samples.

Line 529- %???

We added the percentages at lines 576 and 577 in the revised manuscript changes not marked.

Line 530- Why only felsic rocks??? there also zircon grains in gabbro-dioritic rocks; see Pereira et al 2017- Geologica Acta; Orejana et al., 2020- Geoscience Frontiers

We have corrected this statement and now it reads igneous rocks (line 578 in the revised manuscript changes not marked).

Line 531-could you be more specific???

We have described the sources at lines 578 to 583 in the revised manuscript changes not marked: "…occupying more than one third of the outcrops of the whole Iberian Massif, and essentially, ca. one half of the Central Iberian Zone (e.g. Arranz and Lago, 2004; Bea, 2004; Casquet and Galindo, 2004; Gallastegui et al., 2004; Ribeiro et al., 2019). Furthermore, they could have been sourced from the oldest granitoids within the Variscan remnants in the Betic Chain, essentially the older orthogneisses in the NFC with U-Pb ages of ca. 301 Ma (Gómez-Pugnaire et al., 2004, 2012)."

Line 534-%?

We have added the percentages of the components in the description.

Line 535-This is not correct... there are important Ordovician (see Montero et al., 2008. Geological Magazine; Rubio-Ordonez et al. 2012. Geological Magazine; Pereira et al., 2018. Journal of Iberian Geology) and also Devonian magmatism in the CIZ (Gutierrez-Alonso et al., 2008- Tectonophysics)

Line 538- of what??

Line 540- You must be cation with this kind of statement because you can have sources of Devonian grains that derived from primary sources and/or from intermediate sediment repositories (as result of several cycles of recycling)...

We have rewritten the whole **subsection 5.2 Provenance of zircon in Late Carboniferous samples**, in order to the comment of both reviewers. This rewriting included: correction of inaccuracies, adding the suggested references, reordering the paragraphs within the text, and adding the suggested MDS plots and results. The later included adding new Figures 15 and 17, while the old figures comparing the KDEs (old Figures 19 and 21) are now in the Supplementary material as Figures S5 and S6. The results of the K-S test and MDS study demonstrated that we were wrong when we proposed the similarity of the Maláguide Complex and the Ossa-Morena Zone. We have corrected this, and changed our interpretation accordingly in new Figure 16 (paleogeography during the Late Carboniferous), and in the Graphical abstract.

Line 554- which rocks??? too vague..

This paragraph has been deleted.

Lines 558 to 561, and 565 to 566- %????

We have added the percentages of the components in the text.

Line 562- these sources for Neoproterozoic grains are also present in the Meguma and West Avalonia terranes (Nova Scotia)

We have added to the text at lines 607 and 608 in the revised manuscript changes not marked: "…in Gondwana and the peri-Gondwanan terranes, as in the Meguma and West Avalonia terranes in Gondwana and the peri-Gondwanan terranes, like the Meguma and West Avalonia terranes."

Line 590- ???

We have added to the text in lines 614 to 616 in the revised manuscript changes not marked: "…and surrounding areas, as the Pyrenees, Montagne Noire and Mouthoumet massifs (Martínez et al., 2016) (Fig. S5 in the Supplementary material)."

Line 605 and 606- delete

We have deleted the references.

Lines 612 to 617- These works on the Late Carboniferous basins of the Ossa-Morena and South-Portuguese zones do not show what is mentioned here ... I advise you to reread the text of these publications more carefully ...

We have rewritten the whole paragraph. It now reads in lines 656 to 671 in the revised manuscript changes not marked: "Dinis et al. (2018) and Pereira et al. (in press) studied the Late Carboniferous sediments from the Ossa-Morena (Santa Susana Fm: samples StSz2 and StSz4 from Dinis et al., 2018, and SS-1 and SS-2 from Pereira et al., in press). In the MDS plot, they do not show any similarity with the samples from NFC, AC or the Cantabrian Zone, except in the case of the comparison between AG-17 and SS-2 and StSz4 samples. The Santa Susana Fm samples plot far from the other two clusters on the MDS diagram. (Fig. 15). The main difference is the lack of the Stenian and Neoarchean populations in the latter samples. Furthermore, Pereira et al. (2014) studied the South Portuguese Zone of the Iberian Massif (Fig. S5 in Supplementary material), where Late Carboniferous sediments were deposited in the Mira Fm

(Serpukhovian-Bashkirian, samples ST-8 and SC-6 from Pereira et al., 2014) and in the Brejeira Fm (Bashkirian-Moscovian, samples AJ-1, AM-3, and TH-5 from Pereira et al., 2014). Samples from both the Mira and Brejeira Fms essentially show no similarity with the samples from the NFC, AC and Cantabrian Zone in the MDS plot, although the AM-3, and TH-5 samples show some similarity with the cluster from sample AG-17 and those from NE Iberian Peninsula and South France (Martinez et al., 2016) (Fig. 15)."

Lines 672, 694, 709, and 723 - I suggest to merge Sections 6.3-6.5

We have merged them into the new **Section 5.3. Permian to Triassic samples from the NFC, AC and MC.**

Line 731- It would be very interesting to discuss what tectonic processes will have induced these differences ... would it have been tectonic movements that conditioned the exposure to erosion of different blocks?

In order to discuss the processes after the unroofing of the Late Variscan granitoids, we have added a last paragraph (lines 821 to 829 in the revised manuscript changes not marked): "A major question is what tectonic process induced these differences. Vissers (1992) found an Upper Carboniferous to Permian extensional event in the Pyrenees synchronous with uplift and emergence of large parts of the crust and deposition of continental sediments in fault-bounded extensional half-grabens. Subsequently, García-Navarro and Fernández (2004) found an Early Permian faulting event in the SW Iberian Peninsula where strike-slip and normal faults generated the intracontinental, Early Permian El Viar basin. Those data suggest that during the Permian to Early Triassic breakup of Pangea, tectonic uplift along major normal faults may have exposed different levels of Variscan crust, including the Late-Variscan granitoids, to erosion."

Lines 733 and 735- age range???

We have added the age ranges in the text.

Line 777- ages???

We have added the ages in the text.

Line 780- ?????

We have rewritten the sentence and now it reads (lines 836 to 839 in the revised manuscript changes not marked): "…confirming that after experiencing HP metamorphism during Oligocene-Early Miocene times (Zindler et al., 1983; Blichert-Toft et al., 1999; Sánchez-Rodriguez and Gebauer, 2000; Platt et al., 2003; Esteban et al., 2007), the AC rocks were exhumated and eroded at the surface during the Middle Miocene."

Line 781- which ones??

We have changed the sentence and it now reads (lines 839 and 840 in the revised manuscript changes not marked): "It is noteworthy that these unconformable Middle Miocene sediments were formed …"

Line 792- age???

We have added the age of the late Variscan event in lines 850 and 851 in the revised manuscript changes not marked: "…by the Late Carboniferous-Early Permian Late Variscan magmatic event"

Line 792- When???

We have added the age of the metamorphism in lines 852 and 853 in the revised manuscript changes not marked: "…was metamorphosed from Oligocene to Middle Miocene times to form…"

Line 805- ????

We have changed Line 865 in the revised manuscript changes not marked: "… partially melt, leading to the formation of migmatites."

Line 809-...Ma ???

you must explain if these igneous rocks represent volcanic rocks contemporaneous with deposition or post-deposition intrusive rocks...

We have changed this sentence, and now it reads (lines 875 to 878 in the revised manuscript changes not marked): "Orthogneisses in the NFC may have volcanic or plutonic parent rocks, but as they are located in the uppermost part of the Lomo de Bas succession, they can indicate a minimum depositional age for these rocks (Sakmarian-Artinskian, 294 ± 2 Ma and 289 ± 3 Ma), regardless of their igneous classification."

Lines 827 to 829- How do you explain this difference???

We have modified the text to explain the difference. Lines 899 to 901 in the revised manuscript changes not marked reads: "This data can be explained if zircon grains from the main Variscan orogenic relief were recycled, while unroofing of footwalls of faults also exposed Late Variscan granitoids at the surface. It is possible that these zircon grains …"

Line 833- why felsic rocks???

Because there are Jurassic mafic rocks in the area that are not the source of zircon grains.

Figure 3- difficult to read

We have changed the size of the text and dots in Figure 3.

Figure 5- schists

We have changed the word in the new Figure 4.

Figure 6 and 7-these basaltic dikes are from the Alpujarride Complex? or they are intrusions on the Piar Group??? and thus belong to the Malaguide Complex???

We have deleted these figures according to Reviewer#1. However, these basalt dikes intruded in both complexes during Paleogene-Early Neogene times.

Figures 9, 10, 13, 14, 17 and 18-difficult to read

???

We have changed all the pies with the percentages of the zircon data in old Figures 9, 10, 13, 14, 17 and 18: we have changed their sizes and their colours in order to make them easier to read. We have also deleted mention of 0 to 541 Ma in all the figures.

Figure 10- this one is concordant??

UNIVERSIDAD DE GRANADA

Yes, it is. It corresponds to Analysis AG13z6c (see table S1 in the Supplementary material)

Ages						Concordia
207Pb/206Pb	1σ	207Pb/235U	1σ	206Pb/238U	1σ	
2346	13	2274	13	2196	23	97

Figure 15- ???

We have changed maximum, for population at ca. 16 Ma in the new Figure 11.

Figure 16-???

We have changed main population, for population at ca. 283 Ma in the new Figure 12.

Table 1- geographic coordinates???

We have added the coordinates in the new Table 2.

We have also followed the minor questions marked in the PDF file by the Reviewer#2 and changed them accordingly.

Yours sincerely,

Antonio Jabaloy Sánchez
Corresponding Author

Graphical Abstract

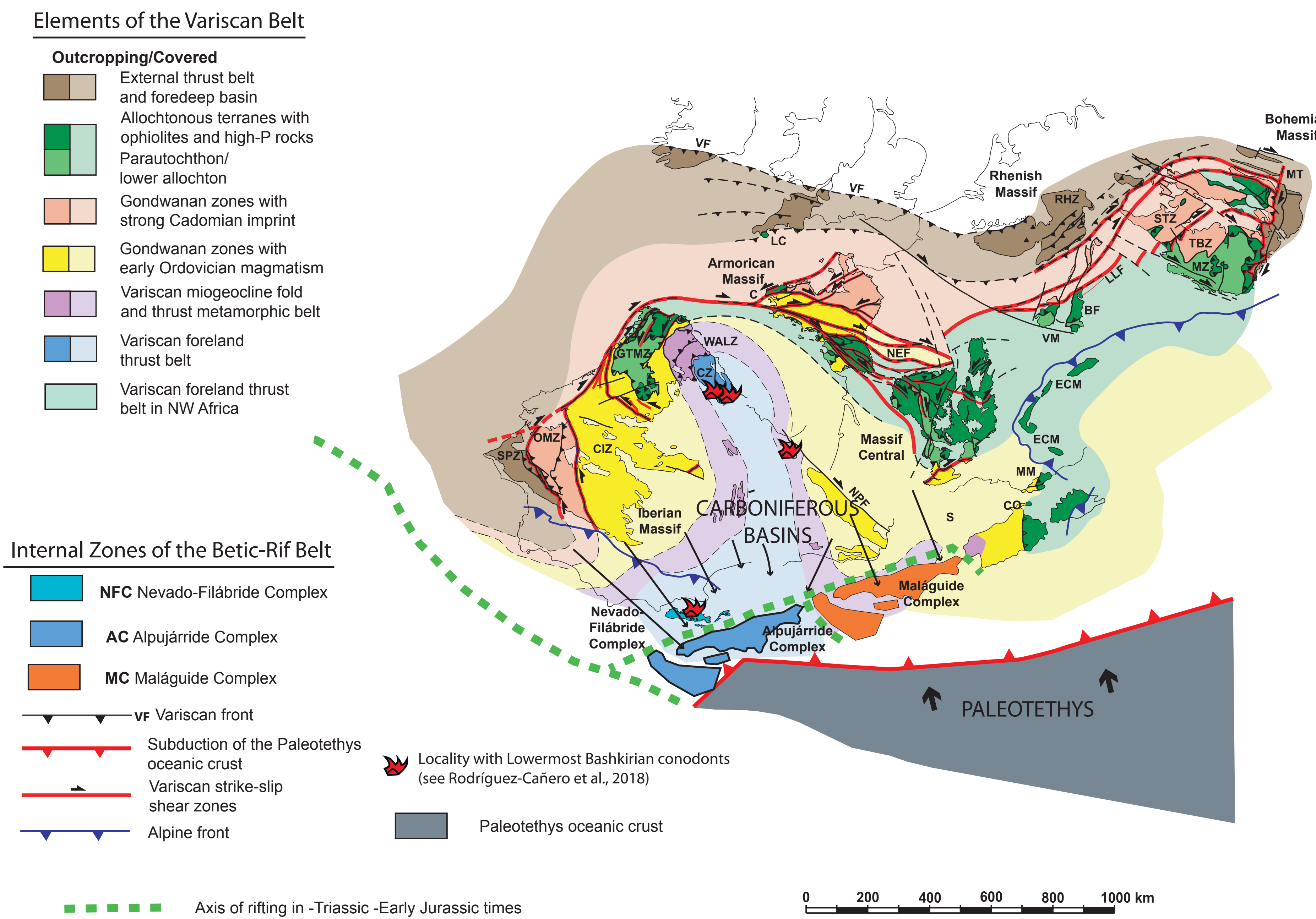

Maximum depositional ages of graphite rich rocks of the Nevado-Filábride and Alpujárride complexes are Late Carboniferous

Graphite-rich rocks of the Nevado-Filábride and Alpujárride complexes were likely deposited in Carboniferous foreland basins eastwards of the Iberian Massif

The Maláguide Complex located near the NE Iberian Peninsula

Maximum depositional age of Tahal, Meta-detrital and Saladilla Fms are Early Permian

Manuscript

U-Pb geochronology of detrital and igneous zircons from the Águilas Arc in the Internal Betics (SE Spain): implications for Carboniferous-Permian paleogeography of Pangea

Antonio Jabaloy-Sánchez[1], Cristina Talavera[2], Martín Jesús Rodríguez-Peces[3], Mercedes Vázquez-Vílchez[4], Noreen Joyce Evans[5]

[1]Departamento de Geodinámica, Universidad de Granada, 18002 Granada, Spain.

[2]School of Geosciences, University of Edinburgh, The King's Building, James Hutton Road, EH9 3FE, Edinburgh, UK.

[3]Departamento de Geodinamica, Estratigrafía y Paleontología, Universidad Complutense de Madrid, Madrid, Spain.

[4]Departmento de Didáctica de las Ciencias Experimentales, Universidad de Granada, Granada, Spain.

[5]School of Earth and Planetary Sciences/John de Laeter Center, Curtin University, Bentley 6845, Australia.

Abstract

The Águilas Arc (SE Spain) comprises the three tectonic complexes of the Internal Betic Chain. New U-Pb detrital zircon and U-Pb zircon ages of metaigneous rocks in the Nevado-Filábride Complex provide a Late Carboniferous depositional age for the Lomo de Bas schists and quartzites, while the maximum depositional age of the Tahal Fm is confirmed as Permian-Triassic. In the Alpujárride Complex, the maximum depositional age of the Micaschists and Quartzite Fm is Late Carboniferous and the Meta-detrital Fm was deposited in the Early Permian. Furthermore, the maximum depositional age of the Saladilla Fm in the Maláguide Complex is also Early Permian. The age distribution patterns for the Carboniferous rocks of the Nevado-Filábride and Alpujárride complexes are similar to those from the Cantabrian, West Asturian-Leonese, and Central-Iberian zones of the Iberian Massif, suggesting deposition in

Carboniferous foreland basins located eastwards of the Iberian Massif. However, the zircon age distribution patterns for the Nevado-Filábride and Alpujárride complexes show differences to those of the Carboniferous rocks from the Maláguide Complex, and the South Portuguese and Ossa-Morena zones of the Iberian Massif, while patterns in Maláguide and Ossa-Morena samples show some similarities. Thus, the paleogeographic location of the Maláguide Complex seems different from that of the Nevado-Filábride and Alpujárride complexes, and it was probably located near the Ossa-Morena Zone.

The samples with Early Permian maximum depositional ages from the three complexes contain more Paleozoic zircons relative to the older Carboniferous samples, but have similar age distribution patterns, suggesting that they were deposited in the same basin. Samples from unconformable Middle Miocene sediments have Early Permian youngest zircon populations and age distribution patterns corresponding to a mixing of zircons from the Alpujárride and Maláguide complexes. Furthermore, there is no record of any major felsic rocks formation event after the Early Permian in those two complexes.

1. Introduction

The Variscan-Alleghanian belt (i.e. Martínez Catalán et al., 1997; Matte, 2001; Simancas, 2019) was formed during the Late Paleozoic collision of two major continents: Laurussia (Laurentia-Baltica) and Gondwana. The southern front of the Variscan segment of this orogenic belt is poorly understood due to Pangea break-up (e.g. Wilson, 1997; Marzoli et al., 1999) and Alpine reworking (Simancas, 2019). Numerous fragments resulting from Gondwana break-up were dispersed and recycled during the Alpine orogeny, and superposition of metamorphic and deformational Alpine events overprinted most Variscan features.

Several of these fragments are included now within the Internal Zones of the Betic-Rif orogen as tectono-metamorphic complexes. These complexes hold clues to the Variscan and Late-Variscan evolution of the southern domains of the Variscan belt and its relationship with the Gondwanan foreland (i.e. Gómez-Pugnaire et al., 2004, 2012; Sánchez-Navas et al., 2014, 2017; Jabaloy-Sánchez et al., 2018; Rodríguez-Cañero et al., 2018). Zircon U-Pb dating of metamorphosed sedimentary sequences and igneous rocks can provide temporal constraints on this evolution, especially in an area where detrital zircon geochronological data are scarce.

Here, we present U-Pb zircon data from metasedimentary and metaigneous rocks of the Águilas Arc in the eastern Betic Chain, in an effort to provide maximum depositional ages for these rocks, paleogeographic information about the possible sources and, hence, paleolocation of the different tectonic complexes of the Betic-Rif orogenic system. We will then discuss the implication of these data for both the Variscan and Alpine evolution of this orogenic system.

2. Geological setting

The Betic-Rif orogen is an arcuate Alpine mountain belt outcropping in both South Spain and North Morocco (Fig. 1). According to Balanyá and García-Dueñas (1987), this belt comprises: i) a central allochthonous terrain, the so-called Alborán Domain, ii) the South Iberian Domain, which includes the rocks deposited at the southern paleomargin of the Iberian Peninsula, iii) the North African Domain, comprising rocks deposited at the northwestern paleomargin of Africa, and iv) the Flysch Trough units with slope/rise and abyssal plain deposits (e.g. Chalouan et al., 2008, and references therein). Furthermore, the Alborán Domain, as was originally defined by Balanyá and García-Dueñas (1987), included three metamorphic complexes, namely (from bottom to top): the Nevado-Filábride Complex (NFC), the Alpujárride Complex (AC) and the Maláguide Complex (MC) (Fig. 1).

Recently this subdivision has been redefined and a new tectonic frame with only three major domains is emerging. Pratt et al. (2015) and Azdimousa et al. (2019) have indicated that the whole Maghrebian Flysch Domain was part of the North African Domain. Moreover, the Alborán Domain has been redefined and now only comprises two tectonic complexes: the lower AC and the upper MC (see Gómez-Pugnaire et al., 2012, and references therein). Accordingly, the NFC is now considered part of the southern paleomargin of the Iberian Peninsula, which was subducted below the Alborán Domain (Gómez-Pugnaire et al., 2012).

In the Central part of the Betic-Chain, the previously mentioned metamorphic complexes were deformed by three mayor E-W trending antiforms, but eastwards, left-handed, roughly N-S trending strike-slip faults rotated and translated the folds towards the North to form the Águilas tectonic Arc (Figs. 1, 2).

2.1. Nevado-Filábride Complex

The NFC is composed of the upper Mulhacén tectonic units (Puga et al., 2002), which underwent Alpine HP metamorphism at 18-15 Ma (López Sánchez-Vizcaíno et al., 2001; Gómez-Pugnaire et al., 2004, 2012; Platt et al., 2006; Kirchner et al., 2016), and the lower Veleta tectonic units (Gómez-Pugnaire and Franz, 1988; Puga et al., 2002; Rodríguez-Cañero et al., 2018) (Fig. 2).

Within the Águilas tectonic Arc, the lower Veleta units are represented by the Lomo de Bas units (Fig. 3), which are tectonically overlaid by the Mulhacén units (Álvarez and Aldaya, 1985; Álvarez, 1987). The Lomo de Bas units comprise a lower tectonic unit made of ca. 1000 m of alternating graphite-bearing grey and black quartz-schists, garnet and chloritoid-bearing micaschists, and ferruginous quarzitic levels (Laborda-López et al., 2013, 2015a, b) (Fig. 4). These rocks include orthogneiss bodies derived from metamorphosed, acidic volcanic rocks (Álvarez and Aldaya, 1985; Álvarez, 1987). An upper tectonic unit tectonically overlays the lower unit, and its succession begins with a 600 to 800 m thick lower member of fine-grained metamorphic rocks. These are mostly graphite-bearing micaschists, quartz schists, and phyllites, which are intercalated with ferruginous quartzite beds (Laborda-López et al., 2015a, b). These rocks are overlaid by 80 to 140 m thick low-grade black marbles, with abundant fossils of Early-Middle Devonian age (Emsian-Eifelian, c.f. Lafuste and Pavillon, 1976; Laborda-López et al., 2013, 2015a, b). The succession ends with 130 to 500 m thick graphitic schists, phyllites, and quartzites (Laborda-López et al., 2015a, b) (Fig. 4).

In the studied area, the Mulhacén unit succession (Álvarez and Aldaya, 1985; Álvarez, 1987) begins with grey schists and metapsammites of the Permian-Triassic Tahal Fm (Voet, 1967; Jabaloy-Sánchez et al., 2018; Santamaría-López and Sanz de Galdeano, 2018). Moving up section is the Metaevaporite Fm, and marbles, calc-schists, micaschists, and quartzites of the Marbles and Calc-Schists Fms (see Voet, 1967; López Sánchez-Vizcaino et al., 1997) (Fig. 4). The succession includes metabasite bodies.

2.2. Alpujárride Complex

In the studied area, the AC includes a thin lower Miñarros unit, which overlies the brittle-ductile extensional shear zone developed at the NFC/AC contact (Figs. 3 and 5) (Álvarez and Aldaya, 1985; Álvarez, 1987; Booth-Rea et al., 2009). The Miñarros unit has ca. 15 m of thickness and comprises brecciaed ferruginous marbles and white quartzitic mylonites with unknown ages (Álvarez, 1987) (Fig. 5).

Álvarez and Aldaya (1985) and Álvarez (1987) identified several AC tectonic units thrusting over the Miñarros mylonites and breccias (i.e. the Talayón unit, Águilas unit and Las Palomas unit), and Booth-Rea et al. (2009) grouped them into only one tectonic unit, the so-called Las Estancias-Talayón-Palomas unit. Hereafter, and for simplicity, we call it Las Palomas unit. Las Palomas unit has the most complete succession in the area, which begins with ca. 300 m of graphite-bearing micaschists and phyllites alternating with micaceous quartzites from the Micaschists and Quartzite Fm, with a probable Late Paleozoic age (Álvarez and Aldaya, 1985; Álvarez, 1987) (Fig. 5). The succession follows up with ca. 600 m of phyllites and quartzites from the Meta-detrital Fm made of a quartzite-rich lower member and a phyllite-rich upper member with Permian to Middle Triassic ages (Martín-Rojas et al., 2010; García-Tortosa et al., 2012) (Fig. 5). The Middle to Late Triassic Meta-carbonate Fm overlays the previous rocks and is composed of ca. 50 m of marbles and calc-schists (García-Tortosa et al., 2012) with (Fig. 5).

The Ramonete unit crops out above the Las Palomas unit (Figs. 3, 5) (Álvarez and Aldaya, 1985; Álvarez, 1987; Booth-Rea et al., 2009) and contains only Mesozoic rocks: phyllites and quartzites of the Middle Triassic Meta-detrital Fm (see Simon and Visscher, 1983; Maate et al., 1993; García-Tortosa et al., 2002; Martín-Rojas et al., 2010), and calcitic and dolomitic marbles and calcschists from the Middle-Upper Triassic Meta-carbonate Fm (García-Tortosa et al., 2002).

Álvarez and Aldaya (1985), and Álvarez (1987) defined the Cantal unit as an AC tectonic unit thrusting over the Las Palomas unit, or limited by left-handed strike-slip faults (Figs. 3, 5 and 6). However, García-Tortosa et al. (2000) included this unit within the NFC and discussed its adscription to the AC. The Cantal unit is composed of ca. 330 m of migmatitic and felsic gneisses with kyanite and sillimanite bearing schists, graphite bearing schist with staurolite and black marbles and quartzites (see Álvarez and Aldaya, 1985; Álvarez, 1987; Booth-Rea et al., 2009) (Fig. 5).

2.3. Maláguide Complex

The MC occurs as small outcrops on top of the AC (Figs. 3 and 6). Towards the east, in the Vélez Rubio area (Fig. 7), the MC succession includes ca. 1000 m of greywackes, slates, conglomerates and lesser marbles and black cherts of the Ordovician to Carboniferous Piar Group (see Martín-Algarra, 1987) overlain by a detached Mesozoic to Cenozoic cover of ca. 500 m of red conglomerates, sandstones, and pelites, with gypsum of the Middle-Late Triassic Saladilla Fm (Perri et al., 2013) (Fig. 8). The succession follows up with ca. 300 m of Late Triassic to Early Cretaceous limestones, dolostones and marls (Geel, 1973), unconformably overlaid by ca. 200 m of Eocene Nummulite-rich limestones and marls (Geel, 1973) (Fig. 8).

In the Águilas Arc area, this succession is usually incomplete and thinned by normal faults, omitting the thick Paleozoic succession of the Piar Group, (see Aldaya et al., 1991) (Fig. 8). The main outcrops of this complex correspond to the Cabo Cope and Albaida areas (Álvarez and Aldaya, 1985; Álvarez, 1987; García-Tortosa, 2002) (Figs. 3 and 8), with a succession beginning with ca. 40 m of red pelites, sandstones and gypsum of the Middle-Late Triassic Saladilla Fm. Following up section there are ca. 130 m of Late Triassic to Jurassic dolostones, marls, and oolitic limestones (García-Tortosa, 2002, and references therein) (Fig. 8). On top, there is an unconformity overlain by ca. 50 m of Oligocene conglomerates and calcarenites (Durand-Delga et al., 1962; Álvarez, 1987).

Unconformably overlying both the MC and AC, there are Middle Miocene sedimentary rocks with a succession that includes red Langhian-Early Serravallian conglomerates and sandstones with clasts from both complexes (Figs. 3 and 6).

3. Sampling localities

Seventeen samples from the Águilas Arc were studied. Eight samples were collected from the NFC, nine from the AC, two from the MC, and two from the Middle Miocene sedimentary rocks (Table 1).

The samples collected from the NFC were located in both the Lomo de Bas units and in the Mulhacen units. Samples AG-12 and AG-14 come from quartzites of the lower Lomo de Bas unit, while samples AG-17 and AG-18 are from the uppermost quartzite intercalations within the upper Lomo de Bas unit (Fig. 4, Table 1). Samples AG-13 and AG-16 originate from two orthogneiss bodies within this lower tectonic unit (Fig. 4), and samples AG-1 and AG-2 are from two quartzites of the upper part of the Tahal Fm within the Mulhacén tectonic ensemble (Figs. 3 and 4).

Nine samples were collected from the tectonic units of the AC: six samples come from the Las Palomas unit (AG-4, AG-5, AG-6, AG-7, AG-9 and AG-11) (Figs. 3 and 5, Table 1). Samples AG-4 and AG-5 are from quartzites at the base of the Micaschists and Quartzite Fm attributed to the Upper Paleozoic (Álvarez and Aldaya, 1985; Álvarez, 1987) (Fig. 5). Samples AG-6, and AG-7 come from quartzites near the upper levels of the same Micaschists and Quartzite Fm (Fig. 5). Samples AG-9 and AG-11 are from quartzites within the Middle Triassic Meta-detrital Fm of the Las Palomas unit (Martin-Rojas et al., 2010; García Tortosa, 2002) (Fig. 5). Sample AG-15 is from the Middle Triassic Meta-detrital Fm of the Ramonete unit, and sample AG-19 comes from the quartzitic mylonites of the Miñarros unit (Figs. 3 and 5).

Sample AG-26 comes from the Cabezo Blanco orthogneiss body (Fig. 6), within the migmatitic and felsic gneisses with kyanite and sillimanite bearing schists, graphite bearing schist with staurolite and black marbles and quartzites of the Cantal unit (see Álvarez and Aldaya, 1985; Álvarez, 1987; Booth-Rea et al., 2009) (Fig. 5).

Two samples from the Middle-Late Triassic Saladilla Fm of the MC (LP-16-AZ and AG-10) were also collected (Figs. 3 and 7, Table 1). Sample AG-10 is a quartzite from the Cabo Cope area of the Águilas Arc (Fig. 3), and sample LP-16-AZ comes from a quartzite from a lower Maláguide unit of the las Estancias Range near Vélez Rubio (Fig. 7). Two samples (AG-3 and AG-20) were collected from the Middle Miocene red conglomerates and sandstones unconformably covering both the AC and the MC (Fig. 3, Table 1).

4. Analytical methods

Zircon grains were separated using standard heavy-liquid and magnetic techniques in the Department of Geodynamics of the University of Granada. Grains were handpicked and mounted in epoxy, polished, cleaned and gold coated for cathodoluminescence (CL) imaging on a Mira3 FESEM instrument at the John de Laeter Centre (JdLC), Curtin University, Perth, Australia and a Carl Zeiss SIGMA HD VP Field Emission SEM at the School of Geosciences, the University of Edinburgh, Scotland, the United Kingdom. Representative CL images have been selected and interpreted in the results section. In CL images, the lower-U regions are brightly illuminated and higher-U regions are dark, or even black, poorly illuminated regions. U-Th-Pb geochronological analyses of samples AG-16 and AG-26 were carried out on the SHRIMP IIe/mc instrument of the IBERSIMS lab, University of Granada, Spain, and sample AG-13 was analysed on the Cameca IMS1270 at the NERC Ion Micro-

Probe Facility, the University of Edinburgh, United Kingdom (see S1 Supplementary material for a detailed description of the methodologies). Laser ablation inductively coupled plasma mass spectrometry (LA-ICPMS) data collection on the remaining samples was performed at the GeoHistory Facility, JdLC, Curtin University, Perth, Australia. Ages in the text and figures are quoted as $^{206}Pb/^{238}U$ dates for zircons younger than 1500 Ma and as $^{207}Pb/^{206}Pb$ dates for zircons older than 1500 Ma. Distribution of detrital zircon ages were calculated using DensityPlotter 8.5 (Vermeesch, 2012), with a bin of 40 Ma. An adaptive bandwidth of 40 Ma was applied for the Kernel Density Estimators (KDE); except in the zoom windows from 0 to 541 Ma, where a bin of 10 Ma and an adaptive bandwidth of 10 Ma were applied. Errors used in the calculation are at the 1σ level.

5. Results

In this section, we present the distribution histograms and KDE diagrams with the U-Pb results from the detrital zircons of the three different complexes (NFC, AC, and MC). For each complex, we have combined and described the U-Pb data for each formation and/or unit. A synthesis of the analyses and the results is listed in Tables S1 in the Supplementary material. The full description, CL images for representative zircon grains, representative Concordia plots, youngest zircon populations and detailed U-Pb analytical datasets of each individual sample are also provided in the supplementary information (Figs. 1 to 10 in S3 and Table S1in the Supplementary material).

Furthermore, we present the Concordia plots and KDE diagrams with the U-Pb results from the igneous zircon cores and metamorphic rims from the studied orthogneisses. CL images for representative zircon grains, and detailed U-Pb analytical datasets of each individual sample are also provided in the supplementary information (Figs. x 1 to x 10 in S3 and Table S1 in the Supplementary material).

5.1. Nevado-Filábride Complex

5.1.1. LA-ICPMS results from metadetrital samples

The CL images for samples AG-12, AG-14, AG-17 and AG-18 mostly show zircon grains with continuous oscillatory zoning (Fig. 1 in S3 Supplementary material). There are also some composite grains with cores overgrown by low or high U rims and a few grains with sector zoning and grains that are structureless (Fig. 1 in S3 Supplementary material).

Independent of their location within the upper or lower Lomo de Bas tectonic unit, samples AG-12, AG-14, AG-17 and AG-18 yielded similar ages for the youngest zircon analysed, and similar youngest zircon population ages. The youngest zircons have $^{206}Pb/^{238}U$ dates between 284 ± 14 Ma (sample AG-12) and 323 ± 5 Ma (sample AG-18), while the youngest populations show $^{206}Pb/^{238}U$ mean ages between 321 ± 2 Ma (sample AG-17, MSWD = 0.55 and probability = 0.65) and 336 ± 2 Ma (sample AG-14, MSWD = 1.10 and probability = 0.36).

These samples also have similar age distribution patterns showing a very noticeable Ediacaran component with peak ages between ca. 557 and ca. 618 Ma (Fig. 9). There are also significant Mesoproterozoic and Paleoproterozoic contributions. The former clearly stands out in samples AG-12 and AG-18 with ages clustering at ca. 1001 and 1025 Ma, respectively, and the latter in samples AG-14 and AG-17 with ages grouping at ca. 1893 and 2032 Ma, and ca. 2011 Ma, respectively (Fig. 9). Despite having similar age distribution patterns, there is a noteworthy difference; the percentage of Paleozoic dates in sample AG-17 (36%) is twice as high as that in the other three samples (15% to 19%) (Fig. 9).

Combining a total of 522 concordant or nearly concordant dates obtained from these four samples of Lomo de Bas quartzites, a new age distribution pattern with dates ranging from 284 to 3195 Ma is shown in Fig. 9. These dates are Paleozoic (21%), Neoproterozoic (45%), Mesoproterozoic (9%), Paleoproterozoic (20%), Neoarchean (5%) and Mesoarchean (1%) (Fig. 9). Within the 111 Paleozoic zircon grains, there are Early Permian (2% with respect to the total amount of Paleozoic grains), Carboniferous (44%), Devonian (12%), Silurian (2%), Ordovician (7%) and Cambrian dates (33%) (Fig. 9).

The CL imaging of zircons from the Tahal Fm of the Mulhacén tectonic ensemble (samples AG-1 and AG-2) shows grains with continuous oscillatory zoning and partially resorbed cores overgrown by low and high U rims (Fig. 2 in S3 Supplementary material). There are also grains with sector zoning and structureless grains (Fig. 1 in S3 Supplementary material).

Individually, samples AG-1 and AG-2 contain Jurassic zircons with the youngest zircon grains yielding $^{206}Pb/^{238}U$ dates of 195 ± 8 Ma, and 179 ± 5 Ma, respectively. They also have a Permian age, within uncertainty, for the youngest zircon population at 275 ± 8 Ma (MSWD = 1.4 and probability = 0.25) and 277 ± 4 Ma (MSWD = 1.12 and probability = 0.35), respectively. Their age distribution patterns are also comparable with Carboniferous and Ediacaran peaks at ca. 334 and 331 Ma, and ca. 610 and 598 Ma, respectively (Fig. 10). However, there are some differences: i) a minor Early Tonian peak in sample AG-1 at ca. 939 Ma; ii) a higher percentage of Mesozoic and Paleozoic dates in sample AG-2; iii) greater percentage of

Mesoproterozoic and Paleoproterozoic zircons in sample AG-1; and iv) lack of Mesoarchean dates in sample AG-2 (Fig. 10).

The 259 concordant or nearly concordant dates from samples AG-1 and AG-2 were combined in an age distribution pattern with dates from 179 to 2811 Ma, which are mainly Neoproterozoic (43.5%), Paleozoic (32%) and Paleoproterozoic (13%), with minor Mesozoic (2%), Mesoproterozoic (7%), Neoarchean (2%) and Mesoarchean dates (0.5%) (Fig. 10). The 83 Paleozoic zircon grains have Permian (23% with respect to the total amount of Paleozoic grains), Carboniferous (52%), Devonian (7%), Silurian (2%), Ordovician (7%) and Cambrian dates (9%), while the six Mesozoic zircon grains have two Jurassic and four Triassic dates (Fig. 10).

5.1.2. SIMS results of sample AG-13 (orthogneiss) – Lower Lomo de Bas tectonic unit

Twenty-six grains from this orthogneiss were analysed and 27 of the 31 analyses yielded concordant or nearly concordant dates between 191 and 2345 Ma (Fig. 11). Eleven dates plot in a single population with a ^{204}Pb corrected ^{206}Pb/^{238}U mean age of 294 ± 2 Ma (MSWD = 0.75 and probability = 0.68) (Fig. 11). These dates are from zircons with continuous oscillatory zoning, Th/U ratios between 0.030 and 0.615 and common Pb content from 0.05% to 0.26% (Table S1 in Supplementary material). Therefore, this mean age could represent the best estimate of the crystallization age of the protolith.

There are also seven 7 slightly younger dates between 264 and 286 Ma (Fig. 12). These dates are from grains with continuous oscillatory zoning (Fig. 3 in S3 Supplementary material), and one rim from a composite grain, Th/U ratios between 0.062 and 0.692 and much higher common Pb content up to 0.35% (Table S1 in

Supplementary material). Thus, they were not taking into account for the age calculation.

The youngest ^{204}Pb corrected ^{206}Pb/^{238}U date for this dataset is 191 ± 3 Ma (Table S1 in Supplementary material). This date is from the rim of a composite grain, has a Th/U ratio of 0.011 and could be related to a metamorphic event in this area.

5.1.3. SHRIMP IIe/mc datations on zircons from sample AG-16 (orthogneiss) – Lower Lomo de Bas tectonic unit

Sample AG-16 provided scarce euhedral bipyramidal prismatic zircons with dimensions between 80 and 200 μm. The CL imaging shows partially resorbed cores overgrown by low or high U rims with well-defined oscillatory zoning and a few grains with continuous oscillatory zoning (Fig. 4 in S3 Supplementary material).

Twenty-one U-Pb analyses on 18 different crystals yielded 15 concordant or nearly concordant dates (discordance <5%) ranging from 284 to 674 Ma (Fig. 11). Eight of those 13 analyses plotted as a single population with a ^{207}Pb corrected ^{206}Pb/^{238}U mean age of 289 ± 3 Ma (MSWD = 1.4 and probability = 0.20) (Fig. 12) and were from grains with continuous oscillatory zoning, U and Th contents of 205-1415 and 53-426 ppm, respectively, and Th/U ratios between 0.07 and 1.03 (Table S1 in Supplementary material). This mean age is therefore considered the best estimate of the crystallization age of the protolith for the orthogneiss. The remaining dates (330 to 674 Ma) were from cores of composite grains and grains with continuous oscillatory zoning and are considered inherited cores and xenocrysts, respectively (Fig. 12).

5.2. Alpujárride Complex

5.2.1. LA-ICPMS results from samples from the Micaschists and Quartzite Fm

The CL images of zircons of samples AG-4, AG-5, AG-6 and AG-7 from the Micaschists and Quartzite Fm show grains with continuous oscillatory zoning and complex grains with a partially resorbed core overgrown by low or high U rim. There are also a few grains with sector zoning and structureless grains (Fig. 5 in S3 Supplementary material).

Some similarities are distinguished on the age distribution patterns of these four samples (Fig. 13). There are two main peaks: i) a main Ediacaran peak with ages between ca. 600 and 631 Ma; and ii) a secondary Early Tonian-Late Stenian peak with ages between ca. 996 and 1040 Ma.

However, some differences are noteworthy: i) samples AG-6 and AG-7, located at the top of the formation, have an Early Orosirian-Late Rhyacian population at ca. 2055 and 2033 Ma, respectively, that is absent in samples AG-4 and AG-5 at the base of the formation (Fig. 13); ii) samples from the top of the formation also have a Paleoarchean component that is lacking at the bottom; iii) there were no Mesoarchean dates found in sample AG-6; iv) the age of the youngest zircon grains decreases from the bottom to the top of the formation; that is, from 328 ± 10 Ma and 306 ± 6 Ma in samples AG-4 and AG-5, respectively, to 296 ± 4 Ma and 299 ± 7 Ma in samples AG-6 and AG-7, respectively; and finally, v) the youngest zircon population in sample AG-5 is Late Carboniferous (308 ± 4 Ma) contrasting with those from the other three samples that are Cambrian-Early Ediacaran (sample AG-4, 551 ± 5 Ma; sample AG-6, 507 ± 10 Ma; and sample AG-7; 558 ± 7 Ma (Text S2 and Fig. S4 in Supplementary material).

Combining the 562 concordant or nearly concordant U-Pb data for the four samples of Micaschits and Quartzite Fm produces an age distribution pattern composed of Paleozoic (11%), Neoproterozoic (51%), Mesoproterozoic (11%), Paleoproterozoic (17%), Neoarchean (8%), Mesoarchean (1.5%) and Paleoarchean dates (0.5%) (Fig. 13).

These cluster into five main peaks at ca. 309, 602, 1039, 2054 and 2547 Ma (Fig. 13). Within the 63 Paleozoic zircon grains, there are: Permian (5% with respect to the total amount of Paleozoic grains), Carboniferous (32%), Devonian (9%), Ordovician (14%) and Cambrian dates (40%) (Fig. 13).

5.2.2. LA-ICPMS results from samples from the Middle Triassic Meta-detrital Fm

The CL imaging of zircons from samples AG-9, AG-11, and AG-15 shows grains with continuous oscillatory zoning and some partially resorbed cores with low or high U overgrowths. There are also grains with sector zoning (Fig. 6 in S3 Supplementary material).

Their youngest zircon grains have $^{206}Pb/^{238}U$ dates ranging between 214 ± 2 and 288 ± 4 Ma, while their youngest zircon populations have $^{206}Pb/^{238}U$ mean ages varying between 287 ± 1 Ma (sample AG-11, MSWD = 1.11 and probability = 0.35) and 474 ± 3 Ma (sample AG-15, MSWD = 0.71 and probability = 0.54).

The age distribution pattern from these samples displays two or three main populations: a Permian-Late Carboniferous peak (ca. 287 Ma in samples AG-9, and AG-11), one or two Ediacaran-Cryogenian peaks (from ca. 546 to ca. 661 Ma, in all samples) and a Tonian-Stenian peak (from ca. 963 to ca. 1016 Ma in samples AG-9 and AG-15) (Fig. 14).

The dates of samples AG-9, AG-11, and AG-15 from the Meta-detrital Fm range from 214 Ma to 2941 Ma, and are Paleozoic (17% to 39%), Neoproterozoic (34% to 57%), Mesoproterozoic (6% to 13%), Paleoproterozoic (7% to 13%) and Neoarchean (4% to 7%) in age. It is worthy to note that only sample AG-15 yielded a few Mesoarchean dates (1%) (Fig. 14). When we combine the 392 concordant or nearly concordant U-Pb data AG-9, AG-11, and AG-15, we obtain an age distribution pattern composed of Mesozoic (0.5%), Paleozoic (30%), Neoproterozoic (44%), Mesoproterozoic (9%), Paleoproterozoic (11%), Neoarchean (5%), and Mesoarchean dates (0.5%) (Fig. 14). These cluster into five main peaks at ca. 316, 588, 990, 7960, and 2610 Ma (Fig. 14). Within the 119 Paleozoic zircon grains, there are: Permian (33% with respect to the total amount of Paleozoic grains), Carboniferous (28%), Devonian (3%), Silurian (3%), Ordovician (17%), and Cambrian dates (16%) (Fig. 14).

5.2.3. LA-ICPMS results from samples from the Miñarros quartz mylonites

The CL images of zircon grains from the Miñarros quartz mylonites (sample AG-19) show grains with continuous oscillatory zoning and composite grains with cores overgrown by low and high U rims (Fig. 7 in S3 Supplementary material). One hundred and fifty one analyses were performed on selected zircons and 145 yielded concordant or nearly concordant dates between 297 and 3105 Ma. Those dates are Palaeozoic (30%), Neoproterozoic (42%), Mesoproterozoic (7%), Paleoproterozoic (15%), Neoarchean (5%) and Mesoarchean (1%), and cluster into six main populations at ca. 300, 305, 550, 566, 622 and 986 Ma (Fig. 14). The 43 Paleozoic zircon grains include Permian (7% with respect to the total amount of Paleozoic grains), Carboniferous (46%), Devonian (5%), Ordovician (19%), and Cambrian dates (23%) (Fig. 14).The youngest zircon $^{206}Pb/^{238}U$ date is 297 ± 5 Ma and the youngest zircon population, comprising 10 dates, has a mean $^{206}Pb/^{238}U$ age of 300 ± 1 Ma (MSWD = 0.64 and probability = 0.76).

5.2.4. SHRIMP IIe/mc datations on zircons from sample AG-26 (orthogneiss)

Zircon grains from AG-26 are abundant and euhedral bipyramidal prisms with lengths of about 250 to 80 µm and widths of 100 to 50 µm. Most are brownish translucent crystals. CL imaging shows composite grains with partially resorbed cores overgrown by thick high U rims. Most of the cores show continuous oscillatory zoning truncated by the dark rims (Fig. 8 in S3 Supplementary material). Both domains were targeted for the analysis.

Sixteen U-Pb measurements on 16 different dark rims yielded 14 concordant or nearly concordant dates ranging from 14 to 250 Ma (Fig. 15). Six dates plot in a single population with a ^{207}Pb corrected ^{206}Pb/^{238}U age of 15.8 ± 0.2 Ma (MSWD = 0.69, probability = 0.63) (Fig. 15). These dates are from zircon with U and Th contents between 4006 and 7413, and 6 and 14 ppm, respectively, and Th/U between 0.001 and 0.004 (Table S1 in Supplementary material).

Thirty analyses were performed on 30 cores from different crystals and all these analyses yielded concordant or nearly concordant dates between 30 and 288 Ma (Fig. 16). Fifteen analyses plot in a single population with a ^{207}Pb corrected ^{206}Pb/^{238}U age of 283 ± 2 Ma (MSWD = 0.76 and probability = 0.71) (Fig. 16). These analyses are from zircons with U and Th contents between 377 and 1919, and 32 and 137 ppm, respectively, and Th/U between 0.05 and 0.21 (Table S1 in Supplementary material).

5.3. Maláguide Complex and unconformable Middle Miocene red conglomerates and sandstones

Samples LP-16-AZ and AG-10 contained zircon grains displaying either continuous oscillatory zoning, partially resorbed cores overgrown by low or high U rims, or sector zoning. There were also a few structureless zircon grains (Fig. 9 in S3 Supplementary material)

The youngest zircon grains in these two samples have ^{206}Pb/^{238}U ages of 277 ± 7 and 283 ± 15 Ma, respectively, while the youngest zircon populations have mean

$^{206}Pb/^{238}U$ ages of 279 ± 3 Ma (MSWD = 0.57 and probability = 0.63) and 492 ± 8 Ma (MSWD = 1.3 and probability = 0.28), respectively.

The age distribution patterns of samples AG-10 and LP-16-AZ are significantly different (Fig. 17). The two main populations in sample AG-10 are Ediacaran (ca. 602 Ma) and Stenian (ca. 1074 Ma), while in sample LP-16-AZ, they are Carboniferous (ca. 305 Ma) and Ediacaran (ca. 608 Ma). The percentage of Paleozoic grains in sample LP-16AZ is also almost four times higher than that in sample AG-10, while the Neoproterozoic component in sample AG-10 is almost double that in sample LP-16-AZ. Furthermore, Mesoarchean and Neoarchean dates are lacking in sample LP-16-AZ, which does contain a Paleoarchean population.

The dates from the two samples (Fig. 17) include Paleozoic (14 to 52%), Neoproterozoic (33 to 50%), Mesoproterozoic (5 to 9 %), and Paleoproterozoic (9 to 20%). Sample AG-10 also includes Neoarchean (6%), and Mesoarchean (1%) zircon grains, while sample LP-16-AZ also includes Paleoarchean (1%) zircon grains. Within the Paleozoic zircon population, the main difference is the increase (by one order of magnitude) in the number of Carboniferous and Permian grains from 3 and 2 in sample AG-10 to 33 and 18 in sample LP-16-AZ, respectively. The character of the remaining Paleozoic grains is similar in AG-10 and LP-16-AZ (3 and 2 Devonian grains, 1 and 1 Silurian grains, 2 and 10 Ordovician grains, and 7 and 6 Cambrian grains in each sample, respectively).

Samples AG-3 and AG-20 from the unconformable Middle Miocene red conglomerates and sandstones contain zircon grains with either continuous oscillatory zoning or sector zoning (Fig. 10 in S3 Supplementary material). There are also some composite grains with a partially resorbed core overgrown by a thick rim, very similar to those previously described in the Micaschists and Quartzite Fm of the AC. Sample

AG-20 also includes a few structureless zircon grains (Fig. 10 in S3 Supplementary material)

The youngest zircons from samples AG-3 and AG-20 have $^{206}Pb/^{238}U$ dates of 248 ± 8 and 177 ± 7 Ma, respectively, while their youngest zircon populations have mean $^{206}Pb/^{238}U$ ages of 582 ± 7 Ma (MSWD = 1.3 and probability = 0.23) and 292 ± 3 Ma (MSWD = 0.91 and probability = 0.47), respectively.

The age distribution patterns of AG-3 and AG-20 are slightly different (Fig. 18). There is only one main population in sample AG-3 (Early Ediacaran: ca. 605 Ma), while there are three main populations in sample AG-20 (Late Ediacaran: ca. 574 Ma; Cryogenian: ca. 691 Ma; Orosirian: ca. 2007 Ma). Moreover, the percentage of Paleozoic zircon grains in sample AG-20 is almost three times higher than that in AG-3. The Mesoarchean component in sample AG-3 is fourteen times greater than that in sample AG-20. Paleoarchean zircons are absent in sample AG-20 (Fig. 18). Regarding the Mesozoic component, sample AG-3 contains one Triassic zircon grain, while sample AG-20 contains one Jurassic zircon grain. The number of Paleozoic grains also differs, with 11 and 31 grains in samples AG-3 and AG-20, respectively. The main difference in the Paleozoic component is the lack of Permian grains in sample AG-3 and the content of Carboniferous grains (three in AG-3 to eight in AG-20). Samples AG-3 and AG-20 contain the same number of number of Devonian grains (4), and a similar number of Silurian (1 and 3, respectively), Ordovician (1 and 5, respectively), and Cambrian grains (2 and 4, respectively).

6. Discussion

6.1. Depositional age of the graphite-bearing formations of the Nevado-Filábride and Alpujárride complexes

Within the upper or lower Lomo de Bas units, the four studied samples yielded youngest zircons with dates between 284 ± 14 and 323 ± 5 Ma, while their youngest populations vary between 321 ± 2 and 336 ± 2 Ma (see text S2 and Fig. S4 in Supplementary material). Therefore, the youngest dates point towards Early Permian-Late Carboniferous maximum depositional ages (MDA). However, as data from the orthogneisses samples AG-13 and AG-26 highlight, some of the youngest zircon dates can be related to Mesozoic metamorphic events and/or Pb loss. Therefore, we prefer the more conservative approach of using the youngest detrital zircon populations, and thus, we propose a MDA between 321 ± 2 and 336 ± 2 Ma for the quartzites of the Lomo de Bas (i.e., Carboniferous).

The minimum depositional age of these rocks is defined by samples AG-13 and AG-16, the orthogneiss bodies within the Lomo de Bas blacks schists and quartzites (Álvarez and Aldaya, 1985; Álvarez, 1987) with ^{206}Pb/^{238}U ages for the protoliths of 294 ± 2 Ma (MSWD = 0.75 and probability = 0.68) and 289 ± 3 Ma (MSWD = 1.4 and probability = 0.20), respectively. The ages of both orthogneisses just overlap within uncertainty and, together with the previous MDA, define a depositional age for the quartzitic rocks of the Lomo de Bas units between Bashkirian (Late Carboniferous) and Artinskian-Sakmarian (Early Permian).

This Late Carboniferous age agrees with the presence of Early-Middle Devonian fossils in the dark marbles below the quartzites of the upper tectonic unit (Eifelian-Emsian, c.f. Lafuste and Pavillon, 1976; Laborda-López et al., 2013, 2015a, b), and also supports the presence of several superposed tectonic units as suggested by Laborda-López et al. (2013, 2015a, b).

The youngest ^{206}Pb/^{238}U zircon dates in samples from the Micaschists and Quartzite Fm of the AC (AG-4, AG-5, AG-6 and AG-7) are Early Permian-Late

Carboniferous (328 ± 10 Ma and 296 ± 4 Ma), but the youngest populations in these samples are highly variable; Cambrian-Late Ediacaran (between 507 and 558 Ma) in samples AG-4, AG-6 and AG-7, and Late Carboniferous (308 Ma) in sample AG-5 at the base of the Micaschists and Quartzite Fm. A MDA of Late Pennsylvanian age is proposed for the AC Micaschists and Quartzite Fm.

6.2. Provenance of zircon in Late Carboniferous samples

The studied samples from both the Lomo de Bas rocks and the Micaschists and Quartzite Fm include Carboniferous grains (49 grains in the NFC, and 20 grains in the AC) that could have been sourced from Late-Variscan and Variscan felsic rocks, widely distributed within the whole Iberian Massif and surrounding areas (e.g. Arranz and Lago, 2004; Bea, 2004; Casquet and Galindo, 2004; Gallastegui et al., 2004; Ribeiro et al., 2019). The Carboniferous rocks of both the NFC and AC also include a number of Early Ordovician, Silurian and Devonian dates (23 grains in the NFC and 15 grains in the AC with dates between 484 and 365 Ma), which have no known source in pre-Carboniferous rocks from the Central Iberian, Cantabrian, and West Asturian-Leonese zones of the Iberian Massif. The nearest source of these zircon grains could be in the Avalonian terranes. In fact, felsic magmatism was developed during rifting, spreading, and later subduction of the Rheic Ocean (e.g. Sánchez Martínez et al., 2007, 2012). In the surrounding Variscan terranes, Devonian zircon source rocks are only found within the Sehoul Block in the Western Moroccan Meseta (Tahiri et al., 2010). However, metasediments containing those Devonian grains have also been described: i) in the Late Devonian Debdou-Mekkam Metasediments in the Eastern Moroccan Meseta (Accotto et al., 2020), ii) in Late Paleozoic metasediments from both the South Portuguese and Ossa-Morena zones (Pereira et al., 2012, 2014, 2017; Pérez-Cáceres et al., 2017), iii) in the Carboniferous rocks from the Cantabrian Zone (Pastor-Galán et al., 2013), and, iv) in the syn-orogenic rocks below the allochthonous complexes of the Galicia-Tras-Os-Montes (Martínez Catalan et al., 2008).

As previously mentioned, these Devonian grains are interpreted as having been derived from Avalonian terranes, based on two slightly different hypotheses. The first is that they were sourced from an unexposed magmatic arc along the Avalonian convergent margin during Middle-Late Devonian subduction of the Rheic Ocean (Pereira et al., 2012, 2017; Pérez-Cáceres et al., 2017; Accotto et al., 2020). The second possibility is that they were directly sourced from eroded rocks within the Rheic Ocean suture zone, where zircon grains of these ages occur (e.g. Fernandez-Suarez et al., 2002; Sánchez-Martínez et al., 2007; Martínez Catalán et al., 2008; Pastor-Galán et al., 2013).

However, the main detrital zircon component in the Carboniferous rocks of both the NFC and AC is pre-Cambrian, with two main populations: i) an Early Neoproterozoic population between ca. 574 and 602 Ma (Ediacaran-Cryogenian) (Text S2 in Supplementary material), and ii) a Mesoproterozoic population between ca. 1014 and 1039 Ma (Stenian) (Fig. 19; Text S2 in Supplementary material). These populations represent the Cadomian-Pan-African orogeny developed in Gondwana and the Tonian-Stenian magmatic event that took place in the Arabian Shield (see Bea et al., 2010), respectively. Furthermore, the NFC and AC Carboniferous rock also contain an Orosirian (ca. 2.0-2.1 Ga), recording the Eburnean orogeny, and a Neoarchean (ca. 2.5-2.7 Ga) population. Similar age patterns with these four peaks are found within the Carboniferous and older rocks from the Central Iberian, Cantabrian, and West Asturian-Leonese zones of the Iberian Massif (see Talavera et al., 2012, 2015; Pastor-Galán et al., 2013; Fernández-Suárez et al., 2014; Shaw et al., 2014; Gutierrez-Alonso et al., 2015) (Fig. 19). If we focus on the Pre-Carboniferous rocks, Fernandez Suarez et al.

(2014) studied the age of zircon from Ediacaran and Early Cambrian rocks of the Cantabrian and Central Iberian zones and found two populations ca. 0.55-0.75 Ga and ca. 0.85-1.15 Ga, and also minor Paleoproterozoic (ca. 1.9–2.1 Ga) and Archean (ca. 2.4–2.6 Ga) populations (Fig. 19D). Talavera et al. (2012, 2015) also determined similar age patterns in Ediacaran to Early Ordovician rocks of the Central Iberian Zone. Shaw et al. (2014) sampled and studied the Lower Ordovician Armorican quartzite trough the Central Iberian, Cantabrian, and West Asturian-Leonese zones, and their age pattern (n=1173) also shows the above-mentioned peaks with Ediacaran-Cryogenian (ca. 617 Ma), Tonian-Stenian (ca. 1.21 Ga), Orosirian (ca. 2.0 Ga), and Neoarchean (ca. 2.6 Ga) populations (Fig. 19D). Furthermore, Gutierrez-Alonso et al. (2015) studied Silurian-Devonian sedimentary rocks from the same two paleogeographic zones and found also the same four populations: Ediacaran–Cryogenian (c. 0.55–0.8 Ga), Tonian–Stenian (0.85–1.2 Ga), Palaeoproterozoic (c. 1.8–2.2 Ga) and Archaean (c. 2.5–3.3 Ga) (Fig.19C). In summary, the same four age peaks were found in all these works, albeit with differences in the proportion of grains in each population (Fig. 19). Stephan et al. (2019) include those areas with similar pre-Ediacaran age patterns to their East African-Arabian zircon province, and included the Central Iberian, Cantabrian, and West Asturian-Leonese zones of the Iberian Massif.

We can also compare the results presented here with those obtained on samples of a similar age from the Betic Cordillera, Iberian massif and surrounding areas. In the Betic Cordilleras, the Lomo de Bas units have usually been interpreted as part of the Veleta units of the NFC (i.e. Álvarez and Aldaya, 1985; Álvarez, 1987), and their quartzites correlated with the Late Carboniferous Aulago Fm in the Sierra de Filabres area (Jabaloy-Sanchez et al., 2018; Rodríguez-Cañero et al., 2018), which also include the Ediacaran-Cryogenian and Stenian populations mentioned above (Fig. 19A). The main difference is a larger proportion of Devonian and Carboniferous zircon grains within the Lomo the Bas rocks (13 and 49 grains, respectively), when compared to those from the Aulago Fm (7 and 4 grains, respectively; Jabaloy-Sánchez et al., 2018) (Fig. 19A). Furthermore, the age pattern of sample Ri119 from the Paleozoic basement of a tectonic unit of the Sebtide/Alpujárride Complex in the Internal Rif (n=144 analyses, Azdimousa et al., 2019) also yields a similar pattern to that in Late Carboniferous samples from the AC and NFC with two main populations at ca. 532 and 992 Ma (Fig. 19B).

Pereira et al. (2014, 2020) studied the Late Carboniferous sediments from the Ossa-Morena and South Portuguese zones of the Iberian Massif (see Pereira et al., 2012, 2014, 2020, and references therein) (Fig. 19H). Within these rocks, those from the Ossa-Morena Zone were deposited in a continental environment (Santa Susana Fm Pereira et al., 2020), with an age pattern that includes a main Early Carboniferous population at ca. 354 Ma, but also Cryogenian (ca. 647 Ma) and Rhyacian (ca. 2128 Ma) secondary populations (Pereira et al., 2020) (Fig. 19H). However, the age patterns lack the Stenian and Neoarchean populations present in the NFC and AC samples (Fig. 19). Furthermore, marine detritic sediments were also deposited in the South-Portuguese Zone, and their age patterns are very similar to those of the Ossa-Morena Zone. Those marine detritic sediments from the South-Portuguese Zone include the Devonian (ca. 405 Ma), Ediacaran-Cryogenian (ca. 639 Ma), and Orosirian populations (ca. 2068 Ma), and they lack the Stenian and Neoarchean ones (Brejeira and Mira Fms from Pereira et al., 2014) (Fig. 19).

On the other hand, Upper Carboniferous samples from the Cantabrian Zone studied by Pastor-Galán et al. (2013) yield very similar age distribution patterns to those of the Lomo de Bas (NFC) and Micaschists and quartzites Fm (AC), with the only difference being the existence of an Early Carboniferous peak (ca. 335 Ma, “Variscan”) in the rocks from the Betic Cordillera (Fig. 19C). Martínez et al. (2016) analyzed Late Carboniferous rocks from the NE Iberian Peninsula and South France, including samples from the Catalonian Massif, Minorca, Montagne Noire Massif, Mouthoumet Massif, Pyrenees, and Priorat, but the age patterns show differences only in the Stenian and Neoarchean populations. The samples from Martinez et al (2016) usually lack a Stenian peak (Montagne Noire Massif, Mouthoumet Massif, Pyrenees, and Priorat Massif) or it is a minor one (Catalonian Massif and Minorca), and the Neoarchean population is also absent in the Catalonian Massif, Mouthoumet Massif, Pyrenees, and Priorat Massif areas, but not in the samples from Minorca and Montagne Noire Massif (Fig. 19E and F).

All these data suggest that the Late Carboniferous sediments of both the NFC and the AC were sourced from Variscan rocks containing zircon grains from the Cantabrian, West Asturian-Leonese, and Central-Iberian zones of the Iberian Massif, but they also include a small amount of zircons derived from the Avalonian terranes. Furthermore, the sediments incorporated a small number of zircon grains derived from the Late-Variscan felsic rocks. The sediments were mainly pelites rich in organic material, quartz-rich sandstones (quartzwackes in the case of the NFC, Jabaloy, 1993; Rodríguez-Cañero et al., 2018), and black limestones (with conodonts in the case of the NFC rocks; Rodríguez-Cañero et al., 2018) suggesting deposition in open marine anoxic environments (Rodríguez-Cañero et al., 2018). This points to the Carboniferous foreland basins developed in the Cantabrian Zone of the Iberian Massif (see Matte, 2001, Rodríguez-Cañero et al., 2018; Jabaloy-Sánchez et al., 2018) as the most likely paleogeographic location of both complexes (Fig. 20).

In Late Carboniferous times, the Variscan belt was already formed in Western and Central Europe (e.g. Matte, 2001), and most of the rocks of the Cantabrian, West Asturian-Leonese, Central-Iberian zones were deformed and stacked with the rocks of the Rheic Ocean suture zone (i.e. Pastor-Galán et al., 2013). Rocks from the Variscan belt, including rocks from those three stacked zones, were being eroded at Late Carboniferous, and their zircons had been stored within the coetaneous sediments in the Cantabrian Zone (see Pastor-Galán et al., 2013), and NFC (Jabaloy-Sánchez et al., 2018). Our data indicate the same case for the rocks of the AC (Fig. 20).

On the other hand, the published data from the samples from the MC with Carboniferous-Early Permian ages have Early Carboniferous (at ca. 329 and 347 Ma respectively), Early Ordovician-Cambrian (ca. 445 and 491 Ma), Ediacaran-Cryogenian (ca. 589 and 649 Ma), Tonian (ca. 932 Ma), and Orosirian populations (ca. 2002 and 2080 Ma) (Marbella conglomerate from Esteban et al., 2017, Fig. 19A; sample Ri121 from Azdimousa et al., 2019, Fig 19G). However, they show a difference in the number of Neoarchean zircon grains (ca. 2.6 Ga), which are more abundant in the sample Ri121 from Azdimousa et al., 2019, Fig. 19G). The age distribution patterns for both samples also include a small number of Devonian zircons, most likely sourced in the Avalonian terranes, such as the Sehoul block (Accotto et al., 2020). Those data suggest that the main source area for the Marbella conglomerate described in Esteban et al. (2017) was the West African Craton and derived terranes (i.e. Ossa-Morena Zone according to Esteban et al., 2017). However, the age pattern of sample Ri121 from Azdimousa et al. (2019) is very similar to that found in the NFC and AC Carboniferous rocks, suggesting the same source areas. Therefore, the paleogeographic location of the MC seems slightly different from that of the NFC and AC, and in this location the sediments were sourced from the Cantabrian, West Asturian-Leonese, Central-Iberian zones, or the Ossa Morena Zone (Esteban et al., 2017) and/or the Moroccan Variscides (Figs. 19, 20).

6.3. Lower Permian orthogneisses from the NFC (Cantal unit)

The sample AG-26 from the Cabezo Blanco orthogneiss within the Cantal unit yielded zircons with textures similar to those described by Gómez-Pugnaire et al., (2004, 2012) in the NFC. The CL imaging of these grains shows cores with continuous oscillatory zoning truncated by dark U-rich rims. These cores yielded a ^{207}Pb corrected ^{206}Pb/^{238}U age of 283 ± 2 Ma while the dark overgrowths have yielded a ^{207}Pb corrected ^{206}Pb/^{238}U age of 15.8 ± 0.2 Ma. We propose the former age as the age of the igneous protolith of the Cabezo Blanco orthogneiss and the latter age as the age of a metamorphic event affecting this orthogneiss. Similar metamorphic ages have been determined within zircons from the NFC (López Sánchez-Vizcaíno et al., 2001, 15.0 ± 0.6 Ma; Gómez-Pugnaire et al., 2004, 2012, 16.5 ± 0.4 Ma and 17.3±0.4 Ma respectively). Furthermore, similar ages were also determined from Lu-Hf on garnets (Platt et al., 2006, between 18 and 14 Ma) and multimineral isochrons on samples of this complex (Kirchner et al., 2016; three ages of 20.1 ± 1.1, 16.0 ± 0.3, and 13.3 ± 1.3 Ma). However, the metamorphic zircons from the AC typically have slightly older ages (Sánchez-Rodriguez and Gebauer, 2000, 19.9 ± 1.7 Ma.; Platt et al., 2003, ages between 22.7 and 21.3 Ma, Esteban et al., 2007, 19.2 ± 1.1 Ma), and the AC has yielded additional older ages including a garnet Lu-Hf age of 25 ± 1 Ma (Blichert-Toft et al., 1999), and a garnet and clinopyroxene Sm-Nd age of 21.5 ± 1.8 Ma (Zindler et al., 1983). Therefore, we propose that the Cantal unit is part of the NFC as already proposed by García-Tortosa (2002).

6.4. Permian to Triassic metadetrital samples from the NFC

Samples AG-1 and AG-2 come from two quartzites in the upper part of the Tahal Fm within the Mulhacén units. They yielded very similar zircon age patterns, the youngest zircon $^{206}Pb/^{238}U$ dates being Jurassic (195 ± 8 Ma and 179 ± 5 Ma, respectively) and the youngest zircon population being Early Permian (275 ± 8 Ma and 277 ± 4 Ma, respectively). These data match the 259 concordant-nearly concordant analyses from the Tahal Fm published by Jabaloy-Sánchez et al. (2018), in which youngest zircon population was Early Permian (275 ± 2 Ma) as well (Fig. 21C).

An estimate of the MDA for the sources of the Tahal Fm based on the youngest zircons points to Jurassic. However, our preference is a more conservative estimate for the MDA based on the youngest populations and our proposal is an age younger than Early Permian (275 ± 8 Ma), in agreement with the data provided by Jabaloy-Sánchez et al. (2018), and Santamaría-López and Sanz de Galdeano (2018) for the same rocks in Sierra Nevada and Sierra de los Filabres.

6.5. Permian to Triassic metadetrital samples from the AC

The youngest zircon dates for samples AG-9, AG-11, and AG-15 from the Meta-detrital Fm of the AC are Triassic-Early Permian (between 214 ± 2 Ma and 288 ± 4 Ma) and the youngest zircon populations are Early Permian (287 ± 2, AG-9, and 287 ± 1, AG-11) to Early Ordovician (474 ± 3 Ma, AG-15). We have used the same approach described above to estimate the MDA of the Meta-detrital Fm, proposing an Early Permian (Artinskian) MDA for this formation, older than the Middle Triassic stratigraphic age (247 to ca. 237 Ma, see Simon and Visscher, 1983; Maate et al., 1993; García Tortosa et al., 2002; Martín-Rojas et al., 2010). Furthermore, the youngest zircon $^{206}Pb/^{238}U$ date and the youngest zircon population in sample AG-19 from the Miñarros unit are 297 ± 5 Ma and 300 ± 1 Ma, respectively, indicating an older MDA (Gzhelian, Late Pennsylvanian). Samples AG-9, AG-11, AG-15 and AG-19 have similar age patterns to the samples from the Tahal Fm (NFC).

6.6. Permian to Triassic metadetrital samples from the MC

The youngest zircon grains from samples AG-10 and LP-16-AZ from the Saladilla Fm of the MC yielded $^{206}Pb/^{238}U$ dates between 277 ± 7 and 282 ± 15 Ma. Moreover, the youngest zircon populations were 492 ± 8 Ma and 279 ± 3 Ma, respectively, pointing to an Early Permian MDA.

6.7. Provenance for zircon of the the Permian to Triassic meta-detrital samples

A common feature of the samples with a Permian MDA from the three complexes (NFC, AC and MC) is an increase in the number of Paleozoic zircons with respect to the older Carboniferous samples (Fig. 21). In fact, the Permian MDA samples show an increase in the number of Permian and Carboniferous zircon grains indicating erosion of Variscan and Late-Variscan felsic rocks in the source areas. In the NFC, the Tahal Fm contains 21% to 27 % Permian-Carboniferous grains (the values are the percentage of the total number of analyses of each sample), while the Carboniferous Lomo de Bas quartzites have 5% to 18% Carboniferous grains, with only two Permian grains. Within the AC, the Meta-detrital Fm has variable contents of Permian-Carboniferous grains (from 3 to 31%, the values are the percentage of the total number of analyses of each sample), while the Carboniferous Micaschists and Quartzite Fm has 3% to 6%. Furthermore, in the MC, the Saladilla Fm also displays a variable content of Permian-Carboniferous grains (from 4% to 38%); while the Lower Carboniferous Morales Fm (sample Ri121 from Azdimousa et al., 2019) has 6% Carboniferous grains, and the Permian Marbella Conglomerate (Esteban et al., 2017) has 12 % Permian and Carboniferous grains.

Samples from the Tahal Fm (NFC) have Carboniferous populations between ca. 331 and ca. 334 Ma (“Variscan”), Ediacaran populations between ca. 598 and ca. 610 Ma (“Cadomian”-“Pan-African”), and a Tonian population at ca. 939 Ma (Fig. 21). If the “Variscan grains” are excluded (i.e. post- Late Devonian grains which are younger than 370 Ma), the age distribution pattern is similar to that of the Aulago Fm (Jabaloy-Sánchez et al., 2018) and of the Lomo de Bas quartzites, except for a lower number of Tonian-Stenian (ca. 1.0 Ga) and Neoarchean (ca. 2.61 Ga) grains (Fig. 20).

The age distribution patterns for samples from the Meta-detrital Fm (AC) are similar to those in the above mentioned samples from the Tahal Fm (NFC) (Fig. 21). Samples from the Meta-detrital Fm also have Permian (“Late-Variscan” at 287Ma), Ediacaran-Cryogenian (“Pan-African”, from ca. 546 to ca. 660 Ma) populations, with minor Tonian-Stenian (from ca. 963 to ca. 1016 Ma) and Rhyacian (“Eburnean”, ca. 2060 Ma) populations (Fig. 21). If the <370 Ma zircon grains are excluded, the age distribution pattern is similar to that obtained by combining the Micaschists and Quartzite Fm (AC) datasets (Fig. 21).

In the Saladilla Fm (MC), there are Permian (“Late-Variscan” between ca. 279 and 305 Ma), and Ediacaran-Cryogenian populations (“Pan-African”, from ca. 602 to 677 Ma), with minor Stenian (ca. 1074 Ma), Orosirian (“Eburnean”, ca. 1937 Ma) and Neoarchean (ca. 2106 Ma) peaks (Fig. 21). They differ from the data of the Carboniferous-Early Permian samples from the same MC (Esteban et al., 2017; Azdimousa et al., 2019), not only in the presence of the Early Permian population, but also in the Stenian and Neoarchean peaks. This distinction in the age patterns is due to the erosion and incorporation of material from Late-Variscan felsic rocks and the increasing number of zircons sourced from the Cantabrian, West Asturian-Leonese and Central-Iberian zones.

The similarity between the age patterns of samples with Early Permian MDA from the three complexes and those of the Permian-Early Triassic from the Iberian ranges (Sánchez Martínez et al., 2012) suggests that they were deposited in the same Permian-Triassic basins.

6.8. Unconformable Middle Miocene red conglomerates and sandstones

The samples from Middle Miocene sediments have only two Mesozoic zircon grains and their youngest zircon population has a mean $^{206}Pb/^{238}U$ age of 292 ± 3 Ma, pointing to an Early Permian MDA. Their age distribution patterns correspond to mixing of zircons from the AC and MC that were eroded at the surface during the Middle Miocene. It is noteworthy that those sediments were formed at the surface at the same time that the Cantal unit (sample AG-26) and the NFC were experiencing metamorphism in depth. However, the most important conclusions is that there is no record of any major felsic rock formation event after the Early Permian times in the AC or MC, although several stages of continental rifting and the subduction of the AC took place during this period (e.g. Jabaloy-Sánchez et al., 2019).

The U-Pb zircon data presented here have implications for the evolution of both the Variscan and Alpine chains in the western Mediterranean area. The main implications for the Variscan chain is the existence of Late Carboniferous sedimentary basins eastwards of the Iberian Massif, which recorded the erosion of the Variscan Chain formed during the Late-Devonian Carboniferous, and were also affected by the Late Variscan magmatic event. The sediment in these basins was metamorphosed to form the graphite-rich successions of the NFC and AC during the Alpine orogeny.

During the Permian-Triassic, the break-up of Pangea took place and resulted in the formation of three different paleogeographic realms:

i) the Nevado-Filábride realm continued near the Iberian Massif southeastern paleomargin,

ii) the Alpujárride realm separated from the Iberian Massif by rifting during the Triassic-Jurassic (Martín Rojas et al. 2009; Puga et al., 2011),

iii) the Maláguide realm separated from the southern paleomargin of Iberia (Esteban et al., 2107) during the Jurassic (e.g., Martín-Martín et al. 2006).

Those three realms amalgamated during the Cenozoic; first, the AC subducted below the MC, and later, the NFC subducted below the two previously amalgamated complexes at Early Middle Miocene times. During these processes, the Cantal unit was partially fused, leading to the formation of migmatites.

7. Conclusions

New U-Pb detrital zircon ages in rocks from the Águilas Arc provide maximum depositional ages for their protoliths. U-Pb zircon ages of orthogneisses help to constrain their true depositional ages. In the NFC, the true depositional age of the Lomo de Bas schists and quartzites is Late Carboniferous (ranging between 321 ± 2 and 293 ± 2 Ma), while the MDA of the Tahal Fm is confirmed as Early Permian. In the AC, the MDA of the Micaschists and Quartzite Fm is also Late Carboniferous (308 ± 4 Ma), and that of the Meta-detrital Fm is Early Permian (287 ± 1 Ma). Furthermore, the MDA of the Saladilla Fm (Maláguide Complex) is also Early Permian (279 ± 3 Ma).

The age patterns from the Upper Carboniferous rocks of the NFC and AC are similar, and also similar to those from Upper Carboniferous of the Cantabrian Zone of the Iberian Massif, suggesting similar source areas. The most likely paleogeographical location of both complexes was in Late Carboniferous marine basins located eastwards of the Iberian Massif. However, the age patterns show differences compared with those from the Upper Carboniferous rocks of the MC, and from the South Portuguese and Ossa-Morena zones of the Iberian Massif. On the other hand, age patterns from Upper Carboniferous rocks of the MC show some similarities with those from the Ossa-Morena Zone. Therefore, the paleogeographic location of the MC could have been different from that of the NFC and AC, and it was probably located near the Ossa-Morena Zone and the other rocks derived from the West African Craton.

The samples with Early Permian MDA from the three complexes (NFC, AC, and MC) have more Paleozoic zircons than the Late Carboniferous samples, and similar age patterns, suggesting that they were deposited in the same basin, likely the long-lived Iberian Permian-Triassic depositional basins. Samples from the unconformable Middle Miocene sediments have Early Permian MDA (292 ± 3 Ma) and age distribution patterns corresponding to a mixing of zircons from the AC and MC, and thus, do not record formation of felsic rocks since the Early Permian.

Acknowledgements

We are indebted to Mike Hall and Brad McDonald for their technical support on sample preparation and LA-ICPMS, respectively. The CL imaging was carried out in Curtin University's Microscopy & Microanalysis Facility, whose instrumentation has been partially funded by the University, State and Commonwealth Governments, and the Scanning Electron Microscope (SEM) Facility at the University of Edinburgh. Analysis in the John de Laeter Centre GeoHistory Facility was enabled by AuScope (auscope.org.au) and the Australian Government via the National Collaborative Research Infrastructure Strategy (NCRIS). This work is supported by grants CGL2016-75224-R, and CGL2015-71692-P (MINECO/FEDER, Spain) and RNM-208 (Junta de Andalucía, Spain). This is the IBERSIMS Publication No. 70.

References

Accotto, C., Martínez Poyatos, D.J., Azor, A., Jabaloy-Sánchez, A., Talavera, C., Evans, N.J., Azdimousa, A., 2020. Tectonic evolution of the Eastern Moroccan Meseta: from Late Devonian fore-arc sedimentation to Early Carboniferous collision of an Avalonian promontory. Tectonics

Accotto, C., Martínez Poyatos, D.J., Azor, A., Talavera, C., Evans, N.J., Jabaloy-Sánchez, A., Azdimousa, A., Tahiri, A.; El Hadi, H., 2019. Mixed and recycled detrital zircons in the Paleozoic rocks of the Eastern Moroccan Meseta: paleogeographic inferences. Lithos 338-339, 73-86. Doi: 10.1016/j.lithos.2019.04.011

Aldaya, F., Álvarez, F., Galindo-Zaldívar, J., González-Lodeiro, F., Jabaloy, A., Navarro-Vilá, F., 1991. The Maláguide-Alpujárride contact (Betic Cordilleras, Spain): a brittle extensional detachment, Comptes Rendus de l'Académie des Sciences de Paris 313, 1447-1453.

Álvarez, F., 1987. Subhorizontal shear zones and their relation to nappe movements in the Cantal and Miñarros units. Eastern Betic Zone (Spain). Geologie en Mijnbouw 66, 101-110.

Álvarez, F., Aldaya, F., 1985. Las unidades de la Zona Bética en la región de Águilas-Mazarrón (Prov. de Murcia). Estudios Geológicos 41, 139-146.

Arranz, E., Lago, M., 2004. El plutonismo sin- y tardi-varisco en los Pirineos. In: Vera, J.A., (Ed.) Geología de España, SGE-IGME, Madrid, 263-266.

Azdimousa, A., Jabaloy-Sánchez, A., Talavera, C., Asebriy, L., González-Lodeiro, F., Evans, N.J. 2019. Detrital zircon U-Pb ages in the Rif Belt (northern Morocco): Paleogeographic implications. Gondwana Research 70, 133-150. Doi 10.1016/j.gr.2018.12.008

Balanyá, J.C., García-Dueñas, V., 1987. Les directions structurales dans le Domaine d'Alborán de part et d'autre du Détroit de Gibraltar. Comptes Rendus de l'Académie des Sciences de Paris 304, 929-932.

Bea, F., 2004. La naturaleza del magmatismo de la Zona Centroibérica: consideraciones generales y ensayo de correlación. In: Vera, J.A., (Ed.) Geología de España, SGE-IGME, Madrid, 128-133.

Bea, F., Montero, P., Talavera, C., Abu Anbar, M., Scarrow, J., Molina, J.F., Moreno, J.A., 2010. The palaeogeographic position of Central Iberia in Gondwana during the Ordovician: evidence from zircon geochronology and Nd isotopes. Terra Nova 22, 341-346.

Booth-Rea, G., Silva Barroso, P.G., (2008). Mapa Geológico de España escala 1:50.000. Edición Digital. Hoja 975, Puerto Lumbreras. Instituto Geológico y Minero de España, Madrid.

Blichert-Toft, J., Albarède, F., Kornprobst, J., 1999, Lu-Hf isotope systematics of garnet pyroxenites from Beni Bousera, Morocco: Implications for basalt origin. Science 283, 1303-1306

Booth-Rea, G., Silva Barroso, P.G., Bardají Azcárate, T., Martín Serrano, A., (2009). Mapa Geológico de España escala 1:50.000. Edición Digital. Hoja 997, Águilas. Instituto Geológico y Minero de España, Madrid.

Casquet, C., Galindo, C., 2004. Magmatismo varisco y postvarisco en la Zona de Ossa-Morena. In: Vera, J.A., (Ed.) Geología de España, SGE-IGME, Madrid, 194-198.

Chalouan, A., Michard, A., El Kadiri, K., Negro, F., Frizon de Lamotte, D., Soto J.I., Saddiqi, O., 2008. The Rif Belt. In: Michard, A., Frizon de Lamotte, D., Saddiqi, O., Chalouan, A., (Eds.) Continental Evolution: The Geology of Morocco. Lecture Notes in Earth Sciences, vol 116, pp. 203-302, Springer-Verlag, Berlin Heidelberg.

Dallmeyer, R.D., Martínez Catalán, J.R., Arenas, R., Gil Ibarguchi, J.I., Gutiérrez-Alonso, G., Farias, P., Aller, J., Bastida, F., 1997. Diachronous Variscan tectonothermal activity in the NW Iberian Massif: Evidence from 40Ar/39Ar dating of regional fabrics. Tectonophysics 277, 307–337. Doi:10.1016/s0040-1951(97)00035-8

Durand-Delga, M.; Escalier des Orres, P., Fernex, F., 1962. Sur la présence de Jurassique et d'Oligocène a l'ouest de Carthagene (Espagne méridionale)". Comptes Rendus de l'Académie des Sciences de Paris 255, 1755-1753.

Espinosa Godoy, J., Herrera López, J.L., Pérez Rojas, A., 1972. Mapa Geológico de España escala 1:50.000. Hoja 997bis, Cope. Instituto Geológico y Minero de España, Madrid

Esteban, J.J., Cuevas, J., Tubía, J.M., Liati, A., Seward, D., Gebauer, D., 2007. Timing and origin of zircon-bearing chlorite schists in the Ronda peridotites (Betic Cordilleras, Southern Spain). Lithos 99, 121-135.

Esteban, J.J., Cuevas, J., Tubía, J.M., Gutiérrez-Alonso, G., Larionov, A., Sergeev, S., Hofmann, M., 2017. U–Pb detrital zircon ages from the Paleozoic Marbella

Conglomerate of the Malaguide Complex (Betic Cordilleras, Spain). Implications on Paleotethyan evolution. Lithos 290-291, 34-47.

Fernández-Fernández, E.M., Jabaloy-Sánchez, A., Nieto, F., González-Lodeiro, F., 2007. Structure of the Maláguide Complex near Vélez Rubio (Eastern Betic Cordillera, SE Spain). Tectonics 26, TC4008, doi:10.1029/2006TC002019

Fernández-Suárez, J., Gutiérrez-Alonso, G., Jeffries, T.E., 2002. The importance of along-margin terrane transport in northern Gondwana: insights from detrital zircon parentage in Neoproterozoic rocks from Iberia and Brittany. Earth and Planetary Science Letters 204, 75-88.

Fernández-Suárez, J., Gutiérrez-Alonso, G., Pastor-Galán, D., Hofmann, M., Murphy, J.B., Linnemann, U., 2014. The Ediacaran–Early Cambrian detrital zircon record of NW Iberia: possible sources and paleogeographic constraints. International Journal of Earth Sciences 103, 1335–1357. Doi: 10.1007/s00531-013-0923-3

Gallastegui et al., 2004. Magmatismo. In: Vera, J.A., (Ed.) Geología de España, SGE-IGME, Madrid, 63-68

García Tortosa, F.J., Leyva Cabello, F., Bardaji Azcárate, T., 2012. Mapa Geológico de España escala 1:50.000. Edición Digital. Hoja 976, Mazarrón. Instituto Geológico y Minero de España, Madrid.

García Tortosa, F.J., López-Garrido, A.C., Sanz de Galdeano, C., 2000. Présence du complexe tectonique Malaguide à l'ouest de Carthagéne (zone interne Bétique, Espagne). Comptes Rendus de l'Académie des Sciences de Paris 330, 139-146.

García-Tortosa, F.J., 2002. Los Complejos Tectónicos Alpujárride y Maláguide en el sector oriental de la Zona Interna Bética. Estratigrafía, relaciones tectónicas y evolución paleogeográfica durante el Triásico. PhD Thesis, Universidad de Granada.

Geel, T., 1973. The geology of the Betic of Malaga, the Subbetic and the zone between these two units in the Velez Rubio area (Southern, Spain). GUA Papers of Geology.

Gómez-Pugnaire, M.T., Franz, G., 1988. Metamorphic evolution of the Paleozoic series of the Betic Cordilleras (Nevado-Filabride complex, SE Spain) and its relationship with the Alpine orogeny. Geologische Rundschau 77, 619-640.

Gómez-Pugnaire, M.T., Galindo-Zaldívar, J., Rubatto, D., González-Lodeiro, F., López Sánchez-Vizcaíno, V., Jabaloy, A., 2004. A reinterpretation of the Nevado-Filábride and Alpujárride Complex (Betic Cordillera): field, petrography and U-Pb ages from orthogneisses western Sierra Nevada, S Spain). Schweizerische Mineralogische und Petrographische Mitteilungen 84, 303-322.

Gómez-Pugnaire, M.T., Rubatto, D., Fernández-Soler, J.M., Jabaloy, A., López Sánchez-Vizcaíno, V., González-Lodeiro, F., Galindo-Zaldívar, J., Padrón-Navarta, J.A., 2012. U–Pb geochronology of Nevado–Filábride gneisses: evidence for the Variscan nature of the deepest Betic complex (SE Spain). Lithos 146-147, 93-111.

Jabaloy, A., 1993. La estructura de la región occidental de la Sierra de los Filabres (Cordilleras Béticas). Tierras del Sur, Universidad de Granada, Granada, Spain 9, pp. 1-261.

Jabaloy-Sánchez, A., Talavera, C., Gómez-Pugnaire, M.T., López Sánchez-Vizcaíno, V., Vázquez, M., Rodríguez-Peces, M.J., Evans, N.J., 2018, U-Pb ages of detrital zircons from the Internal Betics: A key to deciphering paleogeographic provenance and tectonostratigraphic evolution. Lithos 318–319, 244–266. Doi: 10.1016/j.lithos.2018.07.026

Kirchner, K.L., Behr, W.M., Loewy, S., Stockli, D.F., 2016. Early Miocene subduction in the western Mediterranean: Constraints from Rb-Sr multimineral isochron geochronology. Geochemistry, Geophysics, Geosystems 17. Doi: 10.1002/2015GC006208

Kroner, U., Romer, R.L., 2013. Two plates - Many subduction zones: The Variscan orogeny reconsidered. Gondwana Research 24, 298-329.

Laborda-López, C., Aguirre, J., Donovan, S.K., 2013. Asociaciones de macrofósiles en rocas metamórficas del Complejo Nevado-Filábride (Zonas Internas de la Cordillera Bética) en Águilas, Murcia (SE España). Tafonomía y biocronoestratigrafía, XXIX Jornadas de Paleontología, Abstracts, pp 83-84.

Laborda-López, C., Aguirre, J., Donovan, S.K., 2015a. Surviving metamorphism: taphonomy of fossil assemblages in marble and calc-silicate schist. Palaios 30, 668-679.

Laborda-López, C., Aguirre, J., Donovan, S.K., Navas-Parejo, P., Rodríguez, S., 2015b. Fossil assemblages and biochronology of metamorphic carbonates of the Nevado-Filábride Complex from the Águilas tectonic arc (SE Spain). Spanish Journal of Palaeontology 30, 275-292.

Lafuste, M.L.J., Pavillon, M.J., 1976. Mise en évidence d'Eifélien daté au sein des terrains métamorphiques des zones internes des Cordillères bétiques. Intérêt de ce nouveau repère stratigraphique: Comptes Rendus de l'Académie des Sciences de Paris 283, 1015-1018.

López Sánchez-Vizcaino, V., Connolly, J.A.D., Gómez-Pugnaire, M.T., 1997. Metamorphism and phase relations in carbonate rocks from the Nevado-Filábride Complex (Cordilleras Béticas, Spain): application of the Ttn + Rt + Cal + Qtz + Gr buffer. Contributions to Mineralogy and Petrology 126, 292-302.

López Sánchez-Vizcaíno, V., Rubatto, D., Gómez-Pugnaire, M.T., Tommsdorff, V, Müntener, O., 2001. Middle Miocene high-pressure metamorphism and fast exhumation of the Nevado-Filábride Complex, SE Spain, Terra Nova 13, 327-332.

Maate, A., Sole De Porta, A.N., Martín-Algarra, A., 1993. Données paléontologiques nouvelles sur le Carnien des séries rouges des Maghrébides (Ghomarides et Dorsale calcaire du Rif septentrional, Maroc). Comptes Rendus de l'Académie des Sciences de Paris 316, 137-143.

Martín-Algarra, A., 1987. Evolución geológica alpina del contacto entre las Zonas Internas y las Zonas Externas de la (Cordillera Bética). Ph D Thesis, Universidad de Granada Martin-Algarra, 1987.

Martínez Catalán, J.R., Arenas, R., Díaz García, F., Abati, J., 1997. Variscan accretionary complex of northwest Iberia: Terrane correlation and succession of tectonothermal events. Geology 25, 1103-1106.

Martínez Catalán, J.R., Fernández-Suárez, J., Meireles, C., González clavijo, E., Belousova, E., Saeed, A., 2008, U-Pb detrital zircon ages in synorogenic deposits of the NW Iberian Massif (Variscan belt): interplay of Devonian–Carboniferous sedimentation and thrust tectonics. Journal of the Geological Society 165, 687-698.

Martínez Catalán, J.R. 2012. The Central Iberian arc, an orocline centered in the Iberian Massif and some implications for the Variscan belt. International Journal of Earth Sciences 101, 1299-1314.

Martínez Catalán, J.R., 2011. Are the oroclines of the Variscan belt related to late Variscan strike-slip tectonics? Terra Nova 23(4), 241-247.

Martínez-Catalán, J.R., Arenas, R., Díaz-García, F., Abati, J., 1997. Variscan accretionary complex of NW Iberia: terrane correlation and succession of tectonothermal events. Geology 25,1103-1106.

Martín-Martín, M., Martin-Rojas, I., Caracuel, J.E., Estevez-Rubio, A., Martin-Algarra, A., Sandoval, J., 2006. Tectonic framework and extensional pattern of the Malaguide Complex from Sierra Espuña (Internal Betic Zone) during Jurassic–Cretaceous: implications for the Westernmost Tethys geodynamic evolution. International Journal of Earth Sciences 95, 815-826.

Martín-Rojas, I., Somma, R., Delgado, F., Estévez, A., Iannace, A., Perrone, V., Zamparelli, V., 2010. Role of sea-level change and synsedimentary extensional tectonics on facies and architecture of Ladinian-Carnian carbonate depositional systems (Alpujarride complex, Betic Internal Zone, SE Spain). Geogaceta 48, 63-66.

Martín-Rojas, I., Somma, R., Delgado, F., Estevez, A., Iannace, A., Perrone, V., Zamparelli, V., 2009. Triassic continental rifting of Pangea: evidence from the Alpujarride carbonates (Betic Cordillera, SE Spain). Journal of the Geological Society, London 166, 447-458.

Marzoli, A., Renne, P., Piccirillo, E.M., Ernesto, M., DeMin, A., 1999. Extensive 200 million-year-old continental flood basalts of the Central Atlantic Magmatic Province. Science 284, 616-618.

Matte, Ph., 1991. Accretionary history and crustal evolution of the Variscan belt in Western Europe. Tectonophysics 196, 309-337.

Matte, Ph., 2002. Variscides between the Appalachians and the Urals: Similarities and differences between Paleozoic subduction and collision belts. In: Martínez Catalán, J.R., Hatcher, R.D. Jr, Arenas, R., Díaz García, F. (eds), Variscan-Appalachian dynamics: The building of the late Paleozoic basement: Boulder, Colorado, Geological Society of America Special Paper 364, 239-251.

Matte, P., 2001. The Variscan collage and orogeny (480-290 Ma) and the tectonic definition of the Armorica microplate: a review. Terra Nov. 13, 122–128. doi:10.1046/j.1365-3121.2001.00327.x

Murphy, J.B., Gutierrez-Alonso, G., Nance, R.D., Fernandez-Suarez, J., Keppie, J.D., Quesada, C., Strachan, R.A., Dostal, J., 2006. Origin of the Rheic Ocean: rifting along a Neoproterozoic suture? Geology 34, 325-328.

Murphy, J.B., Nance, R.D., Cawood, P.A., 2009. Contrasting modes of supercontinent formation and the conundrum of Pangea. Gondwana Research 15, 408-420.

Nance et al., 2010 Nance, R.D, Gutiérrez-Alonso, G., Keppie, J.D., Linnemann, U., Murphy, J.B., Quesada, C., Strachan, R.A., Woodcock, N.H., 2010. Evolution of the Rheic Ocean. Gondwana Research 17, 194-222. Doi:10.1016/j.gr.2009.08.001

Pastor-Galán, D., Gutiérrez-Alonso, G., Murphy, J.B., Fernández-Suárez, J., Hofmann, M., Linnemann, U., 2013a. Provenance analysis of the Paleozoic sequences of the northern Gondwana margin in NW Iberia: Passive margin to Variscan collision and orocline development. Gondwana Res. 23, 1089–1103. doi:10.1016/j.gr.2012.06.015

Pereira, M.F., Gutiérrez-Alonso, G., Murphy, J.B., Drost, K., Gama, C., Silva, J.B., 2017. Birth and demise of the Rheic Ocean magmatic arc(s): Combined U–Pb and Hf isotope analyses in detrital zircon from SW Iberia siliciclastic strata. Lithos 278-281, 383-399.

Pereira, M.F., Chichorro, M., Johnston, S.T., Gutiérrez-Alonso, G., Silva, J.B., Linnemann, U., Hofmann, M., Drost, K., 2012. The missing Rheic Ocean magmatic arcs: provenance analysis of Late Paleozoic sedimentary clastic rocks of SW Iberia. Gondwana Research 3–4(22), 882-891.

Pereira, M.F., Ribeiro, C., Vilallonga, F., Chichorro, M., Drost, K., Silva, J.B., Albardeiro, L., Hofmann, M., Linnemann, U., 2014. Variability over time in the sources of South Portuguese Zone turbidites: evidence of denudation of different crustal blocks during the assembly of Pangaea. International Journal of Earth Sciences 103, 1453-1470.

Pérez-Cáceres, I., Martínez Poyatos, D., Simancas, J.F., Azor, A., 2017. Testing the Avalonian affinity of the South Portuguese Zone and the Neoproterozoic evolution of SW Iberia through detrital zircon populations. Gondwana Res. 42, 177–192. doi:10.1016/j.gr.2016.10.010

Perri, F., Critelli, S., Martín-Algarra, A., Martín-Martín, M., Perrone, V., Mongelli, G., Zattin, G., 2013. Triassic redbeds in the Malaguide Complex (Betic Cordillera-Spain): Petrography, geochemistry and geodynamic implications. Earth-Science Reviews 117, 1-28.

Platt, J.P., Whitehouse, M.J., Kelley, S.P., Carter, A., Hollick, L., 2003. Simultaneous extensional exhumation across the Alboran Basin: Implications for the causes of late orogenic extension. Geology 31 31, 251-254.

Platt, J.P., Anczkiewicz, R., Soto, J.I., Kelley, S.P., Thirlwall, M., 2006. Early Miocene continental subduction and rapid exhumation in the western Mediterranean. Geology 34, 981-984.

Pratt, J.R., Barbeau, D.L., Garver, J.I., Emran, A., Izykowski, T.M., 2015. Detrital Zircon Geochronology of Mesozoic Sediments in the Rif and Middle Atlas Belts of Morocco: Provenance Constraints and Refinement of the West African Signature. J. Geol. 123, 177–200. doi:10.1086/681218

Puga, E., Fanning, M., Díaz de Federico, A., Nieto, J.M., Beccaluva, L., Bianchini, G., Díaz-Puga, M.A., 2011. Petrology, geochemistry and U-Pb geochronology of the Betic Ophiolites: Inferences for Pangaea break-up and birth of the westernmost Tethys Ocean. Lithos 124, 255-272.

Puga, E., Díaz de Federico, A., Nieto, J.M., 2002. Tectonostratigraphic subdivision and petrological characterisation of the deepest complexes of the Betic zone: a review. Geodinamica Acta 15, 23-43.

Ribeiro, M.L., Castro, A., Almeida, A., González Menéndez, L., Jesus, A. Lains, J.A., Lopes, J.C., Martins, H.C.B., Mata, J., Mateus, A., Moita, P., Neiva, A.M.R., Ribeiro, M.A., Santos, J.F., Solá, A.R., 2019, Variscan magmatism. In: Quesada, C., Oliveira, J.T. (Eds.), The Geology of Iberia: A Geodynamic Approach, Regional Geology Reviews 2, 497-526.

Rodriguez-Cañero, R., Jabaloy-Sánchez, A., Navas-Parejo P, Martín-Algarra, A., 2018. Linking Palaeozoic palaeogeography of the Betic Cordillera to the Variscan Iberian Massif: new insight through the first conodonts of the Nevado-Filábride Complex. International Journal of Earth Sciences (Geologische Rundschau) 107(5), 1791-1806. Doi: 10.1007/s00531-017-1572-8

Sánchez Martínez, S., De la Horra, R., Arenas, R., Gerdes, A., Galán-Abellán, A.B., López-Gómez, J., Barrenechea, J.F., Arche, A., 2012. U-Pb Ages of Detrital Zircons from the Permo-Triassic Series of the Iberian Ranges: A Record of Variable Provenance during Rift Propagation. The Journal of Geology 120, 135-154.

Sánchez-Martínez, S., Arenas, R., García, F.D., Martínez Catalán, J.R., Gómez-Barreiro, J., Pearce, J.A., 2007. Careon ophiolite, NW Spain: suprasubduction zone setting for the youngest Rheic Ocean floor. Geology 35, 53-56.

Sánchez-Rodriguez, L., Gebauer, D., 2000, Mesozoic formation of pyroxenites and gabbros in the Ronda area (southern Spain), followed by early Miocene subduction metamorphism and emplacement into the middle crust: U-Pb sensitive high-resolution ion microprobe dating of zircon: Tectonophysics 316, 19-44.

Sánchez-Navas, A., García-Casco, A., Martín-Algarra, A., 2014. Pre-Alpine discordant granitic dikes in the metamorphic core of the Betic Cordillera: tectonic implications. Terra Nova 26, 477-486. Doi :10.1111/ter.12123

Sánchez-Navas, A., García-Casco, A., Mazzoli, S., Martín-Algarra, A., 2017. Polymetamorphism in the Alpujarride Complex, Betic Cordillera, South Spain. The Journal of Geology 125, 637-657.

Santamaría-López, A., Sanz de Galdeano, C., 2018. SHRIMP U–Pb detrital zircon dating to check subdivisions in metamorphic complexes: a case of study in the Nevado–Filábride complex (Betic Cordillera, Spain). International Journal of Earth Sciences, doi: https://doi.org/10.1007/s00531-018-1613-y

Shaw, J., Gutierrez-Alonso, G., Johnston, S.T., Galan, D.P., Pastor-Galan, D., 2014. Provenance variability along the Early Ordovician north Gondwana margin: Paleogeographic and tectonic implications of U-Pb detrital zircon ages from the Armorican Quartzite of the Iberian Variscan belt. Geological Society of America Bulletin 126, 702-719. Doi:10.1130/B30935.1

Shaw, J., Johnston, S.T., Gutiérrez-Alonso, G., Weil, A.B., 2012. Oroclines of the Variscan orogen of Iberia: paleocurrent analysis and paleogeographic implications. Earth and Planetary Science Letters 329-330, 60-70.

Simancas, F., 2019. Variscan Cycle. In: Quesada, C., Oliveira, J.T. (Eds.), The Geology of Iberia: A Geodynamic Approach, Regional Geology Reviews 2, 1-26.

Simon, O., Visscher, H., 1983. El Pérmico de las Cordilleras Béticas. In: Martínez-Diaz C (Ed.), Carbonífero y Pérmico de España: Actas X Congreso Internacional Carbonífero. IGME, Madrid 453-499.

Stephan, T., Kroner, U., Romer, R.L., 2019. The pre-orogenic detrital zircon record of the Peri-Gondwanan crust. Geological Magazine 156, 281-307. Doi: 10.1017/S0016756818000031

Tahiri, A., Montero, P., El Hadi, H., Martínez Poyatos, D., Azor, A., Bea, F., Simancas, J.F., González Lodeiro, F., 2010. Geochronological data on the Rabat-Tiflet granitoids: their bearing on the tectonics of the Moroccan Variscides. J. African Earth Sci. 57, 1–13. doi:10.1016/j.jafrearsci.2009.07.005

Talavera, C., Montero, P., Martínez Poyatos, D., Williams, I.S., 2012. Ediacaran to Lower Ordovician age for rocks ascribed to the Schist–Graywacke Complex (Iberian Massif, Spain): Evidence from detrital zircon SHRIMP U–Pb geochronology. Gondwana Res. 22, 928–942. doi:10.1016/j.gr.2012.03.008

Vermeesch, P., 2012. On the visualisation of detrital age distributions. Chemical Geology, v.312-313, 190-194, doi: 10.1016/j.chemgeo.2012.04.021 0

Voet, H.W., 1967. Geological investigations in the Northern Sierra de Los Filabres around Macael and Cóbdar, southeastern Spain. Ph.D. Thesis, Amsterdam University, The Netherlands.

Williams, J.R., Platt, J.P., 2017. Superposed and refolded metamorphic isograds, and superposed directions of shear during late-orogenic extension in the Alborán Domain, southern Spain. Tectonics 36, 756-786. Doi:10.1002/ 2016TC004358

Wilson, M., 1997. Thermal evolution of the Central Atlantic passive margins: continental break-up above a Mesozoic super-plume. Journal of the Geological Society of London 154, 491-495.

Zindler, A., Staudigel, H., Hart, S.R., Endres, R., Goldstein, S., 1983, Nd and Sm isotopic study of a mafic layer from Ronda ultramafic complex. Nature 304, 226.

Figure and Table captions:

Figure 1.- (A) Tectonic sketch of the Southwestern Mediterranean Sea; (B) Tectonic map of the Betic Cordillera.

Figure 2.- Geological map of the south-eastern Betic Chain with outcrops of the three tectonic complexes of the Internal zones and the location of the Águilas Arc marked (see Fig. 1B for location).

Figure 3.- Geological map of the central area of the Águilas Arc (modified from Espinosa Godoy et al., 1972; Booth-Rea and Silva-Barroso, 2008; Booth-Rea et al., 2009; García-Tortosa et al., 2012), with the location of the studied samples. See location in Fig. 2.

Figure 4.- Lithological columns of the studied successions in the NFC with the location of the studied samples. Yellow stars: meta-detrital samples; red stars: meta-igneous samples. Both lithological columns have the same vertical scale. Successions for the Lomo de Bas units were compiled from Laborda-López et al. (2013, 2015a, b) and Booth-Rea et al (2009). The succession of the Mulhacén units compiled from Booth-Rea and Silva-Barroso (2008), and Booth-Rea et al. (2009).

Figure 5.- Lithological columns of the studied successions in the AC with the location of the studied samples. Yellow stars: meta-detrital samples; red stars: meta-igneous samples. All lithological columns have the same vertical scale. Successions were compiled with data from Booth-Rea and Silva-Barroso (2008), Booth-Rea et al. (2009), and García-Tortosa et al. (2012).

Figure 6.- Geological map of the southern area of the Águilas Arc, near san Juan de los Terreros village, with the location of the Cabezo Blanco orthogneiss and the AG-26 sample (modified from Booth-Rea et al., 2009). See location in Fig. 2.

Figure 7.- Geological map of the northeastern area of the Sierra de las Estancias with the location of sample LP-16-AZ (modified from Fernández-Fernández et al., 2007). See location in Fig. 2.

Figure 8.- Lithological columns of the studied successions in the MC with the location of the studied samples. Yellow stars: meta-detrital samples. All lithological columns have the same vertical scale. The succession from the Sierra de las Estancias area was compiled from Fernández-Fernández et al. (2007). The succession of the Cabo Cope unit is from Espinosa Godoy et al. (1972), and García-Tortosa et al. (2012).

Figure 9.- Results of U-Pb analyses on detrital zircons from Lomo de Bás units (NFC): combination of Kernel Density Estimates plots (KDE, black lines), frequency (grey bars), and relative abundance of age groups based on $^{206}Pb/^{238}U$ (for dates < 1.5 Ga) and $^{207}Pb/^{206}Pb$ (for dates > 1.5 Ga) ages. (A) sample AG-12; (B) sample AG-14; (C) sample AG-17, (D) sample AG-18, (E) Cumulative KDE (blue line) and frequency

(grey bars) for the Lomo de Bás samples; (F) zoom for the ages ranging from 0 to 541 Ma.

Figure 10.- Results of U-Pb analyses of detrital zircons from Tahal Fm samples (Mulhacén units, NFC): combination of Kernel Density Estimates plots (KDE, black lines), frequency (grey bars), and relative abundance of age groups based on ^{206}Pb/^{238}U (for dates < 1.5 Ga) and ^{207}Pb/^{206}Pb (for dates > 1.5 Ga) ages. (A) sample AG-1; (B) sample AG-2; (C) Cumulative KDE (blue line) and frequency (grey bars) for the samples of the Tahal Fm; (D) zoom for the ages ranging from 0 to 541 Ma.

Figure 11.- Results of U-Pb analyses on the core of zircons from orthogneiss AG-13 (Lomo de Bas units, NFC): (A) conventional Concordia diagram, ^{204}Pb corrected, with the concordant data (95% > Concordia > 105%); (B) conventional Concordia diagram, ^{204}Pb corrected, with the most concordant data; (C) probability density plots (red line) and frequency (blue bars) for the concordant data (95% > Concordia > 105%); (D) weighted average of the most concordant data.

Figure 12.- Results of U-Pb analyses on the core of zircons from the orthogneiss AG-16 (Lomo de Bas units, NFC): (A) conventional Concordia diagram with all the data; (B) conventional Concordia diagram, ^{207}Pb corrected, with the most concordant data (90% > Concordia > 110%); (C) probability density plots (red line) and frequency (blue bars) for the most concordant data; (D) weighted average of the most concordant data.

Figure 13.- Results of U-Pb analyses on detrital zircons from samples from the Micaschists and Quartzite Fm (AC): combination of Kernel Density Estimates plots

(KDE, black lines), frequency (grey bars), and relative abundance of age groups based on $^{206}Pb/^{238}U$ (for dates < 1.5 Ga) and $^{207}Pb/^{206}Pb$ (for dates > 1.5 Ga) ages. (A) sample AG-4; (B) sample AG-5; (C) sample AG-6, (D) sample AG-7, (E) Cumulative KDE (blue line) and frequency (grey bars) for the samples from the Micaschists and Quartzite Fm ; (F) zoom for the ages ranging from 0 to 541 Ma.

Figure 14.- Results of U-Pb analyses on detrital zircons from samples from the Meta-detritic Fm (AC: AG-9, AG-11, and AG-15), and from the Miñarros mylonites and breccias (AC: AG-19): combination of Kernel Density Estimates plots (KDE, black lines), frequency (grey bars), and relative abundance of age groups based on $^{206}Pb/^{238}U$ (for dates < 1.5 Ga) and $^{207}Pb/^{206}Pb$ (for dates > 1.5 Ga) ages. (A) sample AG-9; (B) sample AG-11; (C) sample AG-15, (D) sample AG-19, (E) Cumulative KDE (blue line) and frequency (grey bars) for the samples from the Meta-detritic Fm (AG-9, AG-11, and AG-15); (F) zoom for the ages ranging from 0 to 541 Ma.

Figure 15.- Results of U-Pb analyses on the black rims of zircon from the Cabezo Blanco orthogneiss AG-26 (Cantal unit): (A) conventional Concordia diagram with all the data; (B) conventional Concordia diagram, ^{207}Pb corrected, with the maximum at ca. 16 Ma; (C) probability density plots (red line) and frequency (blue bars) for all then data; (D) weighted average of the ca. 16 Ma age.

Figure 16.- Results of U-Pb analyses on the cores of zircon from the Cabezo Blanco orthogneiss AG-26 (Cantal unit): (A) conventional Concordia diagram with all the data; (B) conventional Concordia diagram, ^{207}Pb corrected, with the main population; (C)

probability density plots (red line) and frequency (blue bars) for all then data; (D) weighted average of the main population.

Figure 17.- Results of U-Pb analyses on detrital zircons from samples from the Saladilla Fm (MC): combination of Kernel Density Estimates plots (KDE, black lines), frequency (grey bars), and relative abundance of age groups based on $^{206}Pb/^{238}U$ (for dates < 1.5 Ga) and $^{207}Pb/^{206}Pb$ (for dates > 1.5 Ga) ages. (A) sample AG-10; (B) sample LP-16-AZ; (C) Cumulative KDE (blue line) and frequency (grey bars) for the samples of the Saladilla Fm; (D) zoom for the ages ranging from 0 to 541 Ma.

Figure 18.- Results of U-Pb analyses on detrital zircons from samples from the unconformable Middle Miocene rocks: combination of Kernel Density Estimates plots (KDE, black lines), frequency (grey bars), and relative abundance of age groups based on $^{206}Pb/^{238}U$ (for dates < 1.5 Ga) and $^{207}Pb/^{206}Pb$ (for dates > 1.5 Ga) ages. (A) sample AG-3; (B) sample AG-20; (C) Cumulative KDE (blue line) and frequency (grey bars) for the samples of the Middle Miocene rocks; (D) zoom for the ages ranging from 0 to 541 Ma.

Figure 19.- Comparison between the combined KDE plots determined in Paleozoic samples of the studied area and other regions of the Iberian Peninsula and South France: (A) Lomo de Bas units vs Aulago Fm (Jabaloy-Sánchez et al., 2018); (B) Micaschists and Quartzite Fm vs sample Ri-119 from the Sebtide Complex (Azdimousa et al., 2019); (C) Silurian-Devonian rocks from the Cantabrian and Central Iberian zones (Gutíerrez-Alonso et al.,2015) vs Late Carboniferous rocks from the Cantabrian Zone (Pastor-Galán et al., 2013); (D) Lower Ordovician Armorican Quartzite (Shaw et al.,

2014) vs Ediacaran and Early Cambrian rocks from the Cantabrian and Central Iberian zones (Fernandez-Suarez et al., 2014); (E) Upper Carboniferous rocks from the Pyrenees (Martínez et al., 2016) vs Upper Carboniferous rocks from the Catalonian Massif (Martínez et al., 2016); (F) Upper Carboniferous rocks from the Montagne Noire and Mouthoumet massifs (Martínez et al., 2016), vs Upper Carboniferous rocks from the Priorat Massif (Martínez et al., 2016), vs Upper Carboniferous rocks from Minorca (Martínez et al., 2016); (G) Upper Carboniferous rocks from MC (sample 121, Azdimousa et al., 2019) vs Early Permian Marbella Conglomerate (Esteban et al., 2017); (H) Upper Carboniferous Mira and Brejeira Fms from the South Portuguesse Zone (Pereira et al., 2014) vs Upper Carboniferous Santa Susana Fm from the Ossa Morena Zone (Pereira et al., 2020).

Figure 20.- Paleogeographic reconstruction of the eastern Variscan belt at Early Bashkirian times (modified from Simancas et al. (2005) for NW Africa and from Martínez-Catalán (2011) and Rodríguez-Cañero et al. (2017) for Europe). The proposed location of the NFC, AC and MC with respect to other Variscan Iberian Terranes is included. CIZ, Central Iberian; CZ, Cantabrian; GTMZ, Galicia-Trás-os-Montes; MGCZ, Mid-German Crystalline; MZ, Moldanubian; OMZ, Ossa-Morena; RHZ, Rheno-Hercynian; SPZ, South Portuguese; STZ, Saxo-Thuringian; TBZ, Teplá-Barrandian; WALZ, West Asturian-Leonese.

Figure 21.- Comparison between the combined KDE plots determined in Permian Triassic rocks of the studied area with those from older rocks from the same complexes. Combined KDE from Permian-Triassic samples from the Iberian Massif and Iberian Chain are also included: (A) Samples from the MC: Upper Carboniferous rocks from

MC (sample 121, Azdimousa et al., 2019), vs Early Permian Marbella Conglomerate (Esteban et al., 2017), vs Middle Triassic Saladilla Fm; (B) Samples from the AC: Micaschists and Quartzite Fm, vs sample Ri-119 from the Sebtide Complex (Azdimousa et al., 2019), vs Early-Middle Triassic Meta-detritic Fm; (C) Samples from the NFC: Aulago Fm (Jabaloy-Sánchez et al., 2018), vs Lomo de Bas units, vs Tahal Fm (combination of the data from Jabaloy-Sánchez et al., 2018 and this work); (D) Permian rocks from the Cantabrian Zone (Pastor-Galán et al., 2013), vs Permian rocks from the Iberian Chain (Sánchez-Martínez et al., 2012), vs Lower Triassic rocks from the Iberian Chain (Sánchez-Martínez et al., 2012).

Table 1.- Details of the samples and the analyses carried out; (*) UTM coordinates, ED_1950 ellipsoid, zone 30 S.

U-Pb geochronology of detrital and igneous zircon grains from the Águilas Arc in the Internal Betics (SE Spain): implications for Carboniferous-Permian paleogeography of Pangea

Antonio Jabaloy-Sánchez[1], Cristina Talavera[2], Martín Jesús Rodríguez-Peces[3], Mercedes Vázquez-Vílchez[4], Noreen Joyce Evans[5]

[1]Departamento de Geodinámica, Universidad de Granada, 18002 Granada, Spain.

[2]School of Geosciences, University of Edinburgh, The King's Building, James Hutton Road, EH9 3FE, Edinburgh, UK.

[3]Departamento de Geodinámica, Estratigrafía y Paleontología, Universidad Complutense de Madrid, Madrid, Spain.

[4]Departmento de Didáctica de las Ciencias Experimentales, Universidad de Granada, Granada, Spain.

[5]School of Earth and Planetary Sciences/John de Laeter Center, Curtin University, Bentley 6845, Australia.

Abstract

New U-Pb detrital zircon and U-Pb zircon ages of metaigneous rocks in the Águilas Arc (Betic Chain, SE Spain) allow us to determine the maximum depositional ages of the rocks. Within the Nevado-Filábride Complex, a Late Carboniferous depositional age for the Lomo de Bas schists and quartzites, and a Permian-Triassic maximum depositional age for the Tahal Fm are determined. Within the Alpujárride Complex, the maximum depositional age of the Micaschists and Quartzite Fm is Late Carboniferous and the Meta-detrital Fm was deposited in the Early Permian. Furthermore, the maximum depositional age of the Saladilla Fm in the Maláguide Complex is also Early Permian. The age distribution patterns for the Carboniferous rocks of the Nevado-Filábride and Alpujárride complexes are similar to those from the

Cantabrian Zone of the Iberian Massif, suggesting deposition in Carboniferous foreland basins located eastwards of the Iberian Massif. However, age patterns in Maláguide and samples from the North-eastern Iberian Peninsula and South France show strong similarities suggesting that it can be located near those areas in the Late Carboniferous times.

The samples with Early Permian maximum depositional ages from the three complexes contain more Paleozoic zircon grains relative to the older Carboniferous samples, but have similar age distribution patterns, suggesting that they were deposited in the same basin. Samples from unconformable Middle Miocene sediments have Early Permian youngest zircon populations and age distribution patterns corresponding to a mixing of detrital zircon grains from the Alpujárride and Maláguide complexes. Furthermore, there is no record of any major felsic rocks formation and/or exhumation event after the Early Permian in those two complexes.

1. Introduction

The Variscan-Alleghanian belt (i.e. Martínez Catalán et al., 1997; Matte, 2001; Simancas, 2019) was formed during the Late Paleozoic collision of two major continents: Laurussia (Laurentia-Baltica) and Gondwana. The southern front of the Variscan segment of this orogenic belt is poorly understood due to post-variscan oroclinal bending, Pangea break-up (e.g. Wilson, 1997; Marzoli et al., 1999) and Alpine reworking (Simancas, 2019). Numerous fragments resulting from Gondwana break-up were dispersed and recycled during the Alpine orogeny, and superposition of metamorphic and deformational Alpine events overprinted most Variscan features.

Several of these fragments are interpreted to be currently included within the Internal Zones of the Betic-Rif orogen as tectono-metamorphic complexes. These complexes hold clues to the Variscan and Late-Variscan evolution of the southern domains of the Variscan belt and its relationship with the Gondwanan foreland (i.e. Gómez-Pugnaire et al., 2004, 2012; Sánchez-Navas et al., 2014, 2017; Jabaloy-Sánchez et al., 2018; Rodríguez-Cañero et al., 2018). Zircon U-Pb dating of metamorphosed sedimentary sequences and igneous rocks can provide temporal constraints on this evolution, especially in an area where detrital zircon geochronological data are scarce.

Here, we present U-Pb zircon data from metasedimentary and metaigneous rocks of the Águilas Arc in the eastern Betic Chain, in an effort to provide maximum depositional ages for these rocks, paleogeographic information about the possible sources and, hence, the paleolocation of the different tectonic complexes of the Betic-Rif orogenic system. We will then discuss the implication of these data for both the Variscan and Alpine evolution of this orogenic system.

2. Geological setting

The Alpine Betic-Rif orogen is an arcuate Alpine mountain belt outcropping in both South Spain and North Morocco and formed essentially during Late Paleogene-Neogene times (e.g. Platt et al., 2003; Chaluan et al., 2008) (Fig. 1). According to Balanyá and García-Dueñas (1987), this belt comprises: i) a central allochthonous terrain, the so-called Alborán Domain, ii) the South Iberian Domain, which includes the Triassic to Neogene rocks deposited at the southern paleomargin of the Iberian Peninsula, iii) the North African Domain, comprising Triassic to Neogene rocks deposited at the north-western paleomargin of Africa, and iv) the Flysch Trough units with Cretaceous to Neogene slope/rise and abyssal plain deposits (e.g. Chalouan et al., 2008, and references therein). Furthermore, the Alborán Domain, as originally defined by Balanyá and García-Dueñas (1987), included three metamorphic complexes, namely (from bottom to top): the Paleozoic to Mesozoic Nevado-Filábride Complex (NFC), the Paleozoic to Mesozoic Alpujárride Complex (AC) and the Paleozoic to Paleogene Maláguide Complex (MC) (Fig. 1).

Recently this subdivision has been redefined and a new tectonic framework with only three major domains is emerging. Pratt et al. (2015) and Azdimousa et al. (2019) have indicated that the whole Maghrebian Flysch Domain was part of the North African Domain. Moreover, the Alborán Domain has been redefined and now only comprises two tectonic complexes: the lower AC and the upper MC (see Gómez-Pugnaire et al., 2012, and references therein). Accordingly, the NFC is now considered part of the southern paleomargin of the Iberian Peninsula, which was overridden below the Alborán Domain at 18 to 15 Ma (see López-Sánchez Vizcaino et al., 2001; Gómez-Pugnaire et al., 2004; 2012; Platt et al., 2006; Kirchner et al., 2016).

In the Central part of the Betic-Chain, the previously mentioned metamorphic complexes were deformed by three major E-W trending Tortonian antiforms, but eastwards, left-lateral, roughly N-S trending strike-slip faults rotated and translated the folds towards the North to form the Águilas tectonic Arc (Figs. 1, 2).

2.1. Nevado-Filábride Complex

The NFC is composed of the upper Mulhacén tectonic units (Puga et al., 2002), which underwent Alpine HP (ca. 1.8 GPa) metamorphism at ca. 18-15 Ma (López Sánchez-Vizcaíno et al., 2001; Gómez-Pugnaire et al., 2004, 2012; Platt et al., 2006; Kirchner et al., 2016), and the lower Veleta tectonic units (Gómez-Pugnaire and Franz, 1988; Puga et al., 2002; Rodríguez-Cañero et al., 2018) (Fig. 2, Table 1).

Within the Águilas tectonic Arc, the lower Veleta units are represented by the Lomo de Bas units (Fig. 3, Table 1), which are tectonically overlain by the Mulhacén units (Álvarez and Aldaya, 1985; Álvarez, 1987). The Lomo de Bas units comprise a lower tectonic unit made of ca. 1000 m of alternating graphite-bearing grey and black quartz-schists, garnet and chloritoid-bearing micaschists, and ferruginous quarzitic levels of unknown ages (Laborda-López et al., 2013, 2015a, b) (Fig. 4, Table 1). These rocks include orthogneiss bodies derived from metamorphosed, felsic rocks of unknown age (Álvarez and Aldaya, 1985; Álvarez, 1987), although other orthogneiss bodies within the CNF have yielded Late Carboniferous to Early Permian U-Pb ages (Gómez-Pugnaire et al., 2004, 2012, and references therein). An upper unit tectonically overlays the lower unit, and its succession begins with 600 to 800 m thick graphite-bearing micaschists, quartz schists, and phyllites, which are intercalated with ferruginous quartzite beds (Laborda-López et al., 2015a, b). These rocks are overlain by 80 to 140 m thick low-grade black marbles, with abundant fossils of Early-Middle Devonian age (Emsian-Eifelian, c.f. Lafuste and Pavillon, 1976; Laborda-López et al., 2013, 2015a, b). The succession ends with 130 to 500 m thick graphitic schists, phyllites, and quartzites (Laborda-López et al., 2015a, b) (Fig. 4, Table 1).

In the studied area, the Mulhacén unit succession (Álvarez and Aldaya, 1985; Álvarez, 1987) begins with grey schists and metapsammites of the Permian-Triassic Tahal Fm (Voet, 1967; Jabaloy-Sánchez et al., 2018; Santamaría-López and Sanz de Galdeano, 2018) (Table 1). Moving up section is the Metaevaporite Fm, attributed Permian-Triassic (Leine, 1968; Vissers, 1981) to Paleogene ages (Puga et al., 1996), followed by the marbles, calc-schists, micaschists and quartzites of the Marbles and Calc-Schists Fm (see Voet, 1967; López Sánchez-Vizcaino et al., 1997), for which pre-Permian to Cretaceous ages have been proposed (Tendero et al., 1993; Gómez-Pugnaire et al., 2012) (Fig. 4, Table 1). The succession includes Jurassic metabasite bodies (Puga et al., 2011).

2.2. Alpujárride Complex

In the studied area, the AC includes a thin lower Miñarros unit, which overlies the brittle-ductile extensional shear zone developed at the NFC/AC contact (Figs. 3 and 5) (Álvarez and Aldaya, 1985; Álvarez, 1987; Booth-Rea et al., 2009). At the base of this Complex, the Miñarros unit is ca. 15 m thick and comprises brecciated ferruginous marbles and white quartzitic mylonites of unknown age (Álvarez, 1987) (Fig. 4, Table 1).

Álvarez and Aldaya (1985) and Álvarez (1987) identified several AC tectonic units thrusting over the Miñarros mylonites and breccias (i.e. the Talayón unit, Águilas unit and Las Palomas unit), and Booth-Rea et al. (2009) grouped them into only one tectonic unit, the so-called Las Estancias-Talayón-Palomas unit. Hereafter, and for simplicity, we call it Las Palomas unit (Table 1). The Las Palomas unit has the most complete succession in the area, beginning with ca. 300 m of graphite-bearing micaschists and phyllites alternating with micaceous quartzites from the Micaschists and Quartzite Fm, with an attributed Late Paleozoic age based on correlation with Paleozoic rocks of the MC (Álvarez and Aldaya, 1985; Álvarez, 1987) (Fig. 4, Table 1). The succession follows up with ca. 600 m of phyllites and quartzites from the Meta-detrital Fm made of a quartzite-rich lower member and a phyllite-rich upper member with Permian to Middle Triassic ages (Martín-Rojas et al., 2010; García-Tortosa et al., 2012) (Fig. 4, Table 1). The Middle to Late Triassic Meta-carbonate Fm overlays this succession and is composed of ca. 50 m of marbles and calc-schists (García-Tortosa et al., 2012) with (Fig. 4, Table 1).

Above the Las Palomas unit, the Ramonete unit crops out (Figs. 3, 4) (Álvarez and Aldaya, 1985; Álvarez, 1987; Booth-Rea et al., 2009) and consists of Mesozoic rocks: phyllites and quartzites of the Middle Triassic Meta-detrital Fm (see Simon and Visscher, 1983; Maate et al., 1993; García-Tortosa et al., 2002; Martín-Rojas et al., 2010), and calcitic and dolomitic marbles and calc-schists from the Middle-Upper Triassic Meta-carbonate Fm (García-Tortosa et al., 2002) (Table 1).

Álvarez and Aldaya (1985), and Álvarez (1987) also defined the Cantal unit as an AC tectonic unit thrusting over the Las Palomas unit, or limited by left-lateral strike-slip faults (Figs. 3 and 4, Table 1). However, García-Tortosa et al. (2000) included this unit within the NFC and discussed its adscription to the AC. The Cantal unit is composed of ca. 330 m of migmatitic and felsic gneisses with kyanite and sillimanite bearing schists, graphite bearing schist with staurolite and black marbles and quartzites (see Álvarez and Aldaya, 1985; Álvarez, 1987; Booth-Rea et al., 2009) (Fig. 4, Table 1).

2.3. Maláguide Complex

The MC occurs as relatively small outcrops tectonically emplaced on top of the AC (Figs. 3 and 4). Towards the east, in the Vélez Rubio area (Figs. 2 and 4, Table 1), the MC succession includes ca. 1000 m of greywackes, slates, conglomerates and lesser marbles and black cherts of the pre-Ordovician to Late Carboniferous Piar Group (see Martín-Algarra, 1987) overlain by detached Mesozoic to Cenozoic cover ca. 500 m thick, consisting of red conglomerates, sandstones, pelites, and gypsum of the Middle-Late Triassic Saladilla Fm (see Perri et al., 2013, and references therein) (Fig. 4, Table 1). The succession follows up with ca. 300 m of Late Triassic to Early Cretaceous limestones, dolostones and marls (Castillón Fm, Geel, 1973), unconformably overlain by ca. 200 m of Eocene Nummulite-rich limestones and marls (Xiquena Fm, Geel, 1973) (Fig. 4, Table 1).

In the Águilas Arc area, this succession is usually incomplete and thinned by normal faults, lacking outcrops of the thick Paleozoic succession of the Piar Group, (see Aldaya et al., 1991) (Fig. 4, Table 1). The main outcrops of this complex correspond to the Cabo Cope and Albaida areas (Álvarez and Aldaya, 1985; Álvarez, 1987; García-Tortosa, 2002) (Figs. 3 and 4, Table 1), where a succession beginning with ca. 40 m of red pelites, sandstones and gypsum of the Middle-Late Triassic Saladilla Fm crops out. Following up section, there is ca. 130 m of Late Triassic to Jurassic dolostones, marls, and oolitic limestones of the Castillon Fm (García-Tortosa, 2002, and references therein) (Fig. 4. Table 1). On top, there is an unconformity overlain by ca. 50 m of Oligocene conglomerates and calcarenites (Durand-Delga et al., 1962; Álvarez, 1987).

Unconformably overlying both the MC and AC, there are Middle Miocene sedimentary rocks with a succession that includes red Langhian-Early Serravallian conglomerates and sandstones with clasts derived from rocks present in both complexes (Figs. 3 and 4).

3. Sampling localities and analytical methods

Twenty one samples from the Águilas Arc were studied. Eight samples were collected from the NFC, nine from the AC, two from the MC, and two from the Middle Miocene sedimentary rocks (Table 2, Figs. 3 and 4).

Zircon grains were separated using standard heavy-liquid and magnetic techniques in the Department of Geodynamics of the University of Granada. Grains were handpicked and mounted in epoxy, polished, cleaned and gold coated for cathodoluminescence (CL) imaging on a Mira3 FESEM instrument at the John de Laeter Centre (JdLC), Curtin University, Perth (Australia) and a Carl Zeiss SIGMA HD VP Field Emission SEM at the School of Geosciences, the University of Edinburgh, Scotland (the United Kingdom). Representative CL images have been selected and interpreted in the results section (Figs. 1 to 10 in S3 Supplementary material). In CL images, the lower-U regions are brightly illuminated and higher-U regions are dark, or even black, poorly illuminated regions.

U-Th-Pb geochronological analyses of samples AG-16 and AG-26 were carried out on the SHRIMP IIe/mc instrument of the IBERSIMS lab, University of Granada, Spain, and sample AG-13 was analysed on the Cameca IMS1270 at the NERC Ion Micro-Probe Facility, the University of Edinburgh, United Kingdom (see S1 Supplementary material for a detailed description of the methodologies). Laser ablation inductively coupled plasma mass spectrometry (LA-ICPMS) data collection on the remaining samples was performed at the GeoHistory Facility, JdLC, Curtin University, Perth, Australia. A more detailed description of the methodology is provided within Text S1 in the Supplementary material.

Ages in the text and figures are quoted as $^{206}Pb/^{238}U$ dates for zircon analysis younger than 1500 Ma and as $^{207}Pb/^{206}Pb$ dates for zircon analysis older than 1500 Ma, while errors are at the 2σ level. The distribution of detrital zircon ages were calculated using DensityPlotter 8.5 (Vermeesch, 2012), with a bin of 40 Ma. An adaptive bandwidth of 40 Ma was applied for the Kernel Density Estimators (KDE); except in the zoom windows of the group of ages younger than c. 541 Ma, where a bin of 10 Ma and an adaptive bandwidth of 10 Ma were applied. Errors used in these KDE calculations are at the 1σ level (Figs. 5, 6, 9, 10, 13 and 14). Mixture Models were used as a first approach to the age distribution plots in order to obtain the age of the main populations, however, the accuracy of these models in unsharpened peaks of the KDE was low (i.e. the age esd off-peak), and so the age of main populations was calculated using a weighted mean and assessed by the mean square weighted deviation (MSWD).

The full description, CL images for representative zircon grains, representative Concordia plots, youngest zircon populations and detailed U-Pb analytical datasets of each individual sample are also provided in the supplementary information (Text S2, Figs. 1 to 10 in S3 and Table S1 in the Supplementary material).

Among the different strategies to estimate the Maximum Depositional Age (MDA) of a sample, we have chosen a more conservative approach where the youngest population is defined as the weighted mean of the youngest cluster of grains with overlapping 2σ uncertainty (see Dickinson and Gehrels, 2009, for the method, and Sharman and Malkowski; 2020, for a discussion). The original method contemplates the use of three or more grains, however, we have worked with four or more grains in the calculation. Most of our samples are metadetrital with grains mostly < 400 Ma. The limited curvature of concordia at these young ages combined with the imprecision of the $^{207}Pb/^{235}U$ age, limits the identification of discordance, and, in fact, any level of Pb loss is masked by the uncertainty of the analysis (Bowring and Schmitz, 2003; Ireland and Williams, 2003; Spencer et al., 2016). Therefore, we have tried to minimize the risk of including dates from grains with Pb loss by applying a very conservative youngest population calculation, calculated using Isoplot software (Ludwig, 2003, 2009).

The Multidimensional Scaling (MDS) technique was used to compare the age patterns for our samples with those of previously published samples from the NFC, AC, MC and the Variscan chain. The MDS is a mean of visualizing the level of similarity of individual datasets in two dimensions. In detrital zircon geochronology MDS is used to graphically represent a quantified comparison between the age patterns of two samples: greater distances between samples represent a greater degree of dissimilarity between points on MDS diagrams (Vermeesch, 2013; Spencer and Kirkland, 2015; Wissink et al., 2018). MDS diagrams were produced using the software Provenance, with a

Kolmogorov-Smirnov test for the measurement of the dissimilarity (Vermeesch et al., 2016). Methodology and results of the Kolmogorov-Smirnov test are given in the Supplementary material (Texts S1 and S2, Tables S2 and S3).

4. Results

In this section, we present the distribution histograms and KDE diagrams with the U-Pb results from the detrital zircon grains from the three different complexes (NFC, AC, and MC). For each complex, we have combined and described the U-Pb data for each formation and/or unit.

4.1. Nevado-Filábride Complex

4.1.1. LA-ICPMS results from metadetrital samples

The CL images for samples AG-12, AG-14, AG-17 and AG-18 mostly show zircon grains with continuous oscillatory zoning (Fig. 1 in S3 Supplementary material). There are also some composite grains with cores overgrown by low or high U rims, a few grains with sector zoning, and grains that are structureless (Fig. 1 in S3 Supplementary material).

Independent of their location within the upper or lower Lomo de Bas tectonic unit, putative Upper Carboniferous samples AG-12, AG-14, AG-17 and AG-18 yielded similar ages for the youngest zircon analysed, and similar youngest zircon population ages. The youngest zircon grains have $^{206}Pb/^{238}U$ dates between 284 ± 14 Ma (sample AG-12) and 323 ± 5 Ma (sample AG-18), while the youngest populations show $^{206}Pb/^{238}U$ mean ages between 321 ± 2 Ma (sample AG-17, MSWD = 0.55 and probability = 0.65) and 336 ± 2 Ma (sample AG-14, MSWD = 1.10 and probability = 0.36).

Samples AG-12, AG-14, and AG-18 also have similar age distribution patterns showing a very noticeable Ediacaran component with peak ages between ca. 557 and ca. 618 Ma (between 17.3% and 24.3%, Fig. 5). There are also significant Mesoproterozoic (between 7% and 12%) and Paleoproterozoic (between 17% and 26%) contributions. The Mesoproterozoic population clearly stands out in samples AG-12 and AG-18 with ages clustering at ca. 1001 (7.2%) and 1025 Ma (6.3%), respectively, and the Paleoproterozoic population is clearly identified in sample AG-14 with ages grouping at ca. 1893 and 2032 Ma (13.2%) (Fig. 5). There is a noteworthy difference in sample AG-17; the percentage of Paleozoic ages (36%) in this sample is twice as high as that in the other three samples (15% to 19%) (Fig. 5).

Combining a total of 406 dates (Concordia ranging between 90% and 110%, Table S1 in Supplementary material) obtained from the most similar samples (AG12, AG14 and AG18 of Lomo de Bas quartzites; see Kolmogorov-Smirnov test-S in table S2 in the Supplementary material), the age distribution pattern is characterised by dates ranging from 283 to 3195 Ma (Fig. 5). Within the 67 Paleozoic zircon grains, there are Early Permian (one grain, 283 ± 14, 1.5% with respect to the total amount of Paleozoic grains), Carboniferous (306 ± 4 to 359 ± 8 Ma, 40%), Devonian (368 ± 6 to 405 ± 6 Ma, 9%), Silurian (442 ± 10 Ma, 1.5%), Ordovician (460 ± 12 to 484 ± 8 Ma, 9%) and Cambrian dates (486 ± 7 to 540 ± 7 Ma, 39%) (Fig. 5).

The CL imaging of zircon grains from the Tahal Fm of the Mulhacén units (samples AG-1 and AG-2) shows grains with continuous oscillatory zoning and partially resorbed cores overgrown by low and high U rims (Fig. 2 in S3 Supplementary material). There are also grains with sector zoning and structureless grains (Fig. 1 in S3 Supplementary material).

Individually, samples AG-1 and AG-2 contain Jurassic zircon grains with the youngest zircon grains yielding $^{206}Pb/^{238}U$ dates of 195 ± 8 Ma, and 179 ± 5 Ma, respectively. Both samples also have youngest zircon populations with Permian ages at 275 ± 8 Ma (MSWD = 1.4 and probability = 0.25) and 277 ± 4 Ma (MSWD = 1.12 and probability = 0.35), respectively. Their age distribution patterns are also comparable, with Carboniferous and Ediacaran peaks at ca. 334 and 331 Ma, and ca. 610 and 598 Ma, respectively (Fig. 6). However, there are some differences: i) a minor Early Tonian peak in sample AG-1 at ca. 939 Ma; ii) a higher percentage of Mesozoic and Paleozoic dates in sample AG-2; iii) greater percentage of Mesoproterozoic and Paleoproterozoic zircon grains in sample AG-1; and iv) lack of Mesoarchean dates in sample AG-2 (Fig. 6).

The 259 dates from samples AG-1 and AG-2 (Concordia ranging between 90% and 110%, Table S1 in Supplementary material) were combined in a KDE age distribution with dates from 179 to 2811 Ma (Fig. 6). The 83 Paleozoic zircon grains have Permian (254 ± 11 to 298 ± 8 Ma, 23% with respect to the total amount of Paleozoic grains), Carboniferous (305 ± 9 to 355 ± 10 Ma, 52%), Devonian (363 ± 11 to 410 ± 12 Ma, 7%), Silurian (424 ± 12 to 428 ± 13 Ma, 2%), Ordovician (454 ± 13 to 482 ± 14 Ma, 7%) and Cambrian dates (506 ± 14 to 540 ± 23 Ma, 9%), while the six Mesozoic zircon grains have two Jurassic (179 ± 5 to 195 ± 8 Ma) and four Triassic (209 ± 9 to 239 ± 9 Ma) dates (Fig. 6).

4.1.2. SIMS results of sample AG-13 (orthogneiss) – Lower Lomo de Bas tectonic unit

Twenty-six grains from this orthogneiss were analysed and 27 of the 31 analyses yielded concordant or nearly concordant dates between 191 and 2345 Ma (Fig. 7). Eleven dates plot in a single population with a ^{204}Pb corrected $^{206}Pb/^{238}U$ mean age of

294 ± 2 Ma (MSWD = 0.75 and probability = 0.68) (Fig. 7). These dates are from zircon grains with continuous oscillatory zoning, Th/U ratios between 0.030 and 0.615 and common Pb content from 0.05% to 0.26% (Table S1 in Supplementary material). Therefore, this mean age could represent the best estimate of the crystallization age of the protolith.

There are also 7 slightly younger dates between 264 and 286 Ma defining a tail negatively skewed towards younger ages (Fig. 7), which may relate to Pb loss undetectable with a discordance filter (see Spencer et al., 2016). These dates are from grains with continuous oscillatory zoning (Fig. 3 in S3 Supplementary material), one rim from a composite grain, Th/U ratios between 0.062 and 0.692 and much higher common Pb contents (up to 0.35%; Table S1 in Supplementary material). Thus, they were not taken into account for the age calculation in order to avoid including dates from grains with possible Pb loss.

The youngest ^{204}Pb corrected $^{206}Pb/^{238}U$ date for this dataset is 191 ± 3 Ma (Table S1 in Supplementary material). This date is from the rim of a composite grain, has a Th/U ratio of 0.011 and could be related to a metamorphic event in this area, linked to the intrusion of Early Jurassic mafic rocks (Puga et al., 2011).

4.1.3. SHRIMP IIe/mc analysis on zircon grains from sample AG-16 (orthogneiss) – Lower Lomo de Bas tectonic unit

Sample AG-16 provided scarce euhedral bipyramidal prismatic zircon crystals with dimensions between 80 and 200 μm. The CL imaging shows partially resorbed cores overgrown by low or high U rims with well-defined oscillatory zoning and a few grains with continuous oscillatory zoning (Fig. 4 in S3 Supplementary material).

Twenty-one U-Pb analyses on 18 different crystals yielded 15 concordant or nearly concordant dates (discordance <5%) ranging from 284 to 674 Ma (Fig. 8). Eight of those 13 analyses plotted as a single population with a ^{207}Pb corrected $^{206}Pb/^{238}U$ mean age of 289 ± 3 Ma (MSWD = 1.4 and probability = 0.20) (Fig. 8). All these analysis were performed in grains with continuous oscillatory zoning, U and Th contents of 205-1415 and 53-426 ppm, respectively, and Th/U ratios between 0.07 and 1.03 (Table S1 in Supplementary material). The obtained mean age is therefore considered the best estimate of the crystallization age of the parent rocks for the orthogneiss. The remaining dates (330 to 674 Ma) were from cores of composite grains and grains with continuous oscillatory zoning and are considered inherited cores and xenocrysts, respectively (Fig. 8).

4.2. Alpujárride Complex

4.2.1. LA-ICPMS results from samples from the Micaschists and Quartzite Fm

The CL images of zircon grains of samples AG-4, AG-5, AG-6 and AG-7 from the Micaschists and Quartzite Fm show grains with continuous oscillatory zoning and complex grains with a partially resorbed core overgrown by low or high U rim. There are also a few grains with sector zoning and structureless grains (Fig. 5 in S3 Supplementary material).

The age distribution patterns of the 4 aforementioned samples show some similarities (Fig. 9, and see Kolmogorov-Smirnov test-S in table S2 in the Supplementary material). There are two main peaks: i) a main Ediacaran peak with ages between ca. 600 and 631 Ma; and ii) a secondary Early Tonian-Late Stenian peak with ages between ca. 996 and 1040 Ma.

However, some differences are also noteworthy: i) samples AG-6 and AG-7, located at the top of the formation, have an Early Orosirian-Late Rhyacian population at ca. 2055 and 2033 Ma, respectively, that is absent in samples AG-4 and AG-5 at the base of the formation (Fig. 9); ii) samples from the top of the formation also have a Paleoarchean component that is lacking at the bottom; iii) there were no Mesoarchean dates found in sample AG-6; iv) the age of the youngest zircon grains decreases from the bottom to the top of the formation; that is, from 328 ± 10 Ma and 306 ± 6 Ma in samples AG-4 and AG-5, respectively, to 296 ± 4 Ma and 299 ± 7 Ma in samples AG-6 and AG-7, respectively; and finally, v) the youngest zircon population in sample AG-5 is Late Carboniferous (308 ± 4 Ma) contrasting with those from the other three samples that are Cambrian-Early Ediacaran (sample AG-4, 551 ± 5 Ma; sample AG-6, 507 ± 10 Ma; and sample AG-7; 558 ± 7 Ma (Text S2 and Fig. S4 in Supplementary material).

Combining the 562 U-Pb data (Concordia ranging between 90% and 110%, Table S1 in Supplementary material) for the four samples of Micaschits and Quartzite Fm produces an age distribution pattern (Fig. 9). These data cluster into five main peaks at ca. 309, 602, 1039, 2054 and 2547 Ma (Fig. 9). Within the 63 Paleozoic zircon grains, there are: Permian (296 ± 4 to 298 ± 7 Ma, 5% with respect to the total amount of Paleozoic grains), Carboniferous (304 ± 5 to 359 ± 9 Ma, 32%), Devonian (365 ± 8 to 390 ± 7 Ma, 9%), Ordovician (448 ± 13 to 482 ± 10 Ma, 14%) and Cambrian dates (460 ± 17 to 541 ± 9 Ma, 40%) (Fig. 9).

4.2.2. LA-ICPMS results from samples from the Middle Triassic Meta-detrital Fm

The CL imaging of zircon grains from samples AG-9, AG-11, and AG-15 shows grains with continuous oscillatory zoning and some partially resorbed cores with low or high U overgrowths. There are also grains with sector zoning (Fig. 6 in S3 Supplementary material).

The youngest zircon grains in these samples have $^{206}Pb/^{238}U$ dates ranging from 214 ± 2 and 288 ± 4 Ma, while their youngest zircon populations have $^{206}Pb/^{238}U$ mean ages varying between 287 ± 1 Ma (sample AG-11, MSWD = 1.11 and probability = 0.35) and 474 ± 3 Ma (sample AG-15, MSWD = 0.71 and probability = 0.54).

The age distribution patterns from these samples display two or three main populations: a Permian-Late Carboniferous peak (ca. 287 Ma in samples AG-9: 16.2%, and AG-11: 6.0%), one or two Ediacaran-Cryogenian peaks (from ca. 546 to ca. 661 Ma, in all samples: 4.4%, 12.0%, and 7.3%) and a Tonian-Stenian peak (from ca. 963 to ca. 1016 Ma in samples AG-9: 19.1% and AG-15: 6.5%) (Fig. 10).

The dates of samples AG-9, AG-11, and AG-15 from the Meta-detrital Fm range from 214 Ma to 2941 Ma, and are Paleozoic (275 ± 3 to 541 ± 7 Ma, 17% to 39%), Neoproterozoic (542 ± 8 to 998 ± 13 Ma, 34% to 57%), Mesoproterozoic (1004 ± 13 to 1552 ± 37 Ma, 6% to 13%), Paleoproterozoic (1655 ± 26 to 2451 ± 24 Ma, 7% to 13%) and Neoarchean (2503 ± 28 to 2762 ± 47 Ma, 4% to 7%) in age. It is worth noting that only sample AG-15 yielded one Mesoarchean date (2941 ± 15 Ma, 1%) and sample AG-11 yielded one Triassic date (214 ± 2 Ma, 1%), (Fig. 10). When we combine the 392 U-Pb data (Concordia ranging between 90% and 110%, Table S1 in Supplementary material) from samples AG-9, AG-11, and AG-15, we obtain a cumulate age distribution pattern (Fig. 10). These data cluster into three main peaks at ca. 287, 570, 964Ma (Fig. 10). Within the 119 Paleozoic zircon grains, there are: Permian (275 ± 3 to 298 ± 8.0 Ma, 32% with respect to the total amount of Paleozoic grains), Carboniferous (299 ± 7 to 356 ± 3 Ma, 29%), Devonian (366 ± 4 to 417 ± 4 Ma, 3%), Silurian (434 ± 11 to 443 ± 4 Ma, 3%), Ordovician (445 ± 6 to 482 ± 7 Ma, 17%), and Cambrian dates (490 ± 7 to 541 ± 7 Ma, 16%) (Fig. 10).

4.2.3. LA-ICPMS results from samples from the Miñarros quartz mylonites

The CL images of zircon grains from the Miñarros quartz mylonites (sample AG-19) show grains with continuous oscillatory zoning and composite grains with cores overgrown by low and high U rims (Fig. 7 in S3 Supplementary material). One hundred and fifty one analyses were performed on selected zircon grains and 145 yielded concordant or nearly concordant dates between 297 and 3105 Ma. Those dates are Palaeozoic (297 ± 5 to 535 ± 8 Ma, 30%), Neoproterozoic (545 ± 6 to 992 ± 13 Ma, 42%), Mesoproterozoic (1002 ± 10 to 1201 ± 12 Ma, 7%), Paleoproterozoic (1707 ± 69 to 2431 ± 20 Ma, 15%), Neoarchean (2528 ± 18 to 2696 ± 21 Ma, 5%) and Mesoarchean (2974 ± 18 to 3105 ± 23 Ma, 1%), and cluster into six main populations at ca. 300, 305, 550, 566, 622 and 986 Ma (Fig. 10). The 43 Paleozoic zircon grains include Permian (297 ± 5 to 298 ± 4 Ma, 7% with respect to the total amount of Paleozoic grains), Carboniferous (299 ± 4 to 320 ± 4 Ma, 46%), Devonian (386 ± 5 to 413 ± 8 Ma, 5%), Ordovician (463 ± 6 to 483 ± 5 Ma, 19%), and Cambrian dates (495 ± 6 to 535 ± 8 Ma, 23%) (Fig. 10).The youngest zircon $^{206}Pb/^{238}U$ date is 297 ± 5 Ma and the youngest zircon population, comprising 10 dates, has a mean $^{206}Pb/^{238}U$ age of 300 ± 1 Ma (MSWD = 0.64 and probability = 0.76).

4.2.4. SHRIMP IIe/mc datations on zircon grains from sample AG-26 (orthogneiss)

Zircon grains from AG-26 are abundant and euhedral bipyramidal prisms with lengths of about 250 to 80 µm and widths of 100 to 50 µm. Most are brownish translucent crystals. CL imaging shows composite grains with partially resorbed cores overgrown by thick high U rims. Most of the cores show continuous oscillatory zoning truncated by the dark rims (Fig. 8 in S3 Supplementary material). Both domains were targeted for the analysis.

Sixteen U-Pb measurements on 16 different dark rims yielded 14 concordant or nearly concordant dates ranging from 14 to 250 Ma (Fig. 11). Six dates plot in a single population with a ^{207}Pb corrected $^{206}Pb/^{238}U$ mean age of 15.8 ± 0.2 Ma (MSWD = 0.69, probability = 0.63) (Fig. 11). These dates are from zircon with U and Th contents between 4006 and 7413, and 6 and 14 ppm, respectively, and Th/U between 0.001 and 0.004 (Table S1 in Supplementary material).

Thirty analyses were performed on 30 cores from different crystals and all these analyses yielded concordant or nearly concordant dates between 30 and 288 Ma (Fig. 12). Fifteen analyses plot in a single population with a ^{207}Pb corrected $^{206}Pb/^{238}U$ mean age of 283 ± 2 Ma (MSWD = 0.76 and probability = 0.71) (Fig. 12). These analyses are from zircon grains with U and Th contents between 377 and 1919, and 32 and 137 ppm, respectively, and Th/U between 0.05 and 0.21 (Table S1 in Supplementary material).

4.3. Maláguide Complex and unconformable Middle Miocene red conglomerates and sandstones

Samples LP-16-AZ and AG-10 contained zircon grains displaying either continuous oscillatory zoning, partially resorbed cores overgrown by low or high U rims, or sector zoning. There were also a few structureless zircon grains (Fig. 9 in S3 Supplementary material)

The youngest zircon grains in these two samples have $^{206}Pb/^{238}U$ ages of 277 ± 7 and 283 ± 15 Ma, respectively, while the youngest zircon populations have mean $^{206}Pb/^{238}U$ ages of 279 ± 3 Ma (MSWD = 0.57 and probability = 0.63) and 492 ± 8 Ma (MSWD = 1.3 and probability = 0.28), respectively.

The age distribution patterns of samples AG-10 and LP-16-AZ are significantly different (Fig. 13). The two main populations in sample AG-10 are Ediacaran (population between 587 ± 14 and 615 ± 16 Ma, mean at ca. 602 Ma: 12.8%) and Stenian (population between 1064 ± 30 and 1085 ± 22 Ma, mean at ca. 1074 Ma: 4.0%), while in sample LP-16-AZ, they are Carboniferous (population between 299 ± 7 and 310 ± 8 Ma, mean at ca. 305 Ma 17.8%) and Ediacaran (population between 597 ± 14 and 618 ± 16 Ma, mean at ca. 608 Ma: 4.4%). The percentage of Paleozoic grains in sample LP-16-AZ is also almost four times higher than that in sample AG-10, while the Neoproterozoic component in sample AG-10 is almost double that in sample LP-16-AZ. Furthermore, Mesoarchean and Neoarchean dates are lacking in sample LP-16-AZ, which does contain a Paleoarchean component.

The dates from the two samples (Fig. 13) include Paleozoic (277 ± 7 to 528 ± 13 Ma, 14 to 52%), Neoproterozoic (546 ± 12 to 992 ± 21 Ma, 33 to 50%), Mesoproterozoic (1002 ± 26 to 1588 ± 21 Ma, 5 to 9 %), and Paleoproterozoic (1793 ± 43 to 2499 ± 33 Ma, 9 to 20%). Sample AG-10 also includes Neoarchean (2515 ± 15 to 2605 ± 32 Ma, 6%), and Mesoarchean (3000 ± 17 Ma, 1%) zircon grains, while sample LP-16-AZ also includes one Paleoarchean (3375 ± 18 Ma, 1%) zircon grain. Within the Paleozoic zircon population, the main difference is the increase (by one order of magnitude) in the number of Carboniferous and Permian grains from 3 and 2 in sample AG-10 to 33 and 18 in sample LP-16-AZ, respectively. The character of the remaining Paleozoic grains is similar in AG-10 and LP-16-AZ (3 and 2 Devonian grains, 1 and 1 Silurian grains, 2 and 10 Ordovician grains, and 7 and 6 Cambrian grains in each sample, respectively).

Samples AG-3 and AG-20 from the unconformable Middle Miocene red conglomerates and sandstones contain zircon grains with either continuous oscillatory zoning or sector zoning (Fig. 10 in S3 Supplementary material). There are also some composite grains with a partially resorbed core overgrown by a thick rim, very similar to those previously described in the Micaschists and Quartzite Fm of the AC. Sample AG-20 also includes a few structureless zircon grains (Fig. 10 in S3 Supplementary material)

The youngest zircons from samples AG-3 and AG-20 have $^{206}Pb/^{238}U$ dates of 248 ± 8 and 177 ± 7 Ma, respectively, while their youngest zircon populations have mean $^{206}Pb/^{238}U$ ages of 582 ± 7 Ma (MSWD = 1.3 and probability = 0.23) and 292 ± 3 Ma (MSWD = 0.91 and probability = 0.47), respectively.

The age distribution patterns of AG-3 and AG-20 are slightly different (Fig. 14). There is only one main population in sample AG-3 (Early Ediacaran: ca. 605 Ma: 12.8%), while there are three main populations in sample AG-20 (Late Ediacaran: ca. 574 Ma, 8.5%; Cryogenian: ca. 691 Ma, 6.4%; Orosirian: ca. 2007 Ma: 6.4%). Moreover, the percentage of Paleozoic (270 ± 6 to 535 ± 12 Ma) zircon grains in sample AG-20 (22%) is almost three times higher than that in AG-3 (300 ± 7 to 508 ± 13, 8%). The Mesoarchean component (2848 ± 31 to 3119 ± 28 Ma) in sample AG-3 (5%) is ten times greater than that in sample AG-20 (with only one grain at 3081 ± 35 Ma, ca. 0.5%). Paleoarchean zircon grains are absent in sample AG-20, but present in sample AG-3 (3205 ± 24 Ma) (Fig. 14). Regarding the Mesozoic component (177 to 249 Ma), sample AG-3 contains one Triassic zircon grain with 248 ± 8 Ma, while sample AG-20 contains one Jurassic zircon grain with 177 ± 7 Ma.

The main difference in the Paleozoic component is the lack of Permian grains in sample AG-3, while sample AG-20 contains 7 grains with dates ranging between 270 ± 6 and 298 ± 7 Ma. They also differ in the content of Carboniferous (3 grains in AG-3; 300 ± 7 to 309 ± 7 Ma, and to 8 grains in AG-20; 304 ± 8 to 334 ± 7 Ma), Silurian (1 grain, 435 ± 17 Ma in AG-3, and 3 grains, from 428 ± 12 to 440 ± 10 Ma in AG-20), Ordovician (1 grain, 446 ± 11 Ma in AG-3, and 5 grains, from 453 ± 10 to 485 ± 10 Ma in AG-20) and Cambrian grains (2 grains, 504 ± 14 to 508 ± 13 Ma in AG-3, and 4 grains, from 487 ± 11 to 535 ± 12 Ma, in AG-20). Samples AG-3 and AG-20 contain the same number of number of Devonian grains (4 grains, 368 ± 10 to 412 ± 11 Ma in AG-3, and 360 ± 9 to 368 ± 10 Ma in AG-20).

5. Discussion

5.1. Depositional age of the graphite-bearing formations of the Nevado-Filábride and Alpujárride complexes

Within the upper or lower Lomo de Bas units, the 4 studied samples yielded youngest zircon grains with 4 dates between 284 ± 14 and 323 ± 5 Ma. As previously stated, we also provide youngest populations (see Dickinson and Gehrels, 2009 for the method, and Sharman and Malkowski; 2020 for a discussion). Their youngest populations vary between 321 ± 2 and 336 ± 2 Ma (see text S2 and Fig. S4 in Supplementary material). Therefore, the youngest dates point towards Early Permian-Late Carboniferous maximum depositional ages (MDA). However, as data from the orthogneisses samples AG-13 and AG-26 highlight, some of the youngest zircon dates can be related to Mesozoic metamorphic events and/or lead loss. Therefore, we prefer the more conservative approach of using the youngest detrital zircon populations. Therefore, we propose a MDA between 321 ± 2 and 336 ± 2 Ma for the quartzites of the Lomo de Bas (i.e., Carboniferous).

The orthogneiss bodies within the Lomo de Bas black schists and quartzites (Álvarez and Aldaya, 1985; Álvarez, 1987) are strongly deformed and metamorphosed, making it difficult to determine whether they represent volcanic rocks or intrusive plutons. However, in either case, these units can help define the minimum depositional age of the Lomo de Bas rocks, as they are located in the uppermost part of the succession (see Fig. 4). If they are volcanic rocks coeval with deposition, they indicate the age of the uppermost layers, and if they are plutons which were intruded post-deposition, they constrain the minimum depositional age of the Lomo de Bas rocks. Samples AG-13 and AG-16 yield $^{206}Pb/^{238}U$ ages for the parent rocks of 294 ± 2 Ma (MSWD = 0.75 and probability = 0.68) and 289 ± 3 Ma (MSWD = 1.4 and probability = 0.20), respectively. The age of both orthogneisses just overlap within uncertainty and, together with the previous MDA, defines a depositional age for the quartzitic rocks of the Lomo de Bas units between Bashkirian (Late Carboniferous) and Artinskian-Sakmarian (Early Permian).

This Late Carboniferous age is compatible with the presence of Early-Middle Devonian fossils in the dark marbles below the quartzites of the upper tectonic unit (Eifelian-Emsian, c.f. Lafuste and Pavillon, 1976; Laborda-López et al., 2013, 2015a, b), and also supports the presence of several superposed tectonic units as suggested by Laborda-López et al. (2013, 2015a, b).

The youngest $^{206}Pb/^{238}U$ zircon dates in samples from the Micaschists and Quartzite Fm of the AC (AG-4, AG-5, AG-6 and AG-7) are Early Permian-Late Carboniferous (328 ± 10 Ma and 296 ± 4 Ma), but the youngest populations in these samples are highly variable; Cambrian-Late Ediacaran (between 507 and 558 Ma) in samples AG-4, AG-6 and AG-7, and Late Carboniferous (308 Ma) in sample AG-5 at the base of the Micaschists and Quartzite Fm. Sample AG-5 indicates a MDA of Late Pennsylvanian age for the AC Micaschists and Quartzite Fm.

5.2. Provenance of zircon in Late Carboniferous samples

The studied samples from both the Lomo de Bas rocks and the Micaschists and Quartzite Fm include Carboniferous grains (8.9% of total grains in the NFC, and 3.6%

of grains in the AC) that could have been sourced from Late-Variscan and Variscan igneous rocks, occupying more than one third of the outcrops of the whole Iberian Massif, and essentially, ca. one half of the Central Iberian Zone (e.g. Arranz and Lago, 2004; Bea, 2004; Casquet and Galindo, 2004; Gallastegui et al., 2004; Ribeiro et al., 2019). Furthermore, they could have been sourced from the oldest granitoids within the Variscan remnants in the Betic Chain, essentially the older orthogneisses in the NFC with U-Pb ages of ca. 301 Ma (Gómez-Pugnaire et al., 2004, 2012). The Carboniferous rocks of both the NFC and AC also include a number of Early Ordovician, Silurian and Devonian dates (4.4% of grains in the NFC and 2.7% of grains in the AC with dates between 484 and 365 Ma). Ordovician zircon grains may have come from the Ollo de Sapo magmatic event (Montero et al., 2007, 2009, Díez-Montes et al., 2010) or other igneous bodies (Rubio-Ordóñez et al. 2012; Talavera et al., 2013; Pereira et al., 2018), while Silurian and Devonian grains may have originated from the volcanic event that is now starting to be recognized in the Central Iberian Zone (Gutiérrez-Alonso et al., 2008), or from the allochthonous complexes where rocks with Silurian and Devonian grains are relatively abundant (see Pastor-Galán et al., 2013, where their sources are explored). For example, they are found within granites in the the Sehoul Block in the Western Moroccan Meseta (Tahiri et al., 2010), and also within metasediments: i) in the Late Devonian Debdou-Mekkam Metasediments in the Eastern Moroccan Meseta (Accotto et al., 2020), ii) in Late Paleozoic metasediments from both the South Portuguese and Ossa-Morena zones (Pereira et al., 2012, 2014, 2017a; Pérez-Cáceres et al., 2017) and iii) in the syn-orogenic rocks below the allochthonous complexes of the Galicia-Tras-Os-Montes (Martínez Catalan et al., 2008).

However, the main detrital zircon component in the Carboniferous rocks of both the NFC and AC is pre-Cambrian, and includes 4 zircon age populations: Ediacaran-

Cryogenian (39.4% in the NFC at ca. 574 Ma, and 5.2% in the AC at ca. 602 Ma), Tonian-Stenian (3.6% in the NFC at ca. 1014 Ma, 5.3% in the AC at ca. 1039 Ma), Orosirian (3.8% in the NFC at ca. 2024 Ma, and 4.8% in the AC at ca. 2054 Ma), and Neoarchean (1.7% in the NFC at ca. 2659 Ma, and 1.6% in the AC at ca. 2547 Ma). The first of these four populations represents the Cadomian-Pan-African orogeny, developed in Gondwana and the peri-Gondwanan terranes, like the Meguma and West Avalonia terranes. The second one represents the Tonian-Stenian magmatic event in the Arabian Shield at ca. 1.0 Ga (see Bea et al., 2010; Fernández-Suárez et al., 2014; Meinhold et al., 2014). The Orosirian population represents the Eburnean orogeny, and the ages of the basement in the cratonic areas of the Saharan Metacraton (see Meinhold et al., 2014).

We can also compare the results presented here with those obtained on samples of a similar age from the Betic Cordillera, Iberian Massif and surrounding areas, as the Pyrenees, Montagne Noire and Mouthoumet massifs (Martínez et al., 2016) (Fig. S5 in the Supplementary material). In the Betic Cordilleras, the Lomo de Bas units have usually been interpreted as part of the Veleta units of the NFC (i.e. Álvarez and Aldaya, 1985; Álvarez, 1987), and their quartzites correlated with the Late Carboniferous Aulago Fm in the Sierra de Filabres area (Jabaloy-Sánchez et al., 2018; Rodríguez-Cañero et al., 2018), which also include the Ediacaran-Cryogenian and Stenian populations mentioned above (Jabaloy-Sánchez et al., 2018) (Fig. S5 in Supplementary material). The main difference is a larger proportion of Devonian and Carboniferous zircon grains within the Lomo the Bas rocks (13 and 49 grains, respectively), when compared to those from the Aulago Fm (7 and 4 grains, respectively; Jabaloy-Sánchez et al., 2018) (Fig. S5 in Supplementary material). Furthermore, the age pattern of sample Ri119 from the Paleozoic basement of a tectonic unit of the Sebtide/Alpujárride

Complex in the Internal Rif (n=144 analyses, Azdimousa et al., 2019) also yields a similar pattern to that in Late Carboniferous samples from the AC and NFC with two main populations at ca. 532 and 992 Ma (Fig. S5 in Supplementary material).

Similar age patterns with these four peaks are found within the Carboniferous and older rocks from the Central Iberian, Cantabrian, and West Asturian-Leonese zones of the Iberian Massif (see Talavera et al., 2012, 2015; Pastor-Galán et al., 2013; Fernández-Suárez et al., 2014; Shaw et al., 2014; Gutierrez-Alonso et al., 2015) (Fig. S5 in Supplementary material).

If we compare the studied samples with the previously discussed age patterns using the MDS plot, we found that all the samples from the Late Carboniferous rocks from the NFC (Jabaloy-Sánchez et al., 2018; this work), AC (Azdimousa et al., 2109; this work) and the Cantabrian Zone (Pastor-Galán et al., 2013) are very similar except for sample AG-17 (Fig. 15). This similarity is indicated by a clustering of all samples from the NFC, AC and the Cantabrian Zone to the upper left of the plot, while sample AG-17 plots near the centre (Fig. 15),

Martínez et al. (2016) analyzed Late Carboniferous rocks from the NE Iberian Peninsula and South France, including samples from the Catalonian Massif, Minorca, Montagne Noire Massif, Mouthoumet Massif, Pyrenees, and Priorat Massif. In order to compare these samples with our data, we have calculated discordance for their dataset, and selected the 780 ages with Concordia between 90% and 110%. The MDS plot shows no similarity with the previously discussed data except for sample AG-17, which together with the samples from Martínez et al. (2016), grouped in a different cluster to those of the NFC, AC and the Cantabrian Zone (Fig. 15). The main differences that explain the observed dissimilarity between these Late Carboniferous samples are the lack of a Stenian peak (Montagne Noire Massif, Mouthoumet Massif, Pyrenees, and

Priorat Massif), or , if present, it is a minor one (Catalonian Massif and Minorca) in the samples from Martinez et al (2016). Furthermore, the Neoarchean population is also absent in the Catalonian Massif, Mouthoumet Massif, Pyrenees, and Priorat Massif areas, but not in the samples from Minorca and Montagne Noire Massif.

Dinis et al. (2018) and Pereira et al. (in press) studied the Late Carboniferous sediments from the Ossa-Morena (Santa Susana Fm: samples StSz2 and StSz4 from Dinis et al., 2018, and SS-1 and SS-2 from Pereira et al., in press). In the MDS plot, they do not show any similarity with the samples from NFC, AC or the Cantabrian Zone, except in the case of the comparison between AG-17 and SS-2 and StSz4 samples. The Santa Susana Fm samples plot far from the other two clusters on the MDS diagram. (Fig. 15). The main difference is the lack of the Stenian and Neoarchean populations in the latter samples. Furthermore, Pereira et al. (2014) studied the South Portuguese Zone of the Iberian Massif (Fig. S5 in Supplementary material), where Late Carboniferous sediments were deposited in the Mira Fm (Serpukhovian-Bashkirian, samples ST-8 and SC-6 from Pereira et al., 2014) and in the Brejeira Fm (Bashkirian-Moscovian, samples AJ-1, AM-3, and TH-5 from Pereira et al., 2014). Samples from both the Mira and Brejeira Fms essentially show no similarity with the samples from the NFC, AC and Cantabrian Zone in the MDS plot, although the AM-3, and TH-5 samples show some similarity with the cluster from sample AG-17 and those from NE Iberian Peninsula and South France (Martinez et al., 2016) (Fig. 15).

All these data suggest that the Late Carboniferous sediments of both the NFC and the AC were sourced and recycled from Variscan rocks containing zircon grains from the Cantabrian, West Asturian-Leonese, and Central-Iberian zones of the Iberian Massif. Furthermore, the sediments incorporated a small number of zircon grains derived from the Late-Variscan felsic rocks. The sediments were mainly pelites rich in organic material, quartz-rich sandstones (quartzwackes in the case of the NFC, Jabaloy, 1993; Rodríguez-Cañero et al., 2018), and black limestones (with conodonts in the case of the NFC rocks; Rodríguez-Cañero et al., 2018) suggesting deposition in open marine anoxic environments (Rodríguez-Cañero et al., 2018). This points to an environment similar to the Carboniferous foreland basins developed in the Cantabrian Zone of the Iberian Massif (see Matte, 2001, Rodríguez-Cañero et al., 2018; Jabaloy-Sánchez et al., 2018) as the most likely paleogeographic location of both complexes (Fig. 16).

In Late Carboniferous times, the Variscan belt was already formed in Western and Central Europe (e.g. Matte, 2001), and most of the rocks of the Cantabrian, West Asturian-Leonese, Central-Iberian zones were deformed and stacked with the rocks of the Rheic Ocean suture zone (i.e. Pastor-Galán et al., 2013). Rocks from the Variscan belt, including rocks from those three stacked zones, were being eroded at Late Carboniferous, and their zircon grains had been stored within the coetaneous sediments in the Cantabrian Zone (see Pastor-Galán et al., 2013), and NFC (Jabaloy-Sánchez et al., 2018). Our data indicate the same case for the rocks of the AC (Fig. 16).

On the other hand, the published data from the samples from the MC with Carboniferous-Early Permian ages have Early Carboniferous (at ca. 329 and 347 Ma respectively), Early Ordovician-Cambrian (ca. 445 and 491 Ma), Ediacaran-Cryogenian (ca. 589 and 649 Ma), Tonian (ca. 932 Ma), and Orosirian populations (ca. 2002 and 2080 Ma) (sample CM-10 from the Marbella Conglomerate from Esteban et al., 2017, and sample Ri121 from Azdimousa et al., 2019, Fig S5 in Supplementary material). However, they show a difference in the number of Neoarchean zircon grains (ca. 2.6 Ga), which are more abundant in sample Ri121 from Azdimousa et al., 2019, Fig. S5 in Supplementary material). In the MDS plot, they are located within the same cluster as sample AG-17 and those from North-eastern Iberian Peninsula and South France.

Therefore, the most likely location of the MC realm was not at the southern paleomargin of Iberia (Esteban et al., 2107), but in the same paleomargin as the North-eastern Iberian Peninsula and South France rocks.

5.3. Permian to Triassic samples from the NFC, AC and MC

Sample AG-26 from the Cabezo Blanco orthogneiss within the Cantal unit yielded zircon grains with textures similar to those described by Gómez-Pugnaire et al., (2004, 2012) in the NFC. The CL imaging of these grains shows cores with continuous oscillatory zoning truncated by dark U-rich rims. These cores yielded a ^{207}Pb corrected $^{206}Pb/^{238}U$ age of 283 ± 2 Ma, while the dark overgrowths have yielded a ^{207}Pb corrected $^{206}Pb/^{238}U$ age of 15.8 ± 0.2 Ma. We propose the former age as the age of the igneous parent rocks of the Cabezo Blanco orthogneiss and the latter age as the age of a metamorphic event affecting this orthogneiss. Similar metamorphic ages have been determined within zircon grains from the NFC (López Sánchez-Vizcaíno et al., 2001, 15.0 ± 0.6 Ma; Gómez-Pugnaire et al., 2004, 2012; 16.5 ± 0.4 Ma and 17.3 ± 0.4 Ma respectively). Furthermore, similar ages were also determined from Lu-Hf on garnets (Platt et al., 2006, between 18 and 14 Ma) and multimineral isochrons on samples of this complex (Kirchner et al., 2016; three ages of 20.1 ± 1.1, 16.0 ± 0.3, and 13.3 ± 1.3 Ma). However, the metamorphic zircon grains from the AC typically have slightly older ages (Sánchez-Rodriguez and Gebauer, 2000, 19.9 ± 1.7 Ma.; Platt et al., 2003; ages between 22.7 and 21.3 Ma; Esteban et al., 2007, 19.2 ± 1.1 Ma), and the AC has yielded additional older ages including a garnet Lu-Hf age of 25 ± 1 Ma (Blichert-Toft et al., 1999), and a garnet and clinopyroxene Sm-Nd age of 21.5 ± 1.8 Ma (Zindler et al., 1983). Therefore, we propose that the Cantal unit is part of the NFC as already proposed by García-Tortosa (2002).

Samples AG-1 and AG-2 come from two quartzites in the upper part of the Tahal Fm within the Mulhacén units. They yielded very similar zircon age patterns, the youngest zircon $^{206}Pb/^{238}U$ dates being Jurassic (195 ± 8 Ma and 179 ± 5 Ma, respectively) and the youngest zircon population being Early Permian (275 ± 8 Ma and 277 ± 4 Ma, respectively). These data match the 259 concordant-nearly concordant analyses from the Tahal Fm published by Jabaloy-Sánchez et al. (2018), in which the youngest zircon population was Early Permian (275 ± 2 Ma) as well (Fig. S6 in Supplementary material).

An estimate of the MDA for the sources of the Tahal Fm based on the youngest zircon grains points to Jurassic. However, our preference is a more conservative estimate for the MDA based on the youngest populations and our proposal is an age younger than Early Permian (275 ± 8 Ma), in agreement with the data provided by Jabaloy-Sánchez et al. (2018), and Santamaría-López and Sanz de Galdeano (2018) for the same rocks in Sierra Nevada and Sierra de los Filabres.

The youngest zircon dates for samples AG-9, AG-11, and AG-15 from the Meta-detrital Fm of the AC are Triassic-Early Permian (between 214 ± 2 Ma and 288 ± 4 Ma) and the youngest zircon populations are Early Permian (287 ± 2, AG-9, and 287 ± 1, AG-11) to Early Ordovician (474 ± 3 Ma, AG-15). We have used the same approach described above to estimate the MDA of the Meta-detrital Fm, proposing an Early Permian (Artinskian) MDA for this formation, older than the Middle Triassic stratigraphic age (ca. 247 to ca. 237 Ma, see Simon and Visscher, 1983; Maate et al., 1993; García Tortosa et al., 2002; Martín-Rojas et al., 2010). Furthermore, the youngest zircon $^{206}Pb/^{238}U$ date and the youngest zircon population in sample AG-19 from the Miñarros unit are 297 ± 5 Ma and 300 ± 1 Ma, respectively, indicating an older MDA

(Gzhelian, Late Pennsylvanian). Samples AG-9, AG-11, AG-15 and AG-19 have similar age patterns to the samples from the Tahal Fm (NFC).

The youngest zircon grains from samples AG-10 and LP-16-AZ from the Saladilla Fm of the MC yielded $^{206}Pb/^{238}U$ dates between 277 ± 7 and 282 ± 15 Ma. Moreover, the youngest zircon populations were 492 ± 8 Ma and 279 ± 3 Ma, respectively, pointing to an Early Permian MDA.

5.4. Provenance for zircon of the Permian to Triassic meta-detrital samples

A common feature of the samples with a Permian MDA from the three complexes (NFC, AC and MC) is an increase in the number of Paleozoic zircon grains with respect to the older Carboniferous samples (Fig. S6 in Supplementary material). The Permian MDA samples show an increase in the number of Permian and Carboniferous zircon grains indicating erosion of Variscan and Late-Variscan felsic rocks in the source areas. In the NFC, the Tahal Fm contains 21% to 27 % Permian-Carboniferous grains (the values are the percentage of the total number of analyses of each sample) (254 to 355Ma), while the Late Carboniferous Lomo de Bas quartzites have 5% to 18% Carboniferous grains, with only two Permian grains. Within the AC, the Meta-detrital Fm has variable contents of Permian-Carboniferous grains (from 3 to 31%, the values are the percentage of the total number of analyses of each sample), while the Late Carboniferous Micaschists and Quartzite Fm has 3% to 6%. Furthermore, in the MC, the Saladilla Fm also displays a variable content of Permian-Carboniferous grains (from 4% to 38%); while the Lower Carboniferous Morales Fm (sample Ri121 from Azdimousa et al., 2019) has 6% Carboniferous grains, and the Permian Marbella Conglomerate (Esteban et al., 2017) has 12 % Permian and Carboniferous grains.

Samples from the Tahal Fm (NFC) have Carboniferous populations between ca. 331 and ca. 334 Ma (“Variscan”), Ediacaran populations between ca. 598 and ca. 610 Ma (“Cadomian”-“Pan-African”), and a Tonian population at ca. 939 Ma (Fig. S6 in Supplementary material). If the “Variscan grains” are excluded (i.e. post- Late Devonian grains which are younger than 370 Ma), the age distribution pattern is similar to that of the Aulago Fm (Jabaloy-Sánchez et al., 2018) and of the Lomo de Bas quartzites, except for a lower number of Tonian-Stenian (ca. 1.0 Ga) and Neoarchean (ca. 2.61 Ga) grains (Figs. S5 and S6 in Supplementary material).

The age distribution patterns for samples from the Meta-detrital Fm (AC) are similar to those in the above mentioned samples from the Tahal Fm (NFC) (Fig. S6 in Supplementary material). Samples from the Meta-detrital Fm also have Permian (“Late-Variscan” at 287Ma), Ediacaran-Cryogenian (“Pan-African”, from ca. 546 to ca. 660 Ma) populations, with minor Tonian-Stenian (from ca. 963 to ca. 1016 Ma) and Rhyacian (“Eburnean”, ca. 2060 Ma) populations (Fig. S6 in Supplementary material). If the <370 Ma zircon grains are excluded, the age distribution pattern is similar to that obtained by combining the Micaschists and Quartzite Fm (AC) datasets (Fig. S6 in Supplementary material).

In the Saladilla Fm (MC), there are Permian (“Late-Variscan” between ca. 279 and 305 Ma), and Ediacaran-Cryogenian populations (“Pan-African”, from ca. 602 to 677 Ma), with minor Stenian (ca. 1074 Ma), Orosirian (“Eburnean”, ca. 1937 Ma) and Neoarchean (ca. 2106 Ma) peaks (Fig. S6 in Supplementary material). They differ from the data of the Carboniferous-Early Permian samples from the same MC (Esteban et al., 2017; Azdimousa et al., 2019), not only in the presence of the Early Permian population, but also in the Stenian and Neoarchean peaks. This distinction in the age patterns is due to the erosion and incorporation of material from Late-Variscan felsic rocks and the increasing number of zircon grains sourced from the Cantabrian, West Asturian-Leonese and Central-Iberian zones.

Comparing these samples with Permian MDA with Permian and Triassic samples from the Iberian Peninsula (Sánchez Martínez et al., 2012; Pastor-Galán et al., 2013; Pereira et al. 2016; Dinis et al., 2018; Gama et al., in press) using the MDS plot, we found that samples from the Tahal Fm (NFC), Meta-detrital Fm (AC) and Saladilla Fm are quite similar, and they project towards the centre of the figure (Fig. 17), while sample LP−16−AZ is slightly separated, thus suggesting that all these samples have the same source area. Furthermore, all show similarities with most of the samples from the Iberian Chain (Sánchez Martínez et al., 2012), Cantabrian Zone (Pastor-Galán et al., 2013), Permian El Viar Basin (Dinis et al., 2018), Triassic Lusitanian Basin (Pereira et al., 2016; Dinis et al., 2018), Triassic Alentejo Basin (Pereira et al., 2017b; Dinis et al., 2018), and Triassic Algarve Basin (Pereira et al., 2017b; Dinis et al., 2018; Gama et al., in press). These similarities can be seen in the MDS plot in which samples PT2, PT4 and PT5 from the Iberian Chain (Sánchez-Martínez et al., 2012), PG2 and PG3 from the Cantabrian Zone (Pastor-Galán et al., 2013), V152 and V154 from the Viar Basin (Dinis et al,., 2018), CM2, SBM-6 and SBM-7 from the Algarve Basin (Pereira et al 2017b; Gama et al., in press), SC−4 from the Alentejo Basin (Pereira et al 2017b), and SO and CO from the Lusitania Basin (Pereira et al., 2016; Dinis et al., 2018) cluster together with the samples from the Betic Cordillera (Fig. 17).

A major question is what tectonic process induced these differences. Vissers (1992) found an Upper Carboniferous to Permian extensional event in the Pyrenees synchronous with uplift and emergence of large parts of the crust and deposition of continental sediments in fault-bounded extensional half-grabens. Subsequently, García-Navarro and Fernández (2004) found an Early Permian faulting event in the SW Iberian

Peninsula where strike-slip and normal faults generated the intracontinental, Early Permian El Viar basin. Those data suggest that during the Permian to Early Triassic breakup of Pangea, tectonic uplift along major normal faults may have exposed different levels of Variscan crust, including the Late-Variscan granitoids, to erosion.

5.5. Unconformable Middle Miocene red conglomerates and sandstones

The samples from Middle Miocene sediments have only two Mesozoic zircon grains (248 ± 8 and 177 ± 7 Ma), and their youngest zircon population has a mean $^{206}Pb/^{238}U$ age of 292 ± 3 Ma, pointing to an Early Permian MDA. Their age distribution patterns correspond to mixing of zircon grains from the AC and MC, confirming that after experiencing HP metamorphism during Oligocene-Early Miocene times (Zindler et al., 1983; Blichert-Toft et al., 1999; Sánchez-Rodriguez and Gebauer, 2000; Platt et al., 2003; Esteban et al., 2007), the AC rocks were exhumated and eroded at the surface during the Middle Miocene. It is noteworthy that these unconformable Middle Miocene sediments were formed at the surface at the same time that the Cantal unit (sample AG-26) and the NFC was experiencing metamorphism in depth. However, the most important conclusions is that there is no record of any major felsic rock formation event after the Early Permian times in the AC or MC, although several stages of continental rifting and the subduction of the AC took place during this period (e.g. Jabaloy-Sánchez et al., 2019).

The U-Pb zircon data presented here have implications for the evolution of both the Variscan and Alpine chains in the western Mediterranean area. The main implications for the Variscan chain is the existence of Late Carboniferous sedimentary basins eastwards of the Iberian Massif, which recorded the erosion of the Variscan Chain formed during the Late Devonian-Carboniferous, and were also affected by the

Late Carboniferous-Early Permian Late Variscan magmatic event. The sedimentary record in these basins was metamorphosed from Oligocene to Middle Miocene times to form the graphite-rich successions of the NFC and AC during the Alpine orogeny.

During the Permian-Triassic, the break-up of Pangea took place and resulted in the formation of three different paleogeographic realms:

i) the Nevado-Filábride realm continued near the Iberian Massif southeastern paleomargin,

ii) the Alpujárride realm separated from the Iberian Massif by rifting during the Triassic-Jurassic (Martín Rojas et al. 2009; Puga et al., 2011),

iii) the Maláguide realm separated from the North-eastern paleomargin of Iberia (Esteban et al., 2107) during the Jurassic (e.g., Martín-Martín et al. 2006).

Those three realms amalgamated during the Cenozoic; first, the AC subducted below the MC, and later, the NFC subducted below the two previously amalgamated complexes at Early Middle Miocene times. During these processes, the Cantal unit was partially melt, leading to the formation of migmatites. Another line of correlation is the age of the felsic intrusive rocks reported here and in previous works (Gómez-Pugnaire et al., 2014; 2012). The Permian age of the volumetrically minor intrusive bodies (301 to 282 Ma, Gómez-Pugnaire et al., 2004, 2012; this work) is similar to granites in the CZ (286 to 297 Ma; Gutiérrez-Alonso et al., 2011), while the significantly more abundant granites in the WALZ and the CIZ are, in general, older (321 to 290 Ma, Martins et al., 2019, and references therein).

7. Conclusions

New U-Pb detrital zircon ages in rocks from the Águilas Arc provide maximum depositional ages for their parent rocks. Orthogneisses in the NFC may have volcanic or plutonic parent rocks, but as they are located in the uppermost part of the Lomo de Bas succession, they can indicate a minimum depositional age for these rocks (Sakmarian-Artinskian, 294 ± 2 Ma and 289 ± 3 Ma), regardless of their igneous classification. In the NFC, the true depositional age of the Lomo de Bas schists and quartzites is Late Carboniferous to Early Permian (ranging between 321 ± 2 and 289 ± 3 Ma), while the MDA of the Tahal Fm is confirmed as Early Permian. In the AC, the MDA of the Micaschists and Quartzite Fm is also Late Carboniferous (308 ± 4 Ma), and that of the Meta-detrital Fm is Early Permian (287 ± 1 Ma). Furthermore, the MDA of the Saladilla Fm (Maláguide Complex) is also Early Permian (279 ± 3 Ma).

The age patterns from the Upper Carboniferous rocks of the NFC and AC are similar, and also similar to those from Upper Carboniferous of the Cantabrian Zone of the Iberian Massif, suggesting similar source areas. The most likely paleogeographical location of both complexes was in Late Carboniferous marine basins located eastwards of the Iberian Massif. However, the age patterns show differences compared with those from the Upper Carboniferous rocks of the MC, and from the South Portuguese and Ossa-Morena zones of the Iberian Massif. On the other hand, age patterns from Upper Carboniferous rocks of the MC show some similarities with those from the North-eastern Iberian Peninsula and South Francia. Therefore, the paleogeographic location of the MC could have been different from that of the NFC and AC, and it was probably located near the Ossa-Morena Zone and the other rocks derived from the West African Craton.

The samples with Early Permian MDA from the three complexes (NFC, AC, and MC) have more Paleozoic zircon grains than the Late Carboniferous samples, and similar age patterns. This data can be explained if zircon grains from the main Variscan orogenic relief were recycled, while unroofing of footwalls of faults also exposed Late

Variscan granitoids at the surface. It is possible that these zircon grains were deposited in the same basin, likely the long-lived Iberian Permian-Triassic depositional basins. Samples from the unconformable Middle Miocene sediments have Early Permian MDA (292 ± 3 Ma) and age distribution patterns corresponding to a mixing of zircon grains from the AC and MC, and thus, do not record formation of felsic rocks since the Early Permian.

Acknowledgements

This paper is dedicated to the memory of Dr. Fernando Álvarez Lobato, who passed away while this contribution was written. We are indebted to Mike Hall and Brad McDonald for their technical support on sample preparation and LA-ICPMS, respectively. The CL imaging was carried out in Curtin University's Microscopy & Microanalysis Facility, of which instrumentation has been partially funded by the University, State and Commonwealth Governments, and the Scanning Electron Microscope (SEM) Facility at the University of Edinburgh. Analysis in the John de Laeter Centre GeoHistory Facility was enabled by AuScope (auscope.org.au) and the Australian Government via the National Collaborative Research Infrastructure Strategy (NCRIS). This work is supported by grants CGL2016-75224-R, and CGL2015-71692-P (MINECO/FEDER, Spain) and RNM-208 (Junta de Andalucía, Spain). This is the IBERSIMS Publication No. 70.

References

Accotto, C., Martínez Poyatos, D.J., Azor, A., Jabaloy-Sánchez, A., Talavera, C., Evans, N.J., Azdimousa, A., 2020. Tectonic evolution of the Eastern Moroccan Meseta: from Late Devonian fore-arc sedimentation to Early Carboniferous collision of an Avalonian promontory. Tectonics, 38, e2019TC005976,https://doi.org/10.1029/2019TC005976

Accotto, C., Martínez Poyatos, D.J., Azor, A., Talavera, C., Evans, N.J., Jabaloy-Sánchez, A., Azdimousa, A., Tahiri, A.; El Hadi, H., 2019. Mixed and recycled detrital zircons in the Paleozoic rocks of the Eastern Moroccan Meseta: paleogeographic inferences. Lithos 338-339, 73-86, https://doi.org/10.1016/j.lithos.2019.04.011

Aldaya, F., Álvarez, F., Galindo-Zaldívar, J., González-Lodeiro, F., Jabaloy, A., Navarro-Vilá, F., 1991. The Maláguide-Alpujárride contact (Betic Cordilleras, Spain): a brittle extensional detachment, Comptes Rendus de l'Académie des Sciences de Paris 313, 1447-1453.

Álvarez, F., 1987. Subhorizontal shear zones and their relation to nappe movements in the Cantal and Miñarros units. Eastern Betic Zone (Spain). Geologie en Mijnbouw 66, 101-110.

Álvarez, F., Aldaya, F., 1985. Las unidades de la Zona Bética en la región de Águilas-Mazarrón (Prov. de Murcia). Estudios Geológicos 41, 139-146.

Arranz, E., Lago, M., 2004. El plutonismo sin- y tardi-varisco en los Pirineos. In: Vera, J.A., (Ed.) Geología de España, SGE-IGME, Madrid, 263-266.

Azdimousa, A., Jabaloy-Sánchez, A., Talavera, C., Asebriy, L., González-Lodeiro, F., Evans, N.J. 2019. Detrital zircon U-Pb ages in the Rif Belt (northern Morocco): Paleogeographic implications. Gondwana Research 70, 133-150, https://doi.org/10.1016/j.gr.2018.12.008

Balanyá, J.C., García-Dueñas, V., 1987. Les directions structurales dans le Domaine d'Alborán de part et d'autre du Détroit de Gibraltar. Comptes Rendus de l'Académie des Sciences de Paris 304, 929-932.

Bea, F., 2004. La naturaleza del magmatismo de la Zona Centroibérica: consideraciones generales y ensayo de correlación. In: Vera, J.A., (Ed.) Geología de España, SGE-IGME, Madrid, 128-133.

Bea, F., Montero, P., Talavera, C., Abu Anbar, M., Scarrow, J., Molina, J.F., Moreno, J.A., 2010. The palaeogeographic position of Central Iberia in Gondwana during the Ordovician: evidence from zircon geochronology and Nd isotopes. Terra Nova 22, 341-346.

Booth-Rea, G., Silva Barroso, P.G., (2008). Mapa Geológico de España escala 1:50.000. Edición Digital. Hoja 975, Puerto Lumbreras. Instituto Geológico y Minero de España, Madrid.

Blichert-Toft, J., Albarède, F., Kornprobst, J., 1999, Lu-Hf isotope systematics of garnet pyroxenites from Beni Bousera, Morocco: Implications for basalt origin. Science 283, 1303-1306

Booth-Rea, G., Silva Barroso, P.G., Bardají Azcárate, T., Martín Serrano, A., (2009). Mapa Geológico de España escala 1:50.000. Edición Digital. Hoja 997, Águilas. Instituto Geológico y Minero de España, Madrid.

Bowring, S.A., Schmitz, M.D., 2003. High-precision U-Pb zircon geochronology and the stratigraphic record. Reviews in Mineralogy and Geochemistry 53, 305-326, https://doi.org/10.2113/0530305

Casquet, C., Galindo, C., 2004. Magmatismo varisco y postvarisco en la Zona de Ossa-Morena. In: Vera, J.A., (Ed.) Geología de España, SGE-IGME, Madrid, 194-198.

Chalouan, A., Michard, A., El Kadiri, K., Negro, F., Frizon de Lamotte, D., Soto J.I., Saddiqi, O., 2008. The Rif Belt. In: Michard, A., Frizon de Lamotte, D., Saddiqi, O., Chalouan, A., (Eds.) Continental Evolution: The Geology of Morocco.

Lecture Notes in Earth Sciences, vol 116, pp. 203-302, Springer-Verlag, Berlin Heidelberg.

Dallmeyer, R.D., Martínez Catalán, J.R., Arenas, R., Gil Ibarguchi, J.I., Gutiérrez-Alonso, G., Farias, P., Aller, J., Bastida, F., 1997. Diachronous Variscan tectonothermal activity in the NW Iberian Massif: Evidence from 40Ar/39Ar dating of regional fabrics. Tectonophysics 277, 307–337, https://doi.org/10.1016/s0040-1951(97)00035-8

Dickinson, W.R., Gehrels, G.E., 2009. Use of U-Pb ages of detrital zircons to infer maximum depositional ages of strata: a test against a Colorado Plateau Mesozoic database. Earth and Planetary Science Letters 288 (1-2), 115-125, https://doi.org/10.1016/j.epsl.2009.09.013

Díez-Montes, A., Martínez-Catalán, J.R., Bellido Mulas, F., 2010. Role of the Ollo de Sapo massive felsic volcanism of NW Iberia in the Early Ordovician dynamics of northern Gondwana. Gondwana Research 17, 363-376, https://doi.org/10.1016/j.gr.2009.09.001

Dinis, P.A., Fernandes, P., Jorge, R.C.G.S., Rodrigues, B., Chew, D.M., Tassinari, C.G., 2018. The transition from Pangea amalgamation to fragmentation: constraints from detrital zircon geochronology on West Iberia paleogeography and sediment sources. Sedimentary Geology 375, 172-187.

Durand-Delga, M., Escalier des Orres, P., Fernex, F., 1962. Sur la présence de Jurassique et d'Oligocène a l'ouest de Carthagene (Espagne méridionale)". Comptes Rendus de l'Académie des Sciences de Paris 255, 1755-1753.

Espinosa Godoy, J., Herrera López, J.L., Pérez Rojas, A., 1972. Mapa Geológico de España escala 1:50.000. Hoja 997bis, Cope. Instituto Geológico y Minero de España, Madrid

Esteban, J.J., Cuevas, J., Tubía, J.M., Liati, A., Seward, D., Gebauer, D., 2007. Timing and origin of zircon-bearing chlorite schists in the Ronda peridotites (Betic Cordilleras, Southern Spain). Lithos 99, 121-135.

Esteban, J.J., Cuevas, J., Tubía, J.M., Gutiérrez-Alonso, G., Larionov, A., Sergeev, S., Hofmann, M., 2017. U–Pb detrital zircon ages from the Paleozoic Marbella Conglomerate of the Malaguide Complex (Betic Cordilleras, Spain). Implications on Paleotethyan evolution. Lithos 290-291, 34-47.

Fernández-Fernández, E.M., Jabaloy-Sánchez, A., Nieto, F., González-Lodeiro, F., 2007. Structure of the Maláguide Complex near Vélez Rubio (Eastern Betic Cordillera, SE Spain). Tectonics 26, TC4008, https://doi.org/10.1029/2006TC002019

Fernández-Suárez, J., Gutiérrez-Alonso, G., Jeffries, T.E., 2002. The importance of along-margin terrane transport in northern Gondwana: insights from detrital zircon parentage in Neoproterozoic rocks from Iberia and Brittany. Earth and Planetary Science Letters 204, 75-88.

Fernández-Suárez, J., Gutiérrez-Alonso, G., Pastor-Galán, D., Hofmann, M., Murphy, J.B., Linnemann, U., 2014. The Ediacaran–Early Cambrian detrital zircon record of NW Iberia: possible sources and paleogeographic constraints. International Journal of Earth Sciences 103, 1335–1357. https://doi.org/10.1007/s00531-013-0923-3

Gallastegui et al., 2004. Magmatismo. In: Vera, J.A., (Ed.) Geología de España, SGE-IGME, Madrid, 63-68.

Gama, C., Pereira, M.F., Crowley, Q.G., Dias da Silva, Í., Silva, J.B., in press. Detrital zircon provenance of Triassic sandstone of the Algarve Basin (SW Iberia):

Evidence of Gondwanan- and Laurussian-type sources of sediment. Geological Magazine. https://doi.org/10.1017/S0016756820000370

García-Navarro, E., Fernández, C., 2004. Final stages of the Variscan orogeny at the southern Iberian Massif: lateral extrusion and rotation of continental blocks. Tectonics, 23:TC6001. https://doi.org/10.1029/2004TC001646

García Tortosa, F.J., Leyva Cabello, F., Bardaji Azcárate, T., 2012. Mapa Geológico de España escala 1:50.000. Edición Digital. Hoja 976, Mazarrón. Instituto Geológico y Minero de España, Madrid.

García Tortosa, F.J., López-Garrido, A.C., Sanz de Galdeano, C., 2000. Présence du complexe tectonique Malaguide à l’ouest de Carthagéne (zone interne Bétique, Espagne). Comptes Rendus de l’Académie des Sciences de Paris 330, 139-146.

García-Tortosa, F.J., 2002. Los Complejos Tectónicos Alpujárride y Maláguide en el sector oriental de la Zona Interna Bética. Estratigrafía, relaciones tectónicas y evolución paleogeográfica durante el Triásico. PhD Thesis, Universidad de Granada.

Geel, T., 1973. The geology of the Betic of Malaga, the Subbetic and the zone between these two units in the Velez Rubio area (Southern, Spain). GUA Papers of Geology.

Gómez-Pugnaire, M.T., Franz, G., 1988. Metamorphic evolution of the Paleozoic series of the Betic Cordilleras (Nevado-Filabride complex, SE Spain) and its relationship with the Alpine orogeny. Geologische Rundschau 77, 619-640.

Gómez-Pugnaire, M.T., Galindo-Zaldívar, J., Rubatto, D., González-Lodeiro, F., López Sánchez-Vizcaíno, V., Jabaloy, A., 2004. A reinterpretation of the Nevado-Filábride and Alpujárride Complex (Betic Cordillera): field, petrography and U-Pb ages from orthogneisses western Sierra Nevada, S Spain). Schweizerische

Mineralogische und Petrographische Mitteilungen 84, 303-322.

Gómez-Pugnaire, M.T., Rubatto, D., Fernández-Soler, J.M., Jabaloy, A., López Sánchez-Vizcaíno, V., González-Lodeiro, F., Galindo-Zaldívar, J., Padrón-Navarta, J.A., 2012. U–Pb geochronology of Nevado–Filábride gneisses: evidence for the Variscan nature of the deepest Betic complex (SE Spain). Lithos 146-147, 93-111.

Gutiérrez-Alonso, G., Murphy, J.B., Fernández-Suárez, J., Hamilton, M.A., 2008. Rifting along the northern,Gondwana margin and the evolution of the Rheic,Ocean: a Devonian age for the El Castillo volcanic,rocks (Salamanca, Central Iberian Zone). Tectonophysics 461, 157-65, https://doi.org/10.1016/j.tecto.2008.01.013

Gutiérrez-Alonso, G., Fernández-Suárez, J., Jeffries, T.E., Johnston, S.T., Pastor-Galán, D., Murphy, J.B., Franco, M.P., Gonzalo, J.C., 2011. Diachronous post-orogenic magmatism within a developing orocline in Iberia, European Variscides. Tectonics 30, TC5008. http://dx.doi.org/10.1029/2010TC002845

Ireland, T.R., Williams, I.S., 2003. Considerations in zircon geochronology by SIMS. Reviews in Mineralogy and Geochemistry 53, 215-241, https://doi.org/10.2113/0530215

Jabaloy, A., 1993. La estructura de la región occidental de la Sierra de los Filabres (Cordilleras Béticas). Tierras del Sur, Universidad de Granada, Granada, Spain 9, pp. 1-261.

Jabaloy-Sánchez, A., Talavera, C., Gómez-Pugnaire, M.T., López Sánchez-Vizcaíno, V., Vázquez, M., Rodríguez-Peces, M.J., Evans, N.J., 2018, U-Pb ages of detrital zircons from the Internal Betics: A key to deciphering paleogeographic provenance and tectonostratigraphic evolution. Lithos 318–319, 244–266, https://doi.org/10.1016/j.lithos.2018.07.026

Kirchner, K.L., Behr, W.M., Loewy, S., Stockli, D.F., 2016. Early Miocene subduction in the western Mediterranean: Constraints from Rb-Sr multimineral isochron geochronology. Geochemistry, Geophysics, Geosystems 17, https://doi.org/10.1002/2015GC006208

Kroner, U., Romer, R.L., 2013. Two plates - Many subduction zones: The Variscan orogeny reconsidered. Gondwana Research 24, 298-329.

Laborda-López, C., Aguirre, J., Donovan, S.K., 2013. Asociaciones de macrofósiles en rocas metamórficas del Complejo Nevado-Filábride (Zonas Internas de la Cordillera Bética) en Águilas, Murcia (SE España). Tafonomía y biocronoestratigrafía, XXIX Jornadas de Paleontología, Abstracts, pp 83-84.

Laborda-López, C., Aguirre, J., Donovan, S.K., 2015a. Surviving metamorphism: taphonomy of fossil assemblages in marble and calc-silicate schist. Palaios 30, 668-679.

Laborda-López, C., Aguirre, J., Donovan, S.K., Navas-Parejo, P., Rodríguez, S., 2015b. Fossil assemblages and biochronology of metamorphic carbonates of the Nevado-Filábride Complex from the Águilas tectonic arc (SE Spain). Spanish Journal of Palaeontology 30, 275-292.

Lafuste, M.L.J., Pavillon, M.J., 1976. Mise en évidence d’Eifélien daté au sein des terrains métamorphiques des zones internes des Cordillères bétiques. Intérêt de ce nouveau repère stratigraphique: Comptes Rendus de l’Académie des Sciences de Paris 283, 1015-1018.

Leine, L., 1968. Rauhwackes in the Betic Cordilleras, Spain: Nomenclature, description and genesis of weathered carbonate breccias of tectonics origin. PhD Thesis

University of Amsterdam 112 p.

López Sánchez-Vizcaino, V., Connolly, J.A.D., Gómez-Pugnaire, M.T., 1997. Metamorphism and phase relations in carbonate rocks from the Nevado-Filábride Complex (Cordilleras Béticas, Spain): application of the Ttn + Rt + Cal + Qtz + Gr buffer. Contributions to Mineralogy and Petrology 126, 292-302.

López Sánchez-Vizcaíno, V., Rubatto, D., Gómez-Pugnaire, M.T., Tommsdorff, V, Müntener, O., 2001. Middle Miocene high-pressure metamorphism and fast exhumation of the Nevado-Filábride Complex, SE Spain, Terra Nova 13, 327-332.

Ludwig, K.R., 2003, User's Manual for Isoplot 3.00: a Geochronological Toolkit for Microsoft Excel Berkeley Geochronology Center Special Publication 4, p. 4.

Ludwig, K.R., 2009. SQUID II., a user's manual, Berkeley Geochronology Center Special Publication 2, 2455 Ridge Road, Berkeley, CA 94709, USA 22.

Maate, A., Sole De Porta, A.N., Martín-Algarra, A., 1993. Données paléontologiques nouvelles sur le Carnien des séries rouges des Maghrébides (Ghomarides et Dorsale calcaire du Rif septentrional, Maroc). Comptes Rendus de l'Académie des Sciences de Paris 316, 137-143.

Martín-Algarra, A., 1987. Evolución geológica alpina del contacto entre las Zonas Internas y las Zonas Externas de la (Cordillera Bética). Ph D Thesis, Universidad de Granada Martin-Algarra, 1987.

Martínez Catalán, J.R., Arenas, R., Díaz García, F., Abati, J., 1997. Variscan accretionary complex of northwest Iberia: Terrane correlation and succession of tectonothermal events. Geology 25, 1103-1106.

Martínez Catalán, J.R., Fernández-Suárez, J., Meireles, C., González clavijo, E., Belousova, E., Saeed, A., 2008, U-Pb detrital zircon ages in synorogenic deposits of the NW Iberian Massif (Variscan belt): interplay of Devonian–Carboniferous sedimentation and thrust tectonics. Journal of the Geological Society 165, 687-698.

Martínez Catalán, J.R. 2012. The Central Iberian arc, an orocline centered in the Iberian Massif and some implications for the Variscan belt. International Journal of Earth Sciences 101, 1299-1314.

Martínez Catalán, J.R., 2011. Are the oroclines of the Variscan belt related to late Variscan strike-slip tectonics? Terra Nova 23(4), 241-247.

Martínez-Catalán, J.R., Arenas, R., Díaz-García, F., Abati, J., 1997. Variscan accretionary complex of NW Iberia: terrane correlation and succession of tectonothermal events. Geology 25,1103-1106.

Martín-Martín, M., Martin-Rojas, I., Caracuel, J.E., Estevez-Rubio, A., Martin-Algarra, A., Sandoval, J., 2006. Tectonic framework and extensional pattern of the Malaguide Complex from Sierra Espuña (Internal Betic Zone) during Jurassic–Cretaceous: implications for the Westernmost Tethys geodynamic evolution. International Journal of Earth Sciences 95, 815-826.

Martín-Rojas, I., Somma, R., Delgado, F., Estévez, A., Iannace, A., Perrone, V., Zamparelli, V., 2010. Role of sea-level change and synsedimentary extensional tectonics on facies and architecture of Ladinian-Carnian carbonate depositional systems (Alpujarride complex, Betic Internal Zone, SE Spain). Geogaceta 48, 63-66.

Martín-Rojas, I., Somma, R., Delgado, F., Estevez, A., Iannace, A., Perrone, V., Zamparelli, V., 2009. Triassic continental rifting of Pangea: evidence from the Alpujarride carbonates (Betic Cordillera, SE Spain). Journal of the Geological Society, London 166, 447-458.

Martins, H.C.B., Ribeiro, M.A., Almeida, A., 2019. Variscan Magmatism at the Central Iberian Zone, the Central and Northern Border. In: C. Quesada, Oliveira, J.T. (eds.), The Geology of Iberia: A Geodynamic Approach, Regional Geology Reviews, Vol. 2, 510-513. https://doi.org/10.1007/978-3-030-10519-8_13

Marzoli, A., Renne, P., Piccirillo, E.M., Ernesto, M., DeMin, A., 1999. Extensive 200 million-year-old continental flood basalts of the Central Atlantic Magmatic Province. Science 284, 616-618.

Matte, Ph., 1991. Accretionary history and crustal evolution of the Variscan belt in Western Europe. Tectonophysics 196, 309-337.

Matte, Ph., 2002. Variscides between the Appalachians and the Urals: Similarities and differences between Paleozoic subduction and collision belts. In: Martínez Catalán, J.R., Hatcher, R.D. Jr, Arenas, R., Díaz García, F. (eds), Variscan-Appalachian dynamics: The building of the late Paleozoic basement: Boulder, Colorado, Geological Society of America Special Paper 364, 239-251.

Matte, P., 2001. The Variscan collage and orogeny (480-290 Ma) and the tectonic definition of the Armorica microplate: a review. Terra Nov. 13, 122–128, https://doi.org/10.1046/j.1365-3121.2001.00327.x

Meinhold, G., Morton, A.C., Mark Fanning, C., Howard, J.P., Phillips, R.J., Strogen, D., Whitham, A.G., 2014. Insights into crust formation and recycling in North Africa from combined U-Pb, Lu-Hf and O isotope data of detrital zircons from Devonian sandstone of southern Libya. Geological Society, London, Special Publications 386, 281-292, https://doi.org/10.1144/SP386.1

Murphy, J.B., Gutierrez-Alonso, G., Nance, R.D., Fernandez-Suarez, J., Keppie, J.D., Quesada, C., Strachan, R.A., Dostal, J., 2006. Origin of the Rheic Ocean: rifting along a Neoproterozoic suture? Geology 34, 325-328.

Montero, P., Bea, F., González-Lodeiro, F., Talavera, C., Whitehouse, M.J., 2007. Zircon ages of the metavolcanic rocks and metagranites of the Ollo de Sapo Domain in central Spain: Implications for the Neoproterozoic to Early Palaeozoic evolution of Iberia. Geological Magazine 144, 963–976.

Montero, M.P., Talavera, C., Bea, F., González Lodeiro, F., Whitehouse, M. J., 2009. Zircon geochronology of the Ollo de Sapo Formation and the age of the Cambro–Ordovician rifting in Iberia. Journal of Geology 117, 174–191.

Murphy, J.B., Nance, R.D., Cawood, P.A., 2009. Contrasting modes of supercontinent formation and the conundrum of Pangea. Gondwana Research 15, 408-420.

Nance et al., 2010 Nance, R.D, Gutiérrez-Alonso, G., Keppie, J.D., Linnemann, U., Murphy, J.B., Quesada, C., Strachan, R.A., Woodcock, N.H., 2010. Evolution of the Rheic Ocean. Gondwana Research 17, 194-222, https://doi.org/10.1016/j.gr.2009.08.001

Pastor-Galán, D., Gutiérrez-Alonso, G., Murphy, J.B., Fernández-Suárez, J., Hofmann, M., Linnemann, U., 2013. Provenance analysis of the Paleozoic sequences of the northern Gondwana margin in NW Iberia: Passive margin to Variscan collision and orocline development. Gondwana Research 23, 1089-1103, https://doi.org/10.1016/j.gr.2012.06.015

Pereira, M.F., Castro, A., Fernández, C., Rodríguez, C., 2018. Multiple Paleozoic magmatic-orogenic events in the Central Extremadura batholith (Iberian Variscan belt, Spain). Journal of Iberian Geology 44, 309-333.

Pereira, M.F., Chichorro, M., Johnston, S.T., Gutiérrez-Alonso, G., Silva, J.B., Linnemann, U., Hofmann, M., Drost, K., 2012. The missing Rheic Ocean magmatic arcs: provenance analysis of Late Paleozoic sedimentary clastic rocks of SW Iberia. Gondwana Research 3–4(22), 882-891.

Pereira, M.F., Gama, C., Chichorro, M., Silva, J.B., Gutiérrez-Alonso, G., Hofmann, M., Linnemann, U., Gärtner, A., 2016. Evidence for multi-cycle sedimentation and provenance constraints from detrital zircon U-Pb ages: Triassic strata of the Lusitanian basin (western Iberia). Tectonophysics 681, 318-331.

Pereira, M.F., Gama, C., Dias da Silva, I., Silva, J.B., Hofmann, M., Linnemann, U., Gärtner, A., in press. Chronostratigraphic framework and provenance of the Ossa-Morena Zone Carboniferous basins (SW Iberia). Solid Earth Discussions, https://doi.org/10.5194/se-2020-26

Pereira, M.F., Gutiérrez-Alonso, G., Murphy, J.B., Drost, K., Gama, C., Silva, J.B., 2017a. Birth and demise of the Rheic Ocean magmatic arc(s): Combined U–Pb and Hf isotope analyses in detrital zircon from SW Iberia siliciclastic strata. Lithos 278-281, 383-399.

Pereira, M.F., Ribeiro, C., Gama, C., Drost, K., Chichorro, M., Vilallonga, F., Hofmann, M., Linnemann, U., 2017b. Provenance of upper Triassic sandstone, southwest Iberia (Alentejo and Algarve basins): tracing variability in the sources. International Journal of Earth Sciences 106, 43-57. https://doi.org/10.1007/s00531-016-1295-2

Pereira, M.F., Ribeiro, C., Vilallonga, F., Chichorro, M., Drost, K., Silva, J.B., Albardeiro, L., Hofmann, M., Linnemann, U., 2014. Variability over time in the sources of South Portuguese Zone turbidites: evidence of denudation of different crustal blocks during the assembly of Pangaea. International Journal of Earth Sciences 103, 1453-1470.´

Pérez-Cáceres, I., Martínez Poyatos, D., Simancas, J.F., Azor, A., 2017. Testing the Avalonian affinity of the South Portuguese Zone and the Neoproterozoic evolution of SW Iberia through detrital zircon populations. Gondwana Res. 42, 177-192, https://doi.org/10.1016/j.gr.2016.10.010

Perri, F., Critelli, S., Martín-Algarra, A., Martín-Martín, M., Perrone, V., Mongelli, G., Zattin, G., 2013. Triassic redbeds in the Malaguide Complex (Betic Cordillera-Spain): Petrography, geochemistry and geodynamic implications. Earth-Science Reviews 117, 1-28.

Platt, J.P., Whitehouse, M.J., Kelley, S.P., Carter, A., Hollick, L., 2003. Simultaneous extensional exhumation across the Alboran Basin: Implications for the causes of late orogenic extension. Geology 31 31, 251-254.

Platt, J.P., Anczkiewicz, R., Soto, J.I., Kelley, S.P., Thirlwall, M., 2006. Early Miocene continental subduction and rapid exhumation in the western Mediterranean. Geology 34, 981-984.

Pratt, J.R., Barbeau, D.L., Garver, J.I., Emran, A., Izykowski, T.M., 2015. Detrital Zircon Geochronology of Mesozoic Sediments in the Rif and Middle Atlas Belts of Morocco: Provenance Constraints and Refinement of the West African Signature. J. Geol. 123, 177-200, https://doi.org/10.1086/681218

Puga, E., Nieto, J.M., Diaz de Federico, A., Portugal, E., Reyes, E., 1996. The intra-orogenic Soportujar Formation of the Mulhacén Complex; evidence for the polyciclic character of the Alpine orogeny in the Betic Cordilleras. Eclogae Geologicae Helvetiae 89, 129-162.

Puga, E., Fanning, M., Díaz de Federico, A., Nieto, J.M., Beccaluva, L., Bianchini, G., Díaz-Puga, M.A., 2011. Petrology, geochemistry and U-Pb geochronology of the Betic Ophiolites: Inferences for Pangaea break-up and birth of the westernmost Tethys Ocean. Lithos 124, 255-272.

Puga, E., Díaz de Federico, A., Nieto, J.M., 2002. Tectonostratigraphic subdivision and petrological characterisation of the deepest complexes of the Betic zone: a review. Geodinamica Acta 15, 23-43.

Ribeiro, M.L., Castro, A., Almeida, A., González Menéndez, L., Jesus, A. Lains, J.A., Lopes, J.C., Martins, H.C.B., Mata, J., Mateus, A., Moita, P., Neiva, A.M.R., Ribeiro, M.A., Santos, J.F., Solá, A.R., 2019, Variscan magmatism. In: Quesada, C., Oliveira, J.T. (Eds.), The Geology of Iberia: A Geodynamic Approach, Regional Geology Reviews 2, 497-526.

Rodriguez-Cañero, R., Jabaloy-Sánchez, A., Navas-Parejo P, Martín-Algarra, A., 2018. Linking Palaeozoic palaeogeography of the Betic Cordillera to the Variscan Iberian Massif: new insight through the first conodonts of the Nevado-Filábride Complex. International Journal of Earth Sciences (Geologische Rundschau) 107(5), 1791-1806, https://doi.org/10.1007/s00531-017-1572-8

Rubio-Ordóñez, A., Valverde-Vaquero, P., Corretgé, L.G., Cuesta-Fernández, A.,Gallastegui, G., Fernández-González, M., Gerdes, A., 2012. An early Ordovician tonalitic–granodioritic belt along the Schistose-Greywacke Domain of the Central Iberian zone (Iberian Massif, Variscan belt). Geological Magazine 149(5), 927-939, https://doi.org/10.1017/S0016756811001129

Sánchez Martínez, S., De la Horra, R., Arenas, R., Gerdes, A., Galán-Abellán, A.B., López-Gómez, J., Barrenechea, J.F., Arche, A., 2012. U-Pb Ages of Detrital Zircons from the Permo-Triassic Series of the Iberian Ranges: A Record of Variable Provenance during Rift Propagation. The Journal of Geology 120, 135-154.

Sánchez-Martínez, S., Arenas, R., García, F.D., Martínez Catalán, J.R., Gómez-Barreiro, J., Pearce, J.A., 2007. Careon ophiolite, NW Spain: suprasubduction zone setting for the youngest Rheic Ocean floor. Geology 35, 53-56.

Sánchez-Navas, A., García-Casco, A., Martín-Algarra, A., 2014. Pre-Alpine discordant granitic dikes in the metamorphic core of the Betic Cordillera: tectonic implications. Terra Nova 26, 477-486, https://doi.org/10.1111/ter.12123

Sánchez-Navas, A., García-Casco, A., Mazzoli, S., Martín-Algarra, A., 2017. Polymetamorphism in the Alpujarride Complex, Betic Cordillera, South Spain. The Journal of Geology 125, 637-657.

Sánchez-Rodriguez, L., Gebauer, D., 2000, Mesozoic formation of pyroxenites and gabbros in the Ronda area (southern Spain), followed by early Miocene subduction metamorphism and emplacement into the middle crust: U-Pb sensitive high-resolution ion microprobe dating of zircon: Tectonophysics 316, 19-44.

Santamaría-López, A., Sanz de Galdeano, C., 2018. SHRIMP U–Pb detrital zircon dating to check subdivisions in metamorphic complexes: a case of study in the Nevado–Filábride complex (Betic Cordillera, Spain). International Journal of Earth Sciences, https://doi.org/10.1007/s00531-018-1613-y

Sharman, G.R., Malkowski, M.A., 2020, Needles in a haystack: Detrital zircon UePb ages and the maximum depositional age of modern global sediment. Earth-Science Reviews 203, 103109, https://doi.org/10.1016/j.earscirev.2020.103109

Shaw, J., Gutierrez-Alonso, G., Johnston, S.T., Galan, D.P., Pastor-Galan, D., 2014. Provenance variability along the Early Ordovician north Gondwana margin: Paleogeographic and tectonic implications of U-Pb detrital zircon ages from the

Armorican Quartzite of the Iberian Variscan belt. Geological Society of America Bulletin 126, 702-719, https://doi.org/10.1130/B30935.1

Shaw, J., Johnston, S.T., Gutiérrez-Alonso, G., Weil, A.B., 2012. Oroclines of the Variscan orogen of Iberia: paleocurrent analysis and paleogeographic implications. Earth and Planetary Science Letters 329-330, 60-70.

Simancas, F., 2019. Variscan Cycle. In: Quesada, C., Oliveira, J.T. (Eds.), The Geology of Iberia: A Geodynamic Approach, Regional Geology Reviews 2, 1-26.

Simon, O., Visscher, H., 1983. El Pérmico de las Cordilleras Béticas. In: Martínez-Diaz C (Ed.), Carbonífero y Pérmico de España: Actas X Congreso Internacional Carbonífero. IGME, Madrid 453-499.

Spencer, C.J., Kirkland, C.L., 2016. Visualizing the sedimentary response through the orogenic cycle: a multidimensional scaling approach. Lithosphere 8, 29-37, https://doi.org/10.1130/L479.1

Spencer, C.J., Kirkland, C.L., Taylor, R.J.M., 2016. Strategies towards statistically robust interpretations of in situ U-Pb zircon geochronology. Geoscience Frontiers 7, 581-589, http://dx.doi.org/10.1016/j.gsf.2015.11.006

Stephan, T., Kroner, U., Romer, R.L., 2019. The pre-orogenic detrital zircon record of the Peri-Gondwanan crust. Geological Magazine 156, 281-307, https://doi.org/10.1017/S0016756818000031

Tahiri, A., Montero, P., El Hadi, H., Martínez Poyatos, D., Azor, A., Bea, F., Simancas, J.F., González Lodeiro, F., 2010. Geochronological data on the Rabat-Tiflet granitoids: their bearing on the tectonics of the Moroccan Variscides. J. African Earth Sci. 57, 1–13, https://doi.org/10.1016/j.jafrearsci.2009.07.005

Talavera, C., Montero, P., Bea, F., González Lodeiro, F., Whitehouse, M., 2013. U–Pb zircon geochronology of the Cambro–Ordovician metagranites and metavolcanic rocks of central and NW Iberia. International Journal of Earth Sciences 102, 1–23.

Tendero, J.A., Martín-Algarra, A., Puga, E., Díaz de Federico, A., 1993. Lithostratigraphie des métasédiments de l'association ophiolitique Nevado-Filabride (SE Espagne) et mise en evidence d'objets ankéritiques évoquant des foraminiféres planctoniques du Crétacé: conséquences paléogéographiques. Comptes Rendus de l'Académie des Sciences Paris 316, 1115-1122.

Vermeesch, P., 2012. On the visualisation of detrital age distributions. Chemical Geology, v.312-313, 190-194, https://doi.org/10.1016/j.chemgeo.2012.04.021

Vermeesch, P., 2013. Multi-sample comparison of detrital age distributions. Chemical Geology 341, 140-146, https://doi.org/10.1016/j.chemgeo.2013.01.010

Vissers, R.L.M., 1981. A structural study of the Central Sierra de los Filabres (Betic Zone, SE Spain), with emphasis on deformational processes and their relation to the Alpine Metamorphism. GUA Papers of Geology 15, 1- 154.

Vissers, R.L.M., 1992. Variscan extension in the Pyrenees. Tectonics 11(6), 1369-1384. https://doi.org/10.1029/92TC00823

Voet, H.W., 1967. Geological investigations in the Northern Sierra de Los Filabres around Macael and Cóbdar, southeastern Spain. Ph.D. Thesis, Amsterdam University, The Netherlands.

Williams, J.R., Platt, J.P., 2017. Superposed and refolded metamorphic isograds, and superposed directions of shear during late-orogenic extension in the Alborán Domain, southern Spain. Tectonics 36, 756-786, https://doi.org/10.1002/2016TC004358

Wilson, M., 1997. Thermal evolution of the Central Atlantic passive margins: continental break-up above a Mesozoic super-plume. Journal of the Geological Society of London 154, 491-495.

Wissink, G.K., Wilkinson, B.H., Hoke, G.D., 2018. Pairwise sample comparisons and multidimensional scaling of detrital zircon ages with examples from the North American platform, basin, and passive margin settings. Lithosphere 10, 478-491, https://doi.org/ 10.1130/L700.1

Zindler, A., Staudigel, H., Hart, S.R., Endres, R., Goldstein, S., 1983, Nd and Sm isotopic study of a mafic layer from Ronda ultramafic complex. Nature 304, 226.

Figure and Table captions:

Figure 1.- (A) Tectonic sketch of the Southwestern Mediterranean Sea; (B) Tectonic map of the Betic Cordillera.

Figure 2.- Geological map of the south-eastern Betic Chain with outcrops of the three tectonic complexes of the Internal zones and the location of the Águilas Arc marked (see Fig. 1B for location).

Figure 3.- Geological map of the central area of the Águilas Arc (modified from Espinosa Godoy et al., 1972; Booth-Rea and Silva-Barroso, 2008; Booth-Rea et al., 2009; García-Tortosa et al., 2012), with the location of the studied samples. See location in Fig. 2.

Figure 4.- Lithological columns of the studied successions in the NFC, AC and MC with the location of the studied samples. Yellow stars: meta-detrital samples; red stars: meta-igneous samples. Successions for the NFC Lomo de Bas units were compiled from Laborda-López et al. (2013, 2015a, b) and Booth-Rea et al (2009). The succession of the NFC Mulhacén units compiled from Booth-Rea and Silva-Barroso (2008), and Booth-Rea et al. (2009). Successions for the AC were compiled with data from Booth-Rea and Silva-Barroso (2008), Booth-Rea et al. (2009), and García-Tortosa et al. (2012). Succession from the MC Sierra de las Estancias area was compiled from Fernández-Fernández et al. (2007), while the succession of the MC Cabo Cope unit is from Espinosa Godoy et al. (1972), and García-Tortosa et al. (2012).

Figure 5.- Results of U-Pb analyses on detrital zircon grains from Lomo de Bás units (NFC): combination of Kernel Density Estimates plots (KDE, black lines), frequency (grey bars), and relative abundance of age groups based on $^{206}Pb/^{238}U$ (for dates < 1.5 Ga) and $^{207}Pb/^{206}Pb$ (for dates > 1.5 Ga) ages. (A) sample AG-12; (B) sample AG-14; (C) sample AG-17, (D) sample AG-18, (E) Cumulative KDE (blue line) and frequency (grey bars) for the Lomo de Bás samples; (F) zoom for the ages ranging from 0 to 541 Ma.

Figure 6.- Results of U-Pb analyses of detrital zircon grains from Tahal Fm samples (Mulhacén units, NFC): combination of Kernel Density Estimates plots (KDE, black lines), frequency (grey bars), and relative abundance of age groups based on $^{206}Pb/^{238}U$ (for dates < 1.5 Ga) and $^{207}Pb/^{206}Pb$ (for dates > 1.5 Ga) ages. (A) sample AG-1; (B) sample AG-2; (C) Cumulative KDE (blue line) and frequency (grey bars) for the samples of the Tahal Fm; (D) zoom for the ages ranging from 0 to 541 Ma.

Figure 7.- Results of U-Pb analyses on the core of zircon grains from orthogneiss AG-13 (Lomo de Bas units, NFC): (A) conventional Concordia diagram, ^{204}Pb corrected, with the concordant data (95% > Concordia > 105%); (B) conventional Concordia diagram, ^{204}Pb corrected, with the most concordant data; (C) probability density plots (red line) and frequency (blue bars) for the concordant data (95% > Concordia > 105%); (D) weighted average of the most concordant data.

Figure 8.- Results of U-Pb analyses on the core of zircon grains from the orthogneiss AG-16 (Lomo de Bas units, NFC): (A) conventional Concordia diagram with all the data; (B) conventional Concordia diagram, ^{207}Pb corrected, with the most concordant data (90% > Concordia > 110%); (C) probability density plots (red line) and frequency (blue bars) for the most concordant data; (D) weighted average of the most concordant data.

Figure 9.- Results of U-Pb analyses on detrital zircon grains from samples from the Micaschists and Quartzite Fm (AC): combination of Kernel Density Estimates plots (KDE, black lines), frequency (grey bars), and relative abundance of age groups based on $^{206}Pb/^{238}U$ (for dates < 1.5 Ga) and $^{207}Pb/^{206}Pb$ (for dates > 1.5 Ga) ages. (A) sample AG-4; (B) sample AG-5; (C) sample AG-6, (D) sample AG-7, (E) Cumulative KDE (blue line) and frequency (grey bars) for the samples from the Micaschists and Quartzite Fm ; (F) zoom for the ages ranging from 0 to 541 Ma.

Figure 10.- Results of U-Pb analyses on detrital zircon grains from samples from the Meta-detrital Fm (AC: AG-9, AG-11, and AG-15), and from the Miñarros mylonites

and breccias (AC: AG-19): combination of Kernel Density Estimates plots (KDE, black lines), frequency (grey bars), and relative abundance of age groups based on $^{206}Pb/^{238}U$ (for dates < 1.5 Ga) and $^{207}Pb/^{206}Pb$ (for dates > 1.5 Ga) ages. (A) sample AG-9; (B) sample AG-11; (C) sample AG-15, (D) sample AG-19, (E) Cumulative KDE (blue line) and frequency (grey bars) for the samples from the Meta-detrital Fm (AG-9, AG-11, and AG-15); (F) zoom for the ages ranging from 0 to 541 Ma.

Figure 11.- Results of U-Pb analyses on the black rims of zircon from the Cabezo Blanco orthogneiss AG-26 (Cantal unit): (A) conventional Concordia diagram with all the data; (B) conventional Concordia diagram, ^{207}Pb corrected, with the maximum at ca. 16 Ma; (C) probability density plots (red line) and frequency (blue bars) for all then data; (D) weighted average of the ca. 16 Ma age.

Figure 12.- Results of U-Pb analyses on the cores of zircon from the Cabezo Blanco orthogneiss AG-26 (Cantal unit): (A) conventional Concordia diagram with all the data; (B) conventional Concordia diagram, ^{207}Pb corrected, with the main population; (C) probability density plots (red line) and frequency (blue bars) for all then data; (D) weighted average of the main population.

Figure 13.- Results of U-Pb analyses on detrital zircon grains from samples from the Saladilla Fm (MC): combination of Kernel Density Estimates plots (KDE, black lines), frequency (grey bars), and relative abundance of age groups based on $^{206}Pb/^{238}U$ (for dates < 1.5 Ga) and $^{207}Pb/^{206}Pb$ (for dates > 1.5 Ga) ages. (A) sample AG-10; (B) sample LP-16-AZ; (C) Cumulative KDE (blue line) and frequency (grey bars) for the samples of the Saladilla Fm; (D) zoom for the ages ranging from 0 to 541 Ma.

Figure 14.- Results of U-Pb analyses on detrital zircon grains from samples from the unconformable Middle Miocene rocks: combination of Kernel Density Estimates plots (KDE, black lines), frequency (grey bars), and relative abundance of age groups based on $^{206}Pb/^{238}U$ (for dates < 1.5 Ga) and $^{207}Pb/^{206}Pb$ (for dates > 1.5 Ga) ages. (A) sample AG-3; (B) sample AG-20; (C) Cumulative KDE (blue line) and frequency (grey bars) for the samples of the Middle Miocene rocks; (D) zoom for the ages ranging from 0 to 541 Ma.

Figure 15.- A) Multidimensional scaling (MDS) plot of the Late Carboniferous samples from the Betic Cordillera (NFC, AC and MC), Iberian Massif and South France. B) Shepard plot for the MDS.

Figure 16.- Paleogeographic reconstruction of the eastern Variscan belt at Early Bashkirian times (modified from Martínez-Catalán (2011) and Rodríguez-Cañero et al. (2017) for Europe). The proposed location of the NFC, AC and MC with respect to other Variscan Iberian Terranes is included. CIZ, Central Iberian; CZ, Cantabrian; GTMZ, Galicia-Trás-os-Montes; MGCZ, Mid-German Crystalline; MZ, Moldanubian; OMZ, Ossa-Morena; RHZ, Rheno-Hercynian; SPZ, South Portuguese; STZ, Saxo-Thuringian; TBZ, Teplá-Barrandian; WALZ, West Asturian-Leonese.

Figure 17.- A) Multidimensional scaling (MDS) plot of the Permian Triassic samples from the Betic Cordillera (NFC, AC and MC), Iberian Massif and Iberian Chain. B) Shepard plot for the MDS.

Table 1.- Sketch of the Tectonic complexes and units mentioned in the text and available ages from every lithological formation.

Table 2.- Details of the samples and the analyses carried out; (*) UTM coordinates,ED_1950 ellipsoid, zone 30 S.

Declaration of interests

☒ The authors declare that they have no known competing financial interests or personal relationships that could have appeared to influence the work reported in this paper.

☐The authors declare the following financial interests/personal relationships which may be considered as potential competing interests:

Credit Author Statement

Antonio Jabaloy-Sánchez: Conceptualization; Data curation; Formal analysis; Funding acquisition; Investigation; Supervision; Validation; Visualization; Writing - original draft; Writing - review & editing.

Cristina Talavera: Conceptualization; Data curation; Formal analysis; Investigation; Methodology; Resources; Software; Supervision; Validation; Visualization; Writing - original draft; Writing - review & editing.

Martín Jesús Rodríguez-Peces: Conceptualization; Data curation; Investigation; Methodology.

Mercedes Vázquez-Vílchez: Conceptualization; Data curation; Investigation; Methodology; Writing - review & editing.

Noreen Joyce Evans: Formal analysis; Investigation; Methodology; Resources; Software; Supervision; Validation; Writing - review & editing.

U-Pb geochronology of detrital and igneous ~~zircons~~zircon grains from the Águilas Arc in the Internal Betics (SE Spain): implications for Carboniferous-Permian paleogeography of Pangea

Style Definition: Comment Text

Antonio Jabaloy-Sánchez[1], Cristina Talavera[2], Martín Jesús Rodríguez-Peces[3], Mercedes Vázquez-Vílchez[4], Noreen Joyce Evans[5]

[1]Departamento de Geodinámica, Universidad de Granada, 18002 Granada, Spain.

[2]School of Geosciences, University of Edinburgh, The King's Building, James Hutton Road, EH9 3FE, Edinburgh, UK.

[3]Departamento de ~~Geodinamica~~Geodinámica, Estratigrafía y Paleontología, Universidad Complutense de Madrid, Madrid, Spain.

[4]Departmento de Didáctica de las Ciencias Experimentales, Universidad de Granada, Granada, Spain.

[5]School of Earth and Planetary Sciences/John de Laeter Center, Curtin University, Bentley 6845, Australia.

Abstract

~~The Águilas Arc (SE Spain) comprises the three tectonic complexes of the Internal Betic Chain.~~

New U-Pb detrital zircon and U-Pb zircon ages of metaigneous rocks in the Águilas Arc (Betic Chain, SE Spain) allow us to determine the maximum depositional ages of the rocks. Within the Nevado-Filábride Complex ~~provide~~, a Late Carboniferous depositional age for the Lomo de Bas schists and quartzites, ~~while the~~and a Permian-Triassic maximum depositional age ~~of~~for the Tahal Fm ~~is confirmed as Permian-Triassic. In~~are determined. Within the Alpujárride Complex, the maximum depositional age of the Micaschists and Quartzite Fm is Late Carboniferous and the Meta-detrital Fm was deposited in the Early Permian. Furthermore, the maximum depositional age of the Saladilla Fm in the Maláguide Complex is also Early Permian. The age distribution

Formatted: Indent: First line: 0.5"

patterns for the Carboniferous rocks of the Nevado-Filábride and Alpujárride complexes are similar to those from the Cantabrian~~, West Asturian-Leonese, and Central-Iberian zones~~ Zone of the Iberian Massif, suggesting deposition in Carboniferous foreland basins located eastwards of the Iberian Massif. However, ~~the zircon~~ age ~~distribution patterns for the Nevado-Filábride and Alpujárride complexes show differences to those of the Carboniferous rocks from the Maláguide Complex, and the South Portuguese and Ossa-Morena zones of the Iberian Massif, while~~ patterns in Maláguide and ~~Ossa-Morena~~ samples ~~show some~~from the North-eastern Iberian Peninsula and South France show strong similarities~~. Thus, the paleogeographic location of the Maláguide Complex seems different from~~ suggesting that ~~of the Nevado-Filábride and Alpujárride complexes, and~~ it ~~was probably~~can be located near ~~the Ossa-Morena Zone~~those areas in the Late Carboniferous times.

The samples with Early Permian maximum depositional ages from the three complexes contain more Paleozoic ~~zircons~~zircon grains relative to the older Carboniferous samples, but have similar age distribution patterns, suggesting that they were deposited in the same basin. Samples from unconformable Middle Miocene sediments have Early Permian youngest zircon populations and age distribution patterns corresponding to a mixing of ~~zircons~~detrital zircon grains from the Alpujárride and Maláguide complexes. Furthermore, there is no record of any major felsic rocks formation and/or exhumation event after the Early Permian in those two complexes.

1. Introduction

The Variscan-Alleghanian belt (i.e. Martínez Catalán et al., 1997; Matte, 2001; Simancas, 2019) was formed during the Late Paleozoic collision of two major continents: Laurussia (Laurentia-Baltica) and Gondwana. The southern front of the

Variscan segment of this orogenic belt is poorly understood due to post-variscan oroclinal bending, Pangea break-up (e.g. Wilson, 1997; Marzoli et al., 1999) and Alpine reworking (Simancas, 2019). Numerous fragments resulting from Gondwana break-up were dispersed and recycled during the Alpine orogeny, and superposition of metamorphic and deformational Alpine events overprinted most Variscan features.

Several of these fragments are interpreted to be currently included ~~now~~ within the Internal Zones of the Betic-Rif orogen as tectono-metamorphic complexes. These complexes hold clues to the Variscan and Late-Variscan evolution of the southern domains of the Variscan belt and its relationship with the Gondwanan foreland (i.e. Gómez-Pugnaire et al., 2004, 2012; Sánchez-Navas et al., 2014, 2017; Jabaloy-Sánchez et al., 2018; Rodríguez-Cañero et al., 2018). Zircon U-Pb dating of metamorphosed sedimentary sequences and igneous rocks can provide temporal constraints on this evolution, especially in an area where detrital zircon geochronological data are scarce.

Here, we present U-Pb zircon data from metasedimentary and metaigneous rocks of the Águilas Arc in the eastern Betic Chain, in an effort to provide maximum depositional ages for these rocks, paleogeographic information about the possible sources and, hence, the paleolocation of the different tectonic complexes of the Betic-Rif orogenic system. We will then discuss the implication of these data for both the Variscan and Alpine evolution of this orogenic system.

2. Geological setting

The Alpine Betic-Rif orogen is an arcuate Alpine mountain belt outcropping in both South Spain and North Morocco ~~(Fig. 1).~~and formed essentially during Late Paleogene-Neogene times (e.g. Platt et al., 2003; Chaluan et al., 2008) (Fig. 1). According to Balanyá and García-Dueñas (1987), this belt comprises: i) a central allochthonous terrain, the so-called Alborán Domain, ii) the South Iberian Domain, which includes the Triassic to Neogene rocks deposited at the southern paleomargin of the Iberian Peninsula, iii) the North African Domain, comprising Triassic to Neogene rocks deposited at the ~~northwestern~~north-western paleomargin of Africa, and iv) the Flysch Trough units with Cretaceous to Neogene slope/rise and abyssal plain deposits (e.g. Chalouan et al., 2008, and references therein). Furthermore, the Alborán Domain, as ~~was~~ originally defined by Balanyá and García-Dueñas (1987), included three metamorphic complexes, ~~-~~namely (from bottom to top): the Paleozoic to Mesozoic Nevado-Filábride Complex (NFC), the Paleozoic to Mesozoic Alpujárride Complex (AC) and the Paleozoic to Paleogene Maláguide Complex (MC) (Fig. 1).

Recently this subdivision has been redefined and a new tectonic ~~frame~~framework with only three major domains is emerging. Pratt et al. (2015) and Azdimousa et al. (2019) have indicated that the whole Maghrebian Flysch Domain was part of the North African Domain. Moreover, the Alborán Domain has been redefined and now only comprises two tectonic complexes: the lower AC and the upper MC (see Gómez-Pugnaire et al., 2012, and references therein). Accordingly, the NFC is now considered part of the southern paleomargin of the Iberian Peninsula, which was ~~subducted~~overridden below the Alborán Domain ~~(~~at 18 to 15 Ma (see López-Sánchez Vizcaino et al., 2001; Gómez-Pugnaire et al., 2004; 2012; Platt et al., 2006; Kirchner et al., 2016).

In the Central part of the Betic-Chain, the previously mentioned metamorphic complexes were deformed by three ~~mayor~~major E-W trending Tortonian antiforms, but eastwards, left-~~handed~~lateral, roughly N-S trending strike-slip faults rotated and translated the folds towards the North to form the Águilas tectonic Arc (Figs. 1, 2).

2.1. Nevado-Filábride Complex

The NFC is composed of the upper Mulhacén tectonic units (Puga et al., 2002), which underwent Alpine HP (ca. 1.8 GPa) metamorphism at ca. 18-15 Ma (López Sánchez-Vizcaíno et al., 2001; Gómez-Pugnaire et al., 2004, 2012; Platt et al., 2006; Kirchner et al., 2016), and the lower Veleta tectonic units (Gómez-Pugnaire and Franz, 1988; Puga et al., 2002; Rodríguez-Cañero et al., 2018) (Fig. 2, Table 1).

Within the Águilas tectonic Arc, the lower Veleta units are represented by the Lomo de Bas units (Fig. 3, Table 1), which are tectonically ~~overlaid~~overlain by the Mulhacén units (Álvarez and Aldaya, 1985; Álvarez, 1987). The Lomo de Bas units comprise a lower tectonic unit made of ca. 1000 m of alternating graphite-bearing grey and black quartz-schists, garnet and chloritoid-bearing micaschists, and ferruginous quarzitic levels of unknown ages (Laborda-López et al., 2013, 2015a, b) (Fig. 4, Table 1). These rocks include orthogneiss bodies derived from metamorphosed, ~~acidic volcanic~~felsic rocks of unknown age (Álvarez and Aldaya, 1985; Álvarez, 1987~~).~~), although other orthogneiss bodies within the CNF have yielded Late Carboniferous to Early Permian U-Pb ages (Gómez-Pugnaire et al., 2004, 2012, and references therein). An upper ~~tectonic~~ unit tectonically overlays the lower unit, and its succession begins with ~~a~~ 600 to 800 m thick ~~lower member of fine-grained metamorphic rocks. These are mostly~~ graphite-bearing micaschists, quartz schists, and phyllites, which are intercalated with ferruginous quartzite beds (Laborda-López et al., 2015a, b). These rocks are ~~overlaid~~overlain by 80 to 140 m thick low-grade black marbles, with abundant fossils of Early-Middle Devonian age (Emsian-Eifelian, c.f. Lafuste and Pavillon, 1976; Laborda-López et al., 2013, 2015a, b). The succession ends with 130 to 500 m thick graphitic schists, phyllites, and quartzites (Laborda-López et al., 2015a, b) (Fig. 4, Table 1).

In the studied area, the Mulhacén unit succession (Álvarez and Aldaya, 1985; Álvarez, 1987) begins with grey schists and metapsammites of the Permian-Triassic Tahal Fm (Voet, 1967; Jabaloy-Sánchez et al., 2018; Santamaría-López and Sanz de Galdeano, 2018) (Table 1). Moving up section is the Metaevaporite Fm, ~~and~~ attributed Permian-Triassic (Leine, 1968; Vissers, 1981) to Paleogene ages (Puga et al., 1996), followed by the marbles, calc-schists, micaschists~~,~~ and quartzites of the Marbles and Calc-Schists ~~Fms~~Fm (see Voet, 1967; López Sánchez-Vizcaino et al., 1997), for which pre-Permian to Cretaceous ages have been proposed (Tendero et al., 1993; Gómez-Pugnaire et al., 2012) (Fig. 4, Table 1). The succession includes Jurassic metabasite bodies~~.~~ (Puga et al., 2011).

2.2. Alpujárride Complex

In the studied area, the AC includes a thin lower Miñarros unit, which overlies the brittle-ductile extensional shear zone developed at the NFC/AC contact (Figs. 3 and 5) (Álvarez and Aldaya, 1985; Álvarez, 1987; Booth-Rea et al., 2009). ~~The~~At the base of this Complex, the Miñarros unit ~~has~~is ca. 15 m ~~of thickness~~thick and comprises ~~brecciaed~~brecciated ferruginous marbles and white quartzitic mylonites ~~with~~of unknown ~~ages~~age (Álvarez, 1987) (Fig. ~~5~~4, Table 1).

Álvarez and Aldaya (1985) and Álvarez (1987) identified several AC tectonic units thrusting over the Miñarros mylonites and breccias (i.e. the Talayón unit, Águilas unit and Las Palomas unit), and Booth-Rea et al. (2009) grouped them into only one tectonic unit, the so-called Las Estancias-Talayón-Palomas unit. Hereafter, and for simplicity, we call it Las Palomas unit~~.~~ (Table 1). The Las Palomas unit has the most complete succession in the area, ~~which begins~~beginning with ca. 300 m of graphite-bearing micaschists and phyllites alternating with micaceous quartzites from the

Micaschists and Quartzite Fm, with ~~a probable~~an attributed Late Paleozoic age based on correlation with Paleozoic rocks of the MC (Álvarez and Aldaya, 1985; Álvarez, 1987) (Fig. ~~5~~4, Table 1). The succession follows up with ca. 600 m of phyllites and quartzites from the Meta-detrital Fm made of a quartzite-rich lower member and a phyllite-rich upper member with Permian to Middle Triassic ages (Martín-Rojas et al., 2010; García-Tortosa et al., 2012) (Fig. ~~5~~4, Table 1). The Middle to Late Triassic Meta-carbonate Fm overlays ~~the previous rocks~~this succession and is composed of ca. 50 m of marbles and calc-schists (García-Tortosa et al., 2012) with (Fig. ~~5~~4, Table 1).

~~The~~Above the Las Palomas unit, the Ramonete unit crops out ~~above the Las Palomas unit~~ (Figs. 3, ~~5~~4) (Álvarez and Aldaya, 1985; Álvarez, 1987; Booth-Rea et al., 2009) and ~~contains only~~consists of Mesozoic rocks: phyllites and quartzites of the Middle Triassic Meta-detrital Fm (see Simon and Visscher, 1983; Maate et al., 1993; García-Tortosa et al., 2002; Martín-Rojas et al., 2010), and calcitic and dolomitic marbles and ~~calcschists~~calc-schists from the Middle-Upper Triassic Meta-carbonate Fm (García-Tortosa et al., 2002) (Table 1).

Álvarez and Aldaya (1985), and Álvarez (1987) also defined the Cantal unit as an AC tectonic unit thrusting over the Las Palomas unit, or limited by left-~~handed~~lateral strike-slip faults (Figs. 3~~, 5~~ and ~~6~~4, Table 1). However, García-Tortosa et al. (2000) included this unit within the NFC and discussed its adscription to the AC. The Cantal unit is composed of ca. 330 m of migmatitic and felsic gneisses with kyanite and sillimanite bearing schists, graphite bearing schist with staurolite and black marbles and quartzites (see Álvarez and Aldaya, 1985; Álvarez, 1987; Booth-Rea et al., 2009) (Fig. ~~5~~4, Table 1).

2.3. Maláguide Complex

The MC occurs as relatively small outcrops tectonically emplaced on top of the AC (Figs. 3 and ~~6~~4). Towards the east, in the Vélez Rubio area (~~Fig. 7~~Figs. 2 and 4, Table 1), the MC succession includes ca. 1000 m of greywackes, slates, conglomerates and lesser marbles and black cherts of the pre-Ordovician to Late Carboniferous Piar Group (see Martín-Algarra, 1987) overlain by ~~a~~ detached Mesozoic to Cenozoic cover ~~of~~ ca. 500 m thick, consisting of red conglomerates, sandstones, ~~and~~ pelites, ~~with~~and gypsum of the Middle-Late Triassic Saladilla Fm (see Perri et al., 2013, and references therein) (Fig. ~~8~~4, Table 1). The succession follows up with ca. 300 m of Late Triassic to Early Cretaceous limestones, dolostones and marls (Castillón Fm, Geel, 1973), unconformably ~~overlaid~~overlain by ca. 200 m of Eocene Nummulite-rich limestones and marls (Xiquena Fm, Geel, 1973) (Fig. ~~8~~4, Table 1).

In the Águilas Arc area, this succession is usually incomplete and thinned by normal faults, ~~omitting~~lacking outcrops of the thick Paleozoic succession of the Piar Group, (see Aldaya et al., 1991) (Fig. ~~8~~4, Table 1). The main outcrops of this complex correspond to the Cabo Cope and Albaida areas (Álvarez and Aldaya, 1985; Álvarez, 1987; García-Tortosa, 2002) (Figs. 3 and ~~8), with~~4, Table 1), where a succession beginning with ca. 40 m of red pelites, sandstones and gypsum of the Middle-Late Triassic Saladilla Fm crops out. Following up section, there ~~are~~is ca. 130 m of Late Triassic to Jurassic dolostones, marls, and oolitic limestones of the Castillon Fm (García-Tortosa, 2002, and references therein) (Fig. ~~8~~4. Table 1). On top, there is an unconformity overlain by ca. 50 m of Oligocene conglomerates and calcarenites (Durand-Delga et al., 1962; Álvarez, 1987).

Unconformably overlying both the MC and AC, there are Middle Miocene sedimentary rocks with a succession that includes red Langhian-Early Serravallian conglomerates and sandstones with clasts derived from rocks present in both complexes (Figs. 3 and ~~6~~4).

3. Sampling localities and analytical methods

~~Seventeen~~Twenty one samples from the Águilas Arc were studied. Eight samples were collected from the NFC, nine from the AC, two from the MC, and two from the Middle Miocene sedimentary rocks (Table ~~1~~2, Figs. 3 and 4).

~~The samples collected from the NFC were located in both the Lomo de Bas units and in the Mulhacen units. Samples AG-12 and AG-14 come from quartzites of the lower Lomo de Bas unit, while samples AG-17 and AG-18 are from the uppermost quartzite intercalations within the upper Lomo de Bas unit (Fig. 4, Table 1). Samples AG-13 and AG-16 originate from two orthogneiss bodies within this lower tectonic unit (Fig. 4), and samples AG-1 and AG-2 are from two quartzites of the upper part of the Tahal Fm within the Mulhacén tectonic ensemble (Figs. 3 and 4).~~

~~Nine samples were collected from the tectonic units of the AC: six samples come from the Las Palomas unit (AG-4, AG-5, AG-6, AG-7, AG-9 and AG-11) (Figs. 3 and 5, Table 1). Samples AG-4 and AG-5 are from quartzites at the base of the Micaschists and Quartzite Fm attributed to the Upper Paleozoic (Álvarez and Aldaya, 1985; Álvarez, 1987) (Fig. 5). Samples AG-6, and AG-7 come from quartzites near the upper levels of the same Micaschists and Quartzite Fm (Fig. 5). Samples AG-9 and AG-11 are from quartzites within the Middle Triassic Meta-detrital Fm of the Las Palomas unit (Martin-Rojas et al., 2010; García Tortosa, 2002) (Fig. 5). Sample AG-15 is from the Middle Triassic Meta-detrital Fm of the Ramonete unit, and sample AG-19 comes from the quartzitic mylonites of the Miñarros unit (Figs. 3 and 5).~~

Sample AG-26 comes from the Cabezo Blanco orthogneiss body (Fig. 6), within the migmatitic and felsic gneisses with kyanite and sillimanite bearing schists, graphite bearing schist with staurolite and black marbles and quartzites of the Cantal unit (see Álvarez and Aldaya, 1985; Álvarez, 1987; Booth-Rea et al., 2009) (Fig. 5).

Two samples from the Middle-Late Triassic Saladilla Fm of the MC (LP-16-AZ and AG-10) were also collected (Figs. 3 and 7, Table 1). Sample AG-10 is a quartzite from the Cabo Cope area of the Águilas Arc (Fig. 3), and sample LP-16-AZ comes from a quartzite from a lower Maláguide unit of the las Estancias Range near Vélez Rubio (Fig. 7). Two samples (AG-3 and AG-20) were collected from the Middle Miocene red conglomerates and sandstones unconformably covering both the AC and the MC (Fig. 3, Table 1).

4. Analytical methods

Zircon grains were separated using standard heavy-liquid and magnetic techniques in the Department of Geodynamics of the University of Granada. Grains were handpicked and mounted in epoxy, polished, cleaned and gold coated for cathodoluminescence (CL) imaging on a Mira3 FESEM instrument at the John de Laeter Centre (JdLC), Curtin University, Perth, (Australia) and a Carl Zeiss SIGMA HD VP Field Emission SEM at the School of Geosciences, the University of Edinburgh, Scotland, (the United Kingdom.). Representative CL images have been selected and interpreted in the results section. (Figs. 1 to 10 in S3 Supplementary material). In CL images, the lower-U regions are brightly illuminated and higher-U regions are dark, or even black, poorly illuminated regions.

U-Th-Pb geochronological analyses of samples AG-16 and AG-26 were carried out on the SHRIMP IIe/mc instrument of the IBERSIMS lab, University of Granada, Spain, and sample AG-13 was analysed on the Cameca IMS1270 at the NERC Ion Micro-Probe Facility, the University of Edinburgh, United Kingdom (see S1 Supplementary material for a detailed description of the methodologies). Laser ablation inductively coupled plasma mass spectrometry (LA-ICPMS) data collection on the remaining samples was performed at the GeoHistory Facility, JdLC, Curtin University, Perth, Australia. A more detailed description of the methodology is provided within Text S1 in the Supplementary material.

Ages in the text and figures are quoted as $^{206}Pb/^{238}U$ dates for ~~zircons~~zircon analysis younger than 1500 Ma and as $^{207}Pb/^{206}Pb$ dates for ~~zircons~~zircon analysis older than 1500 Ma~~. Distribution~~, while errors are at the 2σ level. The distribution of detrital zircon ages were calculated using DensityPlotter 8.5 (Vermeesch, 2012), with a bin of 40 Ma. An adaptive bandwidth of 40 Ma was applied for the Kernel Density Estimators (KDE); except in the zoom windows ~~from 0 to~~of the group of ages younger than c. 541 Ma, where a bin of 10 Ma and an adaptive bandwidth of 10 Ma were applied. Errors used in ~~the calculation~~these KDE calculations are at the 1σ level~~.~~ (Figs. 5, 6, 9, 10, 13 and 14). Mixture Models were used as a first approach to the age distribution plots in order to obtain the age of the main populations, however, the accuracy of these models in unsharpened peaks of the KDE was low (i.e. the age esd off-peak), and so the age of main populations was calculated using a weighted mean and assessed by the mean square weighted deviation (MSWD).

~~**5. Results**~~

~~In this section, we present the distribution histograms and KDE diagrams with the U-Pb results from the detrital zircons of the three different complexes (NFC, AC, and MC). For each complex, we have combined and described the U-Pb data for each~~

Formatted: Indent: First line: 0.49"

Formatted: Font: Not Bold, No underline

Formatted: Indent: First line: 0.49" formation and/or unit. A synthesis of the analyses and the results is listed in Tables S1 in the Supplementary material. The full description, CL images for representative zircon grains, representative Concordia plots, youngest zircon populations and detailed U-Pb analytical datasets of each individual sample are also provided in the supplementary information (Text S2, Figs. 1 to 10 in S3 and Table S1inS1 in the Supplementary material).

Among the different strategies to estimate the Maximum Depositional Age (MDA) of a sample, we have chosen a more conservative approach where the youngest population is defined as the weighted mean of the youngest cluster of grains with overlapping 2σ uncertainty (see Dickinson and Gehrels, 2009, for the method, and Sharman and Malkowski; 2020, for a discussion). The original method contemplates the use of three or more grains, however, we have worked with four or more grains in the calculation. Most of our samples are metadetrital with grains mostly < 400 Ma. The limited curvature of concordia at these young ages combined with the imprecision of the $^{207}Pb/^{235}U$ age, limits the identification of discordance, and, in fact, any level of Pb loss is masked by the uncertainty of the analysis (Bowring and Schmitz, 2003; Ireland and Williams, 2003; Spencer et al., 2016). Therefore, we have tried to minimize the risk of including dates from grains with Pb loss by applying a very conservative youngest population calculation, calculated using Isoplot software (Ludwig, 2003, 2009).

The Multidimensional Scaling (MDS) technique was used to compare the age patterns for our samples with those of previously published samples from the NFC, AC, MC and the Variscan chain. The MDS is a mean of visualizing the level of similarity of individual datasets in two dimensions. In detrital zircon geochronology MDS is used to graphically represent a quantified comparison between the age patterns of two samples: greater distances between samples represent a greater degree of dissimilarity between points on MDS diagrams (Vermeesch, 2013; Spencer and Kirkland, 2015; Wissink et al., 2018). MDS diagrams were produced using the software Provenance, with a Kolmogorov-Smirnov test for the measurement of the dissimilarity (Vermeesch et al., 2016). Methodology and results of the Kolmogorov-Smirnov test are given in the Supplementary material (Texts S1 and S2, Tables S2 and S3).

4. Results

In this section, we present the distribution histograms and KDE diagrams with the U-Pb results from the detrital zircon grains from the three different complexes (NFC, AC, and MC). For each complex, we have combined and described the U-Pb data for each formation and/or unit. ~~Furthermore, we present the Concordia plots and KDE diagrams with the U-Pb results from the igneous zircon cores and metamorphic rims from the studied orthogneisses. CL images for representative zircon grains, and detailed U-Pb analytical datasets of each individual sample are also provided in the supplementary information (Figs. x 1 to x 10 in S3 and Table S1 in the Supplementary material).~~

~~**5**~~

4.1. Nevado-Filábride Complex

~~5~~4.1.1. LA-ICPMS results from metadetrital samples

The CL images for samples AG-12, AG-14, AG-17 and AG-18 mostly show zircon grains with continuous oscillatory zoning (Fig. 1 in S3 Supplementary material). There are also some composite grains with cores overgrown by low or high U rims ~~and~~, a few grains with sector zoning, and grains that are structureless (Fig. 1 in S3 Supplementary material).

Independent of their location within the upper or lower Lomo de Bas tectonic unit, putative Upper Carboniferous samples AG-12, AG-14, AG-17 and AG-18 yielded similar ages for the youngest zircon analysed, and similar youngest zircon population ages. The youngest ~~zircons~~zircon grains have $^{206}Pb/^{238}U$ dates between 284 ± 14 Ma (sample AG-12) and 323 ± 5 Ma (sample AG-18), while the youngest populations show $^{206}Pb/^{238}U$ mean ages between 321 ± 2 Ma (sample AG-17, MSWD = 0.55 and probability = 0.65) and 336 ± 2 Ma (sample AG-14, MSWD = 1.10 and probability = 0.36).

~~These samples~~Samples AG-12, AG-14, and AG-18 also have similar age distribution patterns showing a very noticeable Ediacaran component with peak ages between ca. 557 and ca. 618 Ma (between 17.3% and 24.3%, Fig. ~~9~~5). There are also significant Mesoproterozoic (between 7% and 12%) and Paleoproterozoic (between 17% and 26%) contributions. The ~~former~~Mesoproterozoic population clearly stands out in samples AG-12 and AG-18 with ages clustering at ca. 1001 (7.2%) and 1025 Ma~~,~~ (6.3%), respectively, and the ~~latter in samples AG-~~Paleoproterozoic population is clearly identified in sample AG-14 ~~and AG-17~~ with ages grouping at ca. 1893 and 2032 Ma~~, and ca. 2011 Ma, respectively~~ (13.2%) (Fig. ~~9). Despite having similar age distribution patterns, there~~5). There is a noteworthy difference in sample AG-17; the percentage of Paleozoic ~~dates~~ages (36%) in this sample ~~AG-17 (36%)~~ is twice as high as that in the other three samples (15% to 19%) (Fig. ~~9~~5).

Combining a total of ~~522 concordant or nearly concordant~~406 dates (Concordia ranging between 90% and 110%, Table S1 in Supplementary material) obtained from ~~these four~~the most similar samples (AG12, AG14 and AG18 of Lomo de Bas quartzites~~,~~

Formatted: Font color: Auto
Formatted: Font color: Auto
Formatted: Font color: Auto
Formatted: Font color: Auto
Formatted: Font color: Auto
Formatted: Font color: Auto
Formatted: Font color: Auto
Formatted: Font color: Auto
Formatted: Font color: Auto
Formatted: Font color: Auto
Formatted: Font color: Auto
Formatted: Font color: Auto
Formatted: Font color: Auto
Formatted: Font color: Auto
Formatted: Font color: Auto
Formatted: Font color: Auto
Formatted: Font color: Auto
Formatted: Font color: Auto
Formatted: Font color: Auto
Formatted: Font color: Auto
Formatted: Font color: Auto
Formatted: Font color: Auto
Formatted: Font color: Auto
Formatted: Font color: Auto

~~a new~~ ; see Kolmogorov-Smirnov test-S in table S2 in the Supplementary material), the age distribution pattern ~~with~~is characterised by dates ranging from ~~284~~283 to 3195 Ma ~~is shown in~~ (Fig. ~~9. These dates are Paleozoic (21%), Neoproterozoic (45%), Mesoproterozoic (9%), Paleoproterozoic (20%), Neoarchean (~~5~~%) and Mesoarchean (1%) (Fig. 9).~~). Within the ~~111~~67 Paleozoic zircon grains, there are Early Permian (~~2~~one grain, 283 ± 14, 1.5% with respect to the total amount of Paleozoic grains), Carboniferous (~~44~~306 ± 4 to 359 ± 8 Ma, 40%), Devonian (~~12~~368 ± 6 to 405 ± 6 Ma, 9%), Silurian (~~2~~442 ± 10 Ma, 1.5%), Ordovician (~~7~~460 ± 12 to 484 ± 8 Ma, 9%) and Cambrian dates (~~33~~486 ± 7 to 540 ± 7 Ma, 39%) (Fig. ~~9~~5).

The CL imaging of ~~zircons~~zircon grains from the Tahal Fm of the Mulhacén ~~tectonic ensemble~~units (samples AG-1 and AG-2) shows grains with continuous oscillatory zoning and partially resorbed cores overgrown by low and high U rims (Fig. 2 in S3 Supplementary material). There are also grains with sector zoning and structureless grains (Fig. 1 in S3 Supplementary material).

Individually, samples AG-1 and AG-2 contain Jurassic ~~zircons~~zircon grains with the youngest zircon grains yielding ^{206}Pb/^{238}U dates of 195 ± 8 Ma, and 179 ± 5 Ma, respectively. ~~They~~Both samples also have ~~a Permian age, within uncertainty, for the~~ youngest zircon ~~population~~populations with Permian ages at 275 ± 8 Ma (MSWD = 1.4 and probability = 0.25) and 277 ± 4 Ma (MSWD = 1.12 and probability = 0.35), respectively. Their age distribution patterns are also comparable, with Carboniferous and Ediacaran peaks at ca. 334 and 331 Ma, and ca. 610 and 598 Ma, respectively (Fig. ~~10~~6). However, there are some differences: i) a minor Early Tonian peak in sample AG-1 at ca. 939 Ma; ii) a higher percentage of Mesozoic and Paleozoic dates in sample AG-2; iii) greater percentage of Mesoproterozoic and Paleoproterozoic ~~zircons~~zircon grains in sample AG-1; and iv) lack of Mesoarchean dates in sample AG-2 (Fig. ~~10~~6).

Formatted: Font color: Auto
Formatted: Font color: Auto
Formatted: Font color: Auto
Formatted: Font color: Auto
Formatted: Font color: Auto
Formatted: Font color: Auto
Formatted: Font color: Auto
Formatted: Font color: Auto
Formatted: Font color: Auto
Formatted: Font color: Auto
Formatted: Font color: Auto
Formatted: Font color: Auto
Formatted: Font color: Auto
Formatted: Font color: Auto
Formatted: Font color: Auto
Formatted: Not Superscript/ Subscript

The 259 ~~concordant or nearly concordant~~ dates from samples AG-1 and AG-2 (Concordia ranging between 90% and 110%, Table S1 in Supplementary material) were combined in ~~an~~a KDE age distribution ~~pattern~~ with dates from 179 to 2811 Ma~~, which are mainly Neoproterozoic (43.5%), Paleozoic (32%) and Paleoproterozoic (13%), with minor Mesozoic (2%), Mesoproterozoic (7%), Neoarchean (2%) and Mesoarchean dates (0.5%)~~ (Fig. ~~10~~6). The 83 Paleozoic zircon grains have Permian (254 ± 11 to 298 ± 8 Ma, 23% with respect to the total amount of Paleozoic grains), Carboniferous (305 ± 9 to 355 ± 10 Ma, 52%), Devonian (363 ± 11 to 410 ± 12 Ma, 7%), Silurian (424 ± 12 to 428 ± 13 Ma, 2%), Ordovician (454 ± 13 to 482 ± 14 Ma, 7%) and Cambrian dates (506 ± 14 to 540 ± 23 Ma, 9%), while the six Mesozoic zircon grains have two Jurassic (179 ± 5 to 195 ± 8 Ma) and four Triassic (209 ± 9 to 239 ± 9 Ma) dates (Fig. ~~10~~6).

~~5~~4.1.2. SIMS results of sample AG-13 (orthogneiss) – Lower Lomo de Bas tectonic unit

Twenty-six grains from this orthogneiss were analysed and 27 of the 31 analyses yielded concordant or nearly concordant dates between 191 and 2345 Ma (Fig. ~~11~~7). Eleven dates plot in a single population with a ^{204}Pb corrected ^{206}Pb/^{238}U mean age of 294 ± 2 Ma (MSWD = 0.75 and probability = 0.68) (Fig. ~~11~~7). These dates are from ~~zircons~~zircon grains with continuous oscillatory zoning, Th/U ratios between 0.030 and 0.615 and common Pb content from 0.05% to 0.26% (Table S1 in Supplementary material). Therefore, this mean age could represent the best estimate of the crystallization age of the protolith.

There are also ~~seven~~ 7 slightly younger dates between 264 and 286 Ma defining a tail negatively skewed towards younger ages (Fig. ~~12~~7), which may relate to Pb loss undetectable with a discordance filter (see Spencer et al., 2016). These dates are from grains with continuous oscillatory zoning (Fig. 3 in S3 Supplementary material),~~ and~~

one rim from a composite grain, Th/U ratios between 0.062 and 0.692 and much higher common Pb ~~content~~ contents (up to 0.35~~% (~~%; Table S1 in Supplementary material). Thus, they were not ~~taking~~taken into account for the age calculation in order to avoid including dates from grains with possible Pb loss.

The youngest ^{204}Pb corrected ^{206}Pb/^{238}U date for this dataset is 191 ± 3 Ma (Table S1 in Supplementary material). This date is from the rim of a composite grain, has a Th/U ratio of 0.011 and could be related to a metamorphic event in this area~~.~~, linked to the intrusion of Early Jurassic mafic rocks (Puga et al., 2011).

~~5~~4.1.3. SHRIMP IIe/mc ~~datations~~analysis on ~~zircons~~zircon grains from sample AG-16 (orthogneiss) – Lower Lomo de Bas tectonic unit

Sample AG-16 provided scarce euhedral bipyramidal prismatic ~~zircons~~zircon crystals with dimensions between 80 and 200 μm. The CL imaging shows partially resorbed cores overgrown by low or high U rims with well-defined oscillatory zoning and a few grains with continuous oscillatory zoning (Fig. 4 in S3 Supplementary material).

Twenty-one U-Pb analyses on 18 different crystals yielded 15 concordant or nearly concordant dates (discordance <5%) ranging from 284 to 674 Ma (Fig. ~~11~~8). Eight of those 13 analyses plotted as a single population with a ^{207}Pb corrected ^{206}Pb/^{238}U mean age of 289 ± 3 Ma (MSWD = 1.4 and probability = 0.20) (Fig. ~~12)~~ ~~and~~8). All these analysis were ~~from~~performed in grains with continuous oscillatory zoning, U and Th contents of 205-1415 and 53-426 ppm, respectively, and Th/U ratios between 0.07 and 1.03 (Table S1 in Supplementary material). ~~This~~The obtained mean age is therefore considered the best estimate of the crystallization age of the ~~protolith~~parent rocks for the orthogneiss. The remaining dates (330 to 674 Ma) were

Formatted: Pattern: Clear

Formatted: Pattern: Clear

Formatted: Pattern: Clear

from cores of composite grains and grains with continuous oscillatory zoning and are considered inherited cores and xenocrysts, respectively (Fig. ~~12~~8).

~~5~~

4.2. Alpujárride Complex

~~5~~4.2.1. LA-ICPMS results from samples from the Micaschists and Quartzite Fm

The CL images of ~~zircons~~zircon grains of samples AG-4, AG-5, AG-6 and AG-7 from the Micaschists and Quartzite Fm show grains with continuous oscillatory zoning and complex grains with a partially resorbed core overgrown by low or high U rim. There are also a few grains with sector zoning and structureless grains (Fig. 5 in S3 Supplementary material).

~~Some similarities are distinguished on the~~ The age distribution patterns of ~~these four~~the 4 aforementioned samples show some similarities (Fig. ~~13~~9, and see Kolmogorov-Smirnov test-S in table S2 in the Supplementary material). There are two main peaks: i) a main Ediacaran peak with ages between ca. 600 and 631 Ma; and ii) a secondary Early Tonian-Late Stenian peak with ages between ca. 996 and 1040 Ma.

However, some differences are also noteworthy: i) samples AG-6 and AG-7, located at the top of the formation, have an Early Orosirian-Late Rhyacian population at ca. 2055 and 2033 Ma, respectively, that is absent in samples AG-4 and AG-5 at the base of the formation (Fig. ~~13~~9); ii) samples from the top of the formation also have a Paleoarchean component that is lacking at the bottom; iii) there were no Mesoarchean dates found in sample AG-6; iv) the age of the youngest zircon grains decreases from the bottom to the top of the formation; that is, from 328 ± 10 Ma and 306 ± 6 Ma in samples AG-4 and AG-5, respectively, to 296 ± 4 Ma and 299 ± 7 Ma in samples AG-6 and AG-7, respectively; and finally, v) the youngest zircon population in sample AG-5 is Late Carboniferous (308 ± 4 Ma) contrasting with those from the other three samples that are Cambrian-Early Ediacaran (sample AG-4, 551 ± 5 Ma; sample AG-6, 507 ± 10 Ma; and sample AG-7; 558 ± 7 Ma (Text S2 and Fig. S4 in Supplementary material).

Combining the 562 ~~concordant or nearly concordant~~ U-Pb data (Concordia ranging between 90% and 110%, Table S1 in Supplementary material) for the four samples of Micaschits and Quartzite Fm produces an age distribution pattern ~~composed of Paleozoic (11%), Neoproterozoic (51%), Mesoproterozoic (11%), Paleoproterozoic (17%), Neoarchean (8%), Mesoarchean (1.5%) and Paleoarchean dates (0.5%) (Fig. 13). These~~(Fig. 9). These data cluster into five main peaks at ca. 309, 602, 1039, 2054 and 2547 Ma (Fig. ~~13~~9). Within the 63 Paleozoic zircon grains, there are: Permian (296 ± 4 to 298 ± 7 Ma, 5% with respect to the total amount of Paleozoic grains), Carboniferous (304 ± 5 to 359 ± 9 Ma, 32%), Devonian (365 ± 8 to 390 ± 7 Ma, 9%), Ordovician (448 ± 13 to 482 ± 10 Ma, 14%) and Cambrian dates (460 ± 17 to 541 ± 9 Ma, 40%) (Fig. ~~13~~9).

~~5~~4.2.2. LA-ICPMS results from samples from the Middle Triassic Meta-detrital Fm

The CL imaging of ~~zircons~~zircon grains from samples AG-9, AG-11, and AG-15 shows grains with continuous oscillatory zoning and some partially resorbed cores with low or high U overgrowths. There are also grains with sector zoning (Fig. 6 in S3 Supplementary material).

~~Their~~The youngest zircon grains in these samples have $^{206}Pb/^{238}U$ dates ranging ~~between~~from 214 ± 2 and 288 ± 4 Ma, while their youngest zircon populations have $^{206}Pb/^{238}U$ mean ages varying between 287 ± 1 Ma (sample AG-11, MSWD = 1.11 and probability = 0.35) and 474 ± 3 Ma (sample AG-15, MSWD = 0.71 and probability = 0.54).

The age distribution ~~pattern~~patterns from these samples ~~displays~~display two or three main populations: a Permian-Late Carboniferous peak (ca. 287 Ma in samples AG-9~~,~~: 16.2%, and AG-11~~),~~: 6.0%), one or two Ediacaran-Cryogenian peaks (from ca. 546 to ca. 661 Ma, in all samples~~)~~: 4.4%, 12.0%, and 7.3%) and a Tonian-Stenian peak (from ca. 963 to ca. 1016 Ma in samples AG-9: 19.1% and AG-15~~)~~: 6.5%) (Fig. ~~14~~10).

The dates of samples AG-9, AG-11, and AG-15 from the Meta-detrital Fm range from 214 Ma to 2941 Ma, and are Paleozoic (275 ± 3 to 541 ± 7 Ma, 17% to 39%), Neoproterozoic (542 ± 8 to 998 ± 13 Ma, 34% to 57%), Mesoproterozoic (1004 ± 13 to 1552 ± 37 Ma, 6% to 13%), Paleoproterozoic (1655 ± 26 to 2451 ± 24 Ma, 7% to 13%) and Neoarchean (2503 ± 28 to 2762 ± 47 Ma, 4% to 7%) in age. It is ~~worthy to note~~worth noting that only sample AG-15 yielded ~~a few~~one Mesoarchean ~~dates (1%)~~date (2941 ± 15 Ma, 1%) and sample AG-11 yielded one Triassic date (214 ± 2 Ma, 1%), (Fig. ~~14~~10). When we combine the 392 ~~concordant or nearly concordant~~ U-Pb data (Concordia ranging between 90% and 110%, Table S1 in Supplementary material) from samples AG-9, AG-11, and AG-15, we obtain ~~an age distribution pattern composed of Mesozoic (0.5%), Paleozoic (30%), Neoproterozoic (44%), Mesoproterozoic (9%), Paleoproterozoic (11%), Neoarchean (5%), and Mesoarchean dates (0.5%)~~ a cumulate age distribution pattern (Fig. ~~14~~10). These data cluster into ~~five~~three main peaks at ca. ~~316, 588, 990, 7960, and 2610 Ma~~287, 570, 964Ma (Fig. ~~14~~10). Within the 119 Paleozoic zircon grains, there are: Permian (~~33~~275 ± 3 to 298 ± 8.0 Ma, 32% with respect to the total amount of Paleozoic grains), Carboniferous (~~28~~299 ± 7 to 356 ± 3 Ma, 29%), Devonian (366 ± 4 to 417 ± 4 Ma, 3%), Silurian (434 ± 11 to 443 ± 4 Ma, 3%), Ordovician (445 ± 6 to 482 ± 7 Ma, 17%), and Cambrian dates (490 ± 7 to 541 ± 7 Ma, 16%) (Fig. ~~14~~10).

~~5~~4.2.3. LA-ICPMS results from samples from the Miñarros quartz mylonites

The CL images of zircon grains from the Miñarros quartz mylonites (sample AG-19) show grains with continuous oscillatory zoning and composite grains with cores overgrown by low and high U rims (Fig. 7 in S3 Supplementary material). One hundred and fifty one analyses were performed on selected ~~zircons~~zircon grains and 145 yielded concordant or nearly concordant dates between 297 and 3105 Ma. Those dates are Palaeozoic (297 ± 5 to 535 ± 8 Ma, 30%), Neoproterozoic (545 ± 6 to 992 ± 13 Ma, 42%), Mesoproterozoic (1002 ± 10 to 1201 ± 12 Ma, 7%), Paleoproterozoic (1707 ± 69 to 2431 ± 20 Ma, 15%), Neoarchean (2528 ± 18 to 2696 ± 21 Ma, 5%) and Mesoarchean (2974 ± 18 to 3105 ± 23 Ma, 1%), and cluster into six main populations at ca. 300, 305, 550, 566, 622 and 986 Ma (Fig. ~~14~~10). The 43 Paleozoic zircon grains include Permian (297 ± 5 to 298 ± 4 Ma, 7% with respect to the total amount of Paleozoic grains), Carboniferous (299 ± 4 to 320 ± 4 Ma, 46%), Devonian (386 ± 5 to 413 ± 8 Ma, 5%), Ordovician (463 ± 6 to 483 ± 5 Ma, 19%), and Cambrian dates (495 ± 6 to 535 ± 8 Ma, 23%) (Fig. ~~14~~10).The youngest zircon $^{206}Pb/^{238}U$ date is 297 ± 5 Ma and the youngest zircon population, comprising 10 dates, has a mean $^{206}Pb/^{238}U$ age of 300 ± 1 Ma (MSWD = 0.64 and probability = 0.76).

Formatted: Font: Italic

~~5~~4.2.4. SHRIMP IIe/mc datations on ~~zircons~~zircon grains from sample AG-26 (orthogneiss)

Zircon grains from AG-26 are abundant and euhedral bipyramidal prisms with lengths of about 250 to 80 µm and widths of 100 to 50 µm. Most are brownish translucent crystals. CL imaging shows composite grains with partially resorbed cores overgrown by thick high U rims. Most of the cores show continuous oscillatory zoning truncated by the dark rims (Fig. 8 in S3 Supplementary material). Both domains were targeted for the analysis.

Sixteen U-Pb measurements on 16 different dark rims yielded 14 concordant or nearly concordant dates ranging from 14 to 250 Ma (Fig. ~~15~~11). Six dates plot in a single population with a ^{207}Pb corrected ^{206}Pb/^{238}U mean age of 15.8 ± 0.2 Ma (MSWD = 0.69, probability = 0.63) (Fig. ~~15~~11). These dates are from zircon with U and Th contents between 4006 and 7413, and 6 and 14 ppm, respectively, and Th/U between 0.001 and 0.004 (Table S1 in Supplementary material).

Thirty analyses were performed on 30 cores from different crystals and all these analyses yielded concordant or nearly concordant dates between 30 and 288 Ma (Fig. ~~16~~12). Fifteen analyses plot in a single population with a ^{207}Pb corrected ^{206}Pb/^{238}U mean age of 283 ± 2 Ma (MSWD = 0.76 and probability = 0.71) (Fig. ~~16~~12). These analyses are from ~~zircons~~zircon grains with U and Th contents between 377 and 1919, and 32 and 137 ppm, respectively, and Th/U between 0.05 and 0.21 (Table S1 in Supplementary material).

~~5~~4.3. Maláguide Complex and unconformable Middle Miocene red conglomerates and sandstones

Samples LP-16-AZ and AG-10 contained zircon grains displaying either continuous oscillatory zoning, partially resorbed cores overgrown by low or high U rims, or sector zoning. There were also a few structureless zircon grains (Fig. 9 in S3 Supplementary material)

The youngest zircon grains in these two samples have ^{206}Pb/^{238}U ages of 277 ± 7 and 283 ± 15 Ma, respectively, while the youngest zircon populations have mean

$^{206}Pb/^{238}U$ ages of 279 ± 3 Ma (MSWD = 0.57 and probability = 0.63) and 492 ± 8 Ma (MSWD = 1.3 and probability = 0.28), respectively.

The age distribution patterns of samples AG-10 and LP-16-AZ are significantly different (Fig. ~~17~~13). The two main populations in sample AG-10 are Ediacaran (population between 587 ± 14 and 615 ± 16 Ma, mean at ca. 602 Ma~~)~~: 12.8%) and Stenian (population between 1064 ± 30 and 1085 ± 22 Ma, mean at ca. 1074 Ma~~),~~: 4.0%), while in sample LP-16-AZ, they are Carboniferous (population between 299 ± 7 and 310 ± 8 Ma, mean at ca. 305 Ma~~)~~ 17.8%) and Ediacaran (population between 597 ± 14 and 618 ± 16 Ma, mean at ca. 608 Ma~~).~~: 4.4%). The percentage of Paleozoic grains in sample LP-~~16AZ~~16-AZ is also almost four times higher than that in sample AG-10, while the Neoproterozoic component in sample AG-10 is almost double that in sample LP-16-AZ. Furthermore, Mesoarchean and Neoarchean dates are lacking in sample LP-16-AZ, which does contain a Paleoarchean ~~population~~component.

The dates from the two samples (Fig. ~~17~~13) include Paleozoic (277 ± 7 to 528 ± 13 Ma, 14 to 52%), Neoproterozoic (546 ± 12 to 992 ± 21 Ma, 33 to 50%), Mesoproterozoic (1002 ± 26 to 1588 ± 21 Ma, 5 to 9 %), and Paleoproterozoic (1793 ± 43 to 2499 ± 33 Ma, 9 to 20%). Sample AG-10 also includes Neoarchean (2515 ± 15 to 2605 ± 32 Ma, 6%), and Mesoarchean (3000 ± 17 Ma, 1%) zircon grains, while sample LP-16-AZ also includes one Paleoarchean (3375 ± 18 Ma, 1%) zircon ~~grains~~grain. Within the Paleozoic zircon population, the main difference is the increase (by one order of magnitude) in the number of Carboniferous and Permian grains from 3 and 2 in sample AG-10 to 33 and 18 in sample LP-16-AZ, respectively. The character of the remaining Paleozoic grains is similar in AG-10 and LP-16-AZ (3 and 2 Devonian grains, 1 and 1 Silurian grains, 2 and 10 Ordovician grains, and 7 and 6 Cambrian grains in each sample, respectively).

Samples AG-3 and AG-20 from the unconformable Middle Miocene red conglomerates and sandstones contain zircon grains with either continuous oscillatory zoning or sector zoning (Fig. 10 in S3 Supplementary material). There are also some composite grains with a partially resorbed core overgrown by a thick rim, very similar to those previously described in the Micaschists and Quartzite Fm of the AC. Sample AG-20 also includes a few structureless zircon grains (Fig. 10 in S3 Supplementary material)

The youngest zircons from samples AG-3 and AG-20 have ^{206}Pb/^{238}U dates of 248 ± 8 and 177 ± 7 Ma, respectively, while their youngest zircon populations have mean ^{206}Pb/^{238}U ages of 582 ± 7 Ma (MSWD = 1.3 and probability = 0.23) and 292 ± 3 Ma (MSWD = 0.91 and probability = 0.47), respectively.

The age distribution patterns of AG-3 and AG-20 are slightly different (Fig. ~~18~~14). There is only one main population in sample AG-3 (Early Ediacaran: ca. 605 Ma~~),~~: 12.8%), while there are three main populations in sample AG-20 (Late Ediacaran: ca. 574 Ma~~;~~, 8.5%; Cryogenian: ca. 691 Ma~~;~~, 6.4%; Orosirian: ca. 2007 Ma~~).~~: 6.4%). Moreover, the percentage of Paleozoic (270 ± 6 to 535 ± 12 Ma) zircon grains in sample AG-20 (22%) is almost three times higher than that in AG-3~~.~~ (300 ± 7 to 508 ± 13, 8%). The Mesoarchean component (2848 ± 31 to 3119 ± 28 Ma) in sample AG-3 (5%) is ~~fourteen~~ten times greater than that in sample AG-20~~.~~ (with only one grain at 3081 ± 35 Ma, ca. 0.5%). Paleoarchean ~~zircons~~ zircon grains are absent in sample AG-20, but present in sample AG-3 (3205 ± 24 Ma) (Fig. ~~18~~14). Regarding the Mesozoic component~~,~~ (177 to 249 Ma), sample AG-3 contains one Triassic zircon grain with 248 ± 8 Ma, while sample AG-20 contains one Jurassic zircon grain~~. The number of Paleozoic grains also differs, with 11 and 31 grains in samples AG-3 and AG-20, respectively. The main difference in the Paleozoic component is the lack of Permian~~

grains in sample AG-3 and the content of Carboniferous grains (three in AG-3 to eight in AG-20). Samples AG-3 and AG-20 contain the same number of number of Devonian grains (4), and a similar number of Silurian (1 and 3, respectively), Ordovician (1 and 5, respectively), and Cambrian grains (2 and 4, respectively). with 177 ± 7 Ma.

6. Discussion

6The main difference in the Paleozoic component is the lack of Permian grains in sample AG-3, while sample AG-20 contains 7 grains with dates ranging between 270 ± 6 and 298 ± 7 Ma. They also differ in the content of Carboniferous (3 grains in AG-3; 300 ± 7 to 309 ± 7 Ma, and to 8 grains in AG-20; 304 ± 8 to 334 ± 7 Ma), Silurian (1 grain, 435 ± 17 Ma in AG-3, and 3 grains, from 428 ± 12 to 440 ± 10 Ma in AG-20), Ordovician (1 grain, 446 ± 11 Ma in AG-3, and 5 grains, from 453 ± 10 to 485 ± 10 Ma in AG-20) and Cambrian grains (2 grains, 504 ± 14 to 508 ± 13 Ma in AG-3, and 4 grains, from 487 ± 11 to 535 ± 12 Ma, in AG-20). Samples AG-3 and AG-20 contain the same number of number of Devonian grains (4 grains, 368 ± 10 to 412 ± 11 Ma in AG-3, and 360 ± 9 to 368 ± 10 Ma in AG-20).

5. Discussion

5.1. Depositional age of the graphite-bearing formations of the Nevado-Filábride and Alpujárride complexes

Within the upper or lower Lomo de Bas units, the four4 studied samples yielded youngest zirconszircon grains with 4 dates between 284 ± 14 and 323 ± 5 Ma, while their. As previously stated, we also provide youngest populations (see Dickinson and Gehrels, 2009 for the method, and Sharman and Malkowski; 2020 for a discussion). Their youngest populations vary between 321 ± 2 and 336 ± 2 Ma (see text S2 and Fig.

S4 in Supplementary material). Therefore, the youngest dates point towards Early Permian-Late Carboniferous maximum depositional ages (MDA). However, as data from the orthogneisses samples AG-13 and AG-26 highlight, some of the youngest zircon dates can be related to Mesozoic metamorphic events and/or ~~Pb~~lead loss. Therefore, we prefer the more conservative approach of using the youngest detrital zircon populations~~, and thus~~. Therefore, we propose a MDA between 321 ± 2 and 336 ± 2 Ma for the quartzites of the Lomo de Bas (i.e., Carboniferous).

~~The minimum depositional age of these rocks is defined by samples AG-13 and AG-16, the~~The orthogneiss bodies within the Lomo de Bas ~~blacks~~black schists and quartzites (Álvarez and Aldaya, 1985; Álvarez, 1987) ~~with~~ are strongly deformed and metamorphosed, making it difficult to determine whether they represent volcanic rocks or intrusive plutons. However, in either case, these units can help define the minimum depositional age of the Lomo de Bas rocks, as they are located in the uppermost part of the succession (see Fig. 4). If they are volcanic rocks coeval with deposition, they indicate the age of the uppermost layers, and if they are plutons which were intruded post-deposition, they constrain the minimum depositional age of the Lomo de Bas rocks. Samples AG-13 and AG-16 yield $^{206}Pb/^{238}U$ ages for the ~~protoliths~~parent rocks of 294 ± 2 Ma (MSWD = 0.75 and probability = 0.68) and 289 ± 3 Ma (MSWD = 1.4 and probability = 0.20), respectively. The ~~ages~~age of both orthogneisses just overlap within uncertainty and, together with the previous MDA, ~~define~~defines a depositional age for the quartzitic rocks of the Lomo de Bas units between Bashkirian (Late Carboniferous) and Artinskian-Sakmarian (Early Permian).

This Late Carboniferous age ~~agrees~~is compatible with the presence of Early-Middle Devonian fossils in the dark marbles below the quartzites of the upper tectonic unit (Eifelian-Emsian, c.f. Lafuste and Pavillon, 1976; Laborda-López et al., 2013, 2015a, b), and also supports the presence of several superposed tectonic units as suggested by Laborda-López et al. (2013, 2015a, b).

The youngest $^{206}Pb/^{238}U$ zircon dates in samples from the Micaschists and Quartzite Fm of the AC (AG-4, AG-5, AG-6 and AG-7) are Early Permian-Late Carboniferous (328 ± 10 Ma and 296 ± 4 Ma), but the youngest populations in these samples are highly variable; Cambrian-Late Ediacaran (between 507 and 558 Ma) in samples AG-4, AG-6 and AG-7, and Late Carboniferous (308 Ma) in sample AG-5 at the base of the Micaschists and Quartzite Fm. ~~A~~Sample AG-5 indicates a MDA of Late Pennsylvanian age~~ is proposed~~ for the AC Micaschists and Quartzite Fm.

~~6~~5.2. Provenance of zircon in Late Carboniferous samples

The studied samples from both the Lomo de Bas rocks and the Micaschists and Quartzite Fm include Carboniferous grains (~~49~~8.9% of total grains in the NFC, and ~~20~~3.6% of grains in the AC) that could have been sourced from Late-Variscan and Variscan ~~felsic~~igneous rocks, ~~widely distributed within~~occupying more than one third of the outcrops of the whole Iberian Massif, and ~~surrounding areas~~essentially, ca. one half of the Central Iberian Zone (e.g. Arranz and Lago, 2004; Bea, 2004; Casquet and Galindo, 2004; Gallastegui et al., 2004; Ribeiro et al., 2019). Furthermore, they could have been sourced from the oldest granitoids within the Variscan remnants in the Betic Chain, essentially the older orthogneisses in the NFC with U-Pb ages of ca. 301 Ma (Gómez-Pugnaire et al., 2004, 2012). The Carboniferous rocks of both the NFC and AC also include a number of Early Ordovician, Silurian and Devonian dates (~~23~~4.4% of grains in the NFC and ~~15~~2.7% of grains in the AC with dates between 484 and 365 Ma~~), which~~). Ordovician zircon grains may have ~~no known source in pre-Carboniferous rocks~~ come from the Ollo de Sapo magmatic event (Montero et al., 2007, 2009, Díez-

Montes et al., 2010) or other igneous bodies (Rubio-Ordóñez et al. 2012; Talavera et al., 2013; Pereira et al., 2018), while Silurian and Devonian grains may have originated from the volcanic event that is now starting to be recognized in the Central Iberian~~,~~ ~~Cantabrian, and West Asturian-Leonese zones of the Iberian Massif. The nearest source of these zircon grains could be in the Avalonian terranes. In fact, felsic magmatism was developed during rifting, spreading,~~ Zone (Gutiérrez-Alonso et al., 2008), or from the allochthonous complexes where rocks with Silurian and ~~later subduction of the Rheic Ocean (e.g. Sánchez Martínez et al., 2007, 2012). In the surrounding Variscan terranes, Devonian zircon source rocks~~ Devonian grains are ~~only~~relatively abundant (see Pastor-Galán et al., 2013, where their sources are explored). For example, they are found within granites in the the Sehoul Block in the Western Moroccan Meseta (Tahiri et al., 2010~~). However,~~), and also within metasediments ~~containing those Devonian grains have also been described~~: i) in the Late Devonian Debdou-Mekkam Metasediments in the Eastern Moroccan Meseta (Accotto et al., 2020), ii) in Late Paleozoic metasediments from both the South Portuguese and Ossa-Morena zones (Pereira et al., 2012, 2014, ~~2017~~2017a; Pérez-Cáceres et al., 2017~~),~~) and iii~~) in the Carboniferous rocks from the Cantabrian Zone (Pastor-Galán et al., 2013), and, iv~~) in the syn-orogenic rocks below the allochthonous complexes of the Galicia-Tras-Os-Montes (Martínez Catalan et al., 2008).

~~As previously mentioned, these Devonian grains are interpreted as having been derived from Avalonian terranes, based on two slightly different hypotheses. The first is that they were sourced from an unexposed magmatic arc along the Avalonian convergent margin during Middle-Late Devonian subduction of the Rheic Ocean (Pereira et al., 2012, 2017; Pérez-Cáceres et al., 2017; Accotto et al., 2020). The second possibility is that they were directly sourced from eroded rocks within the Rheic Ocean~~

Formatted: English (United Kingdom)

Formatted: English (United Kingdom)

Formatted: English (United Kingdom)

Formatted: English (United Kingdom)

~~suture zone, where zircon grains of these ages occur (e.g. Fernandez-Suarez et al., 2002; Sánchez-Martínez et al., 2007; Martínez Catalán et al., 2008; Pastor-Galán et al., 2013).~~

~~However, the main detrital zircon component in the Carboniferous rocks of both the NFC and AC is pre-Cambrian, with two main populations: i) an Early Neoproterozoic population between ca. 574 and 602 Ma (Ediacaran-Cryogenian) (Text S2 in Supplementary material), and ii) a Mesoproterozoic population between ca. 1014 and 1039 Ma (Stenian) (Fig. 19; Text S2 in Supplementary material). These populations represent the Cadomian-Pan-African orogeny developed in Gondwana and the Tonian-Stenian magmatic event that took place in the Arabian Shield (see Bea et al., 2010), respectively. Furthermore, the NFC and AC Carboniferous rock also contain an Orosirian (ca. 2.0-2.1 Ga), recording the Eburnean orogeny, and a Neoarchean (ca. 2.5-2.7 Ga) population.~~ However, the main detrital zircon component in the Carboniferous rocks of both the NFC and AC is pre-Cambrian, and includes 4 zircon age populations: Ediacaran-Cryogenian (39.4% in the NFC at ca. 574 Ma, and 5.2% in the AC at ca. 602 Ma), Tonian-Stenian (3.6% in the NFC at ca. 1014 Ma, 5.3% in the AC at ca. 1039 Ma), Orosirian (3.8% in the NFC at ca. 2024 Ma, and 4.8% in the AC at ca. 2054 Ma), and Neoarchean (1.7% in the NFC at ca. 2659 Ma, and 1.6% in the AC at ca. 2547 Ma). The first of these four populations represents the Cadomian-Pan-African orogeny, developed in Gondwana and the peri-Gondwanan terranes, like the Meguma and West Avalonia terranes. The second one represents the Tonian-Stenian magmatic event in the Arabian Shield at ca. 1.0 Ga (see Bea et al., 2010; Fernández-Suárez et al., 2014; Meinhold et al., 2014). The Orosirian population represents the Eburnean orogeny, and the ages of the basement in the cratonic areas of the Saharan Metacraton (see Meinhold et al., 2014).

Similar age patterns with these four peaks are found within the Carboniferous and older rocks from the Central Iberian, Cantabrian, and West Asturian-Leonese zones of the Iberian Massif (see Talavera et al., 2012, 2015; Pastor-Galán et al., 2013; Fernández-Suárez et al., 2014; Shaw et al., 2014; Gutierrez-Alonso et al., 2015) (Fig. 19). If we focus on the Pre-Carboniferous rocks, Fernandez Suarez et al. (2014) studied the age of zircon from Ediacaran and Early Cambrian rocks of the Cantabrian and Central Iberian zones and found two populations ca. 0.55-0.75 Ga and ca. 0.85-1.15 Ga, and also minor Paleoproterozoic (ca. 1.9–2.1 Ga) and Archean (ca. 2.4–2.6 Ga) populations (Fig. 19D). Talavera et al. (2012, 2015) also determined similar age patterns in Ediacaran to Early Ordovician rocks of the Central Iberian Zone. Shaw et al. (2014) sampled and studied the Lower Ordovician Armorican quartzite trough the Central Iberian, Cantabrian, and West Asturian-Leonese zones, and their age pattern (n=1173) also shows the above-mentioned peaks with Ediacaran-Cryogenian (ca. 617 Ma), Tonian-Stenian (ca. 1.21 Ga), Orosirian (ca. 2.0 Ga), and Neoarchean (ca. 2.6 Ga) populations (Fig. 19D). Furthermore, Gutierrez-Alonso et al. (2015) studied Silurian-Devonian sedimentary rocks from the same two paleogeographic zones and found also the same four populations: Ediacaran–Cryogenian (c. 0.55–0.8 Ga), Tonian–Stenian (0.85–1.2 Ga), Palaeoproterozoic (c. 1.8–2.2 Ga) and Archaean (c. 2.5–3.3 Ga) (Fig.19C). In summary, the same four age peaks were found in all these works, albeit with differences in the proportion of grains in each population (Fig. 19). Stephan et al. (2019) include those areas with similar pre-Ediacaran age patterns to their East African-Arabian zircon province, and included the Central Iberian, Cantabrian, and West Asturian-Leonese zones of the Iberian Massif.

We can also compare the results presented here with those obtained on samples of a similar age from the Betic Cordillera, Iberian massifMassif and surrounding areas.,

Formatted: English (United States)

as the Pyrenees, Montagne Noire and Mouthoumet massifs (Martínez et al., 2016) (Fig. S5 in the Supplementary material). In the Betic Cordilleras, the Lomo de Bas units have usually been interpreted as part of the Veleta units of the NFC (i.e. Álvarez and Aldaya, 1985; Álvarez, 1987), and their quartzites correlated with the Late Carboniferous Aulago Fm in the Sierra de Filabres area (Jabaloy-~~Sanchez~~Sánchez et al., 2018; Rodríguez-Cañero et al., 2018), which also include the Ediacaran-Cryogenian and Stenian populations mentioned above (~~Fig. 19A).~~Jabaloy-Sánchez et al., 2018) (Fig. S5 in Supplementary material). The main difference is a larger proportion of Devonian and Carboniferous zircon grains within the Lomo the Bas rocks (13 and 49 grains, respectively), when compared to those from the Aulago Fm (7 and 4 grains, respectively; Jabaloy-Sánchez et al., 2018) (Fig. ~~19A).~~S5 in Supplementary material). Furthermore, the age pattern of sample Ri119 from the Paleozoic basement of a tectonic unit of the Sebtide/Alpujárride Complex in the Internal Rif (n=144 analyses, Azdimousa et al., 2019) also yields a similar pattern to that in Late Carboniferous samples from the AC and NFC with two main populations at ca. 532 and 992 Ma (Fig. ~~19B).~~ S5 in Supplementary material).

Similar age patterns with these four peaks are found within the Carboniferous and older rocks from the Central Iberian, Cantabrian, and West Asturian-Leonese zones of the Iberian Massif (see Talavera et al., 2012, 2015; Pastor-Galán et al., 2013; Fernández-Suárez et al., 2014; Shaw et al., 2014; Gutierrez-Alonso et al., 2015) (Fig. ~~Pereira et al. (2014, 2020) studied the Late Carboniferous sediments from the Ossa-Morena and South Portuguese zones of the Iberian Massif (see Pereira et al., 2012, 2014, 2020, and references therein) (Fig. 19H). Within these rocks, those from the Ossa-Morena Zone were deposited in a continental environment (Santa Susana Fm Pereira et al., 2020), with an age pattern that includes a main Early Carboniferous~~

Formatted: English (United States)

population at ca. 354 Ma, but also Cryogenian (ca. 647 Ma) and Rhyacian (ca. 2128 Ma) secondary populations (Pereira et al., 2020) (Fig. 19H). However, the age patterns lack the Stenian and Neoarchean populations present in the NFC and AC samples (Fig. 19). Furthermore, marine detritic sediments were also deposited in the South-Portuguese Zone, and their age patterns are very similar to those of the Ossa-Morena Zone. Those marine detritic sediments from the South-Portuguese Zone include the Devonian (ca. 405 Ma), Ediacaran-Cryogenian (ca. 639 Ma), and Orosirian populations (ca. 2068 Ma), and they lack the Stenian and Neoarchean ones (Brejeira and Mira Fms from Pereira et al., 2014) (Fig. 19).

On the other hand, Upper Carboniferous samples from the Cantabrian Zone studied by Pastor-Galán et al. (2013) yield very similar age distribution patterns to those of the Lomo de Bas (NFC) and Micaschists and quartzites Fm (AC), with the only difference being the existence of an Early Carboniferous peak (ca. 335 Ma, “Variscan”) in the rocks from the Betic Cordillera (Fig. 19C). Martínez et al.S5 in Supplementary material).

If we compare the studied samples with the previously discussed age patterns using the MDS plot, we found that all the samples from the Late Carboniferous rocks from the NFC (Jabaloy-Sánchez et al., 2018; this work), AC (Azdimousa et al., 2109; this work) and the Cantabrian Zone (Pastor-Galán et al., 2013) are very similar except for sample AG-17 (Fig. 15). This similarity is indicated by a clustering of all samples from the NFC, AC and the Cantabrian Zone to the upper left of the plot, while sample AG-17 plots near the centre (Fig. 15).

Martínez et al. (2016) analyzed Late Carboniferous rocks from the NE Iberian Peninsula and South France, including samples from the Catalonian Massif, Minorca, Montagne Noire Massif, Mouthoumet Massif, Pyrenees, and Priorat, but Massif. In

Formatted: English (Australia)

Formatted: English (Australia)

order to compare these samples with our data, we have calculated discordance for their dataset, and selected the ~~age patterns show~~780 ages with Concordia between 90% and 110%. The MDS plot shows no similarity with the previously discussed data except for sample AG-17, which together with the samples from Martínez et al. (2016), grouped in a different cluster to those of the NFC, AC and the Cantabrian Zone (Fig. 15). The main differences ~~only in~~that explain the ~~Stenian and Neoarchean populations. The~~observed dissimilarity between these Late Carboniferous samples ~~from Martinez et al (2016)~~ ~~usually~~are the lack of a Stenian peak (Montagne Noire Massif, Mouthoumet Massif, Pyrenees, and Priorat Massif~~)~~), or , if present, it is a minor one (Catalonian Massif and Minorca~~), and~~) in the samples from Martinez et al (2016). Furthermore, the Neoarchean population is also absent in the Catalonian Massif, Mouthoumet Massif, Pyrenees, and Priorat Massif areas, but not in the samples from Minorca and Montagne Noire Massif ~~(Fig. 19E and F).~~.

Dinis et al. (2018) and Pereira et al. (in press) studied the Late Carboniferous sediments from the Ossa-Morena (Santa Susana Fm: samples StSz2 and StSz4 from Dinis et al., 2018, and SS-1 and SS-2 from Pereira et al., in press). In the MDS plot, they do not show any similarity with the samples from NFC, AC or the Cantabrian Zone, except in the case of the comparison between AG-17 and SS-2 and StSz4 samples. The Santa Susana Fm samples plot far from the other two clusters on the MDS diagram. (Fig. 15). The main difference is the lack of the Stenian and Neoarchean populations in the latter samples. Furthermore, Pereira et al. (2014) studied the South Portuguese Zone of the Iberian Massif (Fig. S5 in Supplementary material), where Late Carboniferous sediments were deposited in the Mira Fm (Serpukhovian-Bashkirian, samples ST-8 and SC-6 from Pereira et al., 2014) and in the Brejeira Fm (Bashkirian-Moscovian, samples AJ-1, AM-3, and TH-5 from Pereira et al., 2014). Samples from

Formatted: English (Australia)

Formatted: English (Australia)

Formatted: English (Australia)

Formatted: English (Australia)

Formatted: English (Australia)

Formatted: English (Australia)

Formatted: English (Australia)

Formatted: English (Australia)

Formatted: English (Australia)

Formatted: English (Australia)

Formatted: English (Australia)

both the Mira and Brejeira Fms essentially show no similarity with the samples from the NFC, AC and Cantabrian Zone in the MDS plot, although the AM-3, and TH-5 samples show some similarity with the cluster from sample AG-17 and those from NE Iberian Peninsula and South France (Martinez et al., 2016) (Fig. 15).

All these data suggest that the Late Carboniferous sediments of both the NFC and the AC were sourced and recycled from Variscan rocks containing zircon grains from the Cantabrian, West Asturian-Leonese, and Central-Iberian zones of the Iberian Massif~~, but they also include a small amount of zircons derived from the Avalonian terranes.~~. Furthermore, the sediments incorporated a small number of zircon grains derived from the Late-Variscan felsic rocks. The sediments were mainly pelites rich in organic material, quartz-rich sandstones (quartzwackes in the case of the NFC, Jabaloy, 1993; Rodríguez-Cañero et al., 2018), and black limestones (with conodonts in the case of the NFC rocks; Rodríguez-Cañero et al., 2018) suggesting deposition in open marine anoxic environments (Rodríguez-Cañero et al., 2018). This points to an environment similar to the Carboniferous foreland basins developed in the Cantabrian Zone of the Iberian Massif (see Matte, 2001, Rodríguez-Cañero et al., 2018; Jabaloy-Sánchez et al., 2018) as the most likely paleogeographic location of both complexes (Fig. ~~20~~16).

In Late Carboniferous times, the Variscan belt was already formed in Western and Central Europe (e.g. Matte, 2001), and most of the rocks of the Cantabrian, West Asturian-Leonese, Central-Iberian zones were deformed and stacked with the rocks of the Rheic Ocean suture zone (i.e. Pastor-Galán et al., 2013). Rocks from the Variscan belt, including rocks from those three stacked zones, were being eroded at Late Carboniferous, and their ~~zircons~~zircon grains had been stored within the coetaneous sediments in the Cantabrian Zone (see Pastor-Galán et al., 2013), and NFC (Jabaloy-

Sánchez et al., 2018). Our data indicate the same case for the rocks of the AC (Fig. ~~20~~16).

On the other hand, the published data from the samples from the MC with Carboniferous-Early Permian ages have Early Carboniferous (at ca. 329 and 347 Ma respectively), Early Ordovician-Cambrian (ca. 445 and 491 Ma), Ediacaran-Cryogenian (ca. 589 and 649 Ma), Tonian (ca. 932 Ma), and Orosirian populations (ca. 2002 and 2080 Ma) (sample CM-10 from the Marbella ~~conglomerate~~Conglomerate from Esteban et al., 2017, ~~Fig. 19A;~~and sample Ri121 from Azdimousa et al., 2019, Fig ~~19G).~~S5 in Supplementary material). However, they show a difference in the number of Neoarchean zircon grains (ca. 2.6 Ga), which are more abundant in ~~the~~ sample Ri121 from Azdimousa et al., 2019, Fig. ~~19G). The age distribution patterns for both samples also include a small number of Devonian zircons, most likely sourced in~~S5 in Supplementary material). In the ~~Avalonian terranes, such as the Sehoul block (Accotto et al., 2020). Those data suggest that the main source area for the Marbella conglomerate described in Esteban et al. (2017) was the West African Craton and derived terranes (i.e. Ossa-Morena Zone according to Esteban et al., 2017). However, the age pattern of sample Ri121 from Azdimousa et al. (2019) is very similar to that found in the NFC and AC Carboniferous rocks, suggesting~~MDS plot, they are located within the same ~~source areas.~~cluster as sample AG-17 and those from North-eastern Iberian Peninsula and South France. Therefore, the ~~paleogeographic~~ most likely location of the MC ~~seems slightly different from that of the NFC and AC,~~realm was not at the southern paleomargin of Iberia (Esteban et al., 2107), but in the same paleomargin as the North-eastern Iberian Peninsula and ~~in this location the sediments were sourced from the Cantabrian, West Asturian-Leonese, Central-Iberian zones, or the Ossa~~

~~Morena Zone (Esteban et al., 2017) and/or the Moroccan Variscides (Figs. 19, 20).~~South France rocks.

~~6~~5.3. ~~Lower~~ Permian ~~orthogneisses~~to Triassic samples from the NFC ~~(Cantal unit)~~, AC and MC

~~The sample~~Sample AG-26 from the Cabezo Blanco orthogneiss within the Cantal unit yielded ~~zircons~~zircon grains with textures similar to those described by Gómez-Pugnaire et al., (2004, 2012) in the NFC. The CL imaging of these grains shows cores with continuous oscillatory zoning truncated by dark U-rich rims. These cores yielded a ^{207}Pb corrected ^{206}Pb/^{238}U age of 283 ± 2 Ma, while the dark overgrowths have yielded a ^{207}Pb corrected ^{206}Pb/^{238}U age of 15.8 ± 0.2 Ma. We propose the former age as the age of the igneous ~~protolith~~parent rocks of the Cabezo Blanco orthogneiss and the latter age as the age of a metamorphic event affecting this orthogneiss. Similar metamorphic ages have been determined within ~~zircons~~zircon grains from the NFC (López Sánchez-Vizcaíno et al., 2001, 15.0 ± 0.6 Ma; Gómez-Pugnaire et al., 2004, 2012~~,~~; 16.5 ± 0.4 Ma and 17.3~~±~~ ± 0.4 Ma respectively). Furthermore, similar ages were also determined from Lu-Hf on garnets (Platt et al., 2006, between 18 and 14 Ma) and multimineral isochrons on samples of this complex (Kirchner et al., 2016; three ages of 20.1 ± 1.1, 16.0 ± 0.3, and 13.3 ± 1.3 Ma). However, the metamorphic ~~zircons~~zircon grains from the AC typically have slightly older ages (Sánchez-Rodriguez and Gebauer, 2000, 19.9 ± 1.7 Ma.; Platt et al., 2003~~,~~; ages between 22.7 and 21.3 Ma~~,~~; Esteban et al., 2007, 19.2 ± 1.1 Ma~~-~~), and the AC has yielded additional older ages including a garnet Lu-Hf age of 25 ± 1 Ma (Blichert-Toft et al., 1999), and a garnet and clinopyroxene Sm-Nd age of 21.5 ± 1.8 Ma (Zindler et al., 1983). Therefore, we propose that the Cantal unit is part of the NFC as already proposed by García-Tortosa (2002).

6.4. Permian to Triassic metadetrital samples from the NFC

Samples AG-1 and AG-2 come from two quartzites in the upper part of the Tahal Fm within the Mulhacén units. They yielded very similar zircon age patterns, the youngest zircon $^{206}Pb/^{238}U$ dates being Jurassic (195 ± 8 Ma and 179 ± 5 Ma, respectively) and the youngest zircon population being Early Permian (275 ± 8 Ma and 277 ± 4 Ma, respectively). These data match the 259 concordant-nearly concordant analyses from the Tahal Fm published by Jabaloy-Sánchez et al. (2018), in which the youngest zircon population was Early Permian (275 ± 2 Ma) as well (Fig. 21CS6 in Supplementary material).

An estimate of the MDA for the sources of the Tahal Fm based on the youngest zirconszircon grains points to Jurassic. However, our preference is a more conservative estimate for the MDA based on the youngest populations and our proposal is an age younger than Early Permian (275 ± 8 Ma), in agreement with the data provided by Jabaloy-Sánchez et al. (2018), and Santamaría-López and Sanz de Galdeano (2018) for the same rocks in Sierra Nevada and Sierra de los Filabres.

Formatted: Font: Bold

6.5. Permian to Triassic metadetrital samples from the AC

The youngest zircon dates for samples AG-9, AG-11, and AG-15 from the Meta-detrital Fm of the AC are Triassic-Early Permian (between 214 ± 2 Ma and 288 ± 4 Ma) and the youngest zircon populations are Early Permian (287 ± 2, AG-9, and 287 ± 1, AG-11) to Early Ordovician (474 ± 3 Ma, AG-15). We have used the same approach described above to estimate the MDA of the Meta-detrital Fm, proposing an Early Permian (Artinskian) MDA for this formation, older than the Middle Triassic stratigraphic age (ca. 247 to ca. 237 Ma, see Simon and Visscher, 1983; Maate et al., 1993; García Tortosa et al., 2002; Martín-Rojas et al., 2010). Furthermore, the youngest zircon $^{206}Pb/^{238}U$ date and the youngest zircon population in sample AG-19 from the Miñarros unit are 297 ± 5 Ma and 300 ± 1 Ma, respectively, indicating an older MDA (Gzhelian, Late Pennsylvanian). Samples AG-9, AG-11, AG-15 and AG-19 have similar age patterns to the samples from the Tahal Fm (NFC).

~~6.6. Permian to Triassic metadetrital samples from the MC~~

The youngest zircon grains from samples AG-10 and LP-16-AZ from the Saladilla Fm of the MC yielded $^{206}Pb/^{238}U$ dates between 277 ± 7 and 282 ± 15 Ma. Moreover, the youngest zircon populations were 492 ± 8 Ma and 279 ± 3 Ma, respectively, pointing to an Early Permian MDA.

~~6.7~~5.4. Provenance for zircon of ~~the~~ the Permian to Triassic meta-detrital samples

A common feature of the samples with a Permian MDA from the three complexes (NFC, AC and MC) is an increase in the number of Paleozoic ~~zircons~~zircon grains with respect to the older Carboniferous samples (Fig. ~~21). In fact, the~~S6 in Supplementary material). The Permian MDA samples show an increase in the number of Permian and Carboniferous zircon grains indicating erosion of Variscan and Late-Variscan felsic rocks in the source areas. In the NFC, the Tahal Fm contains 21% to 27 % Permian-Carboniferous grains (the values are the percentage of the total number of analyses of each sample) (254 to 355Ma), while the Late Carboniferous Lomo de Bas quartzites have 5% to 18% Carboniferous grains, with only two Permian grains. Within the AC, the Meta-detrital Fm has variable contents of Permian-Carboniferous grains (from 3 to 31%, the values are the percentage of the total number of analyses of each sample), while the Late Carboniferous Micaschists and Quartzite Fm has 3% to 6%.

Furthermore, in the MC, the Saladilla Fm also displays a variable content of Permian-Carboniferous grains (from 4% to 38%); while the Lower Carboniferous Morales Fm (sample Ri121 from Azdimousa et al., 2019) has 6% Carboniferous grains, and the Permian Marbella Conglomerate (Esteban et al., 2017) has 12 % Permian and Carboniferous grains.

Samples from the Tahal Fm (NFC) have Carboniferous populations between ca. 331 and ca. 334 Ma ("Variscan"), Ediacaran populations between ca. 598 and ca. 610 Ma ("Cadomian"-"Pan-African"), and a Tonian population at ca. 939 Ma (Fig. ~~21).~~S6 in Supplementary material). If the "Variscan grains" are excluded (i.e. post- Late Devonian grains which are younger than 370 Ma), the age distribution pattern is similar to that of the Aulago Fm (Jabaloy-Sánchez et al., 2018) and of the Lomo de Bas quartzites, except for a lower number of Tonian-Stenian (ca. 1.0 Ga) and Neoarchean (ca. 2.61 Ga) grains (~~Fig. 20~~Figs. S5 and S6 in Supplementary material).

The age distribution patterns for samples from the Meta-detrital Fm (AC) are similar to those in the above mentioned samples from the Tahal Fm (NFC) (Fig. ~~21).~~S6 in Supplementary material). Samples from the Meta-detrital Fm also have Permian ("Late-Variscan" at 287Ma), Ediacaran-Cryogenian ("Pan-African", from ca. 546 to ca. 660 Ma) populations, with minor Tonian-Stenian (from ca. 963 to ca. 1016 Ma) and Rhyacian ("Eburnean", ca. 2060 Ma) populations (Fig. ~~21).~~S6 in Supplementary material). If the <370 Ma zircon grains are excluded, the age distribution pattern is similar to that obtained by combining the Micaschists and Quartzite Fm (AC) datasets (Fig. ~~21~~S6 in Supplementary material).

In the Saladilla Fm (MC), there are Permian ("Late-Variscan" between ca. 279 and 305 Ma), and Ediacaran-Cryogenian populations ("Pan-African", from ca. 602 to 677 Ma), with minor Stenian (ca. 1074 Ma), Orosirian ("Eburnean", ca. 1937 Ma) and

Neoarchean (ca. 2106 Ma) peaks (Fig. ~~21).~~S6 in Supplementary material). They differ from the data of the Carboniferous-Early Permian samples from the same MC (Esteban et al., 2017; Azdimousa et al., 2019), not only in the presence of the Early Permian population, but also in the Stenian and Neoarchean peaks. This distinction in the age patterns is due to the erosion and incorporation of material from Late-Variscan felsic rocks and the increasing number of ~~zircons~~zircon grains sourced from the Cantabrian, West Asturian-Leonese and Central-Iberian zones.

~~The similarity between the age patterns of samples with Early Permian MDA from the three complexes and those of the Permian-Early Triassic from the Iberian ranges (Sánchez Martínez et al., 2012) suggests that they were deposited in the same Permian-Triassic basins.~~

~~**6.8**~~Comparing these samples with Permian MDA with Permian and Triassic samples from the Iberian Peninsula (Sánchez Martínez et al., 2012; Pastor-Galán et al., 2013; Pereira et al. 2016; Dinis et al., 2018; Gama et al., in press) using the MDS plot, we found that samples from the Tahal Fm (NFC), Meta-detrital Fm (AC) and Saladilla Fm are quite similar, and they project towards the centre of the figure (Fig. 17), while sample LP−16−AZ is slightly separated, thus suggesting that all these samples have the same source area. Furthermore, all show similarities with most of the samples from the Iberian Chain (Sánchez Martínez et al., 2012), Cantabrian Zone (Pastor-Galán et al., 2013), Permian El Viar Basin (Dinis et al., 2018), Triassic Lusitanian Basin (Pereira et al., 2016; Dinis et al., 2018), Triassic Alentejo Basin (Pereira et al., 2017b; Dinis et al., 2018), and Triassic Algarve Basin (Pereira et al., 2017b; Dinis et al., 2018; Gama et al., in press). These similarities can be seen in the MDS plot in which samples PT2, PT4 and PT5 from the Iberian Chain (Sánchez-Martínez et al., 2012), PG2 and PG3 from the

Cantabrian Zone (Pastor-Galán et al., 2013), V152 and V154 from the Viar Basin (Dinis et al,., 2018), CM2, SBM-6 and SBM-7 from the Algarve Basin (Pereira et al 2017b; Gama et al., in press), SC−4 from the Alentejo Basin (Pereira et al 2017b), and SO and CO from the Lusitania Basin (Pereira et al., 2016; Dinis et al., 2018) cluster together with the samples from the Betic Cordillera (Fig. 17).

A major question is what tectonic process induced these differences. Vissers (1992) found an Upper Carboniferous to Permian extensional event in the Pyrenees synchronous with uplift and emergence of large parts of the crust and deposition of continental sediments in fault-bounded extensional half-grabens. Subsequently, García-Navarro and Fernández (2004) found an Early Permian faulting event in the SW Iberian Peninsula where strike-slip and normal faults generated the intracontinental, Early Permian El Viar basin. Those data suggest that during the Permian to Early Triassic breakup of Pangea, tectonic uplift along major normal faults may have exposed different levels of Variscan crust, including the Late-Variscan granitoids, to erosion.

5.5. Unconformable Middle Miocene red conglomerates and sandstones

The samples from Middle Miocene sediments have only two Mesozoic zircon grains (248 ± 8 and 177 ± 7 Ma), and their youngest zircon population has a mean $^{206}Pb/^{238}U$ age of 292 ± 3 Ma, pointing to an Early Permian MDA. Their age distribution patterns correspond to mixing of ~~zircons~~zircon grains from the AC and MC, confirming that after experiencing HP metamorphism during Oligocene-Early Miocene times (Zindler et al., 1983; Blichert-Toft et al., 1999; Sánchez-Rodriguez and Gebauer, 2000; Platt et al., 2003; Esteban et al., 2007), the AC rocks were exhumated and eroded at the surface during the Middle Miocene. It is noteworthy that ~~those~~these unconformable Middle Miocene sediments were formed at the surface at the same time that the Cantal unit (sample AG-26) and the NFC ~~were~~was experiencing metamorphism in depth. However, the most important conclusions is that there is no record of any major felsic rock formation event after the Early Permian times in the AC or MC, although several stages of continental rifting and the subduction of the AC took place during this period (e.g. Jabaloy-Sánchez et al., 2019).

The U-Pb zircon data presented here have implications for the evolution of both the Variscan and Alpine chains in the western Mediterranean area. The main implications for the Variscan chain is the existence of Late Carboniferous sedimentary basins eastwards of the Iberian Massif, which recorded the erosion of the Variscan Chain formed during the Late~~-~~ Devonian~~-~~-Carboniferous, and were also affected by the Late Carboniferous-Early Permian Late Variscan magmatic event. The ~~sediment~~sedimentary record in these basins was metamorphosed from Oligocene to Middle Miocene times to form the graphite-rich successions of the NFC and AC during the Alpine orogeny.

During the Permian-Triassic, the break-up of Pangea took place and resulted in the formation of three different paleogeographic realms:

i) the Nevado-Filábride realm continued near the Iberian Massif southeastern paleomargin,

ii) the Alpujárride realm separated from the Iberian Massif by rifting during the Triassic-Jurassic (Martín Rojas et al. 2009; Puga et al., 2011),

iii) the Maláguide realm separated from the ~~southern~~North-eastern paleomargin of Iberia (Esteban et al., 2107) during the Jurassic (e.g., Martín-Martín et al. 2006).

Those three realms amalgamated during the Cenozoic; first, the AC subducted below the MC, and later, the NFC subducted below the two previously amalgamated complexes at Early Middle Miocene times. During these processes, the Cantal unit was partially ~~fused, leading to the formation of migmatites.~~ melt, leading to the formation of migmatites. Another line of correlation is the age of the felsic intrusive rocks reported here and in previous works (Gómez-Pugnaire et al., 2014; 2012). The Permian age of the volumetrically minor intrusive bodies (301 to 282 Ma, Gómez-Pugnaire et al., 2004, 2012; this work) is similar to granites in the CZ (286 to 297 Ma; Gutiérrez-Alonso et al., 2011), while the significantly more abundant granites in the WALZ and the CIZ are, in general, older (321 to 290 Ma, Martins et al., 2019, and references therein).

7. Conclusions

New U-Pb detrital zircon ages in rocks from the Águilas Arc provide maximum depositional ages for their ~~protoliths. U-Pb zircon ages of orthogneisses help to constrain their true depositional ages.~~parent rocks. Orthogneisses in the NFC may have volcanic or plutonic parent rocks, but as they are located in the uppermost part of the Lomo de Bas succession, they can indicate a minimum depositional age for these rocks (Sakmarian- Artinskian, 294 ± 2 Ma and 289 ± 3 Ma), regardless of their igneous classification. In the NFC, the true depositional age of the Lomo de Bas schists and quartzites is Late Carboniferous to Early Permian (ranging between 321 ± 2 and ~~293 ± 2~~289 ± 3 Ma), while the MDA of the Tahal Fm is confirmed as Early Permian. In the AC, the MDA of the Micaschists and Quartzite Fm is also Late Carboniferous (308 ± 4 Ma), and that of the Meta-detrital Fm is Early Permian (287 ± 1 Ma). Furthermore, the MDA of the Saladilla Fm (Maláguide Complex) is also Early Permian (279 ± 3 Ma).

The age patterns from the Upper Carboniferous rocks of the NFC and AC are similar, and also similar to those from Upper Carboniferous of the Cantabrian Zone of the Iberian Massif, suggesting similar source areas. The most likely paleogeographical location of both complexes was in Late Carboniferous marine basins located eastwards of the Iberian Massif. However, the age patterns show differences compared with those from the Upper Carboniferous rocks of the MC, and from the South Portuguese and Ossa-Morena zones of the Iberian Massif. On the other hand, age patterns from Upper Carboniferous rocks of the MC show some similarities with those from the ~~Ossa-Morena Zone.~~North-eastern Iberian Peninsula and South Francia. Therefore, the paleogeographic location of the MC could have been different from that of the NFC and AC, and it was probably located near the Ossa-Morena Zone and the other rocks derived from the West African Craton.

The samples with Early Permian MDA from the three complexes (NFC, AC, and MC) have more Paleozoic ~~zircons~~zircon grains than the Late Carboniferous samples, and similar age patterns~~, suggesting~~. This data can be explained if zircon grains from the main Variscan orogenic relief were recycled, while unroofing of footwalls of faults also exposed Late Variscan granitoids at the surface. It is possible that ~~they~~these zircon grains were deposited in the same basin, likely the long-lived Iberian Permian-Triassic depositional basins. Samples from the unconformable Middle Miocene sediments have Early Permian MDA (292 ± 3 Ma) and age distribution patterns corresponding to a mixing of ~~zircons~~zircon grains from the AC and MC, and thus, do not record formation of felsic rocks since the Early Permian.

Acknowledgements

This paper is dedicated to the memory of Dr. Fernando Álvarez Lobato, who passed away while this contribution was written. We are indebted to Mike Hall and Brad McDonald for their technical support on sample preparation and LA-ICPMS, respectively. The CL imaging was carried out in Curtin University's Microscopy & Microanalysis Facility, ~~whose~~of which instrumentation has been partially funded by the University, State and Commonwealth Governments, and the Scanning Electron Microscope (SEM) Facility at the University of Edinburgh. Analysis in the John de Laeter Centre GeoHistory Facility was enabled by AuScope (auscope.org.au) and the Australian Government via the National Collaborative Research Infrastructure Strategy (NCRIS). This work is supported by grants CGL2016-75224-R, and CGL2015-71692-P (MINECO/FEDER, Spain) and RNM-208 (Junta de Andalucía, Spain). This is the IBERSIMS Publication No. 70.

References

Accotto, C., Martínez Poyatos, D.J., Azor, A., Jabaloy-Sánchez, A., Talavera, C., Evans, N.J., Azdimousa, A., 2020. Tectonic evolution of the Eastern Moroccan Meseta: from Late Devonian fore-arc sedimentation to Early Carboniferous collision of an Avalonian promontory. Tectonics, 38, e2019TC005976,https://doi.org/10.1029/2019TC005976

Accotto, C., Martínez Poyatos, D.J., Azor, A., Talavera, C., Evans, N.J., Jabaloy-Sánchez, A., Azdimousa, A., Tahiri, A.; El Hadi, H., 2019. Mixed and recycled detrital zircons in the Paleozoic rocks of the Eastern Moroccan Meseta: paleogeographic inferences. Lithos 338-339, 73-86~~. Doi: ~~, https://doi.org/10.1016/j.lithos.2019.04.011

Aldaya, F., Álvarez, F., Galindo-Zaldívar, J., González-Lodeiro, F., Jabaloy, A., Navarro-Vilá, F., 1991. The Maláguide-Alpujárride contact (Betic Cordilleras, Spain): a brittle extensional detachment, Comptes Rendus de l'Académie des Sciences de Paris 313, 1447-1453.

Álvarez, F., 1987. Subhorizontal shear zones and their relation to nappe movements in the Cantal and Miñarros units. Eastern Betic Zone (Spain). Geologie en Mijnbouw 66, 101-110.

Álvarez, F., Aldaya, F., 1985. Las unidades de la Zona Bética en la región de Águilas-Mazarrón (Prov. de Murcia). Estudios Geológicos 41, 139-146.

Arranz, E., Lago, M., 2004. El plutonismo sin- y tardi-varisco en los Pirineos. In: Vera, J.A., (Ed.) Geología de España, SGE-IGME, Madrid, 263-266.

Azdimousa, A., Jabaloy-Sánchez, A., Talavera, C., Asebriy, L., González-Lodeiro, F., Evans, N.J. 2019. Detrital zircon U-Pb ages in the Rif Belt (northern Morocco): Paleogeographic implications. Gondwana Research 70, 133-150~~. Doi~~ , https://doi.org/10.1016/j.gr.2018.12.008

Balanyá, J.C., García-Dueñas, V., 1987. Les directions structurales dans le Domaine d'Alborán de part et d'autre du Détroit de Gibraltar. Comptes Rendus de l'Académie des Sciences de Paris 304, 929-932.

Bea, F., 2004. La naturaleza del magmatismo de la Zona Centroibérica: consideraciones generales y ensayo de correlación. In: Vera, J.A., (Ed.) Geología de España, SGE-IGME, Madrid, 128-133.

Bea, F., Montero, P., Talavera, C., Abu Anbar, M., Scarrow, J., Molina, J.F., Moreno, J.A., 2010. The palaeogeographic position of Central Iberia in Gondwana during the Ordovician: evidence from zircon geochronology and Nd isotopes. Terra Nova 22, 341-346.

Booth-Rea, G., Silva Barroso, P.G., (2008). Mapa Geológico de España escala 1:50.000. Edición Digital. Hoja 975, Puerto Lumbreras. Instituto Geológico y Minero de España, Madrid.

Blichert-Toft, J., Albarède, F., Kornprobst, J., 1999, Lu-Hf isotope systematics of garnet pyroxenites from Beni Bousera, Morocco: Implications for basalt origin. Science 283, 1303-1306

Booth-Rea, G., Silva Barroso, P.G., Bardají Azcárate, T., Martín Serrano, A., (2009). Mapa Geológico de España escala 1:50.000. Edición Digital. Hoja 997, Águilas. Instituto Geológico y Minero de España, Madrid.

Bowring, S.A., Schmitz, M.D., 2003. High-precision U-Pb zircon geochronology and the stratigraphic record. Reviews in Mineralogy and Geochemistry 53, 305-326, https://doi.org/10.2113/0530305

Casquet, C., Galindo, C., 2004. Magmatismo varisco y postvarisco en la Zona de Ossa-Morena. In: Vera, J.A., (Ed.) Geología de España, SGE-IGME, Madrid, 194-198.

Chalouan, A., Michard, A., El Kadiri, K., Negro, F., Frizon de Lamotte, D., Soto J.I., Saddiqi, O., 2008. The Rif Belt. In: Michard, A., Frizon de Lamotte, D., Saddiqi, O., Chalouan, A., (Eds.) Continental Evolution: The Geology of Morocco. Lecture Notes in Earth Sciences, vol 116, pp. 203-302, Springer-Verlag, Berlin Heidelberg.

Dallmeyer, R.D., Martínez Catalán, J.R., Arenas, R., Gil Ibarguchi, J.I., Gutiérrez-Alonso, G., Farias, P., Aller, J., Bastida, F., 1997. Diachronous Variscan tectonothermal activity in the NW Iberian Massif: Evidence from 40Ar/39Ar dating of regional fabrics. Tectonophysics 277, 307–337~~. Doi:~~, https://doi.org/10.1016/s0040-1951(97)00035-8

Dickinson, W.R., Gehrels, G.E., 2009. Use of U-Pb ages of detrital zircons to infer maximum depositional ages of strata: a test against a Colorado Plateau Mesozoic

Formatted: English (United States)

Formatted: Spanish (Spain)

Formatted: English (United Kingdom)

Formatted: Spanish (Spain)

Formatted: English (United States)

Formatted: English (United States)

database. Earth and Planetary Science Letters 288 (1-2), 115-125, https://doi.org/10.1016/j.epsl.2009.09.013

Díez-Montes, A., Martínez-Catalán, J.R., Bellido Mulas, F., 2010. Role of the Ollo de Sapo massive felsic volcanism of NW Iberia in the Early Ordovician dynamics of northern Gondwana. Gondwana Research 17, 363-376, https://doi.org/10.1016/j.gr.2009.09.001

Dinis, P.A., Fernandes, P., Jorge, R.C.G.S., Rodrigues, B., Chew, D.M., Tassinari, C.G., 2018. The transition from Pangea amalgamation to fragmentation: constraints from detrital zircon geochronology on West Iberia paleogeography and sediment sources. Sedimentary Geology 375, 172-187.

Durand-Delga, M., Escalier des Orres, P., Fernex, F., 1962. Sur la présence de Jurassique et d'Oligocène a l'ouest de Carthagene (Espagne méridionale)". Comptes Rendus de l'Académie des Sciences de Paris 255, 1755-1753.

Espinosa Godoy, J., Herrera López, J.L., Pérez Rojas, A., 1972. Mapa Geológico de España escala 1:50.000. Hoja 997bis, Cope. Instituto Geológico y Minero de España, Madrid

Esteban, J.J., Cuevas, J., Tubía, J.M., Liati, A., Seward, D., Gebauer, D., 2007. Timing and origin of zircon-bearing chlorite schists in the Ronda peridotites (Betic Cordilleras, Southern Spain). Lithos 99, 121-135.

Esteban, J.J., Cuevas, J., Tubía, J.M., Gutiérrez-Alonso, G., Larionov, A., Sergeev, S., Hofmann, M., 2017. U–Pb detrital zircon ages from the Paleozoic Marbella Conglomerate of the Malaguide Complex (Betic Cordilleras, Spain). Implications on Paleotethyan evolution. Lithos 290-291, 34-47.

Fernández-Fernández, E.M., Jabaloy-Sánchez, A., Nieto, F., González-Lodeiro, F., 2007. Structure of the Maláguide Complex near Vélez Rubio (Eastern Betic

Formatted: French (France)

Formatted: French (France)

Formatted: English (Australia)

Cordillera, SE Spain). Tectonics 26, TC4008, https://doi~~:~~.org/10.1029/2006TC002019

Fernández-Suárez, J., Gutiérrez-Alonso, G., Jeffries, T.E., 2002. The importance of along-margin terrane transport in northern Gondwana: insights from detrital zircon parentage in Neoproterozoic rocks from Iberia and Brittany. Earth and Planetary Science Letters 204, 75-88.

Fernández-Suárez, J., Gutiérrez-Alonso, G., Pastor-Galán, D., Hofmann, M., Murphy, J.B., Linnemann, U., 2014. The Ediacaran–Early Cambrian detrital zircon record of NW Iberia: possible sources and paleogeographic constraints. International Journal of Earth Sciences 103, 1335–1357. ~~Doi: ~~https://doi.org/10.1007/s00531-013-0923-3

Gallastegui et al., 2004. Magmatismo. In: Vera, J.A., (Ed.) Geología de España, SGE-IGME, Madrid, 63-68.

Gama, C., Pereira, M.F., Crowley, Q.G., Dias da Silva, Í., Silva, J.B., in press. Detrital zircon provenance of Triassic sandstone of the Algarve Basin (SW Iberia): Evidence of Gondwanan- and Laurussian-type sources of sediment. Geological Magazine. https://doi.org/10.1017/S0016756820000370

García-Navarro, E., Fernández, C., 2004. Final stages of the Variscan orogeny at the southern Iberian Massif: lateral extrusion and rotation of continental blocks. Tectonics, 23:TC6001. https://doi.org/10.1029/2004TC001646

García Tortosa, F.J., Leyva Cabello, F., Bardaji Azcárate, T., 2012. Mapa Geológico de España escala 1:50.000. Edición Digital. Hoja 976, Mazarrón. Instituto Geológico y Minero de España, Madrid.

Formatted: English (United States)

Formatted: English (United States)

Formatted: English (United Kingdom)

Formatted: English (Australia)

Formatted: English (Australia)

García Tortosa, F.J., López-Garrido, A.C., Sanz de Galdeano, C., 2000. Présence du complexe tectonique Malaguide à l'ouest de Carthagéne (zone interne Bétique, Espagne). Comptes Rendus de l'Académie des Sciences de Paris 330, 139-146.

García-Tortosa, F.J., 2002. Los Complejos Tectónicos Alpujárride y Maláguide en el sector oriental de la Zona Interna Bética. Estratigrafía, relaciones tectónicas y evolución paleogeográfica durante el Triásico. PhD Thesis, Universidad de Granada.

Geel, T., 1973. The geology of the Betic of Malaga, the Subbetic and the zone between these two units in the Velez Rubio area (Southern, Spain). GUA Papers of Geology.

Gómez-Pugnaire, M.T., Franz, G., 1988. Metamorphic evolution of the Paleozoic series of the Betic Cordilleras (Nevado-Filabride complex, SE Spain) and its relationship with the Alpine orogeny. Geologische Rundschau 77, 619-640.

Gómez-Pugnaire, M.T., Galindo-Zaldívar, J., Rubatto, D., González-Lodeiro, F., López Sánchez-Vizcaíno, V., Jabaloy, A., 2004. A reinterpretation of the Nevado-Filábride and Alpujárride Complex (Betic Cordillera): field, petrography and U-Pb ages from orthogneisses western Sierra Nevada, S Spain). Schweizerische Mineralogische und Petrographische Mitteilungen 84, 303-322.

Gómez-Pugnaire, M.T., Rubatto, D., Fernández-Soler, J.M., Jabaloy, A., López Sánchez-Vizcaíno, V., González-Lodeiro, F., Galindo-Zaldívar, J., Padrón-Navarta, J.A., 2012. U–Pb geochronology of Nevado–Filábride gneisses: evidence for the Variscan nature of the deepest Betic complex (SE Spain). Lithos 146-147, 93-111.

Gutiérrez-Alonso, G., Murphy, J.B., Fernández-Suárez, J., Hamilton, M.A., 2008. Rifting along the northern,Gondwana margin and the evolution of the

Formatted: French (France)

Rheic Ocean: a Devonian age for the El Castillo volcanic rocks (Salamanca, Central Iberian Zone). Tectonophysics 461, 157-65, https://doi.org/10.1016/j.tecto.2008.01.013

Gutiérrez-Alonso, G., Fernández-Suárez, J., Jeffries, T.E., Johnston, S.T., Pastor-Galán, D., Murphy, J.B., Franco, M.P., Gonzalo, J.C., 2011. Diachronous post-orogenic magmatism within a developing orocline in Iberia, European Variscides. Tectonics 30, TC5008. http://dx.doi.org/10.1029/2010TC002845

Ireland, T.R., Williams, I.S., 2003. Considerations in zircon geochronology by SIMS. Reviews in Mineralogy and Geochemistry 53, 215-241, https://doi.org/10.2113/0530215

Jabaloy, A., 1993. La estructura de la región occidental de la Sierra de los Filabres (Cordilleras Béticas). Tierras del Sur, Universidad de Granada, Granada, Spain 9, pp. 1-261.

Jabaloy-Sánchez, A., Talavera, C., Gómez-Pugnaire, M.T., López Sánchez-Vizcaíno, V., Vázquez, M., Rodríguez-Peces, M.J., Evans, N.J., 2018, U-Pb ages of detrital zircons from the Internal Betics: A key to deciphering paleogeographic provenance and tectonostratigraphic evolution. Lithos 318–319, 244–266~~. Doi: ~~, https://doi.org/10.1016/j.lithos.2018.07.026

Kirchner, K.L., Behr, W.M., Loewy, S., Stockli, D.F., 2016. Early Miocene subduction in the western Mediterranean: Constraints from Rb-Sr multimineral isochron geochronology. Geochemistry, Geophysics, Geosystems 17~~. Doi: ~~, https://doi.org/10.1002/2015GC006208

Kroner, U., Romer, R.L., 2013. Two plates - Many subduction zones: The Variscan orogeny reconsidered. Gondwana Research 24, 298-329.

Laborda-López, C., Aguirre, J., Donovan, S.K., 2013. Asociaciones de macrofósiles en

Formatted: English (United Kingdom)

Formatted: Spanish (Spain)

Formatted: English (United Kingdom)

Formatted: English (United Kingdom)

Formatted: English (United States)

Formatted: English (United States)

rocas metamórficas del Complejo Nevado-Filábride (Zonas Internas de la Cordillera Bética) en Águilas, Murcia (SE España). Tafonomía y biocronoestratigrafía, XXIX Jornadas de Paleontología, Abstracts, pp 83-84.

Laborda-López, C., Aguirre, J., Donovan, S.K., 2015a. Surviving metamorphism: taphonomy of fossil assemblages in marble and calc-silicate schist. Palaios 30, 668-679.

Laborda-López, C., Aguirre, J., Donovan, S.K., Navas-Parejo, P., Rodríguez, S., 2015b. Fossil assemblages and biochronology of metamorphic carbonates of the Nevado-Filábride Complex from the Águilas tectonic arc (SE Spain). Spanish Journal of Palaeontology 30, 275-292.

Lafuste, M.L.J., Pavillon, M.J., 1976. Mise en évidence d'Eifélien daté au sein des terrains métamorphiques des zones internes des Cordillères bétiques. Intérêt de ce nouveau repère stratigraphique: Comptes Rendus de l'Académie des Sciences de Paris 283,- 1015-1018.

Formatted: English (United States)

Leine, L., 1968. Rauhwackes in the Betic Cordilleras, Spain: Nomenclature, description and genesis of weathered carbonate breccias of tectonics origin. PhD Thesis University of Amsterdam 112 p.

López Sánchez-Vizcaino, V., Connolly, J.A.D., Gómez-Pugnaire, M.T., 1997. Metamorphism and phase relations in carbonate rocks from the Nevado-Filábride Complex (Cordilleras Béticas, Spain): application of the Ttn + Rt + Cal + Qtz + Gr buffer. Contributions to Mineralogy and Petrology 126, 292-302.

Formatted: English (United States)

López Sánchez-Vizcaíno, V., Rubatto, D., Gómez-Pugnaire, M.T., Tommsdorff, V, Müntener, O., 2001. Middle Miocene high-pressure metamorphism and fast exhumation of the Nevado-Filábride Complex, SE Spain, Terra Nova 13, 327-332.

Ludwig, K.R., 2003, User's Manual for Isoplot 3.00: a Geochronological Toolkit for Microsoft Excel Berkeley Geochronology Center Special Publication 4, p. 4.

Ludwig, K.R., 2009. SQUID II., a user's manual, Berkeley Geochronology Center Special Publication 2, 2455 Ridge Road, Berkeley, CA 94709, USA 22.

Maate, A., Sole De Porta, A.N., Martín-Algarra, A., 1993. Données paléontologiques nouvelles sur le Carnien des séries rouges des Maghrébides (Ghomarides et Dorsale calcaire du Rif septentrional, Maroc). Comptes Rendus de l'Académie des Sciences de Paris 316, 137-143.

Martín-Algarra, A., 1987. Evolución geológica alpina del contacto entre las Zonas Internas y las Zonas Externas de la (Cordillera Bética). Ph D Thesis, Universidad de Granada Martin-Algarra, 1987.

Martínez Catalán, J.R., Arenas, R., Díaz García, F., Abati, J., 1997. Variscan accretionary complex of northwest Iberia: Terrane correlation and succession of tectonothermal events. Geology 25, 1103-1106.

Martínez Catalán, J.R., Fernández-Suárez, J., Meireles, C., González clavijo, E., Belousova, E., Saeed, A., 2008, U-Pb detrital zircon ages in synorogenic deposits of the NW Iberian Massif (Variscan belt): interplay of Devonian–Carboniferous sedimentation and thrust tectonics. Journal of the Geological Society 165, 687-698.

Martínez Catalán, J.R. 2012. The Central Iberian arc, an orocline centered in the Iberian Massif and some implications for the Variscan belt. International Journal of Earth Sciences 101, 1299-1314.

Martínez Catalán, J.R., 2011. Are the oroclines of the Variscan belt related to late Variscan strike-slip tectonics? Terra Nova 23(4), 241-247.

Formatted: Spanish (Spain)

Formatted: French (France)

Martínez-Catalán, J.R., Arenas, R., Díaz-García, F., Abati, J., 1997. Variscan accretionary complex of NW Iberia: terrane correlation and succession of tectonothermal events. Geology 25,1103-1106.

Martín-Martín, M., Martin-Rojas, I., Caracuel, J.E., Estevez-Rubio, A., Martin-Algarra, A., Sandoval, J., 2006. Tectonic framework and extensional pattern of the Malaguide Complex from Sierra Espuña (Internal Betic Zone) during Jurassic–Cretaceous: implications for the Westernmost Tethys geodynamic evolution. International Journal of Earth Sciences 95, 815-826.

Martín-Rojas, I., Somma, R., Delgado, F., Estévez, A., Iannace, A., Perrone, V., Zamparelli, V., 2010. Role of sea-level change and synsedimentary extensional tectonics on facies and architecture of Ladinian-Carnian carbonate depositional systems (Alpujarride complex, Betic Internal Zone, SE Spain). Geogaceta 48, 63-66.

Martín-Rojas, I., Somma, R., Delgado, F., Estevez, A., Iannace, A., Perrone, V., Zamparelli, V., 2009. Triassic continental rifting of Pangea: evidence from the Alpujarride carbonates (Betic Cordillera, SE Spain). Journal of the Geological Society, London 166, 447-458.

Martins, H.C.B., Ribeiro, M.A., Almeida, A., 2019. Variscan Magmatism at the Central Iberian Zone, the Central and Northern Border. In: C. Quesada, Oliveira, J.T. (eds.), The Geology of Iberia: A Geodynamic Approach, Regional Geology Reviews, Vol. 2, 510-513. https://doi.org/10.1007/978-3-030-10519-8_13

Marzoli, A., Renne, P., Piccirillo, E.M., Ernesto, M., DeMin, A., 1999. Extensive -200 million-year-old -continental -flood -basalts of the Central Atlantic Magmatic Province. Science 284, 616-618.

Matte, Ph., 1991. Accretionary history and crustal evolution of the Variscan belt in Western Europe. Tectonophysics 196, 309-337.

Matte, Ph., 2002. Variscides between the Appalachians and the Urals: Similarities and differences between Paleozoic subduction and collision belts. In: Martínez Catalán, J.R., Hatcher, R.D. Jr, Arenas, R., Díaz García, F. (eds), Variscan-Appalachian dynamics: The building of the late Paleozoic basement: Boulder, Colorado, Geological Society of America Special Paper 364, 239-251.

Matte, P., 2001. The Variscan collage and orogeny (480-290 Ma) and the tectonic definition of the Armorica microplate: a review. Terra Nov. 13, 122–128, https://doi.org/10.1046/j.1365-3121.2001.00327.x

Meinhold, G., Morton, A.C., Mark Fanning, C., Howard, J.P., Phillips, R.J., Strogen, D., Whitham, A.G., 2014. Insights into crust formation and recycling in North Africa from combined U-Pb, Lu-Hf and O isotope data of detrital zircons from Devonian sandstone of southern Libya. Geological Society, London, Special Publications 386, 281-292, https://doi.org/10.1144/SP386.1

Murphy, J.B., Gutierrez-Alonso, G., Nance, R.D., Fernandez-Suarez, J., Keppie, J.D., Quesada, C., Strachan, R.A., Dostal, J., 2006. Origin of the Rheic Ocean: rifting along a Neoproterozoic suture? Geology 34, 325-328.

Montero, P., Bea, F., González-Lodeiro, F., Talavera, C., Whitehouse, M.J., 2007. Zircon ages of the metavolcanic rocks and metagranites of the Ollo de Sapo Domain in central Spain: Implications for the Neoproterozoic to Early Palaeozoic evolution of Iberia. Geological Magazine 144, 963–976.

Montero, M.P., Talavera, C., Bea, F., González Lodeiro, F., Whitehouse, M. J., 2009. Zircon geochronology of the Ollo de Sapo Formation and the age of the Cambro–Ordovician rifting in Iberia. Journal of Geology 117, 174–191.

Formatted: English (United States)

Formatted: English (United Kingdom)

Formatted: English (United Kingdom)

Formatted: English (United Kingdom)

Formatted: English (United Kingdom)

Formatted: English (United States)

Murphy, J.B., Nance, R.D., Cawood, P.A., 2009. Contrasting modes of supercontinent formation and the conundrum of Pangea. Gondwana Research 15, 408-420.

Nance et al., 2010 Nance, R.D, Gutiérrez-Alonso, G., Keppie, J.D., Linnemann, U., Murphy, J.B., Quesada, C., Strachan, R.A., Woodcock, N.H., 2010. Evolution of the Rheic Ocean. Gondwana Research 17, 194-222. Doi:, https://doi.org/10.1016/j.gr.2009.08.001

Pastor-Galán, D., Gutiérrez-Alonso, G., Murphy, J.B., Fernández-Suárez, J., Hofmann, M., Linnemann, U., 2013a2013. Provenance analysis of the Paleozoic sequences of the northern Gondwana margin in NW Iberia: Passive margin to Variscan collision and orocline development. Gondwana Res.Research 23, 1089–1103., https://doi:.org/10.1016/j.gr.2012.06.015

Pereira, M.F., Castro, A., Fernández, C., Rodríguez, C., 2018. Multiple Paleozoic magmatic-orogenic events in the Central Extremadura batholith (Iberian Variscan belt, Spain). Journal of Iberian Geology 44, 309-333.

Pereira, M.F., Pereira, M.F., Gutiérrez-Alonso, G., Murphy, J.B., Drost, K., Gama, C., Silva, J.B., 2017. Birth and demise of the Rheic Ocean magmatic arc(s): Combined U–Pb and Hf isotope analyses in detrital zircon from SW Iberia siliciclastic strata. Lithos 278-281, 383-399.

Pereira, M.F., Chichorro, M., Johnston, S.T., Gutiérrez-Alonso, G., Silva, J.B., Linnemann, U., Hofmann, M., Drost, K., 2012. The missing Rheic Ocean magmatic arcs: provenance analysis of Late Paleozoic sedimentary clastic rocks of SW Iberia. Gondwana Research 3–4(22), 882-891.

Pereira, M.F., Gama, C., Chichorro, M., Silva, J.B., Gutiérrez-Alonso, G., Hofmann, M., Linnemann, U., Gärtner, A., 2016. Evidence for multi-cycle sedimentation

Formatted: English (United States)

Formatted: English (United States)

Formatted: English (United States)

Formatted: Spanish (Spain)

Formatted: Spanish (Spain)

Formatted: Spanish (Spain)

Formatted: Spanish (Spain)

Formatted: Spanish (Spain)

Formatted: English (United Kingdom)

Formatted: English (United Kingdom)

Formatted: Spanish (Spain)

Formatted: English (United Kingdom)

and provenance constraints from detrital zircon U-Pb ages: Triassic strata of the Lusitanian basin (western Iberia). Tectonophysics 681, 318-331.

Pereira, M.F., Gama, C., Dias da Silva, I., Silva, J.B., Hofmann, M., Linnemann, U., Gärtner, A., in press. Chronostratigraphic framework and provenance of the Ossa-Morena Zone Carboniferous basins (SW Iberia). Solid Earth Discussions, https://doi.org/10.5194/se-2020-26

Pereira, M.F., Gutiérrez-Alonso, G., Murphy, J.B., Drost, K., Gama, C., Silva, J.B., 2017a. Birth and demise of the Rheic Ocean magmatic arc(s): Combined U–Pb and Hf isotope analyses in detrital zircon from SW Iberia siliciclastic strata. Lithos 278-281, 383-399.

Pereira, M.F., Ribeiro, C., Gama, C., Drost, K., Chichorro, M., Vilallonga, F., Hofmann, M., Linnemann, U., 2017b. Provenance of upper Triassic sandstone, southwest Iberia (Alentejo and Algarve basins): tracing variability in the sources. International Journal of Earth Sciences 106, 43-57. https://doi.org/10.1007/s00531-016-1295-2

Pereira, M.F., Ribeiro, C., Vilallonga, F., Chichorro, M., Drost, K., Silva, J.B., Albardeiro, L., Hofmann, M., Linnemann, U., 2014. Variability over time in the sources of South Portuguese Zone turbidites: evidence of denudation of different crustal blocks during the assembly of Pangaea. International Journal of Earth Sciences 103, 1453-1470..´

Pérez-Cáceres, I., Martínez Poyatos, D., Simancas, J.F., Azor, A., 2017. Testing the Avalonian affinity of the South Portuguese Zone and the Neoproterozoic evolution of SW Iberia through detrital zircon populations. Gondwana Res. 42, 177–-192.–, https://doi:.org/10.1016/j.gr.2016.10.010

Formatted: English (United Kingdom)

Formatted: English (United Kingdom)

Formatted: Spanish (Spain)

Formatted: English (United Kingdom)

Formatted: English (United States)

Formatted: Spanish (Spain)

Formatted: Spanish (Spain)

Formatted: Spanish (Spain)

Formatted: Spanish (Spain)

Perri, F., Critelli, S., Martín-Algarra, A., Martín-Martín, M., Perrone, V., Mongelli, G., Zattin, G., 2013. Triassic redbeds in the Malaguide Complex (Betic Cordillera-Spain): Petrography, geochemistry and geodynamic implications. Earth-Science Reviews 117, 1-28.

Platt, J.P., Whitehouse, M.J., Kelley, S.P., Carter, A., Hollick, L., 2003. Simultaneous extensional exhumation across the Alboran Basin: Implications for the causes of late orogenic extension. Geology 31 31, 251-254.

Platt, J.P., Anczkiewicz, R., Soto, J.I., Kelley, S.P., Thirlwall, M., 2006. Early Miocene continental subduction and rapid exhumation in the western Mediterranean. Geology 34, 981-984.

Pratt, J.R., Barbeau, D.L., Garver, J.I., Emran, A., Izykowski, T.M., 2015. Detrital Zircon Geochronology of Mesozoic Sediments in the Rif and Middle Atlas Belts of Morocco: Provenance Constraints and Refinement of the West African Signature. J. Geol. 123, 177–-200–, https://doi:.org/10.1086/681218

Puga, E., Nieto, J.M., Diaz de Federico, A., Portugal, E., Reyes, E., 1996. The intra-orogenic Soportujar Formation of the Mulhacén Complex; evidence for the polyciclic character of the Alpine orogeny in the Betic Cordilleras. Eclogae Geologicae Helvetiae 89, 129-162.

Puga, E., Fanning, M., Díaz de Federico, A., Nieto, J.M., Beccaluva, L., Bianchini, G., Díaz-Puga, M.A., 2011. Petrology, geochemistry and U-Pb geochronology of the Betic Ophiolites: Inferences for Pangaea break-up and birth of the westernmost Tethys Ocean. Lithos 124, 255-272.

Puga, E., Díaz de Federico, A., Nieto, J.M., 2002. Tectonostratigraphic subdivision and petrological characterisation of the deepest complexes of the Betic zone: a review. Geodinamica Acta 15, 23-43.

Formatted: English (United States)

Formatted: English (Australia)

Formatted: English (United States)

Formatted: Spanish (Spain)

Formatted: Spanish (Spain)

Formatted: Font: Calibri, Spanish (Spain)

Formatted: Spanish (Spain)

Formatted: English (United Kingdom)

1435 Ribeiro, M.L., Castro, A., Almeida, A., González Menéndez, L., Jesus, A. Lains, J.A., Lopes, J.C., Martins, H.C.B., Mata, J., Mateus, A., Moita, P., Neiva, A.M.R., Ribeiro, M.A., Santos, J.F., Solá, A.R., 2019, Variscan magmatism. In: Quesada, C., Oliveira, J.T. (Eds.), The Geology of Iberia: A Geodynamic Approach, Regional Geology Reviews 2, 497-526.

1440 Rodriguez-Cañero, R., Jabaloy-Sánchez, A., Navas-Parejo P, Martín-Algarra, A., 2018. Linking Palaeozoic palaeogeography of the Betic Cordillera to the Variscan Iberian Massif: new insight through the first conodonts of the Nevado-Filábride Complex. International Journal of Earth Sciences (Geologische Rundschau) 107(5), 1791-1806. Doi: , https://doi.org/10.1007/s00531-017-1572-8

1445 Rubio-Ordóñez, A., Valverde-Vaquero, P., Corretgé, L.G., Cuesta-Fernández, A.,Gallastegui, G., Fernández-González, M., Gerdes, A., 2012. An early Ordovician tonalitic–granodioritic belt along the Schistose-Greywacke Domain of the Central Iberian zone (Iberian Massif, Variscan belt). Geological Magazine 149(5), 927-939, https://doi.org/10.1017/S0016756811001129

1450 Sánchez Martínez, S., De la Horra, R., Arenas, R., Gerdes, A., Galán-Abellán, A.B., López-Gómez, J., Barrenechea, J.F., Arche, A., 2012. U-Pb Ages of Detrital Zircons from the Permo-Triassic Series of the Iberian Ranges: A Record of Variable Provenance during Rift Propagation. The Journal of Geology 120, 135-154.

1455 Sánchez-Martínez, S., Arenas, R., García, F.D., Martínez Catalán, J.R., Gómez-Barreiro, J., Pearce, J.A., 2007. Careon ophiolite, NW Spain: suprasubduction zone setting for the youngest Rheic Ocean floor. Geology 35, 53-56.

1458 Sánchez-Rodriguez, L., Gebauer, D., 2000, Mesozoic formation of pyroxenites and gabbros in the Ronda area (southern Spain), followed by early Miocene

Formatted: English (United States)

Formatted: English (United States)

Formatted: Spanish (Spain)

Formatted: Spanish (Spain)

~~subduction metamorphism and emplacement into the middle crust: U-Pb sensitive high-resolution ion microprobe dating of zircon: Tectonophysics 316, 19-44.~~

Sánchez-Navas, A., García-Casco, A., Martín-Algarra, A., 2014. Pre-Alpine discordant granitic dikes in the metamorphic core of the Betic Cordillera: tectonic implications. Terra Nova 26, 477-486~~. Doi :~~, https://doi.org/10.1111/ter.12123

Sánchez-Navas, A., García-Casco, A., Mazzoli, S., Martín-Algarra, A., 2017. Polymetamorphism in the Alpujarride Complex, Betic Cordillera, South Spain. The Journal of Geology 125, 637-657.

Sánchez-Rodriguez, L., Gebauer, D., 2000, Mesozoic formation of pyroxenites and gabbros in the Ronda area (southern Spain), followed by early Miocene subduction metamorphism and emplacement into the middle crust: U-Pb sensitive high-resolution ion microprobe dating of zircon: Tectonophysics 316, 19-44.

Santamaría-López, A., Sanz de Galdeano, C., 2018. SHRIMP U–Pb detrital zircon dating to check subdivisions in metamorphic complexes: a case of study in the Nevado–Filábride complex (Betic Cordillera, Spain). International Journal of Earth Sciences, ~~doi:~~ https://doi.org/10.1007/s00531-018-1613-y

Sharman, G.R., Malkowski, M.A., 2020, Needles in a haystack: Detrital zircon UePb ages and the maximum depositional age of modern global sediment. Earth-Science Reviews 203, 103109, https://doi.org/10.1016/j.earscirev.2020.103109

Shaw, J., Gutierrez-Alonso, G., Johnston, S.T., Galan, D.P., Pastor-Galan, D., 2014. Provenance variability along the Early Ordovician north Gondwana margin: Paleogeographic and tectonic implications of U-Pb detrital zircon ages from the

Formatted: Spanish (Spain)

Formatted: English (United States)

Formatted: Spanish (Spain)

Formatted: Spanish (Spain)

Formatted: English (United States)

Formatted: English (Australia)

Formatted: English (United States)

Armorican Quartzite of the Iberian Variscan belt. Geological Society of America Bulletin 126, 702-719~~. Doi:~~, https://doi.org/10.1130/B30935.1

Shaw, J., Johnston, S.T., Gutiérrez-Alonso, G., Weil, A.B., 2012. Oroclines of the Variscan orogen of Iberia: paleocurrent analysis and paleogeographic implications. Earth and Planetary Science Letters 329-330, 60-70.

Simancas, F., 2019. Variscan Cycle. In: Quesada, C., Oliveira, J.T. (Eds.), The Geology of Iberia: A Geodynamic Approach, Regional Geology Reviews 2, 1-26.

Simon, O., Visscher, H., 1983. El Pérmico de las Cordilleras Béticas. In: Martínez-Diaz C (Ed.), Carbonífero y Pérmico de España: Actas X Congreso Internacional Carbonífero. IGME, Madrid 453-499.

Spencer, C.J., Kirkland, C.L., 2016. Visualizing the sedimentary response through the orogenic cycle: a multidimensional scaling approach. Lithosphere 8, 29-37, https://doi.org/10.1130/L479.1

Spencer, C.J., Kirkland, C.L., Taylor, R.J.M., 2016. Strategies towards statistically robust interpretations of in situ U-Pb zircon geochronology. Geoscience Frontiers 7, 581-589, http://dx.doi.org/10.1016/j.gsf.2015.11.006

Stephan, T., Kroner, U., Romer, R.L., 2019. The pre-orogenic detrital zircon record of the Peri-Gondwanan crust. Geological Magazine 156, 281-307~~. Doi: ~~, https://doi.org/10.1017/S0016756818000031

Tahiri, A., Montero, P., El Hadi, H., Martínez Poyatos, D., Azor, A., Bea, F., Simancas, J.F., González Lodeiro, F., 2010. Geochronological data on the Rabat-Tiflet granitoids: their bearing on the tectonics of the Moroccan Variscides. J. African Earth Sci. 57, 1–13~~.~~, https://doi~~:~~.org/10.1016/j.jafrearsci.2009.07.005

Talavera, C., Montero, P., ~~Martínez Poyatos, D., Williams, I.S., 2012. Ediacaran to Lower Ordovician age for rocks ascribed to the Schist–Graywacke Complex~~

Formatted: English (United States)
Formatted: English (United States)
Formatted: Spanish (Spain)
Formatted: English (United States)
Formatted: English (United States)
Formatted: Spanish (Spain)
Formatted: Spanish (Spain)
Formatted: English (United States)
Formatted: English (United States)
Formatted: English (United States)
Formatted: English (United Kingdom)

~~(Iberian Massif, Spain): Evidence from detrital~~ Bea, F., González Lodeiro, F., Whitehouse, M., 2013. U–Pb zircon ~~SHRIMP U–Pb~~ geochronology~~. Gondwana Res. 22, 928–942. doi:10.1016/j.gr.2012.03.008~~ of the Cambro–Ordovician metagranites and metavolcanic rocks of central and NW Iberia. International Journal of Earth Sciences 102, 1–23.

Tendero, J.A., Martín-Algarra, A., Puga, E., Díaz de Federico, A., 1993. Lithostratigraphie des métasédiments de l'association ophiolitique Nevado-Filabride (SE Espagne) et mise en evidence d'objets ankéritiques évoquant des foraminiféres planctoniques du Crétacé: conséquences paléogéographiques. Comptes Rendus de l'Académie des Sciences Paris 316, 1115-1122.

Vermeesch, P., 2012. On the visualisation of detrital age distributions. Chemical Geology, v.312-313, 190-194, https://doi~~:~~.org/10.1016/j.chemgeo.2012.04.021~~0~~

Vermeesch, P., 2013. Multi-sample comparison of detrital age distributions. Chemical Geology 341, 140-146, https://doi.org/10.1016/j.chemgeo.2013.01.010

Vissers, R.L.M., 1981. A structural study of the Central Sierra de los Filabres (Betic Zone, SE Spain), with emphasis on deformational processes and their relation to the Alpine Metamorphism. GUA Papers of Geology 15, 1- 154.

Vissers, R.L.M., 1992. Variscan extension in the Pyrenees. Tectonics 11(6), 1369-1384. https://doi.org/10.1029/92TC00823

Voet, H.W., 1967. Geological investigations in the Northern Sierra de Los Filabres around Macael and Cóbdar, southeastern Spain. Ph.D. Thesis, Amsterdam University, The Netherlands.

Williams, J.R., Platt, J.P., 2017. Superposed and refolded metamorphic isograds, and superposed directions of shear during late-orogenic extension in the Alborán

Formatted: English (Australia)
Formatted: English (Australia)
Formatted: Spanish (Spain)
Formatted: French (France)
Formatted: French (France)
Formatted: French (France)
Formatted: French (France)

Domain, southern Spain. Tectonics 36, 756-786~~. Doi:~~, https://doi.org/10.1002/2016TC004358

Wilson, M., 1997. Thermal evolution of the Central Atlantic passive margins: continental break-up above a Mesozoic super-plume. Journal of the Geological Society of London 154, 491-495.

Wissink, G.K., Wilkinson, B.H., Hoke, G.D., 2018. Pairwise sample comparisons and multidimensional scaling of detrital zircon ages with examples from the North American platform, basin, and passive margin settings. Lithosphere 10, 478-491, https://doi.org/ 10.1130/L700.1

Zindler, A., Staudigel, H., Hart, S.R., Endres, R., Goldstein, S., 1983, Nd and Sm isotopic study of a mafic layer from Ronda ultramafic complex. Nature 304, 226.

Figure and Table captions:

Figure 1.- (A) Tectonic sketch of the Southwestern Mediterranean Sea; (B) Tectonic map of the Betic Cordillera.

Figure 2.- Geological map of the south-eastern Betic Chain with outcrops of the three tectonic complexes of the Internal zones and the location of the Águilas Arc marked (see Fig. 1B for location).

Figure 3.- Geological map of the central area of the Águilas Arc (modified from Espinosa Godoy et al., 1972; Booth-Rea and Silva-Barroso, 2008; Booth-Rea et al., 2009; García-Tortosa et al., 2012), with the location of the studied samples. See location in Fig. 2.

Figure 4.- Lithological columns of the studied successions in the NFC, AC and MC with the location of the studied samples. Yellow stars: meta-detrital samples; red stars: meta-igneous samples. ~~Both lithological columns have the same vertical scale.~~ Successions for the NFC Lomo de Bas units were compiled from Laborda-López et al. (2013, 2015a, b) and Booth-Rea et al (2009). The succession of the NFC Mulhacén units compiled from Booth-Rea and Silva-Barroso (2008), and Booth-Rea et al. (2009).

~~**Figure 5.**- Lithological columns of the studied successions in the AC with the location of the studied samples. Yellow stars: meta-detrital samples; red stars: meta-igneous samples. All lithological columns have the same vertical scale.~~ Successions for the AC were compiled with data from Booth-Rea and Silva-Barroso (2008), Booth-Rea et al. ~~(2009~~(2009), and García-Tortosa et al. (2012). Succession from the MC Sierra de las Estancias area was compiled from Fernández-Fernández et al. (2007), while the succession of the MC Cabo Cope unit is from Espinosa Godoy et al. (1972), and García-Tortosa et al. (2012).

Figure ~~6.~~~~- Geological map of the southern area of the Águilas Arc, near san Juan de los Terreros village, with the location of the Cabezo Blanco orthogneiss and the AG-26 sample (modified from Booth-Rea et al., 2009). See location in Fig. 2.~~

~~**Figure 7.**- Geological map of the northeastern area of the Sierra de las Estancias with the location of sample LP-16-AZ (modified from Fernández-Fernández et al., 2007). See location in Fig. 2.~~

~~**Figure 8.** Lithological columns of the studied successions in the MC with the location of the studied samples. Yellow stars: meta-detrital samples. All lithological columns have the same vertical scale. The succession from the Sierra de las Estancias area was compiled from Fernández-Fernández et al. (2007). The succession of the Cabo Cope unit is from Espinosa Godoy et al. (1972), and García-Tortosa et al. (2012).~~

~~Figure 9~~5.- Results of U-Pb analyses on detrital ~~zircons~~zircon grains from Lomo de Bás units (NFC): combination of Kernel Density Estimates plots (KDE, black lines), frequency (grey bars), and relative abundance of age groups based on $^{206}Pb/^{238}U$ (for dates < 1.5 Ga) and $^{207}Pb/^{206}Pb$ (for dates > 1.5 Ga) ages. (A) sample AG-12; (B) sample AG-14; (C) sample AG-17, (D) sample AG-18, (E) Cumulative KDE (blue line) and frequency (grey bars) for the Lomo de Bás samples; (F) zoom for the ages ranging from 0 to 541 Ma.

Figure ~~10~~6.- Results of U-Pb analyses of detrital ~~zircons~~zircon grains from Tahal Fm samples (Mulhacén units, NFC): combination of Kernel Density Estimates plots (KDE, black lines), frequency (grey bars), and relative abundance of age groups based on $^{206}Pb/^{238}U$ (for dates < 1.5 Ga) and $^{207}Pb/^{206}Pb$ (for dates > 1.5 Ga) ages. (A) sample AG-1; (B) sample AG-2; (C) Cumulative KDE (blue line) and frequency (grey bars) for the samples of the Tahal Fm; (D) zoom for the ages ranging from 0 to 541 Ma.

Figure ~~11~~7.- Results of U-Pb analyses on the core of ~~zircons~~zircon grains from orthogneiss AG-13 (Lomo de Bas units, NFC): (A) conventional Concordia diagram, ^{204}Pb corrected, with the concordant data (95% > Concordia > 105%); (B) conventional Concordia diagram, ^{204}Pb corrected, with the most concordant data; (C) probability density plots (red line) and frequency (blue bars) for the concordant data (95% > Concordia > 105%); (D) weighted average of the most concordant data.

Figure ~~12~~8.- Results of U-Pb analyses on the core of ~~zircons~~zircon grains from the orthogneiss AG-16 (Lomo de Bas units, NFC): (A) conventional Concordia diagram with all the data; (B) conventional Concordia diagram, ^{207}Pb corrected, with the most concordant data (90% > Concordia > 110%); (C) probability density plots (red line) and frequency (blue bars) for the most concordant data; (D) weighted average of the most concordant data.

Figure ~~13~~9.- Results of U-Pb analyses on detrital ~~zircons~~zircon grains from samples from the Micaschists and Quartzite Fm (AC): combination of Kernel Density Estimates plots (KDE, black lines), frequency (grey bars), and relative abundance of age groups based on ^{206}Pb/^{238}U (for dates < 1.5 Ga) and ^{207}Pb/^{206}Pb (for dates > 1.5 Ga) ages. (A) sample AG-4; (B) sample AG-5; (C) sample AG-6, (D) sample AG-7, (E) Cumulative KDE (blue line) and frequency (grey bars) for the samples from the Micaschists and Quartzite Fm ; (F) zoom for the ages ranging from 0 to 541 Ma.

Figure ~~14~~10.- Results of U-Pb analyses on detrital ~~zircons~~zircon grains from samples from the Meta-~~detritic~~detrital Fm (AC: AG-9, AG-11, and AG-15), and from the Miñarros mylonites and breccias (AC: AG-19): combination of Kernel Density Estimates plots (KDE, black lines), frequency (grey bars), and relative abundance of age groups based on ^{206}Pb/^{238}U (for dates < 1.5 Ga) and ^{207}Pb/^{206}Pb (for dates > 1.5 Ga) ages. (A) sample AG-9; (B) sample AG-11; (C) sample AG-15, (D) sample AG-19, (E) Cumulative KDE (blue line) and frequency (grey bars) for the samples from the Meta-

~~detritic~~detrital Fm (AG-9, AG-11, and AG-15); (F) zoom for the ages ranging from 0 to 541 Ma.

Figure ~~15~~11.- Results of U-Pb analyses on the black rims of zircon from the Cabezo Blanco orthogneiss AG-26 (Cantal unit): (A) conventional Concordia diagram with all the data; (B) conventional Concordia diagram, ^{207}Pb corrected, with the maximum at ca. 16 Ma; (C) probability density plots (red line) and frequency (blue bars) for all then data; (D) weighted average of the ca. 16 Ma age.

Figure ~~16~~12.- Results of U-Pb analyses on the cores of zircon from the Cabezo Blanco orthogneiss AG-26 (Cantal unit): (A) conventional Concordia diagram with all the data; (B) conventional Concordia diagram, ^{207}Pb corrected, with the main population; (C) probability density plots (red line) and frequency (blue bars) for all then data; (D) weighted average of the main population.

Figure ~~17~~13.- Results of U-Pb analyses on detrital ~~zircons~~zircon grains from samples from the Saladilla Fm (MC): combination of Kernel Density Estimates plots (KDE, black lines), frequency (grey bars), and relative abundance of age groups based on ^{206}Pb/^{238}U (for dates < 1.5 Ga) and ^{207}Pb/^{206}Pb (for dates > 1.5 Ga) ages. (A) sample AG-10; (B) sample LP-16-AZ; (C) Cumulative KDE (blue line) and frequency (grey bars) for the samples of the Saladilla Fm; (D) zoom for the ages ranging from 0 to 541 Ma.

Figure ~~18~~14.- Results of U-Pb analyses on detrital ~~zircons~~zircon grains from samples from the unconformable Middle Miocene rocks: combination of Kernel Density

Estimates plots (KDE, black lines), frequency (grey bars), and relative abundance of age groups based on $^{206}Pb/^{238}U$ (for dates < 1.5 Ga) and $^{207}Pb/^{206}Pb$ (for dates > 1.5 Ga) ages. (A) sample AG-3; (B) sample AG-20; (C) Cumulative KDE (blue line) and frequency (grey bars) for the samples of the Middle Miocene rocks; (D) zoom for the ages ranging from 0 to 541 Ma.

Figure 19. Comparison between the combined KDE plots determined in Paleozoic samples of the studied area and other regions of the Iberian Peninsula and South France: (A) Lomo de Bas units vs Aulago Fm (Jabaloy-Sánchez et al., 2018); (B) Micaschists and Quartzite Fm vs sample Ri-119 from the Sebtide Complex (Azdimousa et al., 2019); (C) Silurian-Devonian rocks from the Cantabrian and Central Iberian zones (Gutíerrez-Alonso et al.,2015) vs Late Carboniferous rocks from the Cantabrian Zone (Pastor-Galán et al., 2013); (D) Lower Ordovician Armorican Quartzite (Shaw et al., 2014) vs Ediacaran and Early Cambrian rocks from the Cantabrian and Central Iberian zones (Fernandez-Suarez et al., 2014); (E) Upper Carboniferous rocks from the Pyrenees (Martínez et al., 2016) vs Upper Carboniferous rocks from the Catalonian Massif (Martínez et al., 2016); (F) Upper Carboniferous rocks from the Montagne Noire and Mouthoumet massifs (Martínez et al., 2016), vs Upper Carboniferous rocks from the Priorat Massif (Martínez et al., 2016), vs Upper Carboniferous rocks from Minorca (Martínez et al., 2016); (G) Upper Carboniferous rocks from MC (sample 121, Azdimousa et al., 2019) vs Early Permian Marbella Conglomerate (Esteban et al., 2017); (H) Upper Carboniferous Mira and Brejeira Fms from the South Portuguesse Zone (Pereira et al., 2014) vs Upper Carboniferous Santa Susana Fm from the Ossa Morena Zone (Pereira et al., 2020).**15.-** A) Multidimensional scaling (MDS) plot of the

Late Carboniferous samples from the Betic Cordillera (NFC, AC and MC), Iberian Massif and South France. B) Shepard plot for the MDS.

Figure ~~20~~16.- Paleogeographic reconstruction of the eastern Variscan belt at Early Bashkirian times (modified from ~~Simancas et al. (2005) for NW Africa and from~~ Martínez-Catalán (2011) and Rodríguez-Cañero et al. (2017) for Europe). The proposed location of the NFC, AC and MC with respect to other Variscan Iberian Terranes is included. CIZ, Central Iberian; CZ, Cantabrian; GTMZ, Galicia-Trás-os-Montes; MGCZ, Mid-German Crystalline; MZ, Moldanubian; OMZ, Ossa-Morena; RHZ, Rheno-Hercynian; SPZ, South Portuguese; STZ, Saxo-Thuringian; TBZ, Teplá-Barrandian; WALZ, West Asturian-Leonese.

Figure ~~**21.-** Comparison between the combined KDE plots determined in Permian Triassic rocks of the studied area with those from older rocks from the same complexes. Combined KDE from Permian-Triassic samples from the Iberian Massif and Iberian Chain are also included: (A) Samples from the MC: Upper Carboniferous rocks from MC (sample 121, Azdimousa et al., 2019), vs Early Permian Marbella Conglomerate (Esteban et al., 2017), vs Middle Triassic Saladilla Fm; (B) Samples from the AC: Micaschists and Quartzite Fm, vs sample Ri-119 from the Sebtide Complex (Azdimousa et al., 2019), vs Early-Middle Triassic Meta-detritic Fm; (C) Samples from the NFC: Aulago Fm (Jabaloy-Sánchez et al., 2018), vs Lomo de Bas units, vs Tahal Fm (combination of the data from Jabaloy-Sánchez et al., 2018 and this work); (D) Permian rocks from the Cantabrian Zone (Pastor-Galán et al., 2013), vs Permian rocks from the Iberian Chain (Sánchez-Martínez et al., 2012), vs Lower Triassic rocks from the Iberian Chain (Sánchez-Martínez et al., 2012).~~**17.-** A) Multidimensional scaling

(MDS) plot of the Permian Triassic samples from the Betic Cordillera (NFC, AC and MC), Iberian Massif and Iberian Chain. B) Shepard plot for the MDS.

Table 1.- Sketch of the Tectonic complexes and units mentioned in the text and available ages from every lithological formation.

Table 2.- Details of the samples and the analyses carried out; (*) UTM coordinates, ED_1950 ellipsoid, zone 30 S.

Figure 1

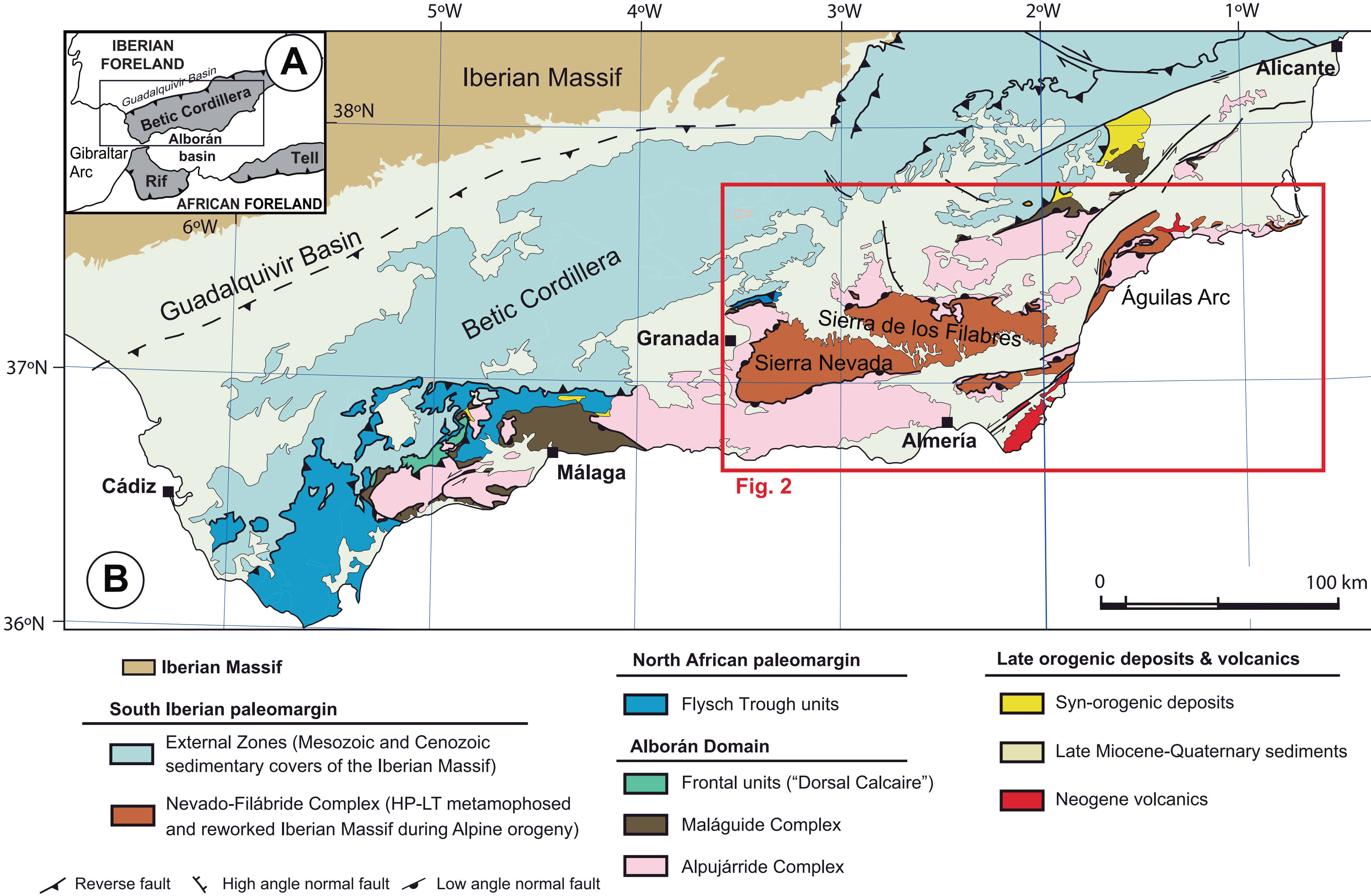

Figure 1

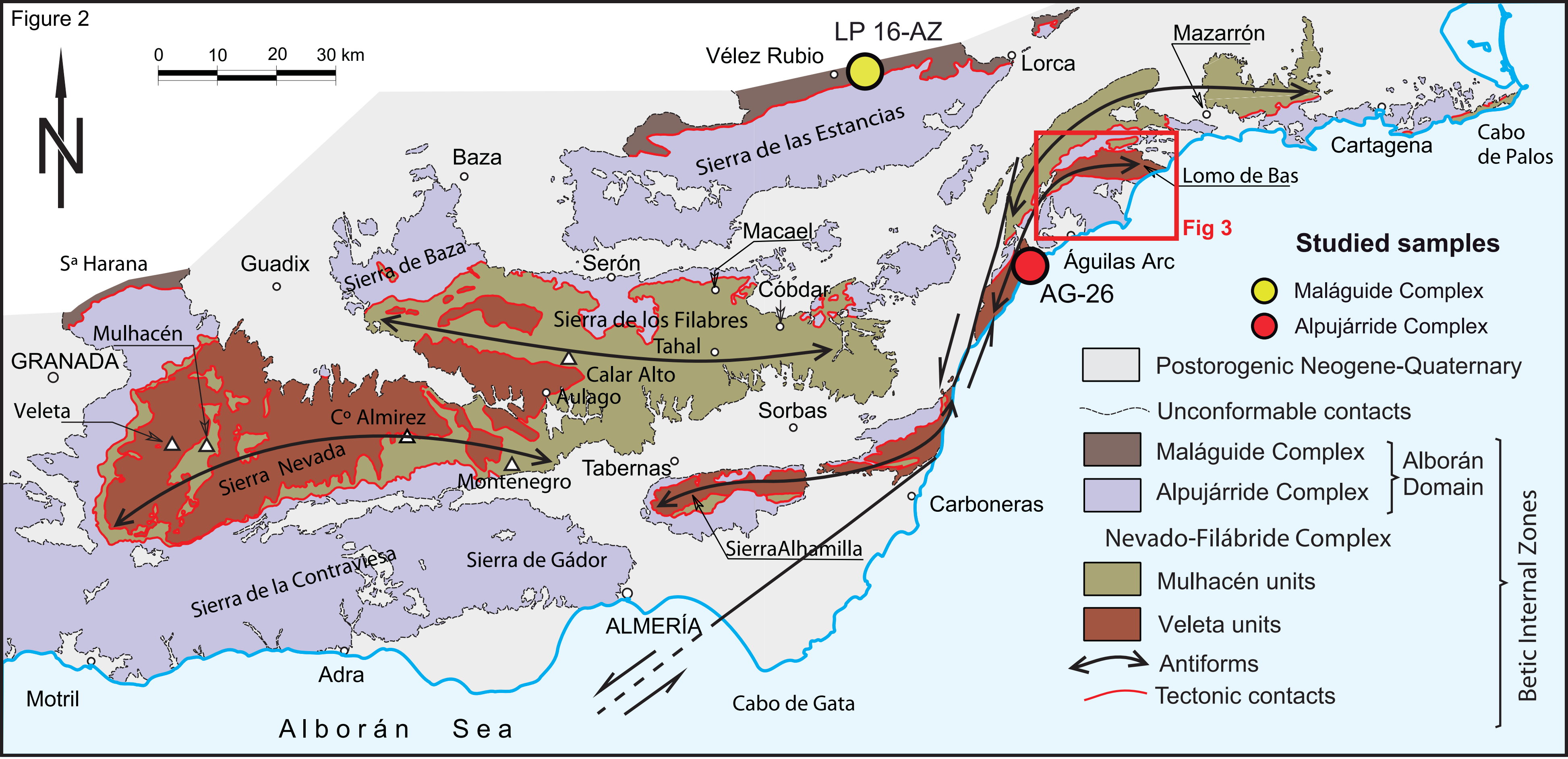

Figure 2
0 10 20 30 km
N
LP 16-AZ
Vélez Rubio
Lorca
Mazarrón
Cartagena
Cabo de Palos
Lomo de Bas
Fig 3
Sierra de las Estancias
Baza
Macael
Serón
Guadix
Sª Harana
Sierra de Baza
Cóbdar
Sierra de los Filabres
Tahal
Calar Alto
Aulago
Sorbas
Águilas Arc
AG-26
Studied samples
Maláguide Complex
Alpujárride Complex
Postorogenic Neogene-Quaternary
Unconformable contacts
Maláguide Complex
Alpujárride Complex
Alborán Domain
Nevado-Filábride Complex
Mulhacén units
Veleta units
Antiforms
Tectonic contacts
Betic Internal Zones
Mulhacén
GRANADA
Veleta
Cº Almirez
Sierra Nevada
Montenegro
Tabernas
Carboneras
Sierra Alhamilla
Sierra de Gádor
Sierra de la Contraviesa
ALMERÍA
Adra
Motril
Cabo de Gata
Alborán Sea

Figure 2

Figure 3

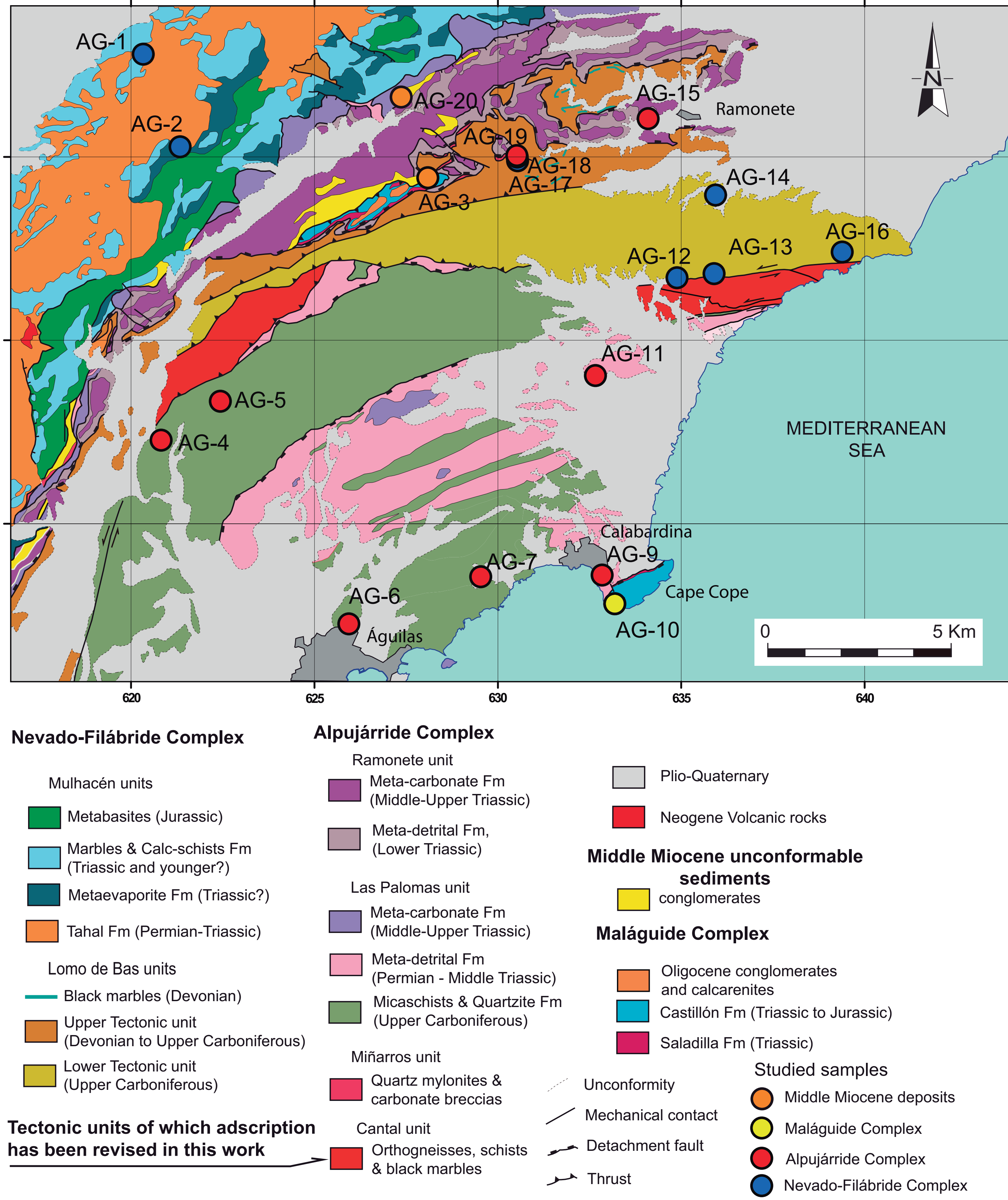

Figure 3

Figure 4

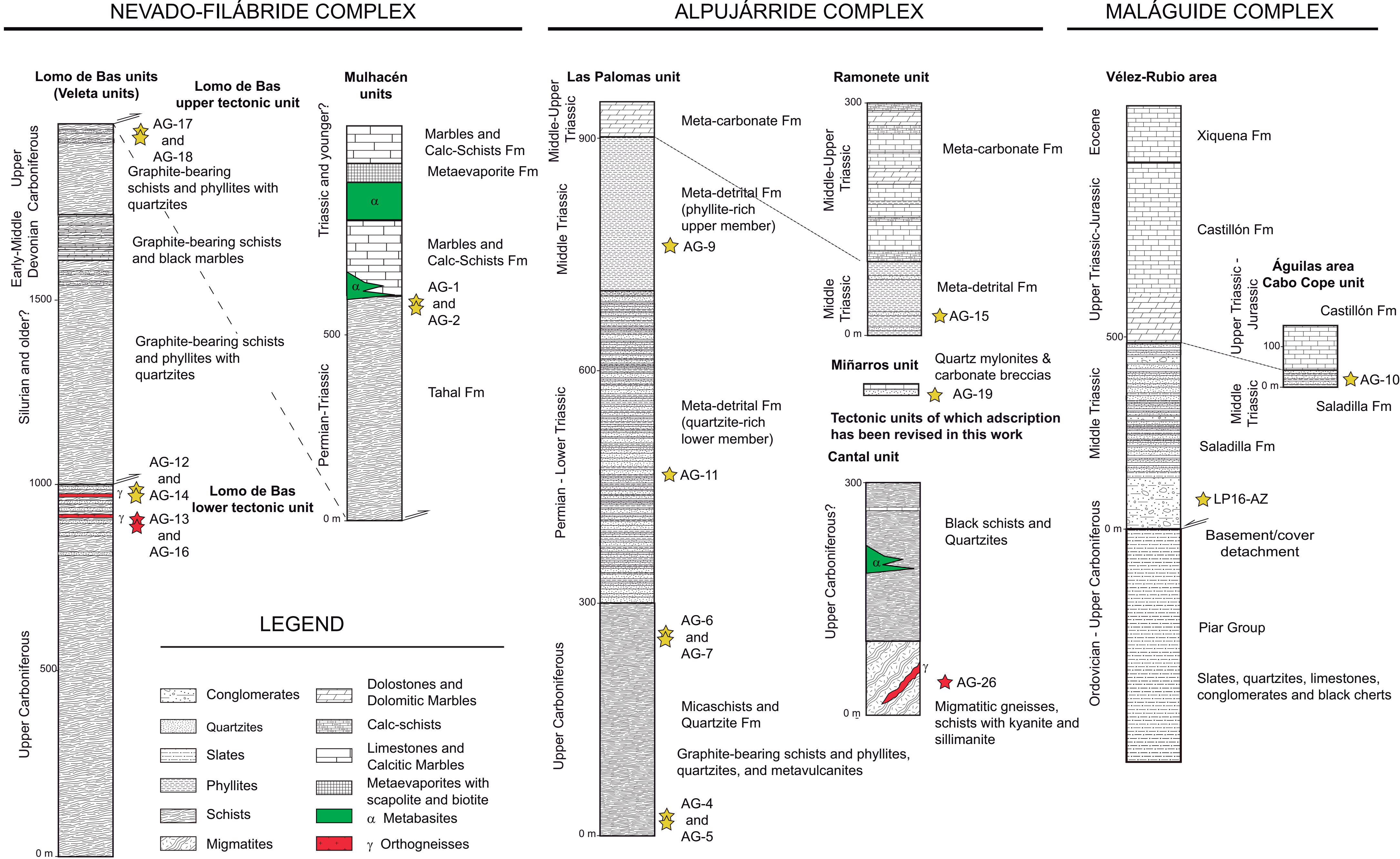

Figure 4

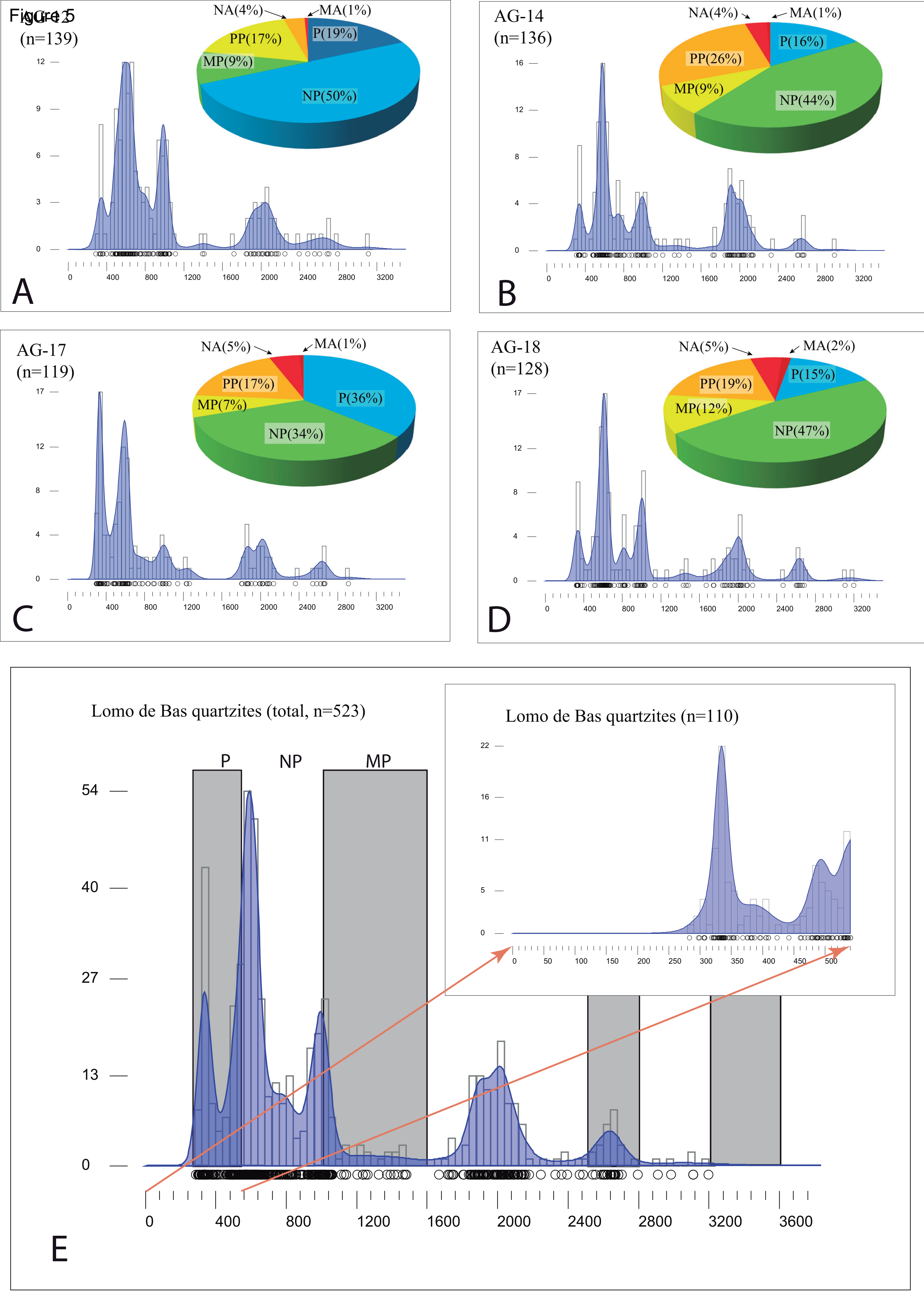
AG-12
(n=139)
NA(4%)
MA(1%)
P(19%)
PP(17%)
MP(9%)
NP(50%)
A
AG-14
(n=136)
NA(4%)
MA(1%)
P(16%)
PP(26%)
MP(9%)
NP(44%)
B
AG-17
(n=119)
NA(5%)
MA(1%)
PP(17%)
P(36%)
MP(7%)
NP(34%)
C
AG-18
(n=128)
NA(5%)
MA(2%)
P(15%)
PP(19%)
MP(12%)
NP(47%)
D
Lomo de Bas quartzites (total, n=523)
P
NP
MP
Lomo de Bas quartzites (n=110)
E

Figure 5

Figure 6

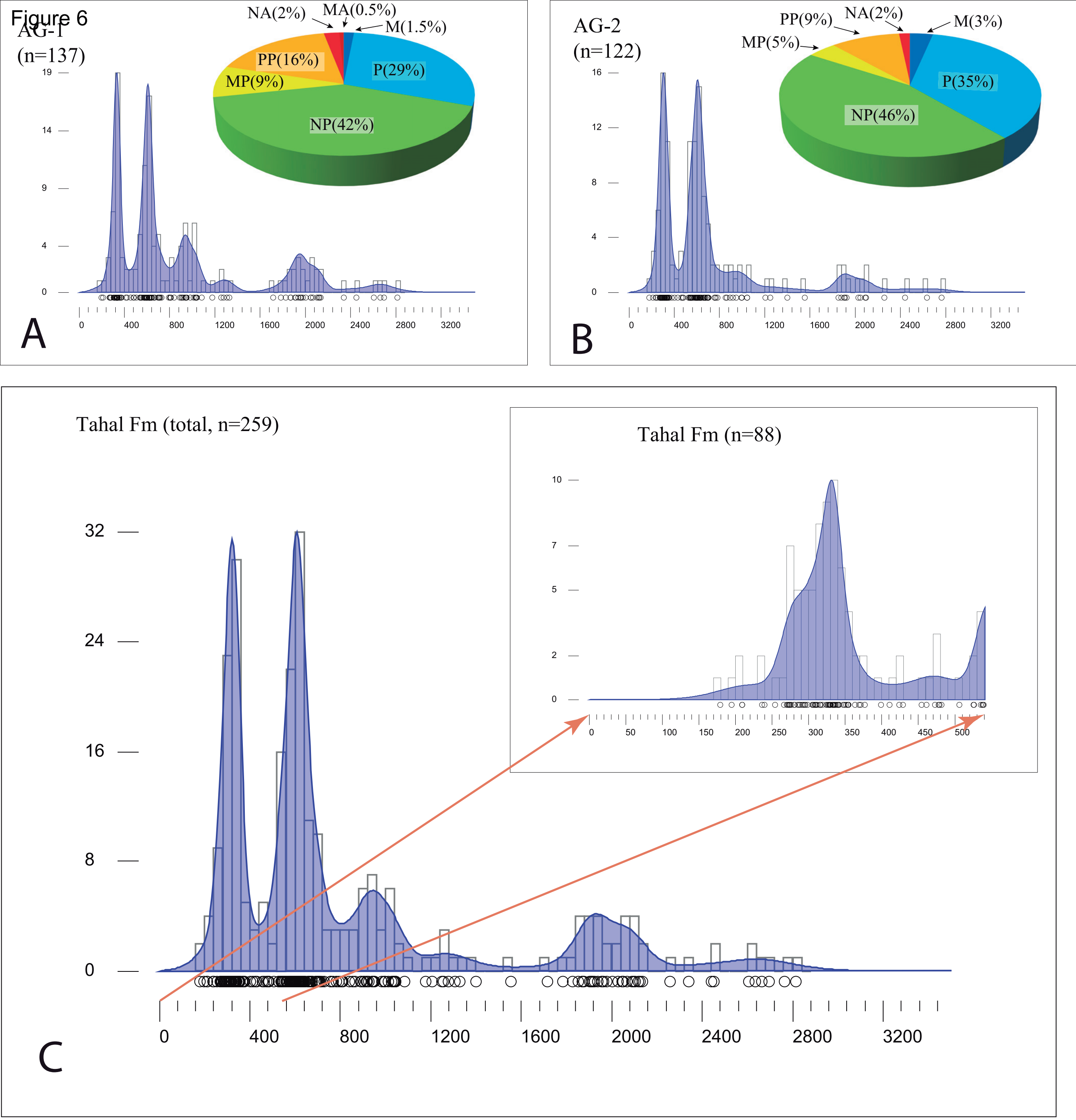

Figure 6

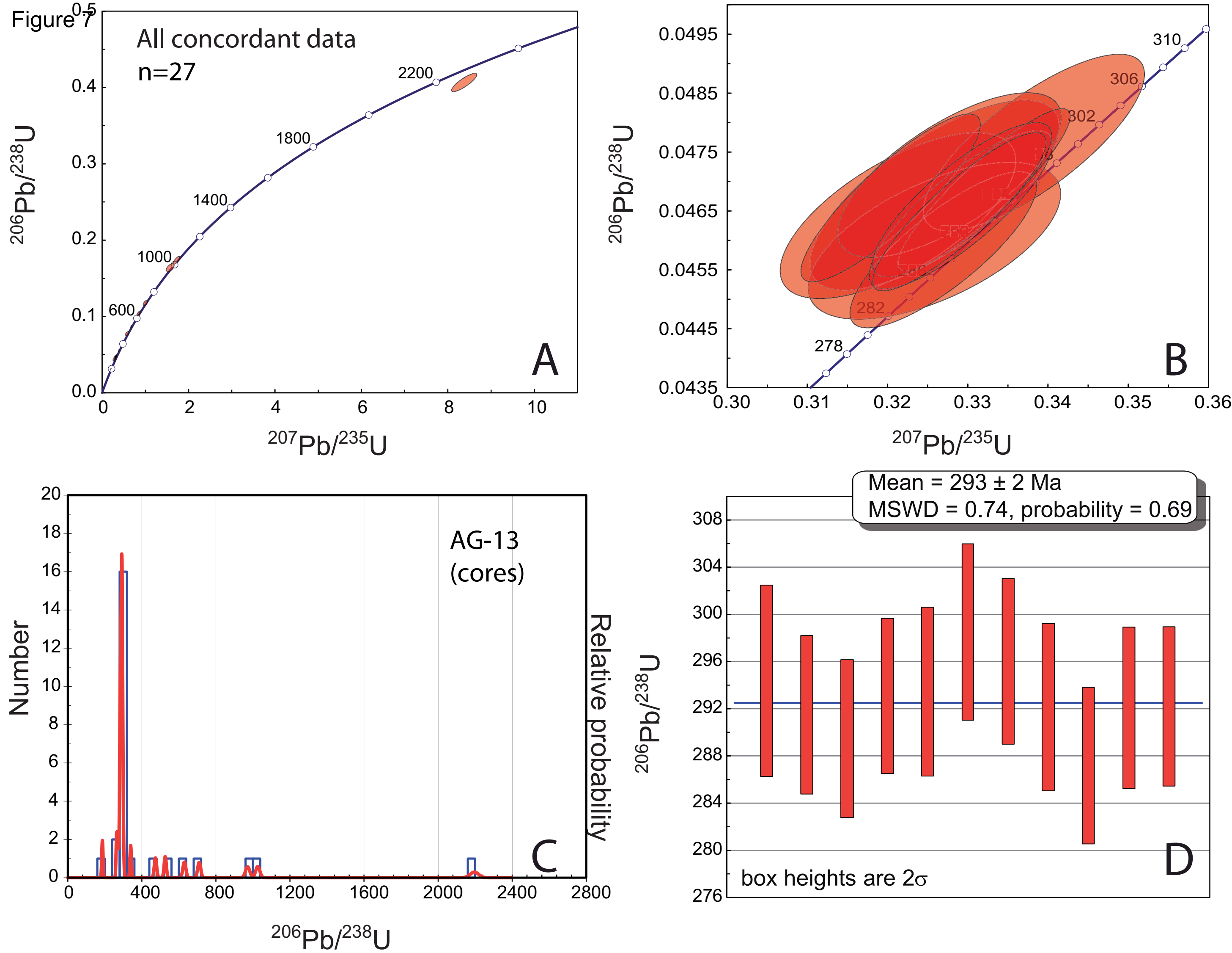
Figure 7
All concordant data
n=27
2200
1800
1400
1000
600
206Pb/238U
207Pb/235U
A
310
306
302
282
278
B
AG-13
(cores)
Number
Relative probability
206Pb/238U
C
Mean = 293 ± 2 Ma
MSWD = 0.74, probability = 0.69
206Pb/238U
box heights are 2σ
D

Figure 7

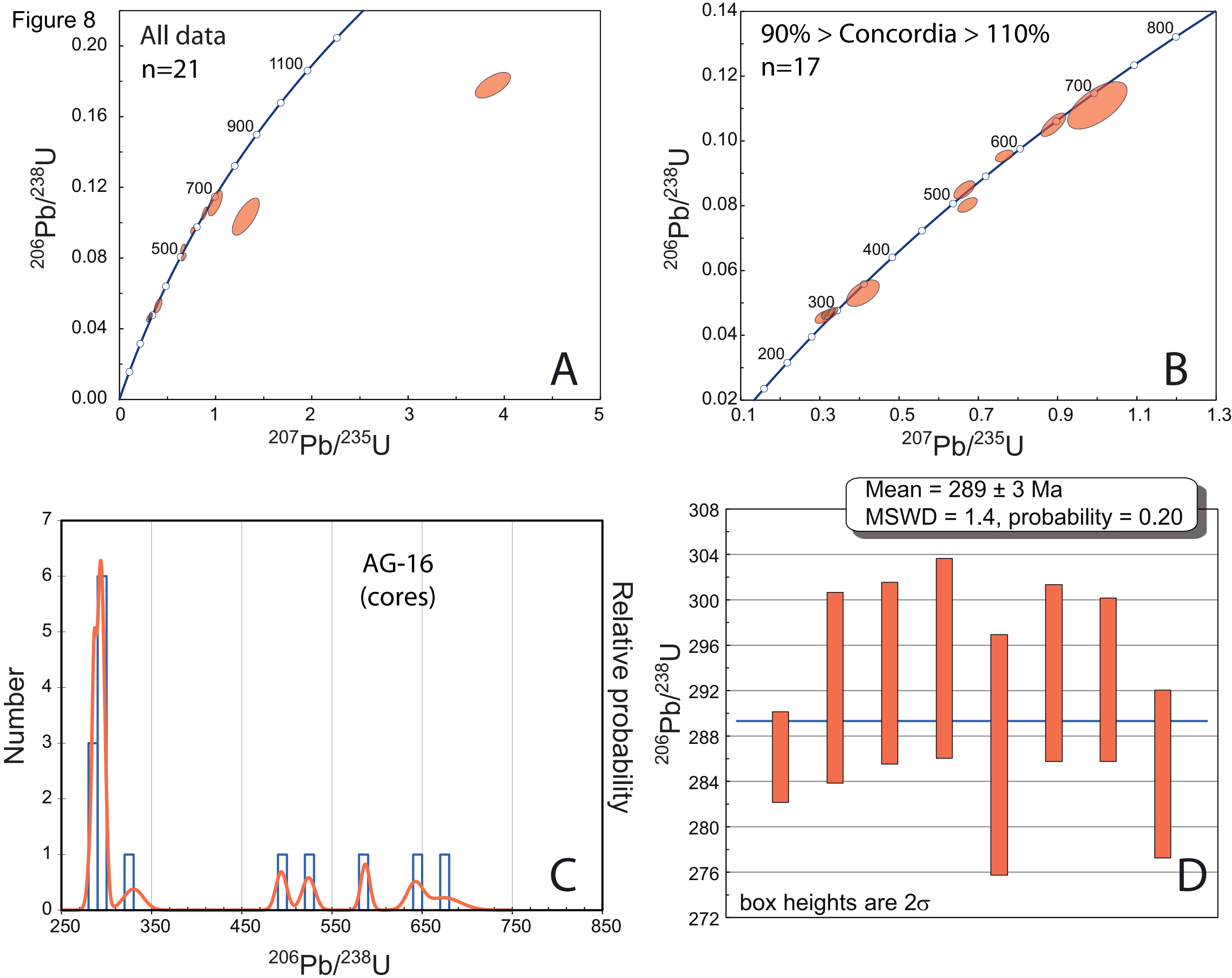
Figure 8
All data
n=21
A
90% > Concordia > 110%
n=17
B
AG-16
(cores)
C
Number
Relative probability
Mean = 289 ± 3 Ma
MSWD = 1.4, probability = 0.20
box heights are 2σ
D
$^{207}Pb/^{235}U$
$^{206}Pb/^{238}U$

Figure 8

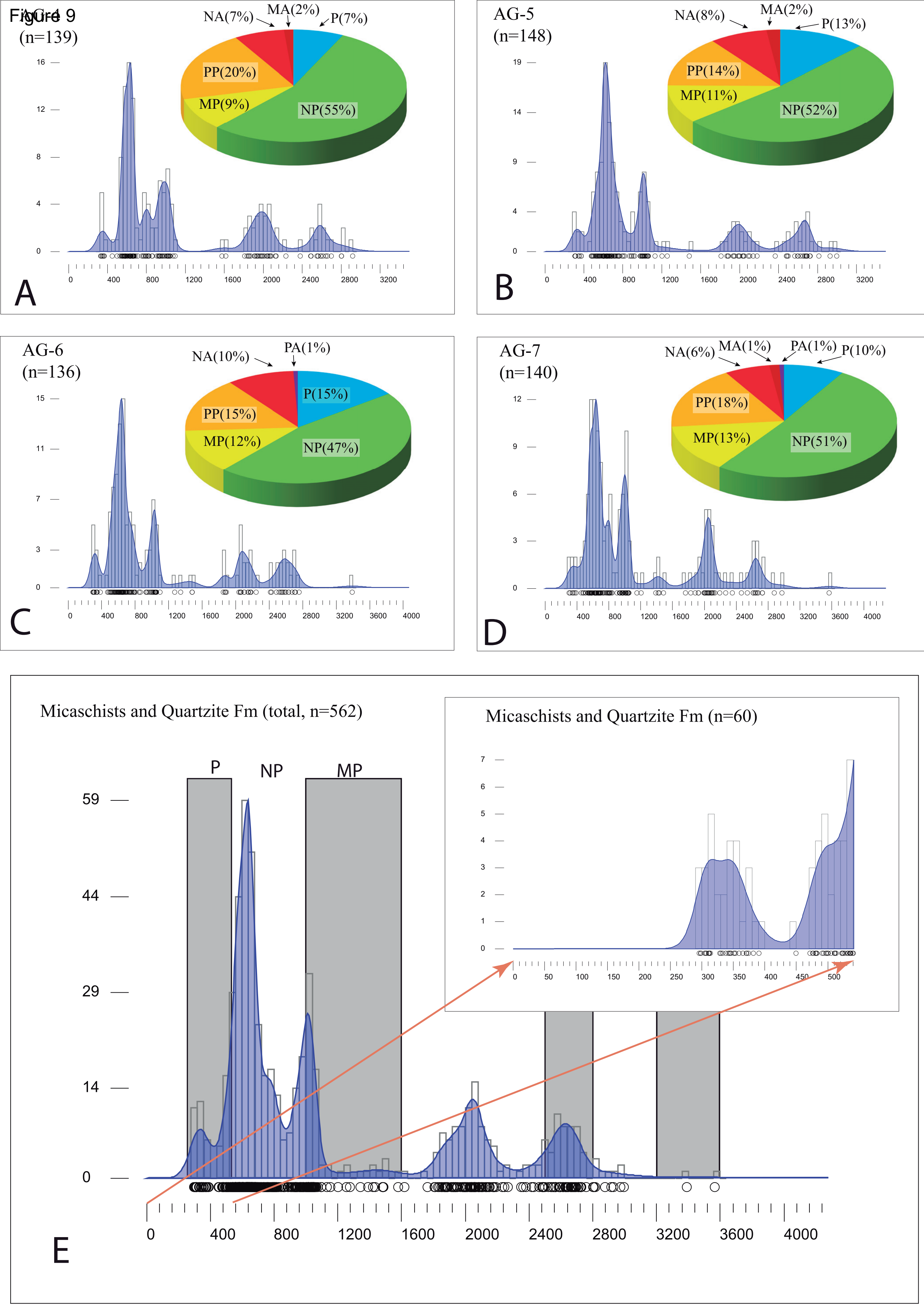
AG-4
(n=139)
NA(7%)
MA(2%)
P(7%)
PP(20%)
MP(9%)
NP(55%)
A
AG-5
(n=148)
NA(8%)
MA(2%)
P(13%)
PP(14%)
MP(11%)
NP(52%)
B
AG-6
(n=136)
NA(10%)
PA(1%)
P(15%)
PP(15%)
MP(12%)
NP(47%)
C
AG-7
(n=140)
NA(6%)
MA(1%)
PA(1%)
P(10%)
PP(18%)
MP(13%)
NP(51%)
D
Micaschists and Quartzite Fm (total, n=562)
P
NP
MP
Micaschists and Quartzite Fm (n=60)
E

Figure 9

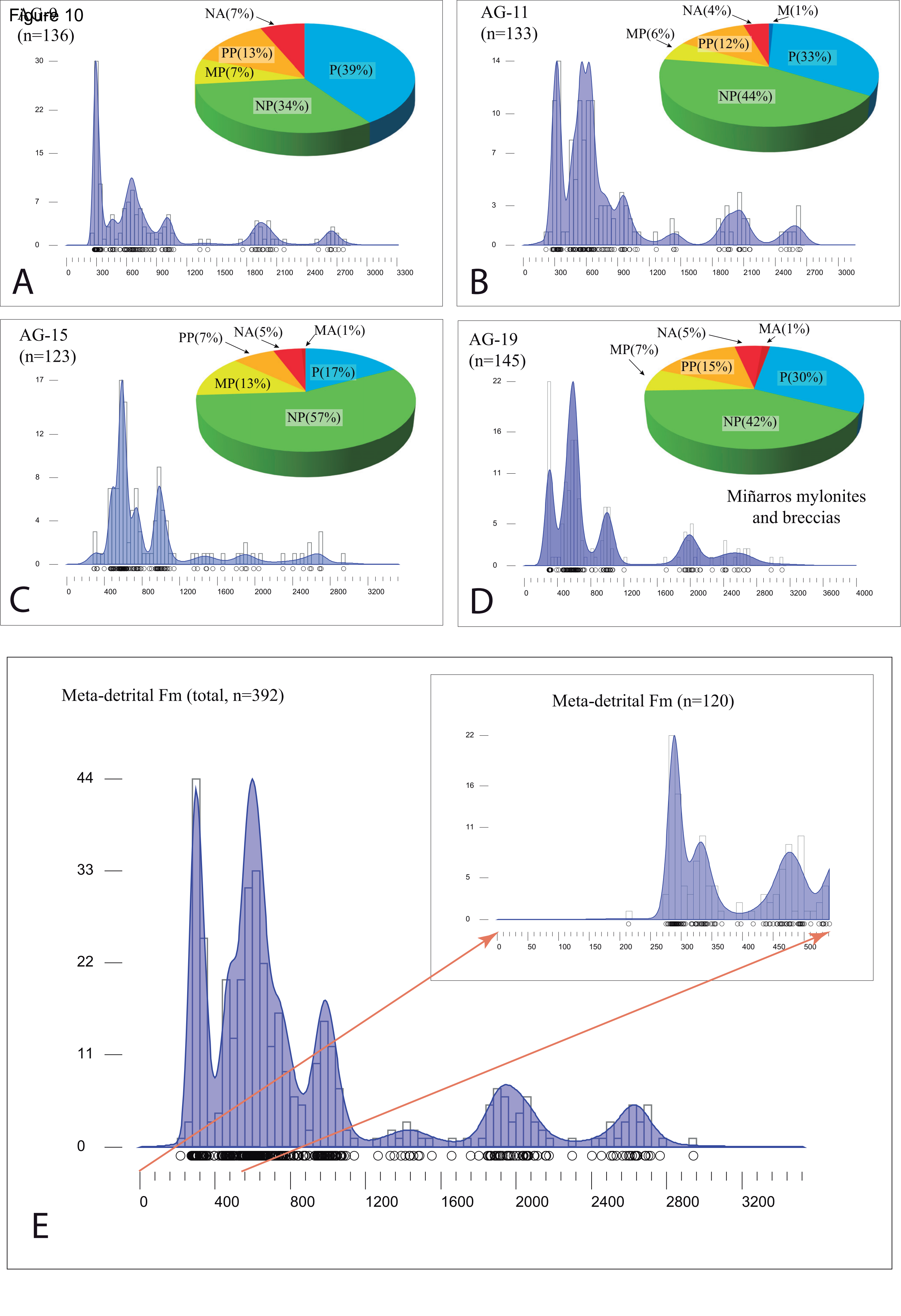

Figure 10
AG-9
(n=136)
NA(7%)
PP(13%)
MP(7%)
P(39%)
NP(34%)
A
AG-11
(n=133)
NA(4%)
M(1%)
MP(6%)
PP(12%)
P(33%)
NP(44%)
B
AG-15
(n=123)
PP(7%)
NA(5%)
MA(1%)
MP(13%)
P(17%)
NP(57%)
C
AG-19
(n=145)
NA(5%)
MA(1%)
MP(7%)
PP(15%)
P(30%)
NP(42%)
Miñarros mylonites and breccias
D
Meta-detrital Fm (total, n=392)
Meta-detrital Fm (n=120)
E

Figure 10

Figure 11

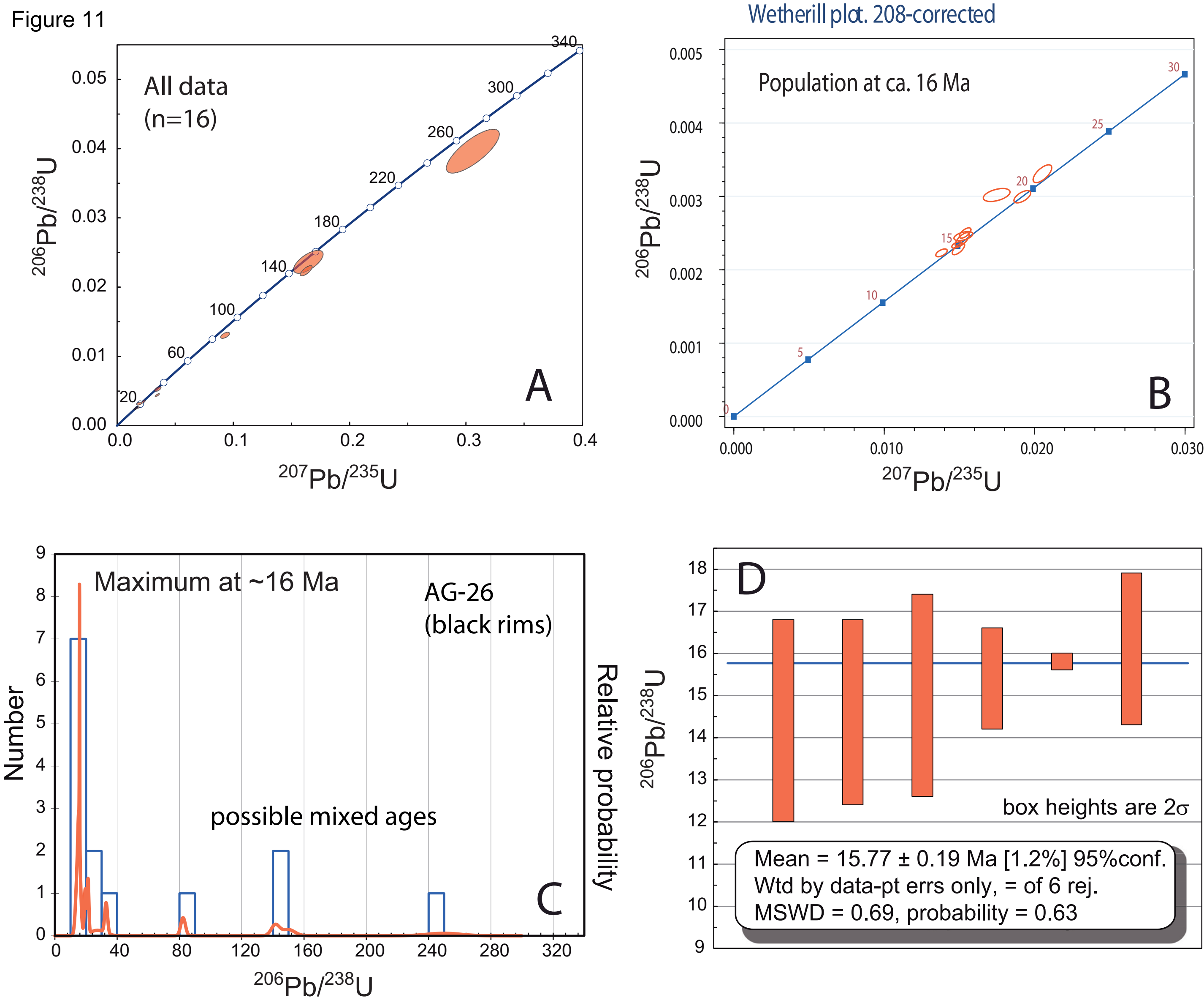

Figure 11

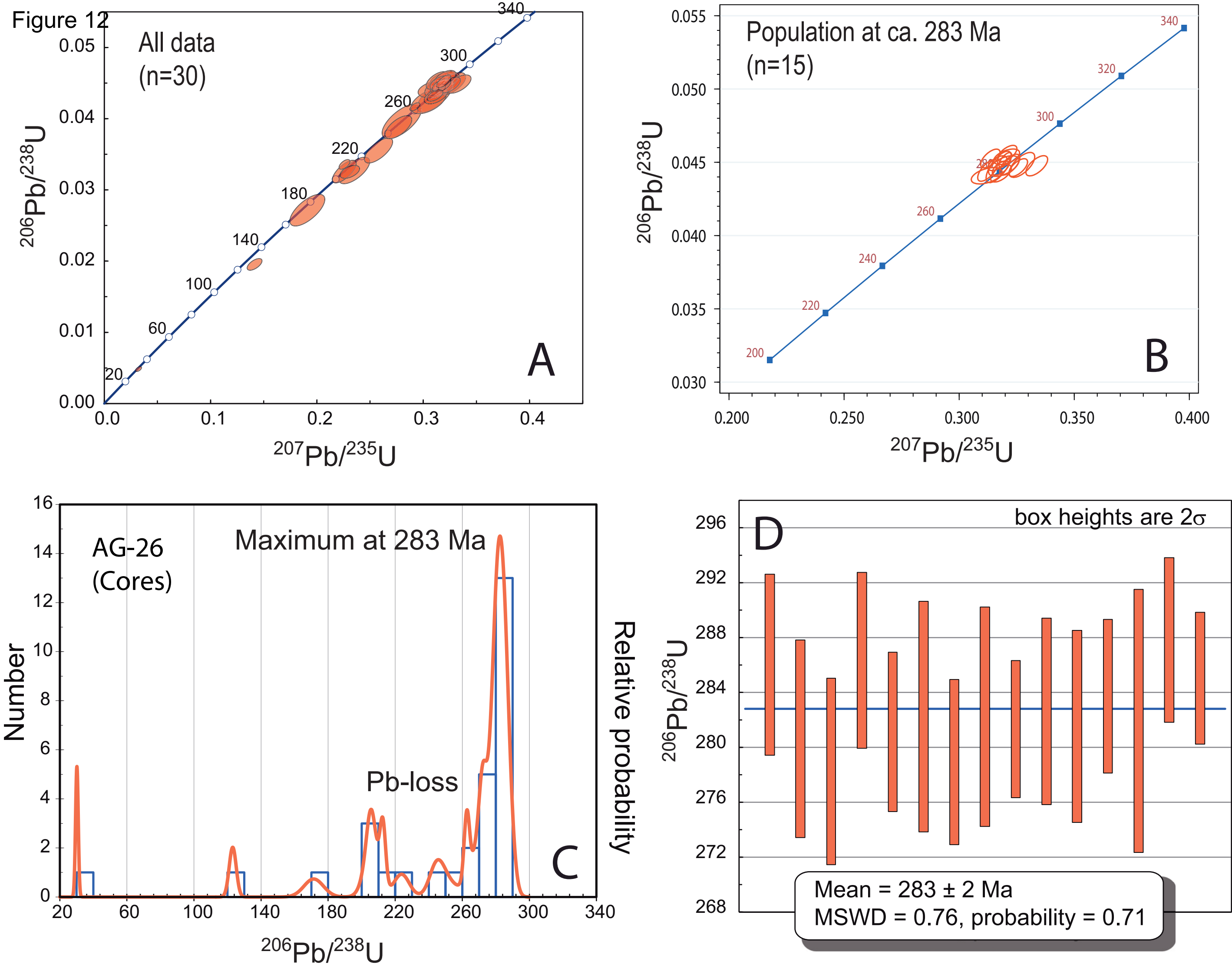
Figure 12
All data
(n=30)
A
Population at ca. 283 Ma
(n=15)
B
AG-26
(Cores)
Maximum at 283 Ma
Pb-loss
C
Number
Relative probability
box heights are 2σ
D
Mean = 283 ± 2 Ma
MSWD = 0.76, probability = 0.71

Figure 12

Figure 13

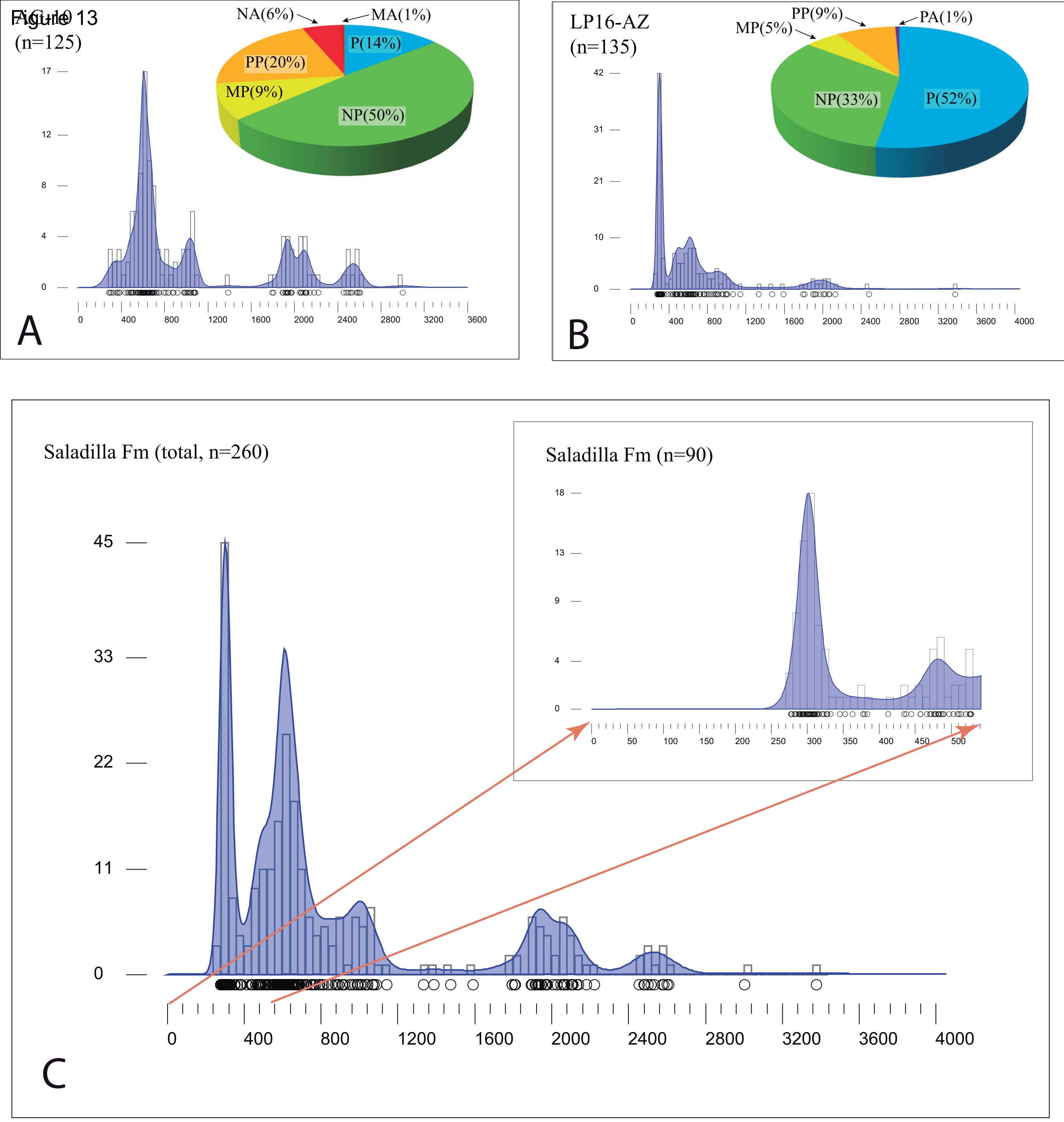

Figure 13

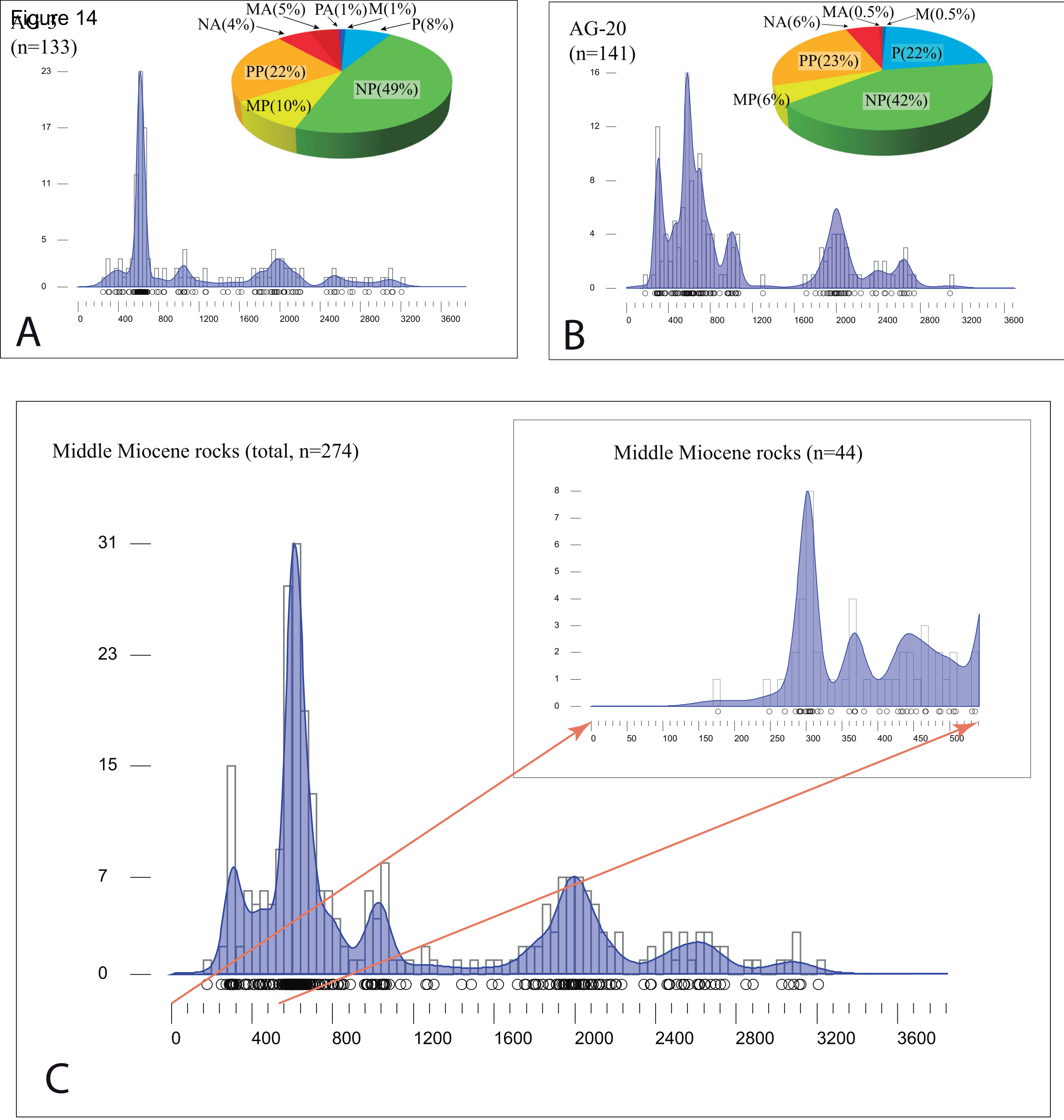

Figure 14
AG-5
(n=133)
NA(4%)
MA(5%)
PA(1%)
M(1%)
P(8%)
PP(22%)
MP(10%)
NP(49%)
A
AG-20
(n=141)
NA(6%)
MA(0.5%)
M(0.5%)
P(22%)
PP(23%)
MP(6%)
NP(42%)
B
Middle Miocene rocks (total, n=274)
Middle Miocene rocks (n=44)
C

Figure 14

Figure 15

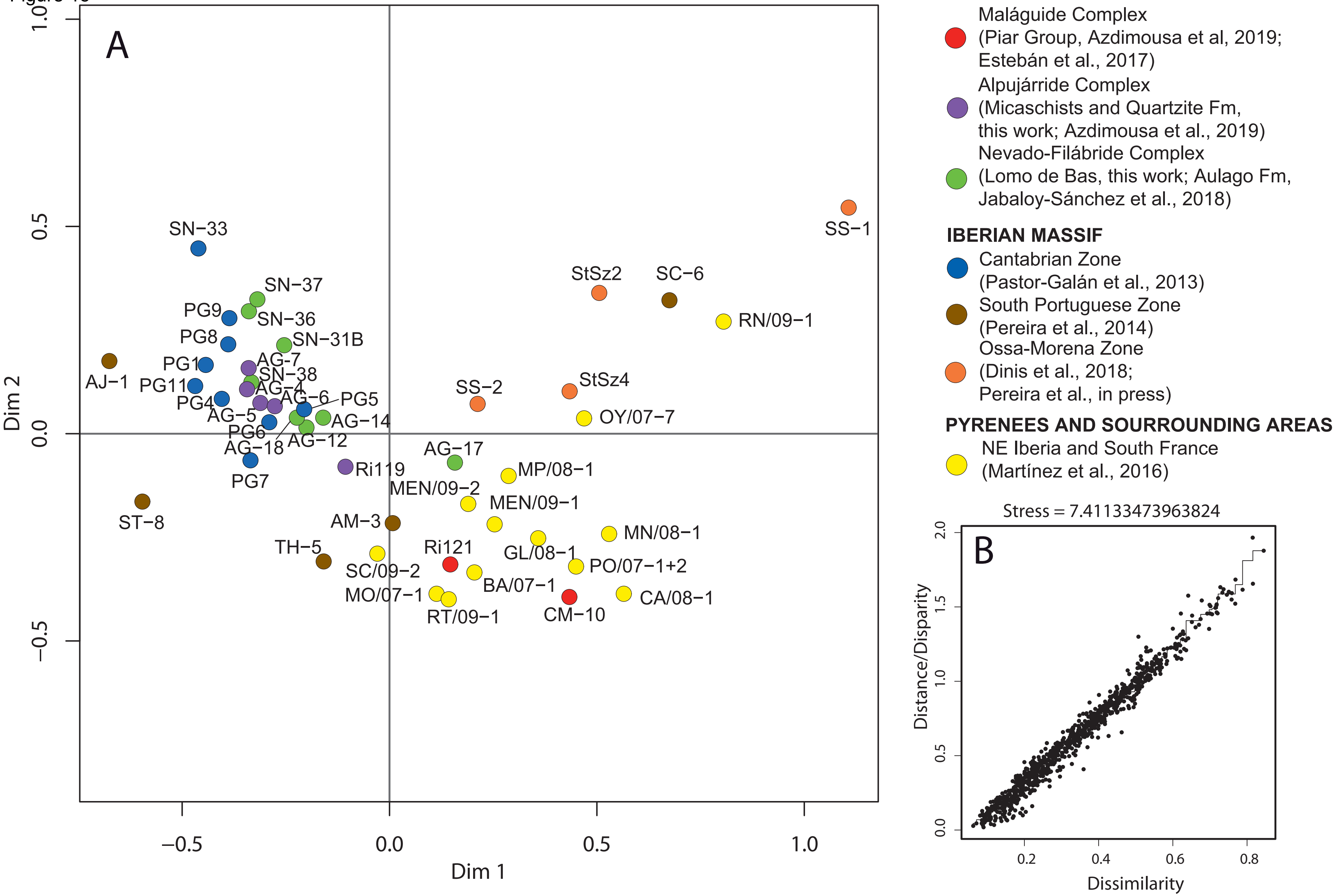
A
Dim 1
Dim 2
BETIC CORDILLERA
Maláguide Complex (Piar Group, Azdimousa et al, 2019; Estebán et al., 2017)
Alpujárride Complex (Micaschists and Quartzite Fm, this work; Azdimousa et al., 2019)
Nevado-Filábride Complex (Lomo de Bas, this work; Aulago Fm, Jabaloy-Sánchez et al., 2018)
IBERIAN MASSIF
Cantabrian Zone (Pastor-Galán et al., 2013)
South Portuguese Zone (Pereira et al., 2014)
Ossa-Morena Zone (Dinis et al., 2018; Pereira et al., in press)
PYRENEES AND SOURROUNDING AREAS
NE Iberia and South France (Martínez et al., 2016)
B
Stress = 7.41133473963824
Distance/Disparity
Dissimilarity

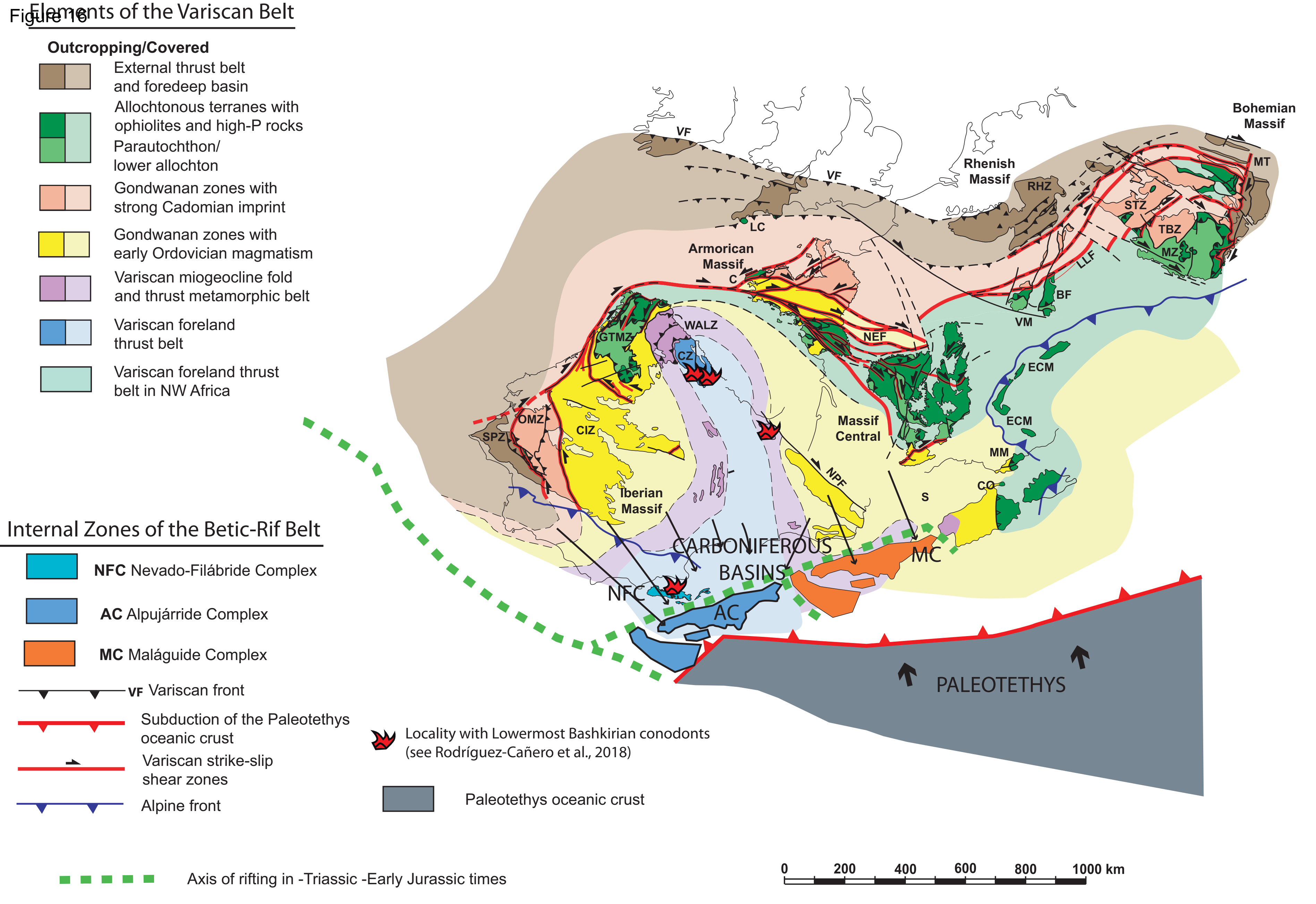
Elements of the Variscan Belt
Outcropping/Covered
External thrust belt and foredeep basin
Allochtonous terranes with ophiolites and high-P rocks
Parautochthon/ lower allochton
Gondwanan zones with strong Cadomian imprint
Gondwanan zones with early Ordovician magmatism
Variscan miogeocline fold and thrust metamorphic belt
Variscan foreland thrust belt
Variscan foreland thrust belt in NW Africa
Internal Zones of the Betic-Rif Belt
NFC Nevado-Filábride Complex
AC Alpujárride Complex
MC Maláguide Complex
VF Variscan front
Subduction of the Paleotethys oceanic crust
Variscan strike-slip shear zones
Alpine front
Locality with Lowermost Bashkirian conodonts (see Rodríguez-Cañero et al., 2018)
Paleotethys oceanic crust
Axis of rifting in -Triassic -Early Jurassic times
0 200 400 600 800 1000 km
VF
Rhenish Massif
Bohemian Massif
MT
RHZ
STZ
TBZ
MZ
LLF
LC
Armorican Massif
C
BF
VM
NEF
WALZ
GTMZ
CZ
ECM
Massif Central
MM
OMZ
SPZ
CIZ
NPF
Iberian Massif
S
CO
CARBONIFEROUS BASINS
MC
NFC
AC
PALEOTETHYS

Figure 16

Figure 17

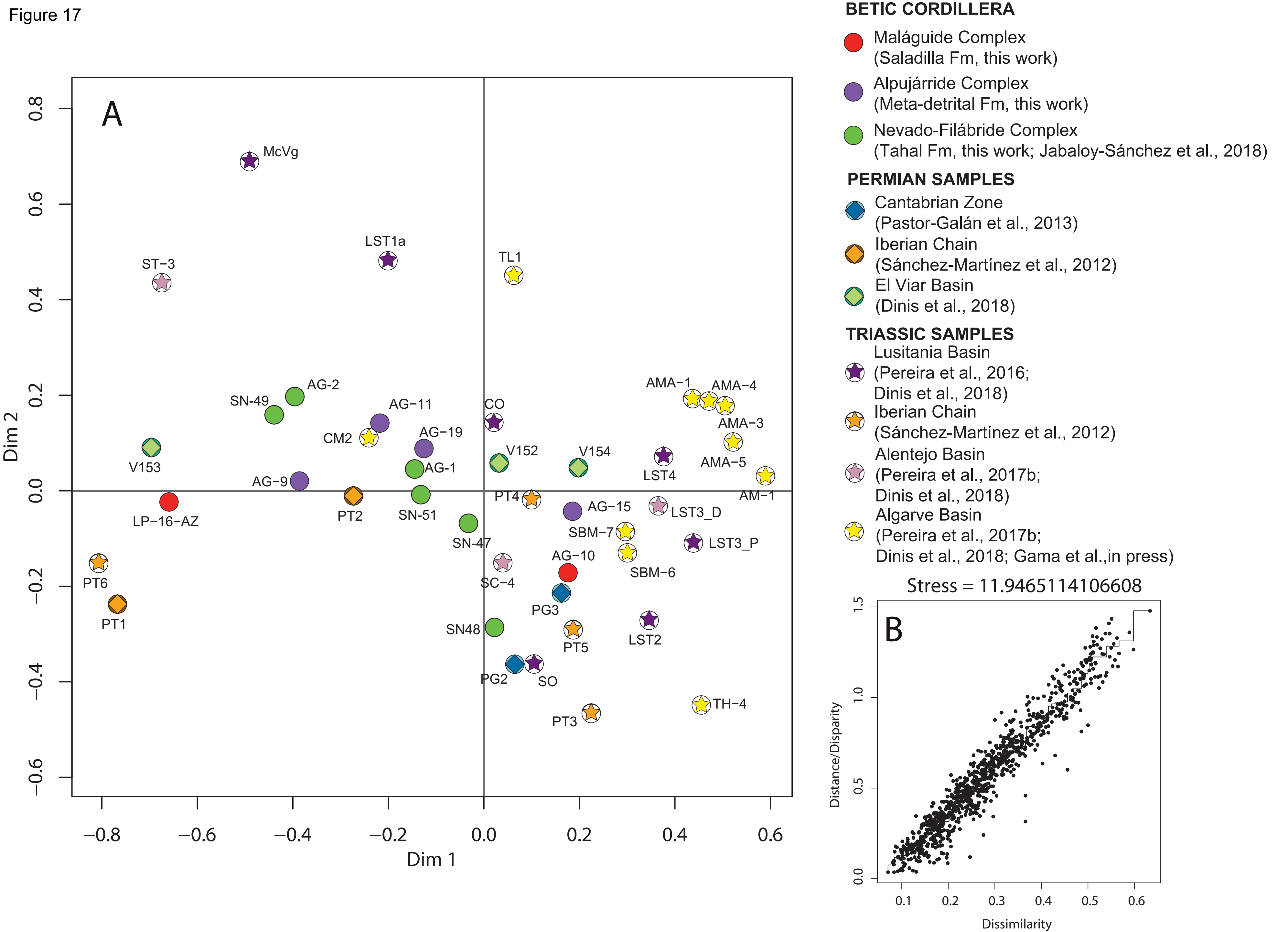
A
B
BETIC CORDILLERA
Maláguide Complex
(Saladilla Fm, this work)
Alpujárride Complex
(Meta-detrital Fm, this work)
Nevado-Filábride Complex
(Tahal Fm, this work; Jabaloy-Sánchez et al., 2018)
PERMIAN SAMPLES
Cantabrian Zone
(Pastor-Galán et al., 2013)
Iberian Chain
(Sánchez-Martínez et al., 2012)
El Viar Basin
(Dinis et al., 2018)
TRIASSIC SAMPLES
Lusitania Basin
(Pereira et al., 2016;
Dinis et al., 2018)
Iberian Chain
(Sánchez-Martínez et al., 2012)
Alentejo Basin
(Pereira et al., 2017b;
Dinis et al., 2018)
Algarve Basin
(Pereira et al., 2017b;
Dinis et al., 2018; Gama et al.,in press)
Stress = 11.9465114106608
Dim 1
Dim 2
Distance/Disparity
Dissimilarity
McVg
LST1a
ST−3
TL1
AG−2
SN-49
AG−11
CO
AMA−1
AMA−4
AMA−3
AMA−5
AM−1
CM2
AG−19
V153
V152
V154
LST4
AG−9
AG−1
PT2
SN-51
PT4
AG−15
LST3_D
LP−16−AZ
SN-47
SBM−7
LST3_P
SBM−6
PT6
SC−4
AG−10
PG3
PT1
SN48
PT5
LST2
PG2
SO
TH−4
PT3

Table 1

Tectonic Complex	NEVADO-FILÁBRIDE COMPLEX (NFC)				Tectonic units of which adscription has been revised in this work		ALPUJÁRRIDE COMPLEX (AC)		MALÁGUIDE COMPLEX (MC)			
Geographical area	**Sierra de Los Filabres area**		**Águilas Arc**		**Águilas Arc**		**Águilas Arc**		**Sierra de las Estancias**		**Águilas Arc**	
Tectonic units	**Mulhacén units**	Marbles and Calc-Schists Fm: atributed from pre-Permian (Gómez-Pugnaire et al., 2012) to Cretaceous ages (Tendero et al., 1993)	**Mulhacén units**	Marbles and Calc-Schists Fm: atributed from pre-Permian (Gómez-Pugnaire et al., 2012) to Cretaceous ages (Tendero et al., 1993)	**Cantal unit**	Black schists and quartzites (unknown age)	**Ramonete unit**	Meta-carbonate Fm: Middle to Late Triassic (García-Tortosa et al., 2012)	**Maláguide succession**	Xiquena Fm (Eocene, Geel, 1973)	**Cabo Cope unit**	-
Tectonic units	**Mulhacén units**	Metaevaporite Fm: atributed from Permian-Triassic (Leine, 1968; Vissers, 1981) to Paleogene ages (Puga et al., 1996)	**Mulhacén units**	Metaevaporite Fm: atributed from Permian-Triassic (Leine, 1968; Vissers, 1981) to Paleogene ages (Puga et al., 1996)	**Cantal unit**	Migmatitic gneisses, schists with kyanite and sillimanite. Orthogneisses. (unknown ages)	**Ramonete unit**	Meta-detrital Fm: Permian to Middle Triassic (Martín-Rojas et al., 2010; García-Tortosa et al., 2012)	**Maláguide succession**	Castillón Fm (Late Triassic to Jurassic, Geel, 1973)	**Cabo Cope unit**	Castillón Fm (Late Triassic to Jurassic, Geel, 1973)
Tectonic units	**Mulhacén units**	Tahal Fm: Permian (Santamaría and Sanz de Galdeano, 2018) to Permian-Early Triassic (Jabaloy-Sánchez et al., 2018)	**Mulhacén units**	Tahal Fm: Permian (Santamaría and Sanz de Galdeano, 2018) to Permian-Early Triassic (Jabaloy-Sánchez et al., 2018)			**Las Palomas unit**	Meta-carbonate Fm: Middle to Late Triassic (García-Tortosa et al., 2012)	**Maláguide succession**	Saladilla Fm (Middle-Late Triassic, Perri et al., 2013)	**Cabo Cope unit**	Saladilla Fm (Middle-Late Triassic, Perri et al., 2013)
Tectonic units	**Veleta units**	Nevada Fm: Late Carboniferous (Santamaría and Sanz de Galdeano, 2018)	**Lomo de Bas units (Veleta units)**	**Lomo de Bas higher unit:** Graphite-bearing micaschist, of unknown ages covering Middle Devonian marbles (Lafuste and Pavillon, 1974; Laborda-López et al., 2013)			**Las Palomas unit**	Meta-detrital Fm: Permian to Middle Triassic (Martín-Rojas et al., 2010; García-Tortosa et al., 2012)	**Maláguide succession**	Piar Group: pre-Ordovician to Late Carboniferous (Martín-Algarra, 1987)		
Tectonic units	**Veleta units**	Aulago Fm Late Carboniferous (Rodríguez-Cañero et al., 2018; Jabaloy-Sánchez et al., 2018)	**Lomo de Bas units (Veleta units)**	**Lomo de Bas higher unit:** Graphite-bearing schists and phyllites with quartzites older than Middle Devonian			**Las Palomas unit**	Micaschists and Quartzite Fm (pre-Permian ages**)**				
Tectonic units	**Veleta units**	Veleta Schists- Late Carboniferous (Santamaría and Sanz de Galdeano, 2018)	**Lomo de Bas units (Veleta units)**	**Lomo de Bas lower unit:** Graphite-bearing micaschist, and quarzites of unknown age			**Miñarro s unit**	Quartz mylonites & carbonate breccias of unknown age				

Table 2

Sample	Tectonic Complex	Tectonic Unit	Lithostratigraphic Formation	Stratigraphic age	Lithology	Location (*)		Type of analyses	Total number of analyses/Conc. analyses
						X	Y		
AG-1	NFC	Mulhacén units	Tahal Fm	Permian-Triassic	quartzite	620445	4158007	LA-ICPMS	150/134
AG-2	NFC	Mulhacén units	Tahal Fm	Permian-Triassic	quartzite	621448	4155480	LA-ICPMS	140/121
AG-12	NFC	Lomo de Bas lower unit	Graphite-bearing micaschist, and ferruginous quarzites	Paleozoic?	quartzite	635001	4151913	LA-ICPMS	150/142
AG-14	NFC	Lomo de Bas lower unit	Graphite-bearing micaschist, and ferruginous quarzites	Paleozoic?	quartzite	636050	4154168	LA-ICPMS	140/136
AG-17	NFC	Lomo de Bas upper unit	Upper graphitic schists, phyllites, and quartzites	Paleozoic?	quartzite	630645	4155136	LA-ICPMS	130/119
AG-18	NFC	Lomo de Bas upper unit	Upper graphitic schists, phyllites, and quartzites	Paleozoic?	quartzite	630642	4155187	LA-ICPMS	133/128
AG-13	NFC	Lomo de Bas lower unit	-	?	orthogneiss	636008	4152026	SIMS	-
AG-16	NFC	Lomo de Bas lower unit	-	?	orthogneiss	639505	4152611	SHRIMP	-
AG-4	AC	Las Palomas unit	Micaschists and Quartzite Fm	Paleozoic?	quartzite	620932	4147486	LA-ICPMS	152/139
AG-5	AC	Las Palomas unit	Micaschists and Quartzite Fm	Paleozoic?	quartzite	622546	4148545	LA-ICPMS	152/146
AG-6	AC	Las Palomas unit	Micaschists and Quartzite Fm	Paleozoic?	quartzite	626053	4142476	LA-ICPMS	150/135
AG-7	AC	Las Palomas unit	Micaschists and Quartzite Fm	Paleozoic?	quartzite	629645	4143760	LA-ICPMS	151/139
AG-19	AC	Miñarros unit	Meta-detritic Fm	?	quartzite	630637	4155209	LA-ICPMS	151/145
AG-9	AC	Las Palomas unit	Meta-detritic Fm	Permian-Middle Triassic	quartzite	632958	4143805	LA-ICPMS	152/136
AG-11	AC	Las Palomas unit	Meta-detritic Fm	Permian-Middle Triassic	quartzite	632773	4149245	LA-ICPMS	147/133
AG-15	AC	Ramonete unit	Meta-detritic Fm	Middle Triassic	quartzite	634212	4156247	LA-ICPMS	143/123
AG-26	AC?	Cantal unit	-	?	orthogneiss	618187	4137767	SHRIMP	-
LP-16-AZ	MC	Lower Maláguide unit (Sierra de Las Estancias)	Saladilla Fm	Middle-Late Triassic	quartzite	588593	4168969	LA-ICPMS	150/138
AG-10	MC	Cabo Cope unit	Saladilla Fm	Middle-Late Triassic	quartzite	633303	4143026	LA-ICPMS	150/126
AG-3	-	-	Conglomerates and sandstones	Middle Miocene	Conglomerate	628202	4154639	LA-ICPMS	151/138
AG-20	-	-	Conglomerates and sandstones	Middle Miocene	Sandstone	627476	4156840	LA-ICPMS	150/141

Supplementary material

Click here to access/download
e-component
Supplementary material.docx

Supplementary material Table S1

Click here to access/download

e-component

Table S1 analytical data.xls

Supplementary material Table S2

Click here to access/download
e-component
Table S2.xls

Supplementary material Table S3

Click here to access/download
e-component
Table S3.xlsx

Click here to access/download
RDM Data Profile XML
GR-D-20-00209_DataProfile.xml